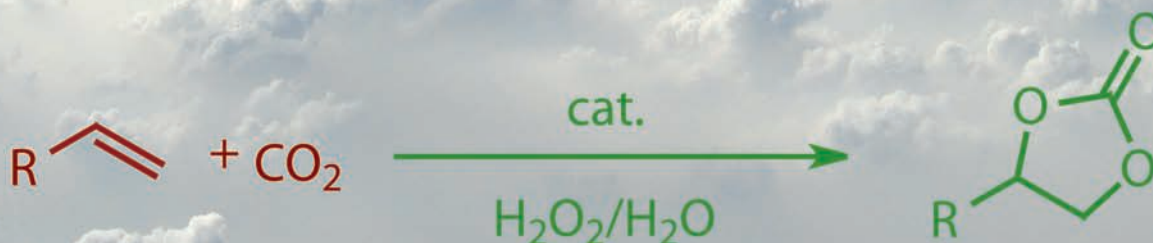


Green Chemistry

Cutting-edge research for a greener sustainable future

www.rsc.org/greenchem

Volume 9 | Number 3 | March 2007 | Pages 193–284



ISSN 1463-9262

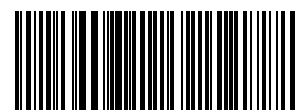
RSC Publishing

Rencurosi *et al.*
HRMAS NMR analysis in neat ionic liquids

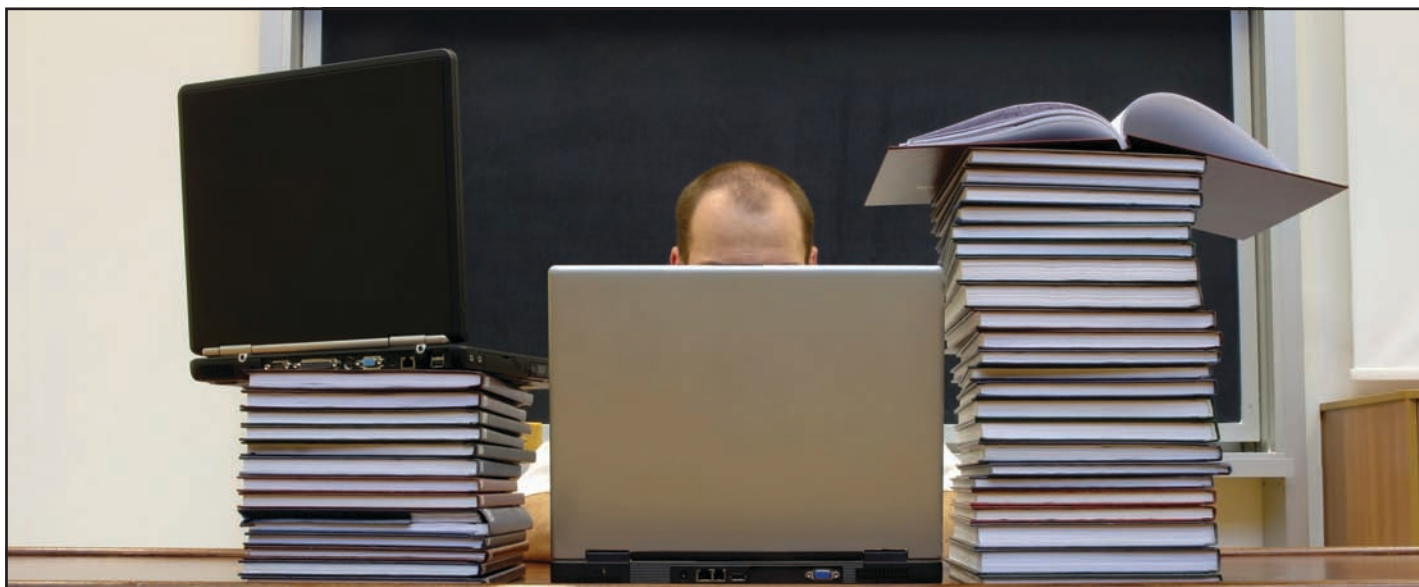
Eghbali and Li
Conversion of carbon dioxide and olefins into cyclic carbonates in water

Carril *et al.*
Recyclable copper-catalyst in aqueous media

Höfer and Bigorra
Green chemistry—a sustainable solution for specialties applications



1463-9262(2007)9:3;1-9



There is an easier way to keep up with research in your field...

An integral part of managing your career as a scientist is staying on top of the news and developments in your field of research and related areas. A good knowledge of your industry is a key component to your success, but finding the time to keep up with the latest research news can pose the greatest challenge.

The solution? By signing up for e-alerts from one of our free news services, you can receive updates about newsworthy and significant research appearing in RSC journals in a quick and easily digestible monthly alert.

Free access. From each news item you can link directly to the source research paper, which is completely free to access and download for a limited period.

New tools to help you. In addition to research news, our news services also feature

- **Instant insights** – whirlwind tours of exciting research areas you should know about
- **Interviews** – leading scientists share their opinions

**Chemical
Technology**

www.rsc.org/chemicaltechnology

**Chemical
Science**

www.rsc.org/chemicalscience

**Chemical
Biology**

www.rsc.org/chembiology

10110633

RSC Publishing

www.rsc.org/ej_alert

Registered Charity Number 207890

Green Chemistry

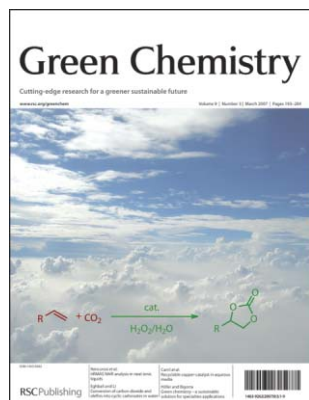
Cutting-edge research for a greener sustainable future

www.rsc.org/greenchem

RSC Publishing is a not-for-profit publisher and a division of the Royal Society of Chemistry. Any surplus made is used to support charitable activities aimed at advancing the chemical sciences. Full details are available from www.rsc.org

IN THIS ISSUE

ISSN 1463-9262 CODEN GRCHFJ 9(3) 193–284 (2007)



Cover

A highly efficient method has been developed to convert alkenes and CO₂ into cyclic carbonates directly in water. Cyclic carbonates were also formed efficiently by using a catalytic amount of bromide ion together with aqueous H₂O₂. Using *N*-bromosuccinimide (NBS) together with DBU in water, alkenes were converted into cyclic carbonates nearly quantitatively.

Image reproduced by permission of C.-J. Li from *Green Chem.*, 2007, 9(3), 213.

CHEMICAL TECHNOLOGY

T17

Chemical Technology highlights the latest applications and technological aspects of research across the chemical sciences.

Chemical Technology

March 2007/Volume 4/Issue 3

www.rsc.org/chemicaltechnology

PERSPECTIVE

203

Green chemistry—a sustainable solution for industrial specialties applications

Rainer Höfer* and Joaquim Bigorra

The development of green chemistry has seen significant effort and progress towards the development of sustainability in industry.

We do not own the world, we borrowed it from our children

Responsible Care

Copli's guiding principle following a saying by Antoine de Saint Exupéry

EDITORIAL STAFF

Editor

Sarah Ruthven

Publishing assistant

Emma Hacking

Team leader, serials production

Stephen Wilkes

Technical editor

Edward Morgan

Administration coordinator

Sonya Spring

Editorial secretaries

Donna Fordham, Jill Segev, Julie Thompson

Publisher

Emma Wilson

Green Chemistry (print: ISSN 1463-9262; electronic: ISSN 1463-9270) is published 12 times a year by the Royal Society of Chemistry, Thomas Graham House, Science Park, Milton Road, Cambridge, UK CB4 0WF.

All orders, with cheques made payable to the Royal Society of Chemistry, should be sent to RSC Distribution Services, c/o Portland Customer Services, Commerce Way, Colchester, Essex, UK CO2 8HP. Tel +44 (0) 1206 226050; E-mail sales@rscdistribution.org

2007 Annual (print + electronic) subscription price: £902; US\$1705. 2007 Annual (electronic) subscription price: £812; US\$1534. Customers in Canada will be subject to a surcharge to cover GST. Customers in the EU subscribing to the electronic version only will be charged VAT.

If you take an institutional subscription to any RSC journal you are entitled to free, site-wide web access to that journal. You can arrange access via Internet Protocol (IP) address at www.rsc.org/ip. Customers should make payments by cheque in sterling payable on a UK clearing bank or in US dollars payable on a US clearing bank. Periodicals postage paid at Rahway, NJ, USA and at additional mailing offices. Airfreight and mailing in the USA by Mercury Airfreight International Ltd., 365 Blair Road, Avenel, NJ 07001, USA.

US Postmaster: send address changes to Green Chemistry, c/o Mercury Airfreight International Ltd., 365 Blair Road, Avenel, NJ 07001. All despatches outside the UK by Consolidated Airfreight.

PRINTED IN THE UK

Advertisement sales: Tel +44 (0) 1223 432246; Fax +44 (0) 1223 426017; E-mail advertising@rsc.org

Green Chemistry

Cutting-edge research for a greener sustainable future

www.rsc.org/greenchem

Green Chemistry focuses on cutting-edge research that attempts to reduce the environmental impact of the chemical enterprise by developing a technology base that is inherently non-toxic to living things and the environment.

EDITORIAL BOARD

Chair

Professor Martyn Poliakoff
Nottingham, UK

Scientific Editor

Professor Walter Leitner
RWTH-Aachen, Germany

Associate Editors

Professor C. J. Li
McGill University, Canada
Professor Kyoko Nozaki
Kyoto University, Japan

Members

Professor Paul Anastas
Yale University, USA
Professor Joan Brennecke
University of Notre Dame, USA
Professor Mike Green
Sasol, South Africa
Professor Buxing Han
Chinese Academy of Sciences,
China
Professor Roshan Jachuck
Clarkson University, USA

Dr Alexei Lapkin
Bath University, UK
Dr Janet Scott
Unilever, UK
Professor Tom Welton
Imperial College, UK

INTERNATIONAL ADVISORY EDITORIAL BOARD

James Clark, York, UK
Avelino Corma, Universidad
Politécnica de Valencia, Spain
Mark Harmer, DuPont Central
R&D, USA
Herbert Hugl, Lanxess Fine
Chemicals, Germany
Makato Misono, Kogakuin
University, Japan
Colin Raston,
University of Western Australia,
Australia

Robin D. Rogers, Centre for Green
Manufacturing, USA
Kenneth Seddon, Queen's
University, Belfast, UK
Roger Sheldon, Delft University of
Technology, The Netherlands
Gary Sheldrake, Queen's
University, Belfast, UK
Pietro Tundo, Università ca
Foscari di Venezia, Italy

INFORMATION FOR AUTHORS

Full details of how to submit material for publication in Green Chemistry are given in the Instructions for Authors (available from <http://www.rsc.org/authors>). Submissions should be sent via ReSource: <http://www.rsc.org/resource>.

Authors may reproduce/republish portions of their published contribution without seeking permission from the RSC, provided that any such republication is accompanied by an acknowledgement in the form: (Original citation) – Reproduced by permission of the Royal Society of Chemistry.

© The Royal Society of Chemistry 2007. Apart from fair dealing for the purposes of research or private study for non-commercial purposes, or criticism or review, as permitted under the Copyright, Designs and Patents Act 1988 and the Copyright and Related Rights Regulations 2003, this publication may only be reproduced, stored or transmitted, in any form or by any means, with the prior permission in writing of the Publishers or in the case of reprographic reproduction in accordance with the terms of licences issued by the Copyright Licensing Agency in the UK. US copyright law is applicable to users in the USA.

The Royal Society of Chemistry takes reasonable care in the preparation of this publication but does not accept liability for the consequences of any errors or omissions.

Ⓢ The paper used in this publication meets the requirements of ANSI/NISO Z39.48-1992 (Permanence of Paper).

Royal Society of Chemistry: Registered Charity No. 207890

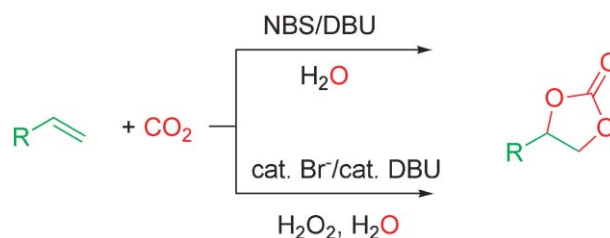
COMMUNICATIONS

213

Conversion of carbon dioxide and olefins into cyclic carbonates in water

Nicolas Eghbali and Chao-Jun Li*

A highly efficient method was developed to convert alkenes and CO₂ into cyclic carbonates directly in water by using *N*-bromosuccinimide (NBS) together with 1,8-diazabicyclo[5.4.0]undec-7-ene (DBU), or by using a catalytic amount of bromide ion together with aqueous H₂O₂.

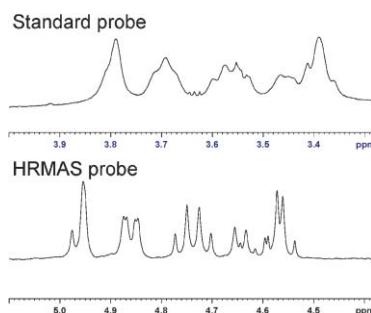


216

HRMAS NMR analysis in neat ionic liquids: a powerful tool to investigate complex organic molecules and monitor chemical reactions

A. Rencurosi, L. Lay, G. Russo, D. Prosperi, L. Poletti* and E. Caneva*

Neat ionic liquids can act as non-deuterated solvents for HRMAS NMR spectroscopy. The high resolution obtained through the HRMAS technique allows the characterization of complex organic molecules and the real time monitoring of chemical reactions in these highly viscous media.

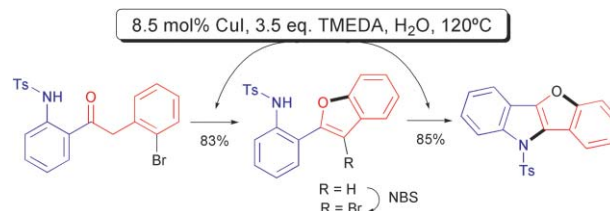


219

Recyclable copper-catalyst in aqueous media: *O*- and *N*-arylation reactions towards the benzofuroindole framework

Mónica Carril, Raul SanMartin,* Esther Domínguez* and Imanol Tellitu

The synthesis of the benzofuroindole skeleton using a recyclable copper-catalytic system in water solution suitable for both key *N*- and *O*-arylation steps is presented.



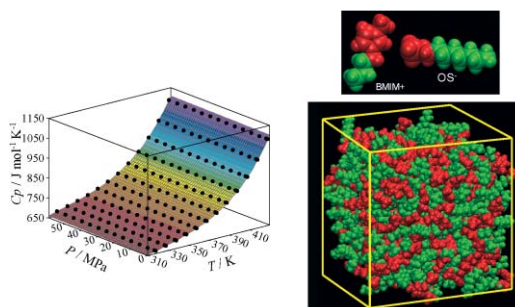
PAPERS

221

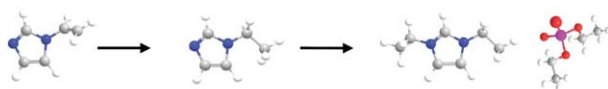
On the properties of 1-butyl-3-methylimidazolium octylsulfate ionic liquid

María J. Dávila, Santiago Aparicio, Rafael Alcalde, Begoña García and José M. Leal*

Combination of thermophysical and molecular modelling studies of ionic liquids provides a solid linkage between macroscopic and microscopic fluid properties. [BMIM][OS], with remarkable properties and favourable green chemistry profile, is a valuable alternative to conventional solvents.



233

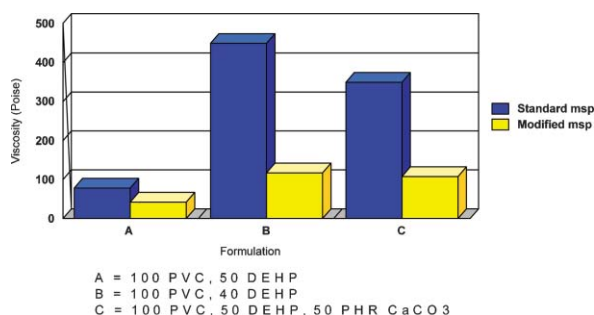


Imidazolium dialkylphosphates—a class of versatile, halogen-free and hydrolytically stable ionic liquids

Esther Kuhlmann, Simone Himmler, Heidi Giebelhaus and Peter Wasserscheid*

A systematic study is presented of the synthesis and properties of dialkylphosphate ionic liquids, halogen-free ionic liquids with great technical potential, especially at low temperature (<200 °C) in contact with water.

243

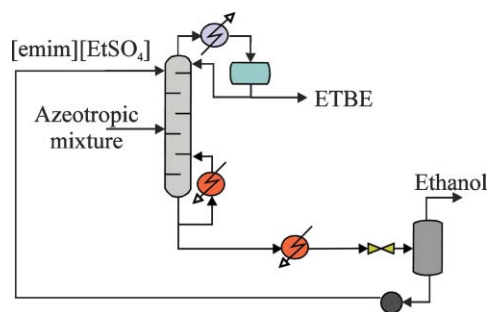


New developments in emulsion-PVC polymerisation to produce polymers with the potential of reduced or zero VOC requirements when used in plastisol applications

Christopher Howick*

A report on work which has modified the microsuspension polymerisation technology of PVC plastisols, allowing full processing without the need for solvents, and as such represents a method of VOC reduction.

247

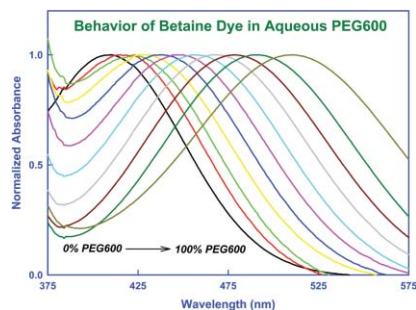


Use of a green and cheap ionic liquid to purify gasoline octane boosters

Alberto Arce,* Héctor Rodríguez and Ana Soto

Rigorous thermodynamic analyses are presented to evaluate the ability of the ionic liquid 1-ethyl-3-methylimidazolium ethylsulfate as an extracting solvent or a distillation entrainer for the separation of ethanol and ETBE.

254



Solute-solvent interactions within aqueous poly(ethylene glycol): solvatochromic probes for empirical determination and preferential solvation

Pallavi Singh and Siddharth Pandey*

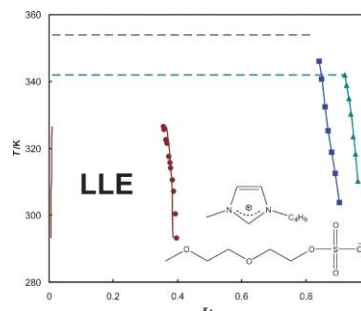
The physicochemical properties (dipolarity/polarizability, H-bond donating acidity, and H-bond accepting basicity) of aqueous poly(ethylene glycols) [PEGs] are shown to depend on the solution composition as well as PEG molecular mass.

262

Liquid phase behaviour of 1-butyl-3-methylimidazolium 2-(2-methoxyethoxy)-ethylsulfate with organic solvents and water

Urszula Domańska* and Andrzej Marciniak

The mutual solubility of [BMIM][MDEGSO₄] with hydrocarbons, ketones, alcohols, 1,1-dimethylpropyl methyl ether and water have been measured for technological use.

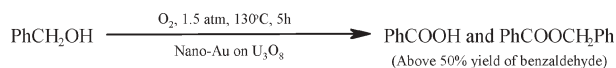


267

Solvent-free selective oxidation of benzyl alcohol by molecular oxygen over uranium oxide supported nano-gold catalyst for the production of chlorine-free benzaldehyde

Vasant R. Choudhary,* Rani Jha and Prabhas Jana

Chlorine-free benzaldehyde can be obtained from a solvent-free liquid phase selective oxidation of benzyl alcohol by molecular oxygen using a reusable U₃O₈ supported nano-gold catalyst.

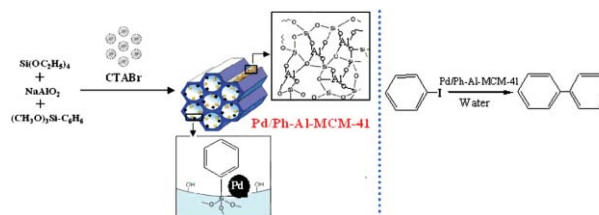


273

Aqueous medium Ullmann reaction over a novel Pd/Ph-Al-MCM-41 as a new route of clean organic synthesis

Hexing Li,* Jia Chen, Ying Wan, Wei Chai, Fang Zhang and Yunfeng Lu

A novel Pd/Ph-Al-MCM-41 catalyst was designed, which exhibited excellent activity, selectivity, and hydrothermal stability in an aqueous-medium Ullmann reaction, owing to the promoting effects of the ordered mesoporous structure, and the Ph- and Al-modifications.




AUTHOR INDEX

- | | | | |
|---------------------------|--------------------------|-------------------------|--------------------------|
| Alcalde, Rafael, 221 | Domańska, Urszula, 262 | Kuhlmann, Esther, 233 | Rencurosi, A., 216 |
| Aparicio, Santiago, 221 | Domínguez, Esther, 219 | Lay, L., 216 | Rodríguez, Héctor, 247 |
| Arce, Alberto, 247 | Eghbali, Nicolas, 213 | Leal, José M., 221 | Russo, G., 216 |
| Bigorra, Joaquín, 203 | García, Begoña, 221 | Li, Chao-Jun, 213 | SanMartin, Raul, 219 |
| Caneva, E., 216 | Giebelhaus, Heidi, 233 | Li, Hexing, 273 | Singh, Pallavi, 254 |
| Carril, Mónica, 219 | Himmeler, Simone, 233 | Lu, Yunfeng, 273 | Soto, Ana, 247 |
| Chai, Wei, 273 | Höfer, Rainer, 203 | Marciniak, Andrzej, 262 | Tellit, Imanol, 219 |
| Chen, Jia, 273 | Howick, Christopher, 243 | Pandey, Siddharth, 254 | Wan, Ying, 273 |
| Choudhary, Vasant R., 267 | Jana, Prabhas, 267 | Poletti, L., 216 | Wasserscheid, Peter, 233 |
| Dávila, María J., 221 | Jha, Rani, 267 | Prosperi, D., 216 | Zhang, Fang, 273 |

FREE E-MAIL ALERTS AND RSS FEEDS


Contents lists in advance of publication are available on the web *via* www.rsc.org/greenchem - or take advantage of our free e-mail alerting service (www.rsc.org/ej_alert) to receive notification each time a new list becomes available.

 Try our RSS feeds for up-to-the-minute news of the latest research. By setting up RSS feeds, preferably using feed reader software, you can be alerted to the latest Advance Articles published on the RSC web site. Visit www.rsc.org/publishing/technology/rss.asp for details.

ADVANCE ARTICLES AND ELECTRONIC JOURNAL

Free site-wide access to Advance Articles and the electronic form of this journal is provided with a full-rate institutional subscription. See www.rsc.org/ejs for more information.

* Indicates the author for correspondence: see article for details.

 Electronic supplementary information (ESI) is available *via* the online article (see <http://www.rsc.org/esi> for general information about ESI).

Take the global perspective

chemistryworld

Chemistry World, the monthly magazine from the Royal Society of Chemistry, has something for everyone

- Daily online news
- Articles on all aspects of the chemical sciences
- Company and individual profiles
- Job vacancies
- Business news analysis
- Award-winning columnists
- Chemistry through the lens
- *Chemistry World* Blog and Podcast



22010759

See Science Come Alive



Introducing Project Prospect

Features include

- IUPAC Gold Book terms linked*
- Hyperlinked compound information in text*
- Ontology terms linked to definitions and related papers*
- RSS feeds with ontology terms and compound structures*

Benefits

- Completely free service*
- At a glance HTML view with additional features accessed by toolbox*
- Downloadable compound structures*
- Printer friendly*

Scientists trawling through the thousands of research papers published every month must wish their computer could do the job for them. This could soon be a reality thanks to **Project Prospect**, an initiative developed by RSC Publishing together with academic partners. Readers can click on named compounds and scientific concepts in an electronic journal article to download structures, understand topics, or link through to electronic databases. Powerful functionality instantly helps researchers to find, understand and share (bio)chemical knowledge with each other quicker than ever before. See the science in journal articles *come alive*: visit the **Project Prospect** website for FAQs, examples, contact information and latest news.

RSC Publishing

www.projectprospect.org

Registered Charity Number 207890



30 years

A measure of our success

Celebrating **30 years** of successful publication, the *New Journal of Chemistry* is the home of new and emerging multidisciplinary work in the chemical sciences. Publishing full papers, letters, opinions and perspectives, *NJC* offers a multitude of benefits to both authors and readers:

- High quality original and significant work
- Fast times to publication
- Owned and published by learned societies

RSC Publishing



CENTRE NATIONAL
DE LA RECHERCHE
SCIENTIFIQUE

www.rsc.org/njc

Registered Charity Number 207890

Green chemistry—a sustainable solution for industrial specialties applications†

Rainer Höfer*^a and Joaquim Bigorra^b

Received 5th May 2006, Accepted 11th December 2006

First published as an Advance Article on the web 10th January 2007

DOI: 10.1039/b606377b

The wellness and sustainability mega-trends will have a decisive influence on the future and, because of this, on the behaviour of consumers. Manufacturers will have to be prepared for the changes that will take place early enough so as not to miss the boat. One of the major goals of sustainability is to maintain an optimal balance between increases in manufacturing output, and a clean and safe environment.

Sustainability will be one of the main drivers for innovation in order to allow the technical industries to care for the well-being of consumers in a safe and healthy environment.

Thus, one area in which significant efforts and progress have been made is in the development of “green” or sustainable chemistry.

1. The history of sustainability

The 20th century has seen a phenomenal growth of the global economy and a continuous improvement of the standard of living in the industrialized countries.

However, since the middle of the last century global consumption of water has tripled. Demand for wood as a construction material has doubled. Demand for wood for heat generation has tripled. Demand for wood as pulp and paper raw material has increased six fold. Consumption of sea fish has increased by five times over the last 50 years. Farmland quality due to intensive live stock farming has seen a steady decrease. Annually *more than* 1000 animals or plants are close to extermination. Since the beginning of the industrial age the concentration of carbon dioxide in the atmosphere has steadily increased (the greenhouse effect). In other words, growth of the economies and increase of living standards, have had their price: exploitation of natural resources to their limits and an ever increasing contamination of the environment¹—an opinion largely shared by politicians, administrations and the wider public.

To a large extent, the history of mankind does mean the history of the relations between human beings and the surrounding nature.²

While the evolution of the human species in prehistoric times was driven by nature, by genetic selection and by geological and climatic changes, since biblical times the western hemisphere, at least, has followed the divine message to “fill the earth and subdue it”. As a result, exploitation of natural resources is nothing new. The Roman Empire developed an extensive agriculture, and in the 2nd century

BC the first compendium about agronomics appeared—“De Agricultura”—written by Cato the Censor.³ The intensive agriculture of the Roman Empire, together with the high energy demand of the Roman society for their popular steam baths, for metal working and production of weapons and the high demand of wood for housing and shipbuilding, are claimed to be at the origin of the first historically known ecological disaster: the complete deforestation, first of Italy (more particularly the Apennine hillside) and later of all areas around the Mediterranean Sea, resulting in enormous erosions, loss of humus soil in the mountains, temporary desiccation of rivers, flash flood after thunderstorms further increasing erosion, formation of karst landscape in the plains followed by climatic changes⁴ in the region which last until our modern times.

An ecological disaster of similar dimensions happened in North America, when squatters and ranchers took the land, transformed it into farmland for pigs and cattle, corn and cotton, clear-cutting broad-leaved and coniferous woods, exterminating great number of wildlife—and aborigines.⁵ And not only wood was exploited beyond limits, but also water—resulting in a drawdown, a lowering of the groundwater. The green plains of former times, in Arizona for example, turned into desert. Out of 70 grass species said to have been known by the Indians less than half a dozen remain—plus bushes and cacti.

More recently, since the Iron Curtain disappeared at the beginning of the 1990s mankind became aware that the Earth is not “endless”, that there are no longer insuperable borders setting limits to migration, that there is no unknown territory left to be discovered, conquered, cultivated or exploited. Maybe this cognition was made public for the first time when, at the beginning of the 1970s, the Club of Rome’s report about “Limits to Growth”⁶ appeared, and together with Rachel Carson’s book “Silent Spring”⁷ and the 1st oil crisis, had an

^aCognis Deutschland GmbH & Co KG, Monheim, Germany

^bCognis Iberia, Castellbisbal, Spain

† Paper presented at the “36 Jornadas Anuales del CED”, Barcelona, 2006

**We do not own the
world, we
borrowed it from
our children**

Responsible Care

Cognis' guiding principle following a saying by Antoine de Saint Exupéry

Fig. 1 Responsible Care.

enormous impact on public opinion worldwide, and started a political debate and thinking process.

The principle of “Responsible Care” became a mission statement for action of companies, and for the thinking of political, religious and social movements and non-governmental organizations (NGOs), leading to the foundation of the “green” movement, and the “Green” political parties. Emanating into the industrial world, “green chemistry” became a concept for economy in chemical synthesis, waste prevention, design and utilization of less hazardous, safer chemicals and chemical auxiliaries, energy efficiency, and use of renewable resources; in other words: for sustainable solutions in the chemical industry.

But “green chemistry” is not really an advancement of “green” political principles into chemistry—on the contrary: the roots of green chemistry go back to the 1950s, when Henkel,⁸ a chemical company, started monitoring surfactant concentrations in the Rhine River and developed the closed bottle test in order to study the biodegradability of surfactants, and since then has strategically steered research and development according to environmental principles, resulting in, for example, the development of zeolithe A as an alternative to phosphates in detergents (in order to avoid eutrophication of sweet water lakes in Germany due to over-fertilization).

The definition and principle of “sustainable development” even goes back to the 18th century, when Hanns Carl Edler von Carlowitz (an official of the Kingdom of Saxony Mining Authority) declared that forestry had to be “sustainable”, which meant that harvesting and seeding had to be in balance.⁹ This was in order to preserve wood supply for the important silver mines in the Erzgebirge.

The far-seeing 18th century principle of sustainability in the final quarter of the 20th century and on the eve of the 3rd millennium entered the scene of world politics when, in 1983, the Assembly of the United Nations asked the Secretary General to appoint a ‘World Commission on Environment and Development’. The idea was to forecast, on a global scale, how man-made activities would affect the environment of the Earth, encompassing the industrial as well as the social and economic aspects. The Secretary General of the UN entrusted

the chair of this committee to Mrs Gro Harlem Brundtland, who was then Prime Minister of Norway. Work on it was completed in March 1987 and it was published later that year under the title *Our Common Future*.¹⁰ Working on that subject, the commission faced a double problem: on the one hand it was obviously human activities which lay behind the deterioration of the environment, especially in the developed nations. On the other hand, it was inconceivable for the UN to create difficulties for the developing nations, for people who had no access to decent living conditions but who, by catching up en masse, would significantly add to the deleterious effects of pollution and degradation of the environment. One of the ways by which the Brundtland commission sought to overcome this dilemma, consisted in the creation of the ‘sustainable development’ concept. This concept was meant to provide a long-term balance between the environment, the economy and the social well being of humanity.

Whereas in prehistoric times of evolution human race was driven by nature, whereas since biblical times humans were filling and subduing the Earth, now, at the doorstep of the 3rd millennium, the concept of balance was born—the conclusion was made that nature and action of humans, among themselves and towards nature, need to be in balance.

Finally, the Nobel Prize for Peace 2004, awarded to Wangari Maathai “for her contribution to sustainable development, democracy and peace”, thus honouring her “Green Belt” initiative and her efforts to promote ecologically viable social, economical and cultural developments in Africa,¹¹ was certainly another step towards sustainable development, particularly as the Norwegian Nobel Committee, through the 2004 award, also found a new, enlarged definition for peace, when stating that “peace on earth depends on our ability to secure our living environment”.

In 1999 sustainability additionally got a financial aspect, when Dow Jones created the DJSI, the Dow Jones Sustainability Index.

2. The sustainability concept in industrial applications

Starch, glucose, cellulose, lignin, tall oil, and natural fats and oils are key base stocks for modern industry relying on renewable resources.¹²

More particularly the production of natural fats and oils starting from 30 million tons in 1960 has reached a fourfold

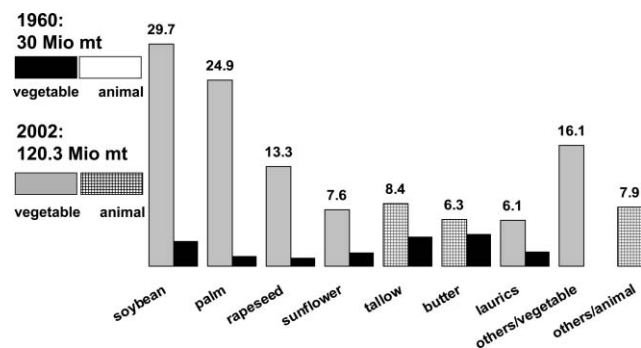


Fig. 2 World Production of oils and fats.

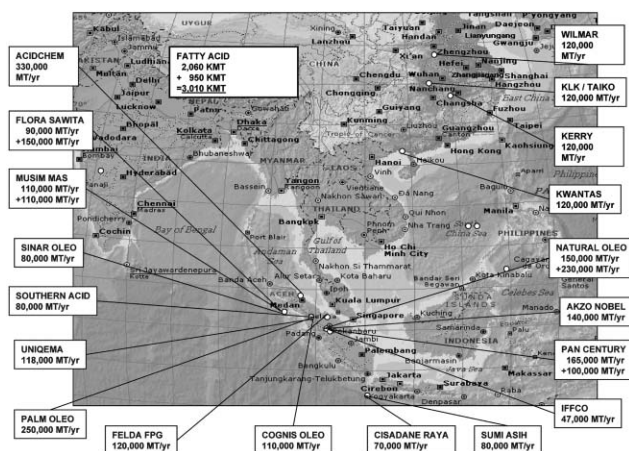


Fig. 3 Fatty acid capacities in Asia.

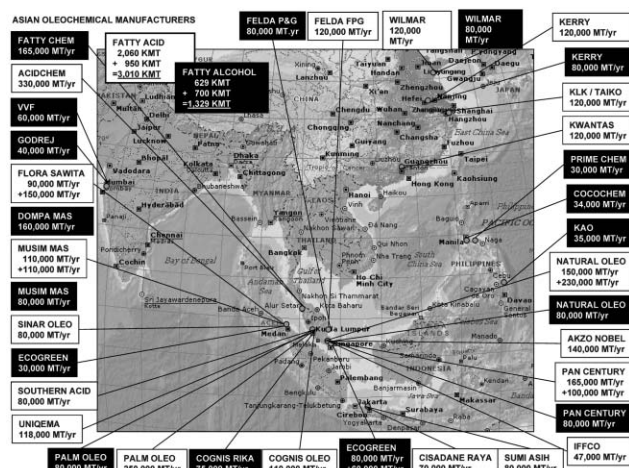


Fig. 4 Oleochemical capacities in Asia.

production volume of 120 million tons in 2002,^{13,14} with a tremendous shift from animal to vegetable base stock; and whereas natural fats and oils have been processed mainly in Europe and in the USA up to now, the years to come will bring a shift to the countries of origin: Asian production of fatty acids will grow by 50% from 2 million tons to 3 million tons, and fatty alcohol production from 800 000 tons to 1.3 million tons, even further shifting the balance between synthetic and natural fatty alcohols to the renewable resources side (see Fig. 5).

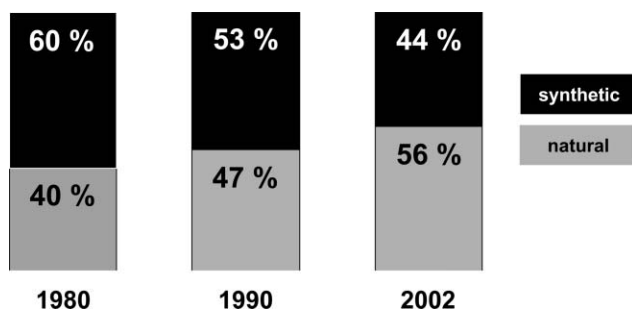


Fig. 5 Change in market share, natural vs. synthetic fatty alcohols.

At the same time the European Biofuel Directive 2003/30/EC will further change the European landscape, obliging the member states of the EC to ensure that a minimum proportion of biofuels and other renewable fuels are placed on their markets as part of the package of measures needed to comply with the Kyoto Protocol. A reference value for these targets will be 2% of all petrol and diesel for transport purposes from December 31st, 2005, and 5.75% by December 31st, 2010, and projects to make the necessary volumes of biodiesel available are already under construction.

Additionally, fueled by regulatory efforts in other countries, the biodiesel industry has demonstrated one of the highest growth rates ever seen in the chemical industry; average annual growth rate during the period 2000–2005 has been in the order of 32%, and world biodiesel demand is forecast to grow from 6.9 million tons in 2006 to 45 million tons in 2010.^{14a} This development will create a third segment of vegetable oil applications, besides food, feed and industrial use, *i. e.* usage as fuel in Europe and other parts of the world.

The increasing production of biodiesel will, however, create an over-supply of glycerol. This has initiated research projects, such as *Solvsafe* as part of the 6th European Framework Program, in order to find new applications for glycerol as a by-product of biodiesel manufacturing.¹⁵ Some changes have already happened: inverting the production of synthetic glycerol from epichlorohydrine, Solvay recently has published that a new 10 000 tons capacity in Tavaux, France will start, designed to produce epichlorohydrine using biodiesel derived glycerine (rather than propylene) as feedstock *via* a catalytic process called “Epicerol”.¹⁶

Green solvents

According to a recent study of the Freedonia Group, the overall world demand for solvents, including hydrocarbon and chlorinated types, is forecast to grow at a 2.3% per year through 2007, and approach 20 million metric tons annually, the lion’s share of 58% being used in the coatings, inks, and adhesives industries. Demand for hydrocarbon and chlorinated solvents, though, will continue its downward trend as a result of environmental regulations, with oxygenated and

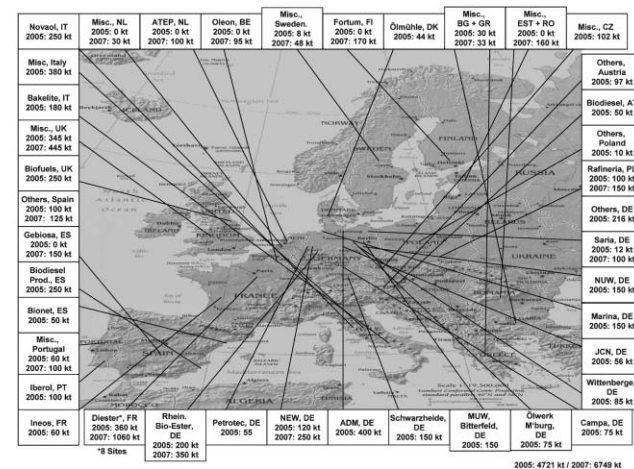


Fig. 6 European Biodiesel capacities.

green solvents replacing them, and growing at an average of 6–7%.

In coatings, by definition a solvent plays only a temporary role: the solvent is in many cases the reaction medium for the synthesis of the binder. After polymerisation, the solvent may remain or it is added to transport the dissolved binder, help to bring it into place, allow and facilitate the formation of a coating or adhesive film or of inks dots—and then should disappear. Volatility is a must for a solvent in coatings.

If transport is the only purpose we also call a solvent “carrier oil”. If a solvent is intended to “stay” in order to facilitate film formation in water-based coatings it is called a “coalescent”, if it is due to solvate macromolecules in order to reduce the glass transition temperature of a plastic material or a film or in order to form a plastisol, it is called “plasticizer”. A “solvent that allows completion of the task, but in an environmentally conscious manner”, by definition constitutes a “green” solvent.¹⁷

Ester solvents are actually the largest group of green solvents. Speciality solvents, such as glycerol carbonate can be used as non-reactive diluents in epoxy or polyurethane systems. Ethyl lactate has been reported as a photo-resist carrier solvent and a clean-up solvent in microelectronics and semiconductor manufacturing, and 2-ethylhexyl lactate can be used as degreaser and as a green solvent in agrochemical formulations, for example for the protection of paddy rice crops.¹⁸

Supercritical carbon dioxide is recommended for spray paint applications because it has high solvation power for many polymers, is non-toxic, and inexpensive. Since CO₂ is so volatile, it is mixed with the coating resin immediately prior to application and the resulting mixture is sprayed onto the substrate.¹⁹

A very peculiar class of solvents are ionic liquids,²⁰ *i. e.*, by definition, salts that are liquid over a wide range of temperature and melt below about 100 °C. Ionic liquids define a class of fluids rather than a small group of individual examples. The most commonly studied systems contain phosphonium, imidazolium or tricaprylmethyl ammonium cations, with varying heteroatom functionality. One regularly suggested advantage of ionic liquids, which positions them as solvents for green chemistry, is the intrinsic lack of vapour

Table 1 Basic formulae for green offset inks^a—varnish

Varnish	Sheet offset ink	Web offset ink
Albertol [®] KP 700 (Vianova Resins)	38%	35%
Albertol [®] KP 854 (Vianova Resins)	—	10%
Alftalat [®] AL (Vianova Resins)	9%	—
Texaprint [®] SKEH (Cognis)	53%	—
Texaprint [®] SLIP (Cognis)	—	55%
Viscosity at 23 °C	480 dPa s at 10/s	80 dPa s at 50/s
Tack 400 m min ⁻¹ at 23 °C	320 dPa s at 50/s	9

^a L. Bothe, Albertol KP 700 – a new resin for monoester based lithographic inks, Technical Information, Vianova Resins (1997)

Table 2 Basic formulae for green offset inks^a—printing ink

Varnish	Sheet offset ink	Web offset ink
Permanent Gelb [®] GRX 82 (Clariant)	12%	12%
Varnish	77%	88%
Texaprint [®] SKEH (Cognis)	11%	—
Viscosity at 23 °C	480 dPa s at 10/s	665 dPa s at 10/s
	320 dPa s at 300/s	275 dPa s at 200/s
Tack 400 m min ⁻¹ at 23 °C	9	11
Gloss at 60 °C and 1.5 g m ⁻²	79	70
tan δ	2.3	2.1

^a L. Bothe, Albertol KP 700 – a new resin for monoester based lithographic inks, Technical Information, Vianova Resins (1997)

pressure. Ionic liquids have created particular scientific interest for extraction or separation technologies, and phase transfer catalysis.

Besides low molecular weight ester solvents, such as methyl acetate or *n*-butyl propionate, higher molecular weight fatty acid esters have already found a broad acceptance as phthalate-free plasticizers²¹ and as biodegradable carrier oils for green inks.²²

ADM and Cognis recently launched a vegetable fatty acid propylene glycol monoester (Archer RC[®], Edenol[®] EFC 100) as a coalescent for decorative paint systems.²³

And Cognis has just started a new plant for the manufacturing of fatty acid dimethylamides, the first plant in Spain (and maybe in Europe) fully dedicated to the production of a green solvent.

In the agrochemical industry, pesticide formulations need solvents in order to dissolve solid actives, or to act as diluents and carriers. More than 25% of all pesticides are formulated as so-called emulsifiable concentrates (ECs). Such concentrates contain 20–80% active ingredient, 20–75% solvent, 5–10% emulsifier, are easy to handle, can be measured volumetrically, and can easily be diluted in place just before application. However, ECs contain high concentrations of organic solvents, which not only represent a fire hazard, but may be toxic and contribute to atmospheric volatile organic compound (VOC) emissions. They may also be phytotoxic to the crop. The most commonly used solvents are the aromatic hydrocarbons, such as C₁₀-alkylbenzene (Solvesso 150, Aromatic 150 Fluid, heavy aromatic solvent, ExxonMobile), primarily utilized as solvents because of their stable physical properties and cost effectiveness. Green solvents for agrosolutions need to perform like

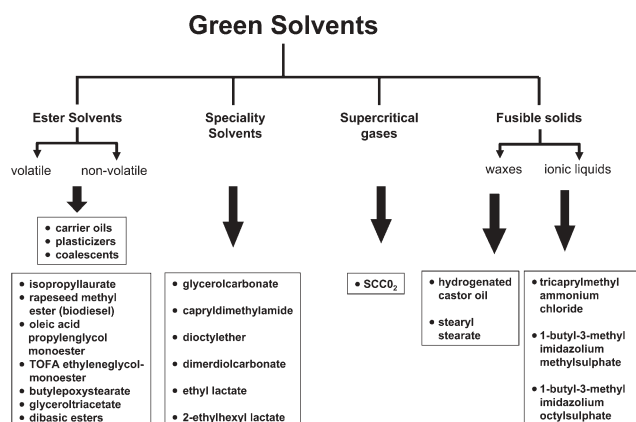


Fig. 7 Green solvents.^{17a}

Table 3 Specifications for oleo-based solvents

	Titer (pour point)/°C	Flash Point/°C	Boiling Point/°C	Visc. at 25 °C/MPa s	Kauri butanol value	Anilin point	Iodine value/Wijs
Short chain fatty acid methylester	-28	75	204–244	2.7	107	<-20	<1
Rapeseed fatty acid methylester	-3	155	335–365	6	66	-1.7	90–110
Soybean fatty acid methylester	-6	170	335–365	10	67	3.69	115–135
<i>n</i> -Butylstearate	22	190	344–384	8.7	42	10	<1
Isobutylstearate	19	>170	341–381	8.4	41	10	2
Soybean fatty acid-2-methylester	-13	180	369–389	9.9	46	-7	85–95
Epoxy stearic acid methylester	—	—	348–386	13.5	>150	-19	—
Di- <i>n</i> -octylether	-7	139	298	3.5	41	27	<1
Capryldimethylamide	—	—	298	6.6	>150	<-20	—

classical solvents, allow ease of handling, simple blending operations and pose no health risk to farm workers. In some pesticide formulations fatty acid methyl esters can directly substitute Aromatic 150 Fluid. The use of lower molecular weight methyl ester can even improve cold stability and reduce the growth of crystals.²⁴

Green lubes and fuels

Lubricants and functional fluids are omnipresent. Because of their widespread use in industrial machinery, in mining, metal working, fibre and textile manufacturing, agriculture, forestry, in construction, road construction and automation, they pollute the environment in small, widely-spread quantities and rarely in large, locally fixed amounts.²⁵ Lubricants are materials used to reduce friction between machinery parts in motion and minimize wear between interacting surfaces.²⁶ Most lubricants are non-aqueous liquids. In the past mineral oil based products were used nearly exclusively, causing the major part of environmental damage by non-proper disposal.

Waxes, which are solids at room temperature, are largely used as lubricants in plastics processing,¹³ where they are used to reduce friction between polymer molecules (internal lubrication) and between the molten polymer and the surrounding machinery parts (external lubrication).

High performance, longer product life and better environmental compatibility will be the driving forces behind foreseeable changes in the worldwide lubricant industry, and, at least in Western Europe, synthetic and quasi-synthetic oils, together with biolubes, will break the dominance of traditional mineral base oils, which tripled in price during the last year's raw material crisis, in a foreseeable future. The selection of rapidly biodegradable lubricants, especially those classified as "not

water pollutant" will reduce the expenses of oil spillage or disposal. The majority of rapidly biodegradable lubricants are based on saturated or unsaturated ester oils. They are divided into five groups: monocarboxylic acid esters (monoesters), dicarboxylic acid esters (diesters), glycerol esters, polyol esters and complex esters.²⁷

Application areas where green lubes have already proved themselves are, for example:

- + environmentally friendly two-stroke oils, especially for outboard engines
- + lubricating chain saw oils
- + latest generation of tractor oils offering higher performance combined with better environmental compatibility
- + readily biodegradable water turbine oils for hydroelectric power stations
- + sustainable synthetic wind turbine oils with a 10 times longer lifetime of lube and turbine gearboxes than with petrolubes or other synthetics. Synthetic wind turbine oils aid and improve the viability of clean, sustainable energy without greenhouse gas emissions, particularly for offshore wind farms where gearbox repair is difficult and expensive.

Drilling fluids for crude oil production are another example where specially designed fatty acid esters demonstrate their character as biolubes and outperform conventional products. In coastal drillings, the demands placed on the lubricants are particularly high. The drilling fluid is pumped to the surface together with the drill cuttings and, after coarse separation, disposed of directly into the sea. A specially developed fatty acid ester (Petrofree[®]) fulfils not only the requirements regarding rapid biodegradability, but also has a better lubricating effect when compared with products based on mineral oil.

Green surfactants

The impact of sustainability on innovation in industrial applications and markets can be demonstrated by taking as an example the coating industry, which has probably undergone the most fundamental changes regarding raw materials, applications, and application technologies related to safety, health, and ecology.

Natural raw materials have been employed for paintings since prehistoric times, when the Chinese people, using the sap of the indigenous lacquer tree, introduced the art of lacquering.²⁸ Gutenberg's inks were based on carbon black and linseed oil. But the coatings and inks industries were born at the beginning of the 19th century, when natural resins, such as

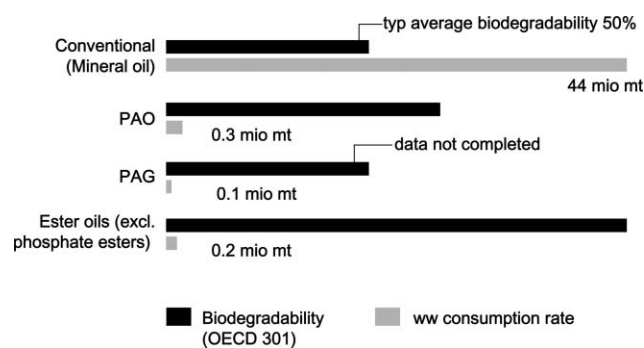


Fig. 8 Relative biodegradability of lubricant base stocks.

shellac, rosin and amber, were largely substituted by synthetic resins,²⁹ and when well performing and cost efficient solvents like benzene, toluene, nitrobenzene, *o*-dichlorobenzene, dichloroethane, Tetralin[®] and Dekalin[®], based on crude and naphtha, and acetylene-, chloro- and nitro-chemistry became available.³⁰ The volatility and flammability of solvents, however, were a steady risk, which has accompanied the coating industry since these early days, and the volatility of solvents, the health risks they create by inhalation, their contribution to air pollution and the green house effect made the coatings, inks and adhesives industries to one of the main targets when environmental and VOC-regulations came into place.

The enormous move of the coating industry towards responsible care by finding water as the major alternative to solvents would not have been possible without the discovery of emulsion polymerisation technology.

Key for emulsion polymerisation³¹ is the emulsifier. By forming micelles the emulsifier can solubilize water-insoluble reactive monomer molecules. A water-soluble initiator starts the polymerisation reaction, which takes place in the micelles. Thus the micelles can be regarded as some kind of living micro-reactors, which grow and form latex particles at the end of the polymerisation process.

The resulting polymer dispersions are largely used in interior and exterior house paints, in textile and paper coating, in leather finishes, floor tile adhesives, and resin re-enforced cements and mortars.

Whereas the world of surfactants for emulsion polymerisation 20 years ago mainly consisted of petrochemical species, the growth of renewable raw materials in general, and the growing importance of vegetable oils in particular, hand in hand with a growing sensitivity for sustainability, initiated a move away from petrochemical emulsifiers towards surfactants derived from natural fats and vegetable oils. In the meantime, green surfactants clearly dominate the emulsion polymerisation technology,³² and this more particularly since natural fatty alcohols are more available and have a bigger market share compared to synthetic fatty alcohols,¹⁴ which—by the way—are not a cheaper alternative anymore.

The breakthrough of green surfactants for emulsion polymerisation happened when equally performing alternatives to alkylphenoethoxylates (APE) and alkyl phenol ether sulfates—until then the workhorses in emulsion polymerisation

technology³³—became available and achieved FDA registration.

Disponil[®] A- and Disponil[®] AFX-types (Cognis) are a new range of such innovative non-ionic “green” emulsifiers^{33a} originally designed for application in emulsion polymerisation, which can also provide innovative solutions in other applications where APEs have been used, such as emulsification of hydrophobic liquids or for dispersing of hydrophobic particles like pigments, resins or fats in water.

APE replacement has been an issue for many years. The EU Risk Reduction Strategy³⁴ proposes to apply marketing and use restrictions to nearly all uses of nonylphenoethoxylates (NPE)s in the following use categories:³⁵

Household detergents³⁶ and cleansers

Personal care and cosmetics (except spermicides)

Industrial and institutional cleaning

Textile industry

Leather industry

Metal working (degreasing, cutting, forming)

Pulp and paper manufacturing

Pesticide and biocide formulations

Veterinary medicine (mandatory zones in the agro industry).

Besides other concerns, the biodegradation of NPE forms NP(EO)_{1–3}, a recalcitrant and very fish toxic metabolite, whereas biodegradation of green alternatives like alkylpolyglycosides or fatty alcohol ethoxylates follow a rapid and complete degradation mechanism leading to the conclusion that polyglycosides and polyglycoethers of short, medium and long chain fatty alcohols and their sulfates, phosphates or sulfosuccinates form a complete base set of green surfactants.

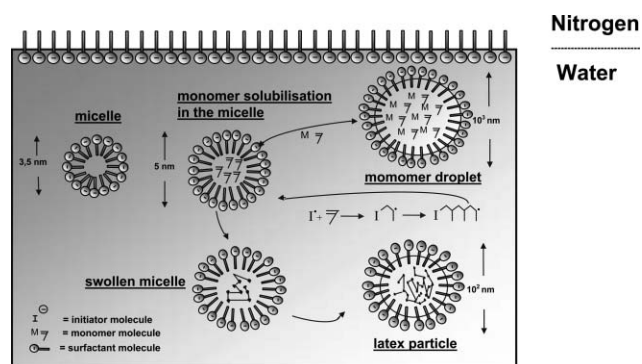


Fig. 9 Emulsion polymerization process.

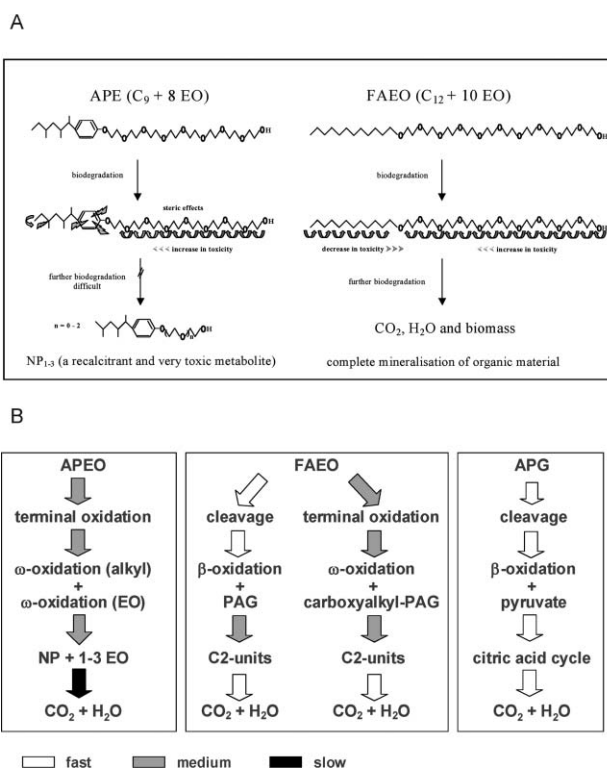


Fig. 10 (a) Ecological properties and (b) biodegradation of non-ionic surfactants.

Green dispersants

Dispersants are used in many technical applications ranging from engine lubricants to fabric washing, from dispersing spilled oil while it is floating on the water surface to solvent borne and water based paint applications.

Incorporation of detergent and dispersant additives into a lubricant helps to control rheology and maintain proper oil fluidity by minimizing thickening and by containing formation of carbon sludge deposits, which occur due to degradation of lubricating oils by oxidation.³⁷ Ashless dispersants are also used in gasoline and diesel fuels to provide fuel injector, carburettor, and valve cleanliness, increasing engine life, and minimizing harmful engine exhaust emissions. The terms detergents and dispersant are often used interchangeably in synthetic lubricants and fuels because the task of both additive types is keeping insoluble combustion debris and oil oxidation products dispersed within the oil.³⁸

Dispersant chemicals are also used in order to respond to marine oil spills at sea, which may be the only means of removing oil from the sea surface, thus minimizing the damage caused by floating oil, for example to birds or sensitive shorelines, particularly when mechanical recovery is not possible.³⁹ In this application dispersants have two main components, a surfactant and a solvent. The solvent acts as a carrier for the surfactant and supports the penetration into the slick. When a dispersant is sprayed onto an oil slick, the interfacial tension between the oil and the water is reduced, breaking up the oil slick, and promoting the formation of finely dispersed oil droplets. There is evidence that dispersed oil degrades more quickly than un-dispersed oil, perhaps because the total surface area of an oil slick increases as dispersants break up the slick into small droplets.

In paints and coatings, dispersants again fulfil another task: here dispersants keep insoluble pigment particles suspended in the binder.

Modern pigments are produced to be primary particles. Commercial pigments viewed through a microscope, show a microstructure with very small, spherical or plate-like primary particles stuck together at their edges and/or planes to form internally hollow secondary structures known as agglomerates. The small size of the primary particles, their surface structure,

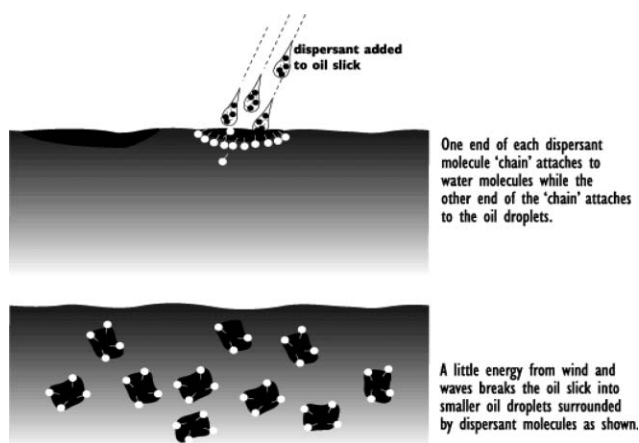


Fig. 11 Breaking of oil slick by action of dispersants.

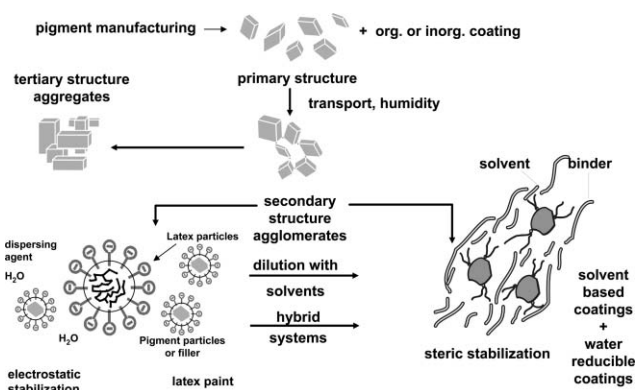


Fig. 12 Pigment dispersions in latex paints vs. solvent-borne and water-reducible coatings.

and their surface energy, result in very high cohesive and adhesive properties, making these agglomerates mechanically very stable. Simply adding these dry pigments as they are delivered to a varnish (*i.e.* a non-pigmented binder in a solvent) would not disturb these secondary structures. A gravelly paint would result, and the dry film would have a matt, inhomogeneous aspect, no colour development, poor hiding power, and would suffer from brilliance and gloss.⁴⁰ In paint making, the dispersion stage consists in grinding, which is the mechanical opening of these secondary structures, the agglomerates, and the addition of a pigment dispersant. This latter is intended to wet the surface of the primary particles, keep them suspended, and stabilize them against re-agglomeration or, even worse, aggregation and settling.

The basic principles for understanding the stabilizing mechanism of dispersants were first investigated 1938 by Verwey and de Boer, who studied the stabilization of various powders in non-aqueous media using oleic acid as the stabilizing agent,⁴¹ and gave one of the first diagrammatic interpretations of the steric stabilization mechanism. The first efficient synthetic dispersing and antissettling agents for inorganic pigments in solvent borne coatings were introduced in the 1950s by Dehydag⁴² (at that time a subsidiary of Henkel, now part of Cognis) under the trademark Texaphor[®]. With the introduction of modern binder systems, such as the durable but poorly wetting solvent-borne polyacrylates or 2 pack polyurethanes in OEM, general industrial, and auto refinish applications, as well as with the growing importance of organic pigments, including the highly hydrophobic carbon black, arose the need for the development of oligomeric or polymeric dispersing agents having a plurality of anchoring groups.⁴³

For the development of dispersing agents for modern aqueous coatings, concepts used in solvent-based coatings were initially transferred to the waterborne field. But there are indeed major differences between aqueous polymer dispersions on one side, and solvent borne and water dilutable systems on the other, with regard to colloidal stabilization, as well as with regard to film formation.⁴⁴ Polymer dispersions (Fig. 9 and 12) contain discrete latex particles stabilized by anionic and/or non-ionic emulsifiers in a continuous water phase. In such ionic surroundings, electrostatic stabilization is the best choice for inorganic pigments and fillers. Thus, organic polyelectrolytes like sodium or ammonium polyacrylate having a

molecular weight range of 3 000 to 10 000 are mainly used as dispersants in latex paints.

The main difference between solvent borne coatings and water dilutable systems (where water is the solvent) is high surface tension at the water/pigment particle interface. Whereas classical solvents by their low surface tension already contribute to wet the pigments, pigment wetting is the major task of a pigment dispersant in aqueous and water dilutable coatings.

So, the function of a dispersant in water dilutable coatings can be compared, to a certain degree, with the task of a detergent in the textile washing process, where the task of the surface active detergent consists in releasing dirt from the fabric and stabilization of the dirt particles in the water phase to prevent their re-deposition.⁴⁵ In clear analogy to the washing process, non-ionic surfactants like certain alkyl phenol ethoxylates already show acceptable dispersant properties, but create the same concerns regarding their eco/toxicological profile as in emulsion polymerization.

In the particular case of coating dispersants, new alkylphenol-free non-ionic alkylene oxide block copolymers⁴⁶ show

even better results. These “green” pigment stabilizing agents derive from vegetable sources, are offered under the trademark Hydropalat[®] and contain at least one if not several hydrophilic moieties, which provide steric stabilization, and are compatible with the surrounding continuous water phase. They also have hydrophobic hydrocarbon chains easily anchoring on the hydrophobic organic pigment surfaces. These new block copolymers are useful for aqueous coatings as well as for modern tinting pastes, and aqueous inks.

3. Sustainability—challenge and driver to innovation

The broad spectrum of technologies employed in chemical industries and the diversity of applications and end user markets makes it clear that “green” can only be used contextually, and the use of a single sustainability metric is not likely to provide a complete picture.⁴⁷ Nonetheless, principles for green chemistry have been established,⁴⁸ and efforts have been made to also develop and employ metrics. For example assessing environmental, health, and safety hazards (EHS) in different effect categories. Assessing the exposure potential by Persistence and Spatial Range (PSR) indicators. Studying the environmental impacts from “cradle to factory” throughout a product’s life using Life-Cycle Inventory (LCI) and from “cradle to grave” throughout Life-Cycle Assessment (LCA, also called Life-Cycle Analysis). Using Cost-Benefit Analysis (CBA) to allow quantification of the socio-economic impacts.^{49,50} Life-Cycle Impact assessment (LCIA) provides additional information to help assess a product system’s LCI results so as to better understand their environmental significance. For the environmental assessment of solvents the *ECOSOLVENT* tool has been developed.⁵¹

Requirements and guidelines for environmental management and LCA have recently become standardised.⁵² LCI, LCA and CBA have been applied for in-depth studies and discussion of oleochemical vs. petrochemical surfactants in household detergents,⁵³ in comparing vegetable oils and mineral oils in lubricant applications, such as hydraulic fluids

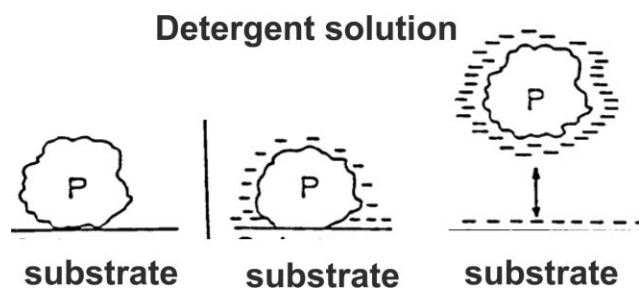


Fig. 13 Stabilization of dirt particles during fabric washing.

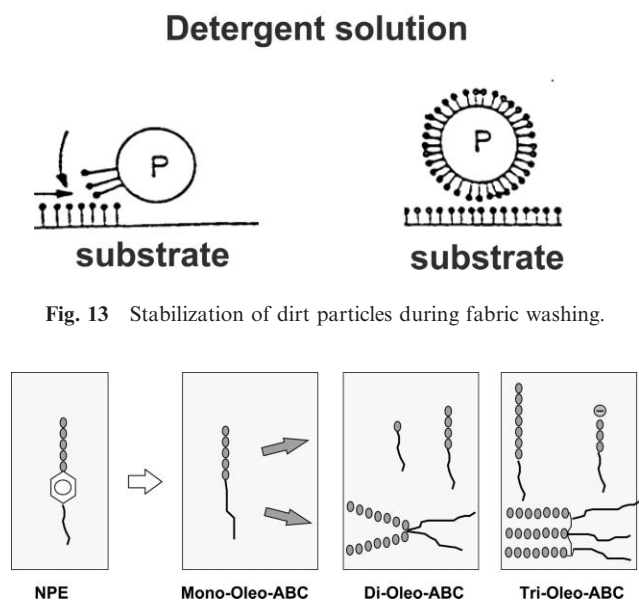


Fig. 14 Green dispersants.

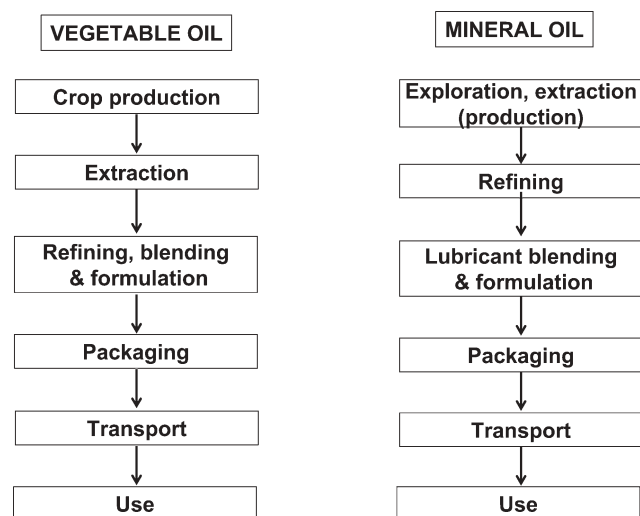


Fig. 15 Life-cycle of chainsaw bar oils made from mineral or vegetable oil.⁵⁰

or chain saw bar oils,⁵⁰ and in comparing vegetable oil vs. petrochemical-based radiation curing coating systems.⁵⁴ In the energy sector, it has been demonstrated that biodiesel reduces the health risks associated with petroleum diesel emissions and delivers significant benefits for the environment and human health. LCI has identified and quantified the advantages of biodiesel as a substitute for petroleum diesel. These advantages are substantial, especially in the area of energy security and control of greenhouse gases.⁵⁵

For comparison of the “green” route vs. the petrochemical route, all process steps from agricultural production, crude oil exploration (“cradle”) and processing leading up to chemical production (“factory gate”) are taken into account. The elementary flow in LCA considers material or energy entering the system being studied that has been drawn from the environment *without previous human transformation*, or material or energy leaving the system being studied that is released into the environment without subsequent human transformation.⁵² So far, LCA elementary flow for petrochemicals starts with exploration but does not include the geological processes for crude oil formation.

What lies ahead ?

Resource economy in crude extraction and crop production, fuel and energy savings in transportation and manufacturing will demand improved lubricants; emission control will continue to target the coating and printing industries to develop emission-free solvent recovery and incineration technologies, and/or emission-free water-based, full solids, radiation curing or powder coating systems. The agro industry will be challenged to continuously develop eco-safe plant and crop protection formulations based on ecologically benign green solvents and adjuvants. Governments and NGOs will continue to challenge the chemical industry to develop innovative and efficient mechanisms to find appropriate substitutes to substances perceived as dangerous or ecologically or hygienically questionable, like some phthalate-based plasticizers in certain applications, for example plastic toys and childcare articles. Alkylphenol ethoxylates or perfluorinated tensides are other examples.

Nicholas Stern’s recently published report on global warming and the economics of climate change⁵⁶ has again demonstrated the need for concerted action which produces a reduction in greenhouse gas emissions.

Marrying the principles of the sustainability concept with established cost, quality and performance standards will be the challenge for economics in general and for the chemical industry in particular. Steering research and development in such a direction will be a powerful concept for innovation.

Aliquat[®], Dekalin[®], Disponil[®] Edenol[®], Hydropalat[®], Petrofree[®], Tetralin[®], Texaphor[®], Texaprint[®] are trademarks of Cognis

References

- 1 C. Brandt, Sustainable Development and Responsible Care – Die chemische Industrie auf dem Weg in eine grüne Zukunft? *Chem. Unserer Zeit*, 2002, **36**(4), 224.
- 2 G. Zirnstein, Ökologie und Umwelt in der Geschichte, *Ökologie und Wirtschaftsforschung*, Metropolis, Marburg, 1994.
- 3 Marcus Portius Cato, *Origines – De Agricultura*.
- 4 H. J. Rieseberg, *Arbeit bis zum Untergang: die Geschichte der Naturzerstörung durch Arbeit*, Raben Verl. von Wittern, München, 1992; H. Metz, R. Pietsch, T. Polgár, F. Vacca and H. Weber, *Die Entwicklung des Waldes in Mitteleuropa*, Papiermacherschule Gernsbach, 2001, <http://www.computus.de/wald/wald.htm>.
- 5 H. J. Rieseberg, *Die verbrauchte Welt: Die Geschichte der Naturzerstörung und Thesen zur Befreiung vom Fortschritt*, Orig.-Ausg. FINIS., Frankfurt/M, Berlin, 1991; J. Diamond, *Collapse*, Penguin Books, London, 2006.
- 6 D. H. Meadows, D. L. Meadows, J. Randers and W. W. Behrens III, *The Limits to Growth*, Universe Books, New York, 1972.
- 7 R. L. Carson, *Silent Spring*, 40th anniversary edn, Houghton Mifflin, Boston, 2002.
- 8 W. Feldkirchen and S. Hilger, *Menschen und Marken*, ed. E. Primosch and W. Zengerling, Auftrag der Henkel KGaA, Düsseldorf, 2001.
- 9 H. C. von Carlowitz, *Sylvicultura oeconomica*, Reprint der Ausg. Leipzig, Braun, 1713/bearb. von K. Irmer, A. Kießling, TU Bergakad. Freiberg, Akad. Buchh., 2000.
- 10 *Our Common Future, The World Commission on Environment and Development*, ed. G. Brundtland, Oxford University Press, Oxford, 1987.
- 11 <http://nobelprize.org/peace/laureates/2004/press.html>.
- 12 R. Höfer, T. Roloff and A. Westfechtel, *Die Verwendung nachwachsender Rohstoffe in Lacken, Farben und Druckfarben*, Fachagentur Nachwachsende Rohstoffe, Gülzower Fachgespräche, Gülzow, 1999.
- 13 R. Höfer, Anwendungstechnische Aspekte der Verwendung natürlicher Öle und ihrer Derivate in der Polymer-Synthese und -Verarbeitung, in *Perspektiven nachwachsender Rohstoffe in der Chemie*, ed. H. Eierdanz, VCH, Weinheim, New York, Basel, Cambridge, Tokyo, 1996.
- 14 P. Renaud, Natural-Based Fatty Alcohols: Completely in Line with the Future? 6th World Surfactants Congress, CESIO, Berlin, 2004; (a) R. Gubler, Biodiesel, *CEH Marketing Research Report*, SRI Consulting, Nov. 2006.
- 15 www.solvsafe.org.
- 16 M. McCoy, *Glycerine surplus*, C&EN 7, February 6, 2006, www.CEN-online.org.
- 17 W. N. Nelson, *Green Solvents in Chemistry*, Oxford University Press, Oxford, New York, 2003; (a) R. Höfer, *Green Chemistry & Sustainability – a solution for the future of industrial applications*, 6th Green Chemistry conference, Barcelona, 2004.
- 18 C. Taranta and R. Buckpesch, Bayer CropScience, Plant protection composition and use thereof, *World Pat.* WO 2005/074685, 2005.
- 19 M. D. Donohue, J. L. Geiger, A. A. Kaimos and K. A. Nielsen, Reduction of volatile organic compound emissions during spray painting, in *Green Chemistry: Designing Chemistry for the Environment*, ed. P. T. Anastas and T. C. Williamson, American Chemical Society, Washington, vol. 626, p. 152, 1996.
- 20 *Ionic Liquids as Green Solvents*, ed. R. D. Rogers and K. R. Seddon, ACS Symposium Series 856, American Chemical Society, Washington, 2003; *Ionic Liquids in Synthesis*, ed. P. Wasserscheid and T. Welton/Wiley-VCH, Weinheim, 2003; T. J. S. Schubert, Ionische Flüssigkeiten – eine Querschnittstechnologie? *Nachr. Chem., Tech. Lab.*, 2005, **53**, 1222; J.-P. Mikkola, P. Virtanen and R. Sjöholm, Aliquat[®] 336 – a versatile and affordable cation source for an entirely new family of hydrophobic ionic liquids, *Green Chem.*, 2006, **8**, 250.
- 21 *Plasticizers in wood coating*, Technical Literature, Cognis.
- 22 R. Höfer, D. Feustel and M. Fies, Derivate natürlicher Öle als Rohstoffe für Lacke und Druckfarben, *Welt der Farben*, 1997, **11**.
- 23 S. Shah, S. Singhal, A. Khan and V. Shah, Advantages of emission-free coalescents using decorative paint systems, *Asia Pac. Coat. J.*, 2005, **18**(3), 31; <http://www.archer-rc.com/>.
- 24 P. R. Skelton and K. L. Turpin, Fatty methyl esters as solvent alternatives for emulsifiable concentrate formulations, in *Pesticide Formulations and Applications Systems*, ed. J. D. Nalewaja, G. R. Goss and R. S. Tann, American Society for Testing and Materials, West Conshohocken, vol. 18, 1998; P. R. Skelton, Pesticide Microemulsion Concentrate Formulations Utilizing Fatty Acid Methyl Esters as Solvent Alternatives, in *Pesticide Formulations and Applications Systems*, ed. J. D. Nalewaja, G. R. Goss and R. S.

- Tann, American Society for Testing and Materials, West Conshohocken, vol. 13, 1993.
- 25 R. Luther, Lubricants in the Environment, in Lubricants and Lubrication, *Ullmann's Encyclopedia of Industrial Chemistry*, Wiley-VCH, Weinheim, New York, Chichester, Brisbane, Singapore, Toronto, 2002.
 - 26 S. Boyde, Green lubricants. Environmental benefits and impacts of lubrication, *Green Chem.*, 2002, **4**, 293.
 - 27 K. Hill, Fats and Oils as Oleochemical Raw Materials, *J. Oleo. Sci.*, 2001, **50**(5), 433.
 - 28 R. Höfer, 6000 Jahre Sinn fürs Schöne – 6000 Jahre Lack, 50 Jahre VILF – mit Erfahrung in die Zukunft, *Schriftenreihe VILF-Vorträge*, vol. 7, p. 23, 2005; M. Kopplin, Ostasiatische Lackkunst, in *Museum für Lackkunst*, BASF Lacke + Farben AG, Münster, 1993.
 - 29 D. Saatweber, A 100 years' success story – Synthetic resins: from Laccain to High Performance Polymers, *ECJ Supplement 2*, November, 2003, www.coatings.de.
 - 30 H. Gnam and W. Sommer, *Die Lösungsmittel und Weichmachungsmittel*, Wissenschaftl. Verlagsges., Stuttgart, 1958.
 - 31 A. Schmidt, Systematik und Eigenschaften von Latices und kolloidalen Systemen, Polymerisation und Terpolymerisation in Emulsionen, in *Houben-Weyl, Methoden der Organischen Chemie*, 4. Aufl., Bd. E20/1, Stuttgart, New York, 1987; C. Baumann, D. Feustel, U. Held and R. Höfer, Stabilizing Systems for the Production of Polymer Dispersions, *Henkel-Referate*, 1997, **33**, 121; D. Distler, *Wäßrige Polymerdispersionen*, Wiley-VCH, Weinheim, New York, Chichester, Brisbane, Singapore, Toronto, 1999; K. Tauer, The role of emulsifiers in the kinetics and mechanisms of emulsion polymerisation, in *Surfactants in Polymers, Coatings, Inks and Adhesives, Applied Surfactant Series*, ed. D. R. Karsa, Blackwell, Oxford, CRC Press, Boca Raton, vol. 1, 2003.
 - 32 A. M. Fernandez, E. Evans, D. Feustel, M. Natale, R. Klima, B. Tuttle, C. Baumann and U. Held, New Green Nonionic Surfactants for Emulsion Polymerization, *Proceedings, 26th International Waterborne, High-Solids & Powder Coatings Symposium*, New Orleans, 1999; J. Bigorra, W. H. Breuer, S. Heldt and Ll. Llauro, Ethoxylated Natural Fatty Alcohol Derivatives, alternative Products to NPEO, *35 Jornadas Anuales del CED*, Barcelona, 2005; A. M. Fernandez, U. Held, A. Willing and W. H. Breuer, New green surfactants for emulsion polymerization, *Progr. Organic Coatings*, 2005, **53**, 246.
 - 33 R. Höfer, Tensioactivos como emulsionantes para la polimerización en emulsión, *Comunicaciones, XVI Jornadas del CED*, Barcelona, 1985; (a) BDI-Umweltpreis, 2005/2006, www.bdi-online.de.
 - 34 CEPAD, Nonylphenol – EU Risk Reduction Strategy, Regulation 793/93/EEC, Status Report of March 2003.
 - 35 EU Directive 2003/53/EG, 18 June 2003, EU Gazette, L178/24 (17 July 2003), <http://europa.eu.int/>.
 - 36 Regulation (EC) No. 648/2004 of the European Parliament and Council on Detergents, 31 March 2004, EU Gazette, L104/1 (8 April 2004), <http://europa.eu.int/>.
 - 37 B. A. Grisso, J. N. Vinci, B. J. Schober and D. C. Visger, Lubrizol, Polymeric dispersant viscosity modifier composition, *World Pat. WO 2005/116174*, 2005.
 - 38 C. C. Colyer and W. C. Gergel, Detergents/dispersants, in *Chemistry and technology of lubricants*, ed. R. M. Mortier and S. T. Orszulik, Blackie, Glasgow, London, VCH, New York, 1992.
 - 39 R. Swanell and F. Daniel, Effect of dispersants on oil biodegradation under simulated marine conditions, *Proceedings, International Oil Spill Conference, Seattle*, 1999, p. 169, <http://www.itopf.com>.
 - 40 R. Höfer, H.-G. Schulte, H. Frommelius and W. Greß, Getting the right mix – Using agents to disperse pigments in lacquers and paints, *Eur. Coat. J.*, 2004, **38**.
 - 41 E. J. W. Verwey and J. H. de Boer, Dilatancy, *Recl. Trav. Chim. Pays-Bas*, 1938, **57**, 383.
 - 42 C. Boller, W. Gündel and A. Kirsthaller, DEHYDAG, Schwebemittel für Pigmente in Lacken und Anstrichstoffen, *Ger. Pat. DE 940 929*, 1952.
 - 43 J. D. Schofield, Polymeric Dispersants, in *Handbook of Coatings Additives, Vol. 2*, ed. L. J. Calbo, Marcel Decker, NY, Basel, Hong Kong, 1992; K. Holmberg, Application of surfactants in paints, in *Surfactants in Polymers, Coatings, Inks and Adhesives, Applied Surfactant Series, Vol. 1*, ed. D. R. Karsa, Blackwell, Oxford, CRC Press, Boca Raton, 2003.
 - 44 G. H. Dekker, Water, the “solvent” of the future, *Double Liaison-Phys. Chem. Peint. Adhes.*, 2003, **531**, 44.
 - 45 M. J. Schwuger, Waschen und Reinigen als Trennprozeß, *Ber. Bunsen-Ges. Phys. Chem.*, 1979, **83**, 1193; G. Jacobi and A. Löhr, *Detergents and Textile Washing*, VCH, Weinheim, 1997.
 - 46 J. Schmitz, H. Frommelius, U. Pegelow, H.-G. Schulte and R. Höfer, A new concept for dispersing agents in aqueous coatings, *Progr. Org. Coatings*, 1999, **35**, 191; R. Höfer, H.-G. Schulte, C. Galopin and G. Félix, Additifs pour la synthèse et la formulation des peintures à l'eau, *Double Liaison-Phys. Chem. Peint. Adhes.*, 2003, **531**, 29.
 - 47 E. Beckman, Sustainability and solvents : Can we have both? in *Book of Abstracts, DECHEMA Symposium, Green Solvents For Processes, Lake Constance*, ed. B. Feißt, DECHEMA, Hrsg., Frankfurt, 2006; E. Beckmann, private communication.
 - 48 P. T. Anastas and J. C. Warner, *Green Chemistry: Theory and Practice*, Oxford University Press, New York, 1998.
 - 49 S. Hellweg, U. Fischer, M. Scheringer and K. Hungerbühler, Environmental assessment of chemicals: methods and application to a case study of organic solvents, *Green Chem.*, 2004, **6**, 418.
 - 50 P. Wightman, R. Eavis, S. Batchelor, K. Walker, R. Bennett, P. Carruthers and R. Tranter, Comparison of rapeseed and mineral oils using Life-Cycle Assessment and Cost-Benefit Analysis, *Ol. Corps Gras, Lipides*, 1999, **6**, 384.
 - 51 K. Hungerbühler and C. Capello, What is a green solvent? in *Book of Abstracts, DECHEMA Symposium, Green Solvents For Processes, Lake Constance*, ed. B. Feißt, DECHEMA, Hrsg., Frankfurt, 2006; K. Hungerbühler, private communication.
 - 52 ISO 14044, 1st edn 2006.
 - 53 F. Hirsinger, Oleochemicals and the Environment, in *Oleochemical Manufacture and Application*, ed. F. Gunstone and R. J. Hamilton, Sheffield Academic Press 300, 2001; M. Stalmans, et al., European Life-Cycle Inventory for Detergent Surfactants Production, *Tenside, Surfactants Deterg.*, 1995, **32**, 84; H.-J. Klüppel, F. Hirsinger, J. Knaut and K.-P. Schick, Ökobilanz von Waschmitteln – Perspektiven und Grenzen, *Henkel-Referate*, 1994, **30**, 49.
 - 54 A. Diehlmann and G. Kreisel, Ökologische Bilanz von UV-härtenden Lacken auf Leinölbasis, *Fabre + Lack*, 2000, **106**, 101.
 - 55 World Energy, <http://www.worldenergy.net/product/emissions.asp>, *Biodiesel Emissions – Life Cycle Inventory of Biodiesel and Petroleum Diesel for Use in an Urban Bus*.
 - 56 N. Stern, Stern Review on the economics of climate change, HM Treasury, London, UK, http://www.hm-treasury.gov.uk/independent_reviews/stern_review_economics_climate_change/stern_review_report.cfm.

Conversion of carbon dioxide and olefins into cyclic carbonates in water

Nicolas Eghbali and Chao-Jun Li*

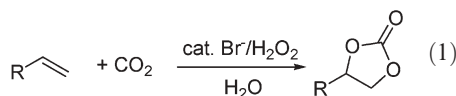
Received 27th October 2006, Accepted 12th December 2006

First published as an Advance Article on the web 21st December 2006

DOI: 10.1039/b615612f

In this manuscript, we have developed a highly efficient method to convert alkenes and CO₂ into cyclic carbonates directly in water by using *N*-bromosuccinimide (NBS) together with 1,8-diazabicyclo[5.4.0]undec-7-ene (DBU) in water, or by using a catalytic amount of bromide ion together with aqueous H₂O₂.

The increased environmental concern of the elevated CO₂ level in the atmosphere calls for innovative means to sequester CO₂ and to utilize it as a raw material to generate chemicals and materials.¹ For the latter, a number of chemical processes have been developed to incorporate CO₂ into organic chemicals and materials² such as carbonates,³ polycarbonates,⁴ and lactones or carboxylic acids.⁵ In this context, the reaction of carbon dioxide with epoxides to form cyclic carbonates⁶ and polycarbonates has seen important development due to their many applications and properties.^{3,7} Polycarbonates are, for example, versatile biodegradable polymers, which can be produced readily from cyclic carbonates.⁷ Although quite efficient, such a reaction usually requires the initial synthesis of an epoxide; an additional step that sometimes involves expensive or toxic reagents and requires chemical separations.⁸ A simpler and even cheaper approach would be the direct synthesis of cyclic carbonates starting from olefins instead of the epoxides. Although such a three-component coupling, also called oxidative-carboxylation of olefins, has been known at least since 1962,⁹ it has not, however, received much attention and only a few reports are available in the literature.¹⁰ Furthermore, low yield, expensive heavy metal oxidizing reagents, and numerous oxidation by-products were often the major problems.¹¹ Herein, we report an efficient direct conversion of alkenes and CO₂ into cyclic carbonates with hydrogen peroxide catalyzed by Br⁻ in water (eqn (1))



The concerns of air-pollution due to the extensive use of volatile organic solvents has led to great interest in searching for novel chemical processes in environmentally friendly solvents¹² such as water,¹³ supercritical CO₂,¹⁴ ionic liquids,¹⁵ and “switchable” solvents.¹⁶ In an attempt to overcome all the shortcomings associated with the previous methods for converting alkenes and CO₂ into cyclic carbonates, we envisioned the utilization of bromohydrin intermediates coupled with a “CO₂ activator” such as an organic base, 1,8-diazabicyclo[5.4.0]undec-7-ene (DBU), in water as a simple, cheap, efficient, and metal-free method. As a preliminary testing of the concept, the stoichiometric conversion of terminal alkenes into alkene carbonates was examined using

N-bromosuccinimide (NBS) together with DBU in water. Results are presented in Table 1. With styrene **1a**, the reaction proceeded excellently, affording a mixture of styrene carbonate **1b** (~89%) and the corresponding bromohydrin **1c** (~10%) after 3 h at 60 °C. No starting material was detected at the end of the reaction. The use of excess DBU was necessary to deprotonate the weakly acidic alcohol and to neutralize hydrobromic acid generated during the reaction. When simple aliphatic olefins such as 1-hexene **6a** and 1-octene **7a** were used, the reaction also proceeded smoothly and efficiently to afford the corresponding cyclic carbonates **6b** and **7b** (Table 1, entries 6, 7).

Following the success of the stoichiometric reaction, a transition-metal free catalytic system was investigated in water. We reasoned that the bromide ion could be readily oxidized to bromine or hypobromous acid, a reagent known to react with olefins in water to form the bromohydrin.¹⁷ Thus, only a catalytic amount of NBS will be needed for the reaction. After the formation of the bromohydrin intermediate, and its subsequent reaction with carbon dioxide, the bromide ions are regenerated and water becomes the only byproduct of the reaction. Inexpensive oxidants, such as 30% aqueous solution of hydrogen peroxide and sodium persulfate, were then examined.

Subsequently, styrene (**1a**) was reacted with 10 mol% of NBS in aqueous hydrogen peroxide. Although the reaction was successful, the yield remained low, most likely due to the high reactivity of NBS towards H₂O₂. Other sources of bromide ion were therefore tested for this transformation. Tetrabutylammonium bromide

Table 1 Conversion of terminal alkenes to alkenecarbonate

Entry	Olefin(R)		Reaction time/h	NMR yield (%) ^d	Product
1 ^b	Ph	1a	3	89 (98)	1b
2 ^b	4-MePh	2a	3	91 (98)	2b
3 ^b	4-SO ₃ Ph	3a	6	95 (100)	3b
4 ^b	PhCH ₂	4a	4	61 (98)	4b
5 ^b	3-MeOPhCH ₂	5a	4	45 (80)	5b
6 ^c	CH ₃ (CH ₂) ₃	6a	5	85 (100)	6b
7 ^c	CH ₃ (CH ₂) ₅	7a	5	63 (78)	7b
8 ^d	H	8a	4	30	8b

^a Based on the olefin; the number in brackets refers to the conversion. ^b Reaction conditions: 1.5 mmol of olefin, 1.5 mmol of NBS, 3 mmol of DBU, 1 mL of water, under a CO₂ pressure of 250–300 psi, 60 °C. ^c 1 mmol of olefin was used and the temperature was kept at 42 °C. ^d Reaction conditions: 40 psi of ethylene, 2.5 mmol of NBS, 5 mmol of KHCO₃, 2 mL of water, under a CO₂ pressure of 350 psi, 60 °C. Yield based on the amount of NBS used.

Department of Chemistry, McGill University, 801 Sherbrooke Street West, Montreal, Quebec, H3A 2K6, Canada. E-mail: cj.li@mcgill.ca

Table 2 Effect of the organic base on the yield of the reaction

Entry ^a	Amine base	NMR yield (%)
1	DBU	17 (20)
2	DMAP	9 (10)
3	Hünig's base	7.5 (10)
4	Triethylamine	>1 (5)
5	1-Methylimidazole	>1 (5)
6	Pyridine	NR
7	<i>N,N,N',N',N''</i> -Pentamethyl-diethylene triamine	NR
8	<i>N</i> -Methyl diphenylamine	NR
9	DABCO	NR
10	<i>N,N</i> -Dimethylaniline	NR
11	<i>N,N,N',N'</i> -Tetramethyldiamine methane	NR

^a All reactions were performed with 3 mmol of styrene (0.2 mL, 1 equiv.), 9 mmol of H₂O₂ (1 mL, 3 equiv.), 0.7 mmol of Bu₄NBr (250 mg, 0.25 equiv.) and 1 mmol of organic base (0.3 equiv.), under a CO₂ pressure of 250–300 psi, 2 h reaction time. The temperature controller was set at 42 °C.

(TBAB) and sodium bromide were both found to be effective. A clean conversion was achieved, leading (in the case of styrene **1a**) to a mixture of **1a** (12%), styrene bromohydrin **1c** (8%) and the desired styrene carbonate **1b** (70%).

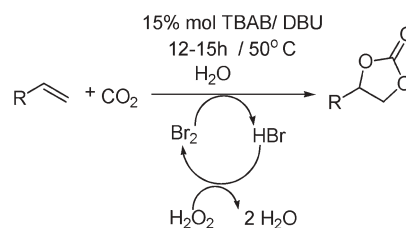
To determine the effect of the organic base, other amines were tested. A quick screening of various bases was carried out by reacting for only 2 h. Results are presented in Table 2. DBU, DMAP and Hünig's base were found to be the most effective for the catalytic reaction.

Other alkenes were then reacted with CO₂ under the optimized conditions (Table 3) (Scheme 1). The water soluble sodium salt of 4-styrene sulfonic acid **3a** gave an even better yield of the desired cyclic carbonates (Table 3, entry 5), although the separation proved to be challenging due to the solubility of the product. Simple alkenes such as 1-hexene **6a** and 1-octene **7a** were also effective under the catalytic conditions (Table 3, entries 6, 7). The ratio of reagents, particularly Br⁻/H₂O₂, was found to be important for the reaction because bromide ion can catalyze the unwanted and non-productive decomposition of hydrogen peroxide to generate O₂ and water.¹⁸ An aqueous solution of sodium persulfate was also effective as the oxidant; however, a lower conversion (*ca.* 14%) from styrene **1a** to styrene carbonate **1b** was observed with a large amount of unreacted starting material being recovered.

Table 3 Conversion of terminal alkenes to alkenecarbonate

Entry	Olefin (R)	Bromide catalyst (equivalent)	Reaction time/h	NMR yield (%) ^a
1 ^b	Ph	1a NBS	15	26 (36) 1b
2 ^b	Ph	1a NaBr	15	65 (80) 1b
3 ^b	Ph	1a TBAB	15	70 (89) 1b
4 ^b	4-MePh	2a TBAB	15	72 (90) 2b
5 ^b	4-SO ₃ Ph	3a TBAB	15	89 (98) 3b
6 ^c	CH ₃ (CH ₂) ₃	6a TBAB	20	47 (72) 6b
7 ^c	CH ₃ (CH ₂) ₅	7a TBAB	20	27 (78) 7b

^a Based on the olefin; the number in brackets refers to the conversion. ^b Reactions conditions: 1.5 mmol of olefin, 0.15 mmol of NBS, 0.2 mmol of DBU, 1 mL of H₂O₂, under a CO₂ pressure of 250–300 psi, 45–55 °C. ^c 1 mmol of olefin was used and the temperature was kept at 40 °C.

**Scheme 1** Bromine-catalyzed direct conversion of alkenes to cyclic carbonate with H₂O₂ in water.

In summary, a simple, direct, and metal-free method was developed to convert CO₂ into cyclic carbonates with alkenes in water.¹⁹ Using *N*-bromosuccinimide (NBS) together with DBU in water, alkenes were converted into cyclic carbonates nearly quantitatively. Cyclic carbonates were also formed efficiently by using a catalytic amount of bromide ion together with aqueous H₂O₂. The scope and applications of this method are under investigation.

Experimental

¹H NMR spectra were recorded at 300 MHz and ¹³C NMR spectra were recorded at 75 MHz. Flash chromatography was performed using SILICYCLE 40–63 μm silica gel, and the column was usually eluted with a 1 : 5 ethyl acetate–hexane mixture (25 to 50%). All the reagents were purchased from Aldrich Chemical Co. and were used without further purification.

Typical procedure for the stoichiometric conversion of alkenes to alkene carbonates using NBS and DBU

In a vial containing a stir bar, NBS (266 mg, 1.5 mmol) was mixed with 1 mL of water. The olefin (1.5 mmol) was added to the mixture followed immediately by the addition of DBU (0.35 mL, 2.4 mmol). The reaction mixture was stirred and the vial placed in a stainless steel autoclave (Parr reactor). The reactor was pressurized with CO₂ gas at an overall pressure of 300/350 psi. The temperature was maintained at 45 or 60 °C (according to the olefin) using a Parr temperature controller. After 3–6 h reaction time, the reactor was cooled down to room temperature and depressurized. Ethyl acetate (1 mL) was used to extract any organic material. After purification by flash chromatography (eluant 1 : 5 ethyl acetate in hexane), the product was characterized by ¹H, ¹³C NMR and GCMS.

Styrene carbonate:²⁰

Isolated yield: 81%. ¹H NMR (CDCl₃, 300 MHz, ppm): δ 4.26 (t, 1H, *J* = 7.26 Hz), 4.71 (t, 1H, *J* = 8.42 Hz), 5.59 (t, 1H, *J* = 8.07), 7.34 (m, 5H); ¹³C NMR (CDCl₃, 75 MHz, ppm): δ 71.1, 77.9, 125.8, 129.1, 129.6, 135.7, 154.8.

4-Methyl styrene carbonate:²¹

Purification was achieved by preparative TLC using toluene as eluant. Isolated yield: 83%. ¹H NMR (CDCl₃, 300 MHz, ppm): δ 2.36 (s, 3H), 4.32 (t, 1H, *J* = 8.1 Hz), 4.75 (t, 1H, *J* = 8.4 Hz), 5.62 (t, 1H, *J* = 7.95 Hz), 7.23 (s, 4H). ¹³C NMR (CDCl₃, 75 MHz, ppm): δ 29.4, 71.4, 78.3, 126.2, 130.1, 132.9, 140.1, 155.1.

4-Styrene carbonate sulfonic acid sodium salt

Although the reaction proceeded well with DBU, the use of KHCO_3 or even NaHCO_3 was preferable. Isolated as a white solid in 68% yield. ^1H NMR (D_2O , 400 MHz, ppm): δ 4.39 (t, 1H, J = 8.4 Hz), 4.86 (t, 1H, J = 8.6 Hz), 5.86 (t, 1H, J = 8.2 Hz), 7.61 (q, 4H, J = 8 Hz). ^{13}C NMR (D_2O , 100 MHz, ppm): δ 71.6, 78.2, 126.2, 127.0, 138.8, 144.3, 156.9. HRMS (FTMS) $\text{C}_9\text{H}_7\text{O}_6\text{S}$ calculated: 242.9963; found: 242.9966.

Allyl benzene carbonate

Purification was achieved by flash chromatography using first 1 : 5 ethyl acetate in hexane, then THF or 1 : 1 ethyl acetate–hexane mixture. Isolated yield: 52%. ^1H NMR (CDCl_3 , 300 MHz, ppm): δ 3.07 (dd, 2H, J = 14.1, 13.8 Hz), 4.168 (t, 1H, J = 6.8 Hz), 4.44 (t, 1H, J = 8.1 Hz), 4.93 (m, 1H), 7.30 (m, 5H). ^{13}C NMR (CDCl_3 , 75 MHz, ppm): δ 39.8, 68.7, 77.0, 127.8, 129.2, 129.5, 134.1, 154.9.

Allyl anisole carbonate

Isolated yield: 41%. ^1H NMR (CDCl_3 , 300 MHz, ppm): δ 3.01 (m, 2H), 3.79 (s, 3H), 4.15 (t, 1H, J = 7.8 Hz), 4.42 (t, 1H, J = 8 Hz), 4.89 (t, 1H, J = 6.8 Hz), 7.00 (dd, 4H). ^{13}C NMR (CDCl_3 , 75 MHz, ppm): δ 27.9, 55.4, 71.1, 78.1, 114.6, 127.8, 129.5, 154.9, 160.7. HRMS $\text{C}_{11}\text{H}_{12}\text{O}_4$ calculated: 208.0736 ; found 208.0737.

1-Hexene carbonate:²⁰

Isolated yield: 79%. ^1H NMR (CDCl_3 , 300 MHz, ppm): δ 0.89 (t, 3H, J = 6.6 Hz), 1.31 (m, 4H), 1.67 (m, 2H), 4.01 (t, 1H, J = 7.1), 4.49 (t, 1H, J = 7.7), 4.65 (m, 1H); ^{13}C NMR (CDCl_3 , 75 MHz, ppm): δ 13.7, 22.15, 26.3, 33.4, 69.3, 77.0, 155.0.

1-Octene carbonate

Purification was achieved by flash chromatography using 1 : 1 ethyl acetate in hexane. Isolated yield: 53%. ^1H NMR (CDCl_3 , 300 MHz, ppm): δ 0.88 (t, 3H, J = 6.5 Hz), 1.26 (m, 8H), 1.72 (m, 2H), 4.01 (t, 1H, J = 6.9), 4.50 (t, 1H, J = 7.2), 4.69 (m, 1H); ^{13}C NMR (CDCl_3 , 75 MHz, ppm): δ 14.0, 22.50, 24.32, 28.80, 31.50, 38.90, 69.40, 77.03, 155.10.

Ethylene carbonate

Isolated yield: 30%. ^1H NMR (CDCl_3 , 300 MHz, ppm): δ 4.51 (s, 4H); ^{13}C NMR (CDCl_3 , 75 MHz, ppm): δ 64.7. GCMS ($\text{C}_3\text{H}_4\text{O}_3$) found: 88.1.

Typical procedure for the conversion of alkenes to alkene carbonates with 30% hydrogen peroxide

In a vial containing a stir bar, TBAB (50 mg, 0.15 mmol) was introduced and dissolved into 1 mL of 30% H_2O_2 (9 mmol, 6 equiv). The olefin (1.5 mmol) was added to the mixture followed immediately by DBU (0.03 mL, 0.2 mmol). The vial was placed in a stainless steel autoclave (Parr reactor) which was pressurized with CO_2 gas at an overall pressure of 350 psi. The reactor was heated at 42 °C or 50 °C using a Parr temperature controller. After reacting for an average of 15 h, the reactor was cooled down to room temperature and depressurized. Ethyl acetate (0.3 mL) was used to extract any organic material.

Acknowledgements

We thank the Canada Research Chair (Tier I) program (to C.J.L.), the CFI, and NSERC for support of our research.

Notes and references

- Green Chemistry: Theory and Practice*, ed. P. T. Anastas and J. C. Warner, Oxford University Press, 1998; I. Omae, *Catal. Today*, 2006, **115**, 33; R. Zevenhoven, S. Eloneva and S. Teir, *Catal. Today*, 2006, **115**, 73.
- A. Behr, *Chem.-Ing.-Tech.*, 1985, **10**, 16.
- A. G. Shaikh and S. Sivaram, *Chem. Rev.*, 1996, **96**, 951.
- For a review, see: H. Arakawa, M. Aresta, J. N. Armor, M. A. Barteau, E. J. Beckman, A. T. Bell, J. E. Bercaw, C. Creutz, E. Dinjus, D. A. Dixon, K. Domen, D. L. DuBois, J. Eckert, E. Fujita, D. H. Gibson, W. A. Goddard, D. W. Goodman, J. Keller, G. J. Kubas, H. H. Kung, J. E. Lyons, L. E. Manzer, T. J. Marks, K. Morokuma, K. M. Nicholas, R. Periana, L. Que, J. Rostrup-Nielsen, W. M. H. Sachtler, L. D. Schmidt, A. Sen, G. A. Somorjai, P. C. Stair, B. R. Stults and W. Tumas, *Chem. Rev.*, 2001, **101**, 953. See also: H. Sugimoto and S. Inoue, *J. Polym. Sci., Part A: Polym. Chem.*, 2004, **42**, 5561.
- A. Behr, *Angew. Chem., Int. Ed. Engl.*, 1988, **27**, 661.
- D. J. Darensbourg and M. W. Holtcamp, *Coord. Chem. Rev.*, 1996, **153**, 155; M. Yoshida and M. Ihara, *Chem.-Eur. J.*, 2004, **10**, 2886.
- J. H. Clements, *Ind. Eng. Chem. Res.*, 2003, **42**, 663.
- As an example, the synthesis of tigliane-daphnane analogs reported by Wender was based on a sequence of epoxidation and carbocyclization: P. A. Wender and F. E. McDonald, *Tetrahedron Lett.*, 1990, **31**, 3691.
- J. A. Verdol, *U.S. Pat.* 3 205 305, 1962.
- S. E. Jacobson, *U.S. Pat.* 4 483 994, 1984; M. Aresta and E. Quaranta, *J. Mol. Catal. A: Chem.*, 1987, **41**, 355; M. Aresta, A. Dibenedetto and I. Tommasi, *Appl. Organomet. Chem.*, 2000, **14**, 799; M. Aresta and A. Dibenedetto, *J. Mol. Catal. A: Chem.*, 2002, **182–183**, 399; R. Srivastava, D. Srinivas and P. Ratnasamy, *Catal. Lett.*, 2003, **91**, 133; J. Sun, S. I. Fujika, B. M. Bhanage and M. Arai, *Catal. Commun.*, 2004, **5**, 83; J. Sun, S. I. Fujika, B. M. Bhanage and M. Arai, *Catal. Today*, 2004, **93–95**, 383; J. Sun, S. I. Fujika, F. Zhao, M. Hasegawa and M. Arai, *J. Catal.*, 2005, **230**, 398; J. Sun, S. I. Fujika and M. Arai, *J. Organomet. Chem.*, 2005, **690**, 3490.
- C. Fumagalli, G. Caprara and P. Roffia, *U.S. Pat.* 4 009 183, 1977; S. E. Jacobson, *U.S. Pat.* 4 325 874, 1982; J. L. Kao, G. A. Wheaton, H. Shalit and M. N. Sheng, *U.S. Pat.* 4 247 465, 1981; G. A. Wheaton, J. L. Kao and M. N. Sheng, *U.S. Pat.* 4 224 223, 1980.
- D. Adam, *Nature*, 2000, **407**, 938; R. Sheldon, *Green Chem.*, 2005, **7**, 267.
- For a recent reviews, C. J. Li, *Chem. Rev.*, 2005, **105**, 3095; U. M. Lindstrom, *Chem. Rev.*, 2002, **102**, 2751; T. H. Chan, L. Li, Y. Yang and W. Lu, *Clean Solvents: Alternative Media for Chemical Reactions and Processing*, ACS Symposium Series, 819, 2002, p. 166; D. Sinou, *Adv. Synth. Catal.*, 2002, **334**, 221; H. Yorimitsu, H. Shinokubo and K. Oshima, *Synlett*, 2002, **5**, 674.
- Chemical Synthesis Using Supercritical Fluids*, ed. P. G. Jessop and W. Leitner, Wiley-VCH, Weinheim, 1999; W. Leitner, *Acc. Chem. Res.*, 2002, **35**, 746; H. F. Jiang, *Curr. Org. Chem.*, 2005, **9**, 289; S. Campestrini and U. Tonellato, *Curr. Org. Chem.*, 2005, **9**, 31.
- Representative literature reviews: *Ionic liquids in Synthesis*, ed. P. Wasserscheid and T. Welton, Wiley-VCH, Weinheim, 2002; T. Welton, *Chem. Rev.*, 1999, **99**, 2071; M. J. Earle and K. R. Seddon, *Pure Appl. Chem.*, 2000, **72**, 1391; T. Welton, *Coord. Chem. Rev.*, 2004, **248**, 2459; T. Welton and P. J. Smith, *Adv. Organomet. Chem.*, 2004, **51**, 251; R. A. Sheldon, R. M. Lau, M. J. Sordedra, F. van Rantwijk and K. R. Seddon, *Green Chem.*, 2002, **4**, 147; J. Muzart, *Adv. Synth. Catal.*, 2006, **348**, 275; S. Pandey, *Anal. Chim. Acta*, 2006, **556**, 38; H. Zhao, S. Xia and P. Ma, *J. Chem. Technol. Biotechnol.*, 2005, **80**, 1089.
- P. G. Jessop, D. J. Heldebrant, X. Li, C. A. Eckert and C. L. Liotta, *Nature*, 2005, **436**, 1102.
- March's Advanced Organic Chemistry*, ed. M. B. Smith and J. March, Wiley-Interscience, New York, 2001.
- W. C. Bray and R. Livingston, *J. Am. Chem. Soc.*, 1923, **45**, 1251.
- N. Eghbali and C. J. Li, *US Pat.* applied, 2006.
- For a recent characterization, see: J.-L. Jiang, G. Feixue, R. Hua and X. Qiu, *J. Org. Chem.*, 2005, **70**, 381–388.
- T. Barlow; and A. Dipple, *Chem. Res. Toxicol.*, 1998, **11**, 44–53.

HRMAS NMR analysis in neat ionic liquids: a powerful tool to investigate complex organic molecules and monitor chemical reactions†

A. Rencurosi,^a L. Lay,^a G. Russo,^a D. Proserpi,^b L. Poletti^{*a} and E. Caneva^{*c}

Received 23rd October 2006, Accepted 19th December 2006

First published as an Advance Article on the web 2nd January 2007

DOI: 10.1039/b615392e

The high resolution magic angle spinning (HRMAS) NMR technique proved to be an effective tool for the analysis of organic solutes and for the observation of an organic reaction in neat ionic liquids.

The growing use of ionic liquids (ILs) as reaction media in organic chemistry reveals a strong interest in this new class of solvents.¹ Notably, they provide a markedly ionic microenvironment for solutes and co-solvents, often influencing the conformation and coordination events,² possibly leading to unpredictable reaction outcomes.³

The unique properties of ILs urgently call for efficient and general analytical methods for the characterization of complex organic molecules dissolved in neat ILs, as well as for the direct monitoring of reactions in these media. Some successful investigations employing mass spectrometry and infrared spectroscopy have already appeared in the literature.⁴ On the other hand, the use of NMR for these purposes is still underemployed. Recent papers describing the use of NMR spectroscopy for the analysis of organic solutes in neat ILs^{2b,5} show that various problems are encountered, such as low resolution of the spectra, due to the high viscosity of ILs;^{5a} the need for deuterated substrates,⁶ with the related influence on chemical shifts;⁷ the problems in assessing the matching routine^{5a} and, notably, difficulty in the correct choice of the chemical shift reference.⁸ The intensity difference of the peaks between neat ILs and solutes is an additional problem, and solvent signal filtering based on the T1 relaxation time values becomes feasible only when solvent and solute show different T1,^{5a} while DOSY techniques require analytes with a molecular weight very different from that of the IL.⁹

These data suggest that there is a strong demand for a general method allowing the effective study of solutes in ILs especially in the case of complex molecules.

We thought that the high resolution magic angle spinning (HRMAS) NMR technique, used successfully for the characterisation of gels and semisolid matrices,¹⁰ could be a powerful tool to overcome the aforementioned problems. Although a paper concerning the use HRMAS spectroscopy for the ¹H-¹³C analysis of ILs immobilized on silica gel has very recently appeared in the

literature,^{5c} the direct investigation of molecules displaying complex spectra and dissolved in neat ILs is still unprecedented.

In this work we set up a routine use of HRMAS NMR as a powerful tool for the characterization of complex organic analytes dissolved in neat ILs through the systematic study of the resolution of their spectra. Even more interestingly, we have shown that this method is easily applied to the direct observation of an organic reaction performed in neat IL.

For this study, three imidazolium-based ILs differing in their side-chain length were chosen, namely 1-butyl-3-methylimidazolium hexafluorophosphate **1**, 1-hexyl-3-methylimidazolium hexafluorophosphate **2** and 1-octyl-3-methylimidazolium hexafluorophosphate **3**. These solvents are analogues in their chemical structure but differ in their viscosity,¹¹ a property strictly related to the resolution of NMR spectra.

A preliminary investigation of the spectra of neat ILs **1–3** revealed that spectra recorded in a 5 mm NMR tube with a coaxial capillary for the external lock (d6 acetone) exhibit low resolution and require further adjustment in chemical shift referencing against the standard,⁸ in order to compensate for the high magnetic susceptibility of ILs.¹² The signals of ¹H HRMAS spectra, however, show chemical shifts which are highly consistent with the spectra of **1–3** dissolved in d6-acetone and a gain in resolution that can be appreciably evidenced with more viscous ILs (see ESI†).

We subsequently performed the same experiments with two organic molecules (compounds **4** and **5**, Fig. 1) dissolved in neat ILs **1–3**.

p-Methoxy benzyl acetate **4** exhibited the resolution data listed in Table 1, reported in terms of full width at half maximum height (FWHM).

The signals of compound **4** observed through ¹H HRMAS NMR showed a remarkable gain in resolution (entries 4–6) as their FWHM was from 25% to 40% lower than that observed for the spectra recorded in a 5 mm tube (entries 1–3) and FWHM values of entries 4–5 were close to that measured in CDCl₃.

We chose methyl 2,3,4,6-tetra-*O*-benzyl- α -D-glucopyranoside **5** (Fig. 1) as the second compound, due to its complex pattern of signals and our interest in the direct observation of carbohydrates dissolved in ILs.¹³ The reference signal was the doublet at

^aDepartment of Organic and Industrial Chemistry, University of Milano, Via Venezian, 21 - 20133, Milano, Italy. E-mail: laura.poletti@unimi.it

^bC.N.R., Istituto di Scienze e Tecnologie Molecolari, via Golgi,

19-20133, Milano, Italy

^cCentro Interdipartimentale Grandi Apparecchiature (C.I.G.A.), Via

Golgi, 19-20133, Milano, Italy. E-mail: enrico.caneva@unimi.it

† Electronic supplementary information (ESI) available: Structures of ILs

1–3, experimental details, HRMAS spectra and spectra recorded in a

conventional probe. See DOI: 10.1039/b615392e

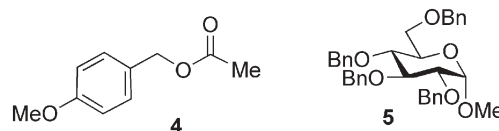


Fig. 1 Chemical structure of compounds **4** and **5**.

Table 1 FWHM of the ^1H NMR spectra of compounds **4** and **5**

Entry	IL	FWHM of compound 4 (CH_2 signal)/Hz	FWHM of compound 5 (benzylic H signal)/Hz
1 ^a	(a) 1	3.7	>11
2 ^a	2	4.1	>>11
3 ^a	3	6.1	>>11
4 ^b	(b) 1	2.8 ^c	4.7 ^d
5 ^b	2	2.5 ^c	8.5 ^d
6 ^b	3	4.0 ^c	9.0 ^d
7 ^e	(c)	1.6	2.3

^a Compounds **4** and **5** dissolved in neat ILs **1–3** ($c = 0.2$ M) in a 5 mm tube provided with a coaxial capillary filled with d_6 acetone.

^b Compounds **4** and **5** dissolved in neat ILs **1–3** ($c = 0.2$ M) in the HRMAS NMR probe. ^c 5 KHz MAS rotation of the HRMAS rotor. ^d 15 KHz MAS rotation of the HRMAS rotor. ^e Compounds **4** and **5** dissolved in CDCl_3 .

$\delta = 4.97$ ppm, $J = 11.0$ Hz in CDCl_3 (benzylic signal), since its position far from the other glucose peaks makes it optimal to monitor the resolution variation of the spectra.

Fig. 2 and entries 4–6 of Table 1 show the significant enhancement of the resolution obtained by the HRMAS technique for compound **5**, including the evaluation of the 11.0 Hz benzylic coupling constant even with the high viscosity of IL **3**. Fig. 2 also shows evidence for the effects on the chemical shifts caused by the magnetic susceptibility of ILs.^{8,12}

An additional experiment showed further evidence of the efficiency of ^1H HRMAS NMR spectroscopy applied to neat ILs. We recorded the spectra of **5** in neat IL **2** in a 5 mm tube provided with an external d_6 DMSO lock at increasing temperatures and compared them with the HRMAS spectrum recorded at 30 °C. A resolution of the spectrum equivalent to that obtained by the HRMAS NMR technique was achieved only at

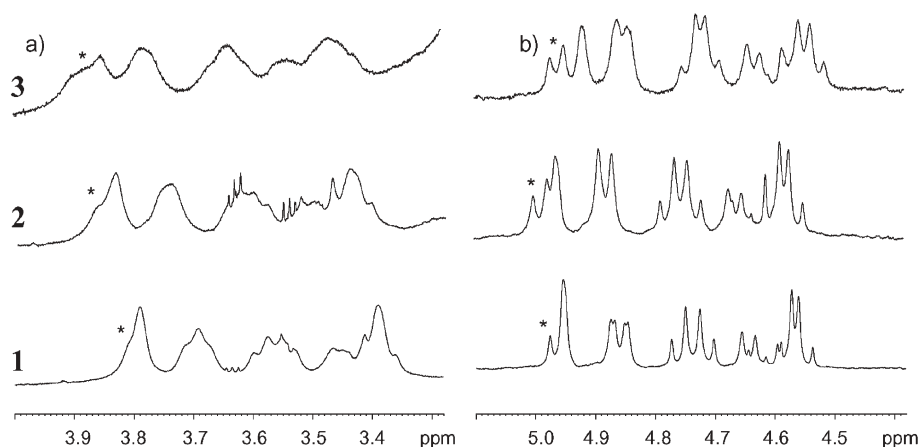


Fig. 2 Resolution behaviour of **5**, dissolved in neat ILs **1–3**, evaluated on benzylic H signal (asterisk). (a) Spectrum in a 5 mm NMR tube with an external lock; (b) spectrum with the HRMAS NMR technique.

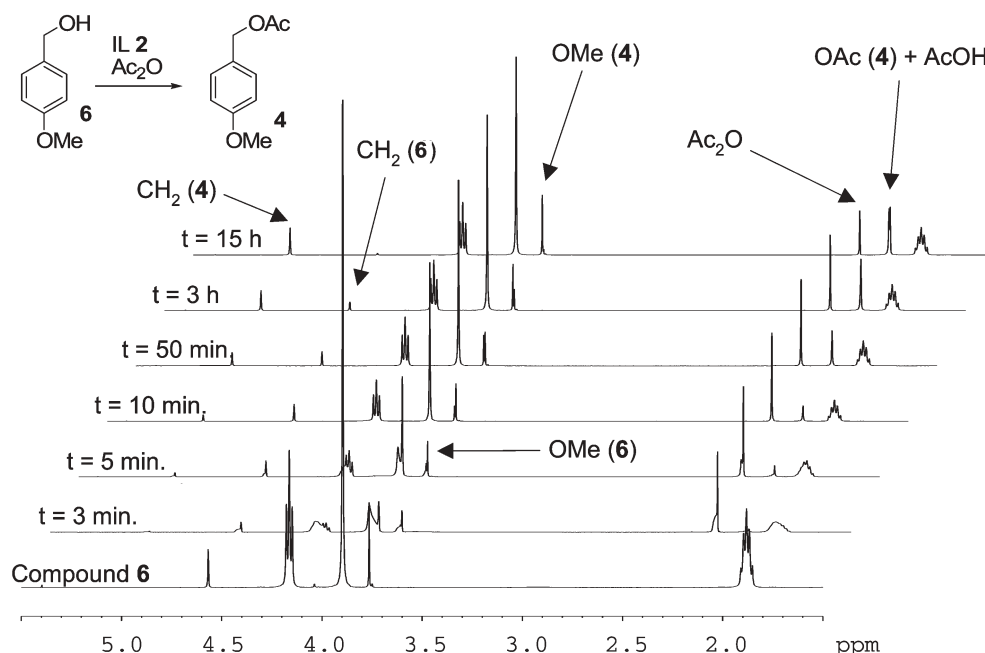


Fig. 3 Time-dependent ^1H HRMAS spectra of the acetylation of **6**.

temperatures over 60 °C, too high for heat-labile organic compounds (see ESI†).

A further challenge in the application of HRMAS spectroscopy to neat ILs was its use in the direct monitoring of a standard organic reaction. To investigate this aspect, we directly performed the acetylation of *p*-methoxybenzyl alcohol **6** in the HRMAS rotor and recorded ¹H HRMAS spectra at regular intervals of time.

The time-dependent intensity of the benzylic signals of compounds **6** and **4** ($\delta = 4.57$ and 5.02 ppm, respectively) can be clearly observed in Fig. 3, together with the concomitant progressive switch of the methyl ether signals ($\delta = 3.76$ ppm for compound **6** and 3.77 ppm for compound **4**) and the appearance of the acetyl signal of **4** ($\delta = 2.03$ ppm) and of acetic acid ($\delta = 2.02$ ppm) as the by-product of the reaction.

It should be noted that the spectra recorded within the first 10 min clearly revealed an initially heterogeneous solution, evidenced by the low resolution of the peaks. However, the rotation of the HRMAS rotor led to a completely homogeneous solution in a few minutes, and the reaction could be followed with optimal resolution until completion.

In conclusion, we have reported an unprecedented successful application of HRMAS NMR spectroscopy to observe complex organic compounds dissolved in neat ILs of different viscosity. Notably the HRMAS technique does not need high solute concentrations (0.2 M, equivalent to that used in common organic reactions) and does not require different molecular weight or relaxation time between the solute and the IL. It involves minimal use of deuterated solvents, leads to reliable chemical shift referencing and to high resolution even with highly viscous ILs.

More interestingly, HRMAS NMR proved to be an excellent tool for the direct observation of a standard organic reaction in neat ILs. This result has important potential applications in the study of reaction intermediates and of the interaction between solutes and solvents in ILs.

Acknowledgements

This work was supported by MIUR (prot. 2004039212) and CNR.

Notes and references

- 1 P. Wasserscheid and T. Welton, *Ionic Liquids in Synthesis*, VCH, Weinheim, 2002 and references therein.
- 2 A. Triolo, O. Russino, U. Keiderling and J. Kohlbrecher, *J. Phys. Chem. B*, 2006, **110**, 1513; R. Madeira Lau, M. Sorgedraeger, G. Carrea, F. Van Rantwijk, F. Secundo and R. Sheldon, *Green Chem.*, 2004, **6**, 483.
- 3 M. Earle, S. Katdare and K. Seddon, *Org. Lett.*, 2004, **6**, 707.
- 4 L. Cammarata, S. Kazarian, P. Salter and T. Welton, *Phys. Chem. Chem. Phys.*, 2001, **3**, 5192; P. Dyson, I. Khalaila, S. Luetzgen, J. McIndoe and D. Zhao, *Chem. Commun.*, 2004, 2204; P. Dyson, J. McIndoe and D. Zhao, *Chem. Commun.*, 2003, 508; G. Jackson and D. Duckworth, *Chem. Commun.*, 2004, 522; C. Tran, S. De Paoli Lacerda and D. Oliveira, *Appl. Spectrosc.*, 2003, **57**, 152.
- 5 R. Giernorth, D. Bankmann and N. Schlörer, *Green Chem.*, 2005, **7**, 279; I. Nicotera, C. Oliviero, W. Henderson, G. Appetecchi and S. Passerini, *J. Chem. Phys. B*, 2005, **109**, 22814; S. Brenna, T. Posset, J. Furrer and J. Blümel, *Chem.–Eur. J.*, 2006, **12**, 2880; D. Fort, R. Swatloski, P. Moyna, R. Rogers and G. Moyna, *Chem. Commun.*, 2006, 714; J.-S. Moulthrop, R. Swatloski, G. Moyna and R. Rogers, *Chem. Commun.*, 2005, 1557.
- 6 G. Owens, A. Durazo and M. Abu-Omar, *Chem.–Eur. J.*, 2002, **8**, 3053.
- 7 S. Lin, M. Ding, C. Chang and S. Lue, *Tetrahedron*, 2004, **60**, 9441.
- 8 R. Harris, E. Becker, S. Menezes, R. Goodfellow and P. Granger, *Pure Appl. Chem.*, 2001, **73**, 1795.
- 9 R. Giernorth and D. Bankmann, *Eur. J. Org. Chem.*, 2005, **21**, 4529.
- 10 W. Power and G. Webb, in *Annual Reports on NMR Spectroscopy*, Academic Press, 2003, vol. 51, pp. 261–295.
- 11 G. Jonathan, A. Visser, W. Reichert, H. Villauer, G. Broker and R. Rogers, *Green Chem.*, 2001, 156.
- 12 Marked differences in the chemical shifts were observed by recording the spectra of ILs in different conditions (see ESI† for conditions, spectra and further references).
- 13 A. Rencurosi, L. Lay, G. Russo, E. Caneva and L. Poletti, *J. Org. Chem.*, 2005, **70**, 7765; A. Rencurosi, L. Lay, G. Russo, E. Caneva and L. Poletti, *Carbohydr. Res.*, 2006, **341**, 903.

Recyclable copper-catalyst in aqueous media: *O*- and *N*-arylation reactions towards the benzofuroindole framework†

Mónica Carril, Raul SanMartin,* Esther Domínguez* and Imanol Tellitu

Received 29th September 2006, Accepted 19th December 2006

First published as an Advance Article on the web 2nd January 2007

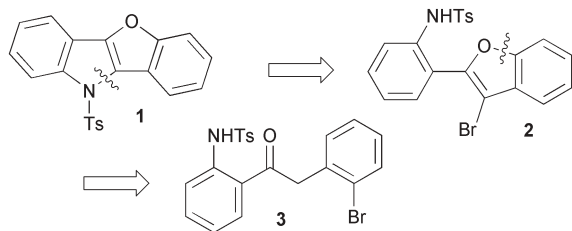
DOI: 10.1039/b614218d

The synthesis of the benzofuroindole skeleton using a recyclable copper-catalytic system in water solution is presented.

In recent years, molecules comprising the benzofuroindole framework of compound **1** as their basic skeleton (Scheme 1) have shown increasing utility as pharmaceuticals. As such, they have proved highly efficient in the treatment of sexual hormone disorders,¹ degenerative brain diseases¹ and different types of cancer due to their extensive antitumour activity.² In addition, they have also demonstrated their relevant role in the modulation of the potassium channels responsible for smooth muscle contraction. This ability renders this type of compounds highly useful for the treatment of irritable bowel syndrome, asthma, congestive heart failure and cerebral vascular diseases, among others.³

Frequently, the synthesis of such valuable compounds implies modifications performed on the non-substituted benzo[4,5]furo-[3,2, *b*]indole core by introduction of different functionalities.² However, the access to the tetracyclic skeleton, depicted in Scheme 1, is not always easily accomplished and it often requires the use of highly elaborated and non-commercial starting materials.^{1,3}

Given the aforementioned valuable properties of this family of compounds as pharmaceuticals, a simple, low cost and environmentally friendly route leading to this benzofuroindole framework would be of great interest for its application to industrial processes. In this context, the use of water as the most benign solvent to perform organic transformations is considered highly advantageous, not only due to its non-toxicity, non-flammability and low cost, but also because of the remarkable increase in chemoselectivity observed when using aqueous media compared to organic solvents.⁴



Scheme 1

Kimika Organikoa II Saila, Zientzia eta Teknologia Fakultatea, Euskal Herriko Unibertsitatea, P.O. Box 644, Bilbao, 48080, Spain.

E-mail: raul.sanmartin@ehu.es; Fax: +34 946012748;

Tel: +34 946015435

† Electronic supplementary information (ESI) available: Experimental procedures and NMR spectra for new compounds. See DOI: 10.1039/b614218d

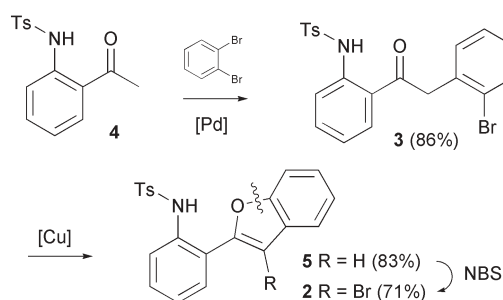
Thus, we envisaged a novel and highly appealing strategy for the construction of the benzofuroindole structure following the sequence depicted in Scheme 1, which consists of the initial formation of benzofuran derivative **2** from diarylethanone **3**, followed by a final intramolecular *N*-arylation step to render the benzofuran-fused indole ring in compound **1**, and employing water as the solvent for the key transformations. Furthermore, the proposed route notably differs from the previously reported ones in that it implies the synthesis of the benzofuran moiety, instead of introducing that heteroaromatic ring already formed as part of one of the starting materials.^{1,3}

First of all, we chose diarylethanone **3** as a precursor mainly because this compound already contains the heteroatoms present in the target molecule **1**, placed in the required positions (Scheme 1). In addition, compound **3** is easily accessible through a palladium-catalysed α -arylation of the acetophenone derivative **4** with 1,2-dibromobenzene, using a partially-aqueous protocol designed by our research group (Scheme 2).⁵

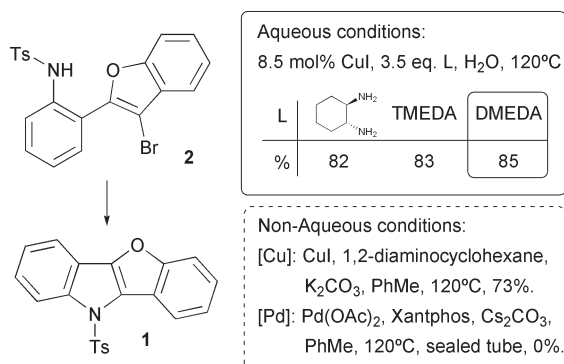
Subsequently, for the construction of the benzofuran ring from diarylethanone **3**, we decided to test our recently developed strategy for the synthesis of benzo[*b*]furans, based on a copper-catalysed intramolecular *O*-arylation performed in neat water solution.⁶ Thus, deoxybenzoin **3** was stirred in the presence of 8.5 mol% of CuI, 3.5 eq. of TMEDA, acting both as the ligand and as the base, and water at 120 °C, delivering the desired heterocycle in good yield (Scheme 2).⁷

Following with the projected route (Scheme 1), prior to the final intramolecular *N*-arylation process, the introduction of a bromine atom at the C-3 position of the benzofuran ring was required. Therefore, benzofuran **5** was treated with NBS, successfully furnishing brominated compound **2** in 71% yield (Scheme 2). The amount of NBS employed (1.05 eq.) and the temperature (0 °C) were critical for the selective monobromination of compound **5**.⁸

The last step of our synthetic proposal involved an intramolecular Goldberg-type reaction between sulfonamide and heteroaryl



Scheme 2



Scheme 3

halide moieties. This kind of transformation has traditionally been accomplished employing mainly copper-catalysis,⁹ although some examples of palladium-catalysed *N*-arylation of amides have also been reported.¹⁰ Nevertheless, such protocols require organic solvents to effect the reaction and, therefore, were not suitable for our purpose, *i.e.*, the design of a more sustainable process to access the valuable benzofuroindole framework.

In this context, we envisaged the extension of the “on-water” chemistry protocol to effect the final *N*-arylation reaction. Such a protocol involves stirring of the substrate with a neat water solution containing 8.5 mol% of CuI and a 1,2-diamine derivative, which not only coordinates to the copper, delivering so the active catalyst, but also acts as the required base for the process. If successful, it would prove that a scheduled use of such an environmentally friendly procedure can accomplish two different key steps of a sequence involving disparing functionalities and reacting centers. Fortunately, as shown in Scheme 3, when substrate **2** was submitted to the aforementioned reaction conditions, the intramolecular *N*-arylation reaction to render the target tetracyclic compound **1** was achieved in good yield.

Interestingly, although DMEDA proved slightly superior, the use of different 1,2-diamine derivatives resulted in hardly any variation in the obtained yields (Scheme 3). Indeed, the presented *N*-arylation reaction proceeded smoothly under identical reaction conditions as those employed for the synthesis of benzofuran **5**. Therefore, we decided to explore the reutilisation of the aqueous solution containing the CuI/TMEDA complex, initially used for the preparation of **5**, to effect the final *N*-arylation. Remarkably, such reutilisation was successfully achieved, and target compound **1** was delivered in 85% yield, thereby employing not only an identical protocol, but also the same aqueous medium (with the catalyst dissolved in it) to accomplish two different copper-catalysed transformations.

Furthermore, at this stage, we decided to compare the efficacy of our newly designed protocol for copper-catalysed *N*-arylation with other copper and palladium-catalysed protocols reported thus far to effect similar transformations in organic solvents. For that purpose, we treated compound **2** under previously described non-aqueous experimental conditions and the results obtained are summarised in Scheme 3. It was observed that the palladium-catalysed reaction conditions¹⁰ tested were inadequate, unreacted substrate **2** was recovered. In contrast, the water-free copper-catalysed protocol,¹¹ furnished the target compound **1** in lower but comparable yield to that obtained when using our aqueous

protocol. However, the non-aqueous method required twice the time of the aqueous one (24 h vs. 12 h).

It can be concluded that we have designed a novel and highly practical methodology for access to the very valuable benzofuroindole framework. Such a structure, not easily attainable by existing methods, is present in a family of relevant pharmaceuticals accessible by means of known modifications performed on the skeleton of compound **1**. The methodology presented herein involves four high yielding steps, three of which imply the use of water, either as an additive or as the solvent, providing a remarkably simple and more sustainable access to the target tetracyclic skeleton. Furthermore, we have demonstrated that the final intramolecular copper-catalysed *N*-arylation reaction can be successfully performed in exclusively aqueous medium, affording the desired benzofuroindole in better yields than those obtained when using non-aqueous conditions. In addition, the use of simple commercially-available starting materials and the recycling of the same water solution containing the copper-catalyst to perform two different arylation reactions render the methodology described herein highly advantageous for its industrial application in terms of low-toxicity, safety and cost.

Acknowledgements

This research was supported by the University of the Basque Country (Project UPV 41.310-13656) and the Spanish Ministry of Education and Science (MEC CTQ2004-03706/BQU). M.C. thanks the Ministry of Education and Science (MEC) for a predoctoral scholarship. The authors also thanks Petronor, S. A. for generous free supply of hexane.

Notes and references

- (a) Z. Sui, X. Zhang and X. Li (Janssen Pharmaceutica N.V., Belg.), *Be. Pat.*, WO 2006/047017 A1, 2006; (b) Z. Sui, X. Zhang and X. Li (Janssen Pharmaceutica N.V., Belg.), *Be. Pat.*, WO 2006/034090, 2006.
- K. W. Bair (Wellcome Foundation Ltd., UK), *UK Pat.*, EP 0447703 A1, 1991.
- (a) J. A. Butera, S. A. Antane, B. Hirth, J. R. Lennox, J. H. Sheldon, N. W. Norton, D. Warga and T. M. Argentieri, *Bioorg. Med. Chem. Lett.*, 2001, **11**, 2093–2097; (b) S. A. Antane, J. A. Butera and J. R. Lennox (American Home Products Corporation, USA), *US Pat.*, 6 288 099, 2001.
- (a) S. Narayan, J. Muldoon, M. G. Finn, V. V. Fokin, H. C. Kolb and K. B. Sharpless, *Angew. Chem., Int. Ed.*, 2005, **44**, 3275–3279; (b) C.-J. Li, *Chem. Rev.*, 2005, **105**, 3095–3165; (c) C.-J. Li and L. Chen, *Chem. Soc. Rev.*, 2006, **35**, 68–82.
- For the preparation of diarylethanone **3** and the effect of water on its synthesis, see: M. Carril, R. SanMartin, I. Tellitu and E. Domínguez, *Org. Lett.*, 2005, **7**, 4787–4789.
- M. Carril, R. SanMartin, I. Tellitu and E. Domínguez, *Org. Lett.*, 2006, **8**, 1467–1470.
- It is remarkable that this transformation is easily scalable. Indeed, the yield reported in this paper was obtained starting from 1.82 g of **3**. For more details see the corresponding ESI†.
- This selective monobromination was only achieved when the *N*-tosyl derivative **3** was employed as the starting material. Other substituents different from tosyl on the amine moiety present in **3**, such as hydrogen or phenyl, led to multiple brominations on the aryl rings.
- (a) K. Kunz, U. Scholz and D. Ganzer, *Synlett*, 2003, 2428–2439; (b) I. P. Beletskaya and A. V. Cheprakov, *Coord. Chem. Rev.*, 2004, **248**, 2337–2364.
- J. Yin and S. L. Buchwald, *J. Am. Chem. Soc.*, 2002, **124**, 6043–6048.
- (a) A. Klapars, J. C. Antilla, X. Huang and S. L. Buchwald, *J. Am. Chem. Soc.*, 2001, **123**, 7727–7729; (b) A. Klapars, X. Huang and S. L. Buchwald, *J. Am. Chem. Soc.*, 2002, **124**, 7421–7428.

On the properties of 1-butyl-3-methylimidazolium octylsulfate ionic liquid†

María J. Dávila, Santiago Aparicio, Rafael Alcalde, Begoña García and José M. Leal*

Received 23rd August 2006, Accepted 8th December 2006

First published as an Advance Article on the web 2nd January 2007

DOI: 10.1039/b612177b

This work reports on a theoretical and experimental study on the ionic liquid 1-butyl-3-methylimidazolium octylsulfate ([BMIM]OS). The halogen-free ionic liquid [BMIM]OS is a stable solvent regarding hydrolysis, whose availability, toxicologically favourable features and well documented biodegradability turns it into a suitable candidate for different multi-ton-scale industrial applications. The pressure–volume–temperature behaviour of this fluid has been evaluated accurately over wide ranges of temperature and pressure, and correlated successfully with the empirical TRIDEN equation. From the measured data the relevant derived coefficients, isothermal compressibility, isobaric expansibility and internal pressure have been calculated. Other valuable properties such as isobaric heat capacity, speed of sound and refractive index were measured at several temperatures and atmospheric pressure. The molecular structure was looked into by quantum computations at the B3LYP/6-31 + g(d) level and classical molecular dynamics simulations in the NPT ensemble with the OPLS-AA forcefield. Both macroscopic and microscopic studies concur in a complex structure involving microheterogeneous polar and non-polar domains, brought about by the aggregation of the non-polar anionic chains.

Introduction

Over the last few years, ionic liquids (ILs) have attracted worldwide scientific interest in academia and industry. On account of their negligible vapour pressure and favourable and easily tunable physical and chemical properties, this class of compounds have found a place as suitable alternatives to volatile organic solvents in synthesis, separation and other applications.¹ ILs constitute quite a promising field; to gain advantage of their novel applications, a detailed and systematic research should be conducted. Although the term green solvent has been used to stand for this class of compounds, so far there is a dearth of reliable information on their toxicology, degradability and environmental effects.² Therefore, prior to its use on a massive scale, the utmost caution must be exercised when handling ILs with either only a limited expertise or absence of a thorough toxicological and environmental study through the whole life cycle.

A detailed survey of recent literature gives away the scarce number of systematic studies on ILs; in fact, most contributions focus too narrowly on halogen-containing ionic liquids. Halogen atoms might occasion major concerns if the anion is insufficiently stable regarding hydrolysis,³ or if costly thermal treatments are needed to leave out release of corrosive HF or HCl; in a green chemistry context, such ILs would be inappropriate for industrial use. Alkylsulfate-based ILs are cheaper and more adequate than halogen-based.^{4a,5} To successfully

cope with this challenge, among the several non-halogenated ILs designed so far [BMIM]OS, derived from inexpensive chemicals, stands out (Fig. 1).⁴ The [BMIM]⁺ cation, based on the imidazole moiety, is prone to microbial degradation,⁶ and the well documented low toxicity and satisfactory biodegradation of the anion part,^{4a} show that this IL has a great deal of promise in a number of multi-ton scale processes.

A major difficulty when dealing with industrial applications of ILs is the scarce number of reliably accurate data on their chemical and physical properties.⁷ The modelling of processes is critically dependent on an accurate knowledge of the thermodynamic behaviour of each component; hence, oversized designs, brought about by absence of reliable data, may result in unnecessary costs or failure in production targets.⁸ To date, the data on the pressure–volume–temperature (PVT)

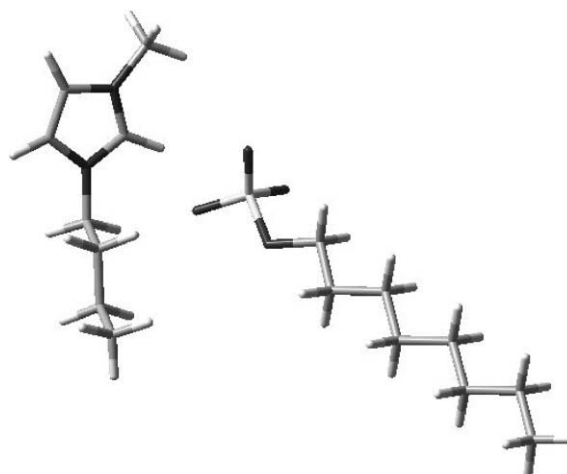


Fig. 1 Structure of [BMIM]OS ion-pair with minimum energy optimized at B3LYP/6-31 + g(d) theoretical level.

Universidad de Burgos. Departamento de Química, 09001, Burgos, Spain. E-mail: jmleal@ubu.es; Fax: +34 947 258831; Tel: +34 947 258062

† Electronic supplementary information (ESI) available: Experimental properties of [BMIM]OS at atmospheric pressure in the 298.15–343.15 K range (Table S1) and experimental and calculated thermo-physical properties in the 0.1–60 MPa, 318.15–428.15 K ranges (Table S2). See DOI: 10.1039/b612177b

behaviour of ILs is pretty scarce; most data have been reported with very low accuracy for only quite a narrow ILs group (mainly PF_6^- and BF_4^- containing ILs) usually at 25 °C, and pushing aside the pressure effect.⁹ In practice, application of ILs runs into difficulties due to the lack of data obtained with well-defined procedures for samples with well-established purity.^{9d,10}

In this work, the thermophysical behaviour of the non-halogenated [BMIM]OS IL was looked into over wide ranges of pressure and temperature. The *PVT* behaviour was evaluated over the 318.15–428.15 K and 0.1–60 MPa ranges. From these readings, the isobaric thermal expansibility, isothermal compressibility and internal pressure have been calculated; these properties are important both for thermodynamic calculations and design of operations such as phase separation, mass transfer or pumping,^{7b} and may provide substantial information on the fluid structure and molecular interactions.^{9d} Likewise, the isobaric heat capacity, speed of sound and refractive index have also been measured at atmospheric pressure over the 298.15–343.15 K temperature range. From isobaric heat capacity and *PVT* data at ambient pressure, isobaric and isochoric heat capacity have been evaluated over a wide pressure range.

Systematic measurement of thermophysical properties enables us to settle useful relationships between the liquid's structure and property values, stressing the cation, anion and substituent effects. In view of the large number of potential ILs,¹¹ economical and time-consuming reasons prevents one from measuring properties for all of them, either pure or mixed; instead, development of semiempirical correlations and predictive models prone to be regularly tested against experimental data is highly recommended.¹² Molecular modelling is a powerful tool that lends insight to the structure of condensed phases; in conjunction with macroscopic studies, it provides a good link between physicochemical properties and molecular structure, thus extending the spectra of possible applications. So far, the number and scope of the molecular modelling studies reported is rather limited. The modelling of ILs requires a good expertise on the fluid structure at microscopic level that often is unavailable.¹³ Moreover, the lack of systematic and accurate data needed also restrains the development of theoretical approaches. In this work, the molecular structure of the non-halogenated [BMIM]OS IL was inferred from the modelling developed on the basis of single ion-pair quantum calculations and condensed phase classical molecular dynamics simulation.

Experimental

Materials and sample preparation

[BMIM]OS, purchased from Fluka (stated purity >95%), is a yellow viscous oil; although its melting point is 34–35 °C,^{4a} at ambient temperatures it remains as an undercooled melt up to 5 °C, where crystallisation begins. Although the yellow colour is indicative of organic impurities arising from the synthesis process, the impurities are in such a low concentration that the physical properties of the IL are almost unaffected within the quoted accuracy limits; in any event, the characteristics and thermophysical properties of the sample used in this work are

in reasonable agreement with those previously reported by Wasserscheid *et al.*^{4a} The two main sources of possible contaminants that could affect remarkably the IL physical properties are chloride, from the synthesis process, and water, on account of its high hygroscopic character. The chloride content, measured by ICP-MS, was <0.1%. To diminish the water content, the IL was heated at 80 °C under vacuum and the water content measured by Karl Fischer titration just prior to measurements. To leave out water contamination, the samples were kept under nitrogen atmosphere after drying, the water content of all samples being <0.05%.

Atmospheric pressure measurements

The isobaric molar heat capacities were measured with a Setaram micro DSC III calorimeter previously described.¹⁴ The measurements were carried out according to the continuous scanning method;¹⁵ toluene (Fluka, >99.8%) was used as the reference material and butan-1-ol (Aldrich, >99.5%) as the calibration liquid. The heat capacities of toluene and butan-1-ol were obtained from Zabransky *et al.*¹⁶ The calorimetric signal is proportional to the volume heat capacity, and the measured density was used to obtain the molar heat capacity with a stated accuracy of $\pm 1 \times 10^{-2} \text{ J mol}^{-1} \text{ K}^{-1}$, with the temperature controlled to $\pm 1 \times 10^{-2} \text{ K}$ by a peltier.

Speeds of sound were evaluated with an Anton Paar DSA 5000 apparatus by measuring the travelling time through the sample of an impulse emitted by a piezoelectric emitter ($\pm 0.5 \text{ m s}^{-1}$), the cell temperature being controlled by a built-in solid state thermostat ($\pm 1 \times 10^{-2} \text{ K}$). The apparatus was calibrated using water (Milli-Q, resistivity 18.2 m Ω cm) and *n*-nonane (Fluka, >99.5%) as standards.

Refractive index ($\pm 5 \times 10^{-5}$) was measured with an automated Leica AR600 refractometer whose temperature was controlled by a Julabo F32 external circulator ($\pm 1 \times 10^{-2} \text{ K}$). The proper calibration was attained using water and a standard supplied by the manufacturer ($n_D = 1.51416$).

PVT behaviour. Apparatus and calibration procedure

The apparatus used in the *PVT* measurements has been described in detail.¹⁷ The system is installed around a high-pressure vibrating tube densimeter. The central element of the system is the Anton Paar DMA 512P high pressure cell, which contains the stainless steel vibrating U-shaped tube and the electronics needed to excite the tube and measure the oscillating period. The cell temperature was controlled to $\pm 1 \times 10^{-2} \text{ K}$ by a Julabo F32 circulating bath, fitted out with a calibrating Pt100 sensor placed in the measuring cell connected to a $\Delta F250$ unit. The circuit pressure was controlled within $\pm 5 \times 10^{-3} \text{ MPa}$ by a Ruska 7615 Digital Pressure controller and measured to $\pm 1 \times 10^{-2} \text{ MPa}$ by a pressure sensor. The pressurising fluid was separated from the sample by a high-pressure liquid-to-liquid separator (Pressurements T3600E) containing a Teflon diaphragm to automatically send out the pressure. The pressure controller and the thermometer were previously calibrated through well defined and traceable procedures. The operation of the whole

system was computer controlled using specially developed software that makes the automatic handling of massive amounts of accurate data feasible. The calibration procedure linking the densimeter oscillation period with the density value has been described.¹⁷ A 14-parameter equation was used, whose values were obtained with toluene (Fluka, >99.8%) and *n*-decane (Aldrich, >99%) as references; the density values of the reference materials were taken from the literature.¹⁸

To prevent the uncertainty in the density readings from being affected by the sample viscosity, a number of corrections are needed.¹⁹ Such corrections rely on both the availability of experimental viscosity data over the pressure and temperature ranges considered and the use of properly defined and evaluated damping equations. The mathematical form of the viscosity corrections for pressures different from atmospheric pressure is still under debate, and different corrections have been suggested which basically depend on the instrument features and the sample viscosity.¹⁹ To properly calculate the correction factor to density, eqn (1) has been put forward:^{19a,b}

$$\frac{\Delta\rho}{\rho} = (-0.5 + 0.45\sqrt{\eta})10^{-4} \quad (1)$$

where ρ , the raw density reading preceding the viscosity correction, was obtained according to the above procedure, $\Delta\rho$ is the difference between the raw and the corrected densities, and η is the sample viscosity in mPa s. To date, only atmospheric pressure viscosity data for [BMIM]OS are available; therefore, to test the viscosity effect on the reported density values, the corrected and non-corrected density data are compared at that pressure (Fig. 2). Only for the lower temperatures, the deviations climbed up to 0.1%, but the main body of the work was completed at temperatures above 318.15 K, that is, where the error is below 0.05%. Bearing in mind the lack of high pressure/high temperature viscosity data for [BMIM]OS and the existence of different corrections,

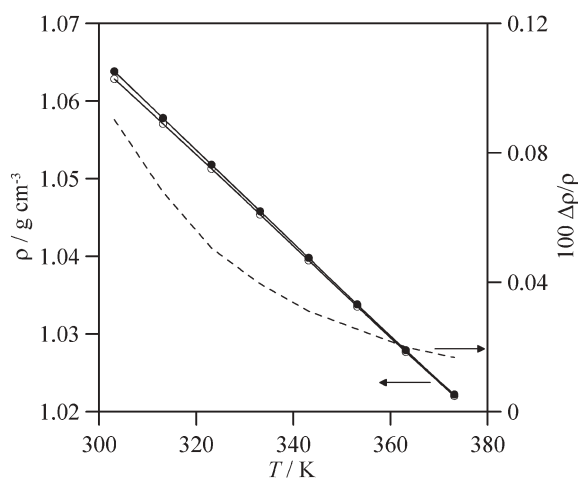


Fig. 2 Experimental raw density data (●), and values after viscosity correction according to eqn (1) and experimental viscosity data from Wasserscheid *et al.*,^{4a} (○). Dashed line: percentage deviation between corrected and non-corrected density data.

whose reliability so far is unclear, the values reported in this work are the raw, non-corrected, density data. Aside from the P and T uncertainties, the main contribution to the experimental uncertainty of density comes from the two reference substances. In light of the full accuracies of all factors involved in the density readings, an accuracy of $\pm 1 \times 10^{-4}$ g cm⁻³ for the raw density data can be assumed.

Quantum calculations

The quantum computations were carried out with the Gaussian 03 package,²⁰ and the Density Functional Theory (DFT), employing the Becke gradient corrected exchange functional²¹ concomitant with the Lee–Yang–Parr correlation functional²² with three parameters (B3LYP)²³ method. The B3LYP gradient corrected method includes some of the electron correlation effects. With only a slightly harder computational effort, the DFT approach usually gives rise to greater accuracy than Hartree–Fock for structural, thermochemical and spectroscopic properties;²⁴ this mix of efficiency and accuracy has turned the method into the most popular functional in modern DFT. Hence, geometry of the isolated monomer ion-pair was fully optimized at the B3LYP/6-31 + g(d) theoretical level.

Molecular dynamics simulations

In the present study, classical molecular dynamics simulations were carried out using the TINKER molecular modelling package.²⁵ All simulations were performed in the NPT ensemble at 318.15 K and 0.1 MPa; the Nosé–Hoover²⁶ method was used to control the temperature and pressure of the simulation system. The motion equations were solved using the Verlet Leapfrog integration algorithm.²⁷ The molecular geometries were constrained according to the shake algorithm.²⁸ Long-range electrostatic interactions were treated with the smooth particle mesh Ewald method.²⁹ The simulated system involves application of periodic boundary conditions in all three directions to a cubic box with 360 ions (9900 atoms). Simulations were performed using a $L/2$ Å cut-off radius for the non-bonded interactions, L being the cubic box side. Imidazolium ILs show only slow microscopic dynamics; therefore, the equilibration simulation time acts out a critical role to ensure statistically significant results. Hence, an initial box was generated using the PACKMOL program.³⁰ This initial configuration was minimized according to the MINIMIZE program in the TINKER package to an *rms* gradient of 0.1 kcal mol⁻¹ Å⁻¹; then a 100 ps NVT molecular dynamics simulation was run starting from the output configuration of the MINIMIZE program. Finally, from the output NVT simulation configuration, a production run of 200 ps, in 1 fs steps, was run in the NPT ensemble at 318.15 K and 0.1 MPa, from which all the reported data are collected. The forcefield developed by Canongia *et al.*,^{13c} based on the OPLS–AA approach, has been successfully applied to analyse alkylimidazolium-containing ILs,^{13a,c} and it was used for molecular dynamics simulations of [BMIM]OS. The forcefield parameters for [BMIM]⁺ were obtained from Canongia *et al.*^{13c} and those for OS⁻ from Schweighofer *et al.*³¹

Results and discussion

Atmospheric pressure measurements

Experimental thermophysical properties at atmospheric pressure are reported in Table S1 (ESI)[†] and plotted in Fig. 3. Despite the 34–35 °C^{4a} melting point reported for [BMIM]OS, this fluid should remain as a subcooled melt for a long time well below this temperature; hence, measurement of the thermophysical properties of this melt are perfectly feasible. The experimental density is slightly higher than the pycnometric value (1.0601 g cm⁻³, difference 0.63%) at 25 °C.^{4a} The long alkyl anion chain gives rise to a less dense IL compared to other ILs containing the [BMIM]⁺ cation and different anions; ILs with more symmetric anions, like PF₆⁻ or BF₄⁻ (spherical in shape), show higher densities^{7b} than this OS⁻ containing IL, whose almost linear shape produces a less dense packaging. Therefore, strongly asymmetric anions like OS⁻ bring about a density fall-off, a well known feature of the cation effect.³² Nevertheless, the density of [BMIM]OS is very low compared to most ILs, in particular those containing [BMIM]⁺, and is comparable to common organic solvents.

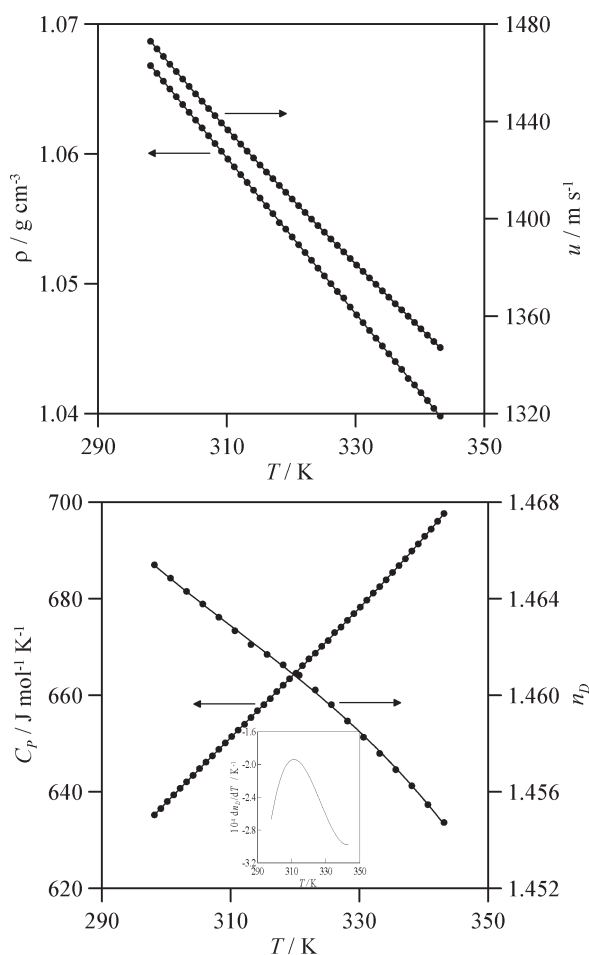


Fig. 3 Experimental thermophysical properties of [BMIM]OS at atmospheric pressure as a function of temperature. Density, ρ , speed of sound, u , refractive index, n_D , and isobaric heat capacity, C_p . Symbols: experimental data, Table S1 (ESI)[†]; lines: guide lines.

Among the properties of [BMIM]OS, the remarkably high isobaric heat capacity and the wide liquid temperature range (~ 300 K),^{4a} turn this fluid into a suitable candidate for a thermal energy storage solvent.^{33a,b} The thermal storage density, E , may be calculated according to eqn (2):^{33b}

$$E = \rho C_p (T_{\text{out}} - T_{\text{in}}) \quad (2)$$

where T_{in} and T_{out} are the input and output temperatures to the storage media. Combination of the properties of Table S1 with $T_{\text{in}} = 308.15$ K (close to the melting point) and $T_{\text{out}} = 614.15$ K (close to the decomposition temperature), yields the value $E = 662$ MJ m⁻³, much higher than those for common storage oils used in industry (around 59 MJ m⁻³).^{33c}

The refractive indices plotted in Fig. 3b show a complex non-linear behaviour. Although the fall with temperature is very mild, the behaviour contrasts with those for the other properties reported in Fig. 3, which is almost linear. The literature available on refractive indices of ILs is very scant,³⁴ and only few studies on the temperature effect are available;³⁵ most studies claim that the temperature effect on the refractive index is almost negligible, reporting even linear fits with temperature^{35a} in opposition to the trend shown in Fig. 3b. Nevertheless, a more detailed analysis of the literature values shows the same trend for different ILs (Fig. 4); although this trend is somehow hidden by the mild variation of the refractive index, Fig. 4 makes clear that, within the range of uncertainty reported in the literature for the experimental data, a non-linear trend is obtained for other [BMIM]⁺ containing ILs. The dn_D/dT function for [BMIM]OS, calculated from a fit of the experimental data and plotted as an insert of Fig. 3b, shows a well defined maximum close to the melting temperature (maximum at 311.40 K, literature value 307–308 K).^{4a}

It is well known that fluids with high density normally show higher refractive index than fluids with low density. However, comparison of the refractive index of [BMIM]OS with more dense ILs indicates that this rule is not true for this fluid, for instance, comparing [BMIM]OS ($\rho = 1.0668$ g cm⁻³,

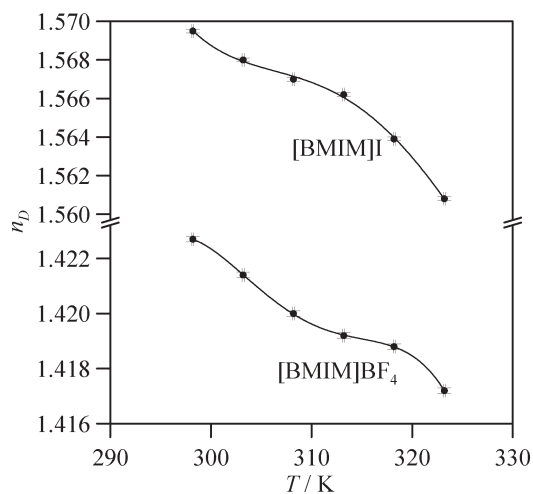


Fig. 4 Literature^{35b} experimental refractive indices for two ILs. Error bars for temperature and refractive indices are also plotted for each point.

$n_D = 1.46540$, at 298.15 K) with [BMIM]PF₆ ($\rho = 1.36 \text{ g cm}^{-3}$, $n_D = 1.409$, at 298.15 K).^{7b} Nevertheless, the refractive indices for [BMIM]OS are in line with those of most common organic solvents.

PVT behaviour

Experimental and calculated thermophysical properties of [BMIM]OS in the 318.15–428.15 K and 0.1–60 MPa ranges, in 10 K and 5 MPa steps, respectively, are reported in Table S2 (ESI)[†] and plotted in Figs. 5, 6 and 9. To rule out the appearance of a solid phase during measurements, the PVT study was carried out from the initial 318.15 K temperature, well above the melting point. The experimental compressed liquid densities were correlated with temperature and pressure according to the 10-parameter TRIDEN equation developed by Ihmehls and Gmehling.³⁶ This approach combines a

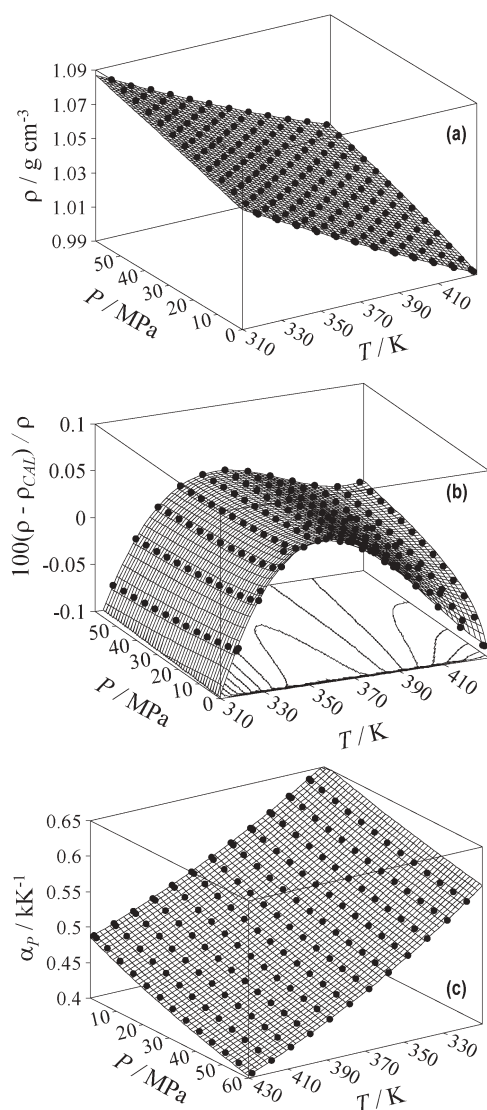


Fig. 5 Experimental density, ρ , percentage deviation between experimental and TRIDEN calculated density, $100(\rho - \rho_{\text{CAL}})/\rho$, and calculated isobaric thermal expansivity, α_p , for [BMIM]OS as a function of pressure and temperature. In part (b) the contour plots of constant percentage deviation are plotted at the bottom of the Figure.

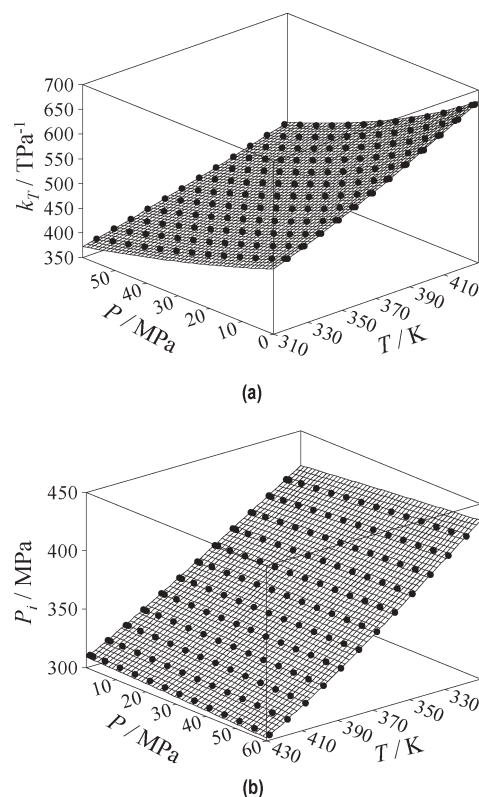


Fig. 6 Calculated isothermal compressibility, k_T , and internal pressure, P_i , for [BMIM]OS as a function of pressure and temperature.

modified version of the Rackett equation for saturation densities (eqn (3)) with the Tait equation for isothermal compressed densities (eqns (3)–(5)).

$$\rho_0 = \frac{A_R}{B_R^{[1+(1-T/C_R)D_R]}} \quad (3)$$

$$\rho = \frac{\rho_0}{1 - C_T \ln \frac{B_T + P}{B_T + P_0}} \quad (4)$$

$$B_T = b_0 + b_1 \frac{T}{E_T} + b_2 \left(\frac{T}{E_T} \right)^2 + b_3 \left(\frac{T}{E_T} \right)^3 \quad (5)$$

The reference pressure $P_0 = 0.1 \text{ MPa}$ was used at all temperatures, and the corresponding reference densities, ρ_0 , were correlated with eqn (3), the C_T Tait parameter being treated as temperature independent. The correlation parameters were deduced using a Levenberg–Marquardt least squares algorithm, and the optimal fitting was assessed by the absolute average percentage deviation (AAD), eqn (6):

$$AAD = \frac{100}{N} \sum_{j=1}^N \left| \frac{\rho_{i,\text{EXP}} - \rho_{i,\text{CAL}}}{\rho_{i,\text{EXP}}} \right| \quad (6)$$

where N is the number of data pairs. Table 1 summarises the calculated parameters and AAD values for [BMIM]OS.

The three-dimensional density plot reported in Fig. 5a enables concurrent analyses of the pressure and temperature effects. No literature data for [BMIM]OS was available in the

Table 1 Fitting parameters of TRIDEN correlation of density, g cm^{-3} , with pressure and temperature, eqn (3)–(5), and average absolute percentage deviation, *AAD*, eqn (6), for [BMIM]OS. The parameters are valid within 318.15 K–428.15 K and 0.1 MPa – 60 MPa temperature and pressure ranges

C_T	b_0/MPa	b_1/MPa	b_2/MPa	b_3/MPa	E_T/K	$A_R/\text{g cm}^{-3}$	B_R	C_R/K	D_R	<i>AAD</i>
0.088004	286.4411	-1.6737	-18.0543	2.2061	106.14	45.9444	4.242588	-1.380552	0.087606	0.0286

pressure/temperature ranges of this study. Hence, comparison with our data is not possible. Nevertheless, the density of [BMIM]OS, as expected, falls when the temperature is raised along isobars and increases with rising pressure along isotherms. It is clear that the cation alkyl chain, and mainly the bulky anion octyl chain, give rise to not very efficient packaging, which is the reason for the low density of the fluid compared with other ILs. This effect is reinforced with increasing temperature, which enables more efficient ion mobility in this inefficient packaging, and thus a lower density, and becomes weakened by increasing pressure, which forces the fluid to a more compact packaging. The presence of bulky, non-symmetrical, non-spherical anions such as OS^- gives rise to low densities over wide T and P ranges. Conversely, pseudo-spherical, highly symmetrical anions, such as BF_4^- or PF_6^- , bring about other effects on [BMIM]⁺-containing ILs; the larger (PF_6^-) anion has the greater density irrespective of pressure and temperature.^{9a,d} Therefore, increasing the anion size does not necessarily hamper the packaging, but rather it increases the density (on account of the higher molecular mass), in contrast with alkylsulfate anions, for which the longer the chain, the more difficult the packaging, and the lower the density.

Fig. 5b plots the percentage deviation between experimental and fitted densities according to the TRIDEN model, the absolute deviations being lower than 0.1%. The very low average deviations, close to the uncertainty of the experimental densities (Table S2, ESI†), and the high fitting quality achieved enable use of this equation, along with the parameters of Table 1, to calculate derived thermophysical properties of [BMIM]OS. The PVT behavior of [BMIM]OS enables calculation of the derived properties isobaric thermal expansivity, α_P (eqn (7)), isothermal compressibility, κ_T (eqn (8)), and internal pressure, P_i (eqn (9)):

$$\alpha_P = -\frac{1}{\rho} \left(\frac{\partial \rho}{\partial T} \right)_P \quad (7)$$

$$\kappa_T = \frac{1}{\rho} \left(\frac{\partial \rho}{\partial P} \right)_T \quad (8)$$

$$P_i = \left(\frac{\partial U}{\partial V} \right)_T = T \frac{\alpha_P}{\kappa_T} - P \quad (9)$$

the derivatives needed being evaluated with the TRIDEN equation and the parameters in Table 1. These properties are shown in Table S2 (ESI)† and plotted in Fig. 5 and 6.

The value deduced for α_P is particularly sensitive to the type of mathematical function used to fit the density data. The temperature effect, along the isobars scale, shows fairly mild deviations from linearity in most cases. To sharply get out of ambiguities,^{9a,b} many authors put forward a linear function; this, however, entails hiding the rather subtle effects that stem

from the non-linear behaviour of most fluids, and therefore a piece of information may be lost. In view that the high quality TRIDEN fitting describes accurately the PVT behaviour of [BMIM]OS, the function does not show any pitfall in the P/T ranges considered; therefore, the α_P values deduced describe the real α_P trend for [BMIM]OS. Fig. 5c and Table S2 (ESI)† show that α_P falls with rising pressure along isotherms and, surprisingly, decreases with increasing temperature along isobars over the working pressure range. The decreasing profile of α_P with rising temperature is quite a rare and interesting anomaly which contrasts with the regular behaviour of most fluids, for which α_P increases with increasing temperature. This behaviour has been reported previously for some alkanols at low temperatures,³⁷ lubricants,^{19a} ILs, such as [BMIM]BF₄^{19a} and [BMIM]PF₆^{19d} and confirmed through molecular simulation studies for several ILs.³⁸ Some authors put down this striking feature to the high ordering of the IL in the liquid phase, with a solid-like structure;^{39a} others, however, consider the anharmonicity effect of intermolecular vibrations together with the P and T effects on the intermolecular potential.^{39b} We shall analyse these features with a molecular dynamics simulation. Nevertheless, α_P was some 2 times smaller for [BMIM]OS compared to conventional organic solvents (but close to water), and most of the studied ILs,^{9d} showing again that the temperature effect on density, and the structural effects beneath, are still more subtle than for common organic fluids.

The isothermal compressibilities (Fig. 6a) show a marked tendency to decrease with P along the isotherms, and to increase with T along the isobars (in contrast with α_P); in view of the diminution of the free intermolecular space this, in fact, should be the regular liquids behaviour. The fluid becomes less compressible as the pressure rises and, at high enough pressure, the system approaches the value corresponding to a closer packed volume. This feature cannot be assessed directly because the highest pressure attained in this work was not high enough to reach that point; however, it has been reported for other ILs,^{9d} and it can be inferred indirectly because it is clear that, for a fixed pressure, the temperature effect on κ_T decreases as the pressure rises (Fig. 6a). For instance at 0.1 MPa, going from 318.15 to 428.15 K gives rise to a 36.62% increase in κ_T ; however at 60 MPa the same temperature rise brings about only 26.14% κ_T . Similar to α_P , the κ_T values for [BMIM]OS are small compared to common organic fluids (and similar to those of water).^{9d} In view that ILs consist purely of ions, the strong Coulomb interactions between them give rise to less compressible fluids than pure organic solvents. Nevertheless, [BMIM]OS is more compressible than other ILs containing the [BMIM]⁺ cation;^{9a,d} this feature can be put down not only to the greater molar volume^{9d} of [BMIM]OS, but also to the non-spherical shape of the OS^- anion that gives rise to a less efficient packaging, a greater free volume, and

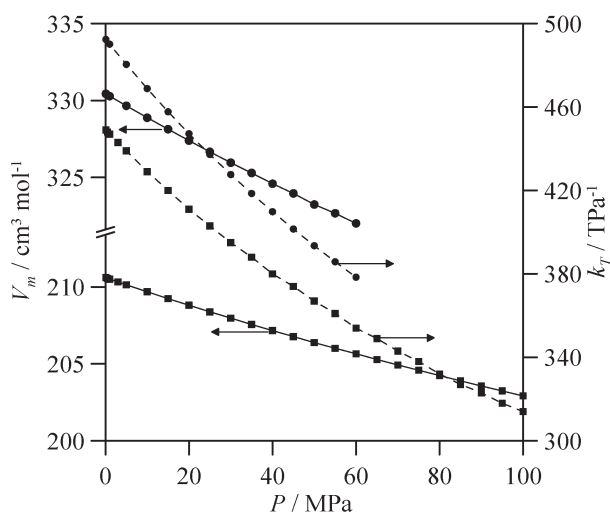


Fig. 7 Molar volume, V_m , and isothermal compressibility, κ_T , of [BMIM]OS, this work, and [BMIM]PF₆, Ref. 9a. Continuous lines: molar volume, dashed lines: isothermal compressibility. (●)[BMIM]OS, (■)[BMIM]PF₆.

thus a more compressible fluid. For comparison, plots of the κ_T values for [BMIM]OS and [BMIM]PF₆^{9a} (Fig. 7), together with the molar volumes for both ILs, bear out the above effects; for instance, at 318.15 K the molar volume of [BMIM]OS is 56.89% larger than that of [BMIM]PF₆, but κ_T for [BMIM]OS was only 9.59% greater; therefore, the difference in free volume between both fluids is the main controlling factor that determines the difference in isothermal compressibility.

Internal pressure (Fig. 6b and Table S2, ESI†) is quite a useful property to analyse liquid structures because it is directly related to the fluid cohesive forces. This property, defined according to eqn (9), indicates that a liquid undergoing an isothermal expansion exerts work against the cohesive forces, entailing internal energy changes.⁴⁰ Another quite valuable property is the so called cohesive energy density, c , defined according to eqn (10):

$$c = \frac{\Delta U}{V_m} = \frac{\Delta H_{\text{vap}} - RT}{V_m} \quad (10)$$

where ΔU is the molar internal energy, V_m stands for the molar volume, and ΔH_{vap} for the molar vaporization enthalpy. The Hildebrand solubility parameter, δ_H , defined as the square root of c , often is used to characterise solubility phenomena. A deal of confusion has emerged between the physical meanings of c and P_i ,⁴⁰ although the two properties bear certain relation, they do not reflect the same structural fluid effects, and only for non-polar/non-associating fluids do they become equivalent. Hence, in order for such solubility phenomena to be unambiguously characterised, knowledge of the δ_H parameters for ILs would be useful from both theoretical and industrial viewpoints.^{13/41} Evaluation of the δ_H parameters requires knowledge of ΔH_{vap} data; however, the volatility of ILs is almost null (one of the main *green* advantages against volatile organic solvents), and thus measuring ΔH_{vap} is not feasible. Although indirect methods for the determination of δ_H have

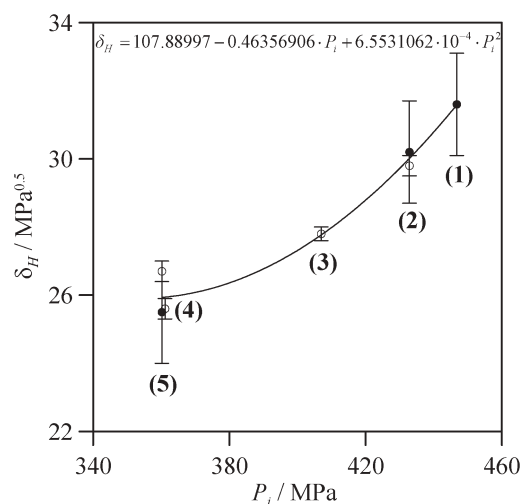


Fig. 8 Relation between the Hildebrand parameter, δ_H , and internal pressure, P_i , for selected ILs. Experimental δ_H from (●) Swiderki *et al.*^{41b} and (○) Lee *et al.*,^{41a} vertical error bars: experimental error. (—) Degree 2 polynomial fitting. (1) [BMIM]BF₄; (2) [BMIM]PF₆; (3) [OMIM]PF₆; (4) [HMIM]NTf₂; (5) [BMIM]NTf₂. α_P and κ_T data for calculation of P_i according to eqn (9) obtained from Gomes de Azevedo *et al.*^{9a} (1,2), Gomes de Azevedo *et al.*^{9b} (4,5) and Gu *et al.*^{9d} (3).

been advocated,⁴¹ it would be useful to generate efficient tools to procure this parameter from experimental PVT data. A number of methods have been put forward for the calculation of δ_H values from equations of state,⁴² but so far they are not convincing because of the strong difference between c and P_i for ILs. Therefore, we tried to find out a relation between P_i and δ_H using available literature data; experimental δ_H and PVT data for ILs are extremely scarce and thus comparison between both properties is quite limited.

The experimental δ_H values are plotted (Fig. 8) as a function of the P_i values calculated from PVT data for all the ILs available, thus providing a relation between both properties for the fluids considered. Although a more detailed study is to be carried out, as a preliminary result and in view of the scarce literature data and the large errors inherent to δ_H by indirect methods, a second degree polynomial fitting linking both properties is put forward here. The relation between both properties may enable the evaluation of δ_H from the P_i , calculated from PVT data, not only at atmospheric pressure but also at different and more extreme conditions. This would enable the characterisation of the solubility of different substances in ILs over wide T and P ranges. Hence, using the fitting equation reported in Fig. 8 for [BMIM]OS we obtained $\delta_H = 28.2 \text{ MPa}^{0.5}$ at 298.15 K and 0.1 MPa; moreover, the value $\Delta U = 263 \text{ kJ mol}^{-1}$ obtained (eqn (10)) was 10 times larger than those of common organic solvents and other ILs.^{41a,b} The remarkably high ΔU value, which accounts for the almost null vapour pressure, can be put down to the solvent's ionic nature and the inherent strong electrostatic interactions.

$$\left(\frac{\partial C_p}{\partial P}\right)_T = -\frac{T}{\rho} \left(\alpha_P^2 + \left(\frac{\partial \alpha_P}{\partial T}\right)_P \right) \quad (11)$$

Eqn (11) was numerically integrated using the experimental C_P data at 0.1 MPa reported in Table S1 (ESI)†. The anomaly reported for α_P (decrease in α_P as T is raised) results in another anomaly in C_P : an increase in C_P as P is raised. The observed rise in C_P with P , although somewhat mild, bears out the high structural ordering of this fluid; for instance, at 318.15 K, a 60 MPa increase in pressure is accompanied by 1.50% increase in C_P ($0.17 \text{ J mol}^{-1} \text{ K}^{-1} \text{ MPa}^{-1}$), and thus it will be very sensitive to experimental and calculation errors. The main source of uncertainty to evaluate the pressure effect on C_P (eqn (11)) stems from the experimental calorimetric data at 0.1 MPa used in the integration process; the high accuracy of these data is passed on to the C_P values calculated at other pressures, and thus the C_P anomaly becomes evident. In any event, the pressure effect on C_P for [BMIM]OS is greater than for other ILs such as [BMIM]PF₆ (without anomalous α_P) or [BMIM]BF₄ (with anomalous α_P) for which C_P is almost constant over wide temperature ranges;^{9a} this can be explained by the pronounced temperature dependence of α_P in [BMIM]OS. Furthermore, the C_P values for [BMIM]OS are greater than those for other common ILs containing the [BMIM]⁺ cation; for instance, the difference with BF₄⁻, PF₆⁻ and NTf₂⁻ containing ILs are 297.5, 253.4 and 76.4 J mol⁻¹ K⁻¹, respectively,^{9a,b} which makes [BMIM]OS a more suitable fluid for energy storage purposes over wide T and P ranges. The increase of C_P with the structural complexity of the anion, and also of the cation,^{9b} is the outcome of the increase of higher vibrational degrees of freedom that improves the fluid energy storage ability.

The isochoric heat capacity, C_V , was calculated according to eqn (12):

$$C_P - C_V = \frac{TV\alpha_P^2}{k_T} \quad (12)$$

The behaviour of C_V is quite similar to that of C_P ; although the pressure dependence of C_V is slightly lower, $0.10 \text{ J mol}^{-1} \text{ K}^{-1} \text{ MPa}^{-1}$, the same anomaly appears. The difference between both heat capacities is plotted in Fig. 9b, it increases as temperature and pressure rise, mainly because of the α_P anomaly.

Quantum calculations

The optimised structure of the [BMIM]⁺/OS⁻ ion-pair is shown in Fig. 1. The interaction among both ions could be envisaged through two different locations of the imidazolium ring: (i) through the hydrogen at the C_r site (carbon placed among the two ring nitrogens), or (ii) through the C_w hydrogen, placed in the opposite ring site. The interaction energy ΔE calculated through both sites is shown in Fig. 10.

The ΔE values calculated for both positions are remarkably large. Values previously reported for ILs with the same cation but with smaller anions,^{13d} such as PF₆⁻, show interaction energies around -325 kJ mol^{-1} , whereas the values for the pair containing OS⁻ are higher than double. Thus, compared to other anions the OS⁻ anion stabilizes remarkably the ion-pair. Interaction through the C_r site is preferred, as the larger (in absolute value) interaction energy reveals. In any event, the energy difference between the two positions is smaller

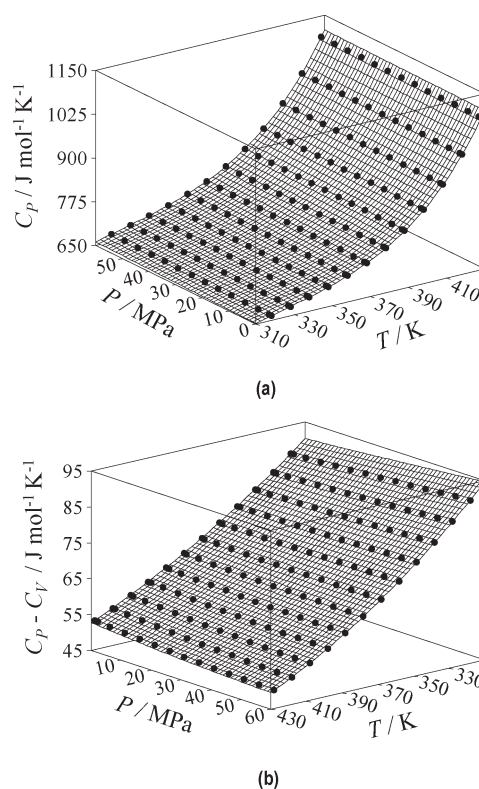


Fig. 9 Experimental (0.1 MPa data) and calculated (other pressures) isobaric heat capacity, C_P , and difference between isobaric and isochoric heat capacity, $C_P - C_V$, for [BMIM]OS as a function of pressure and temperature.

compared to ion-pairs with smaller anions such as PF₆⁻,^{13d,f} hence, although the C_r site is preferred, interactions through the C_w site, with energies only slightly lower, should not be ruled out.

The interaction distance between pairs is also reported in Fig. 10. If the distance between the cation H (at the C_r or C_w sites) and the anion O is lower than 2.7 Å, then it can be regarded as an H-bond. The interaction between both positions gives rise to H bonding through one of the anion oxygens. The shortest anion–cation distance falls well below

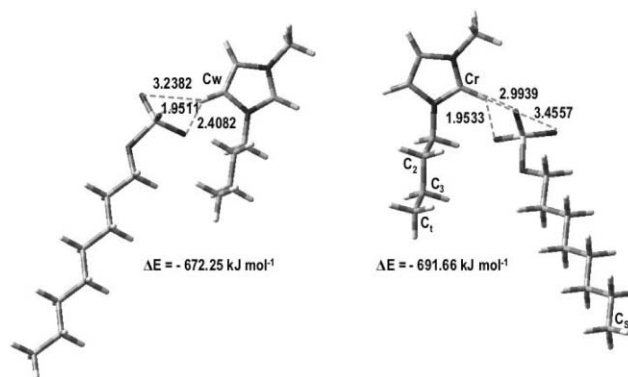


Fig. 10 Structure of [BMIM]OS ion-pair at two different interaction sites with minimum energy optimized at B3LYP/6-31 + g(d) theoretical level. ΔE = interaction energy; figures indicate interatomic distance in Å.

the above limit, and thus strong H bonding should emerge in the fluid for any of the two possible interaction sites. The distance calculated for the [BMIM]⁺–OS[−] ion-pair are remarkably lower than those reported for other ILs with smaller anions such as PF₆[−] and the same cation (2.20 Å),^{13d} a feature borne out by the larger interaction energies obtained for this IL. Thus, the quantum calculations for the [BMIM]⁺–OS[−] ion-pair show strong H-bonding and stable ion-pair effects, with the added effect of a strong fluid structure. The OS[−] anion improves the H-bonding effect on the fluid structure compared to other anions.

Molecular dynamics simulations

The results obtained through classical molecular dynamics simulations enable a detailed analysis of the microstructural features in [BMIM]OS. Various site–site radial distribution functions, (RDF or $g(r)$), were calculated to get a better understanding of the fluid structure. The RDFs are plotted (Fig. 11) for the S atom of the OS[−] anion and different C atoms of the cation in the imidazolium ring (atoms labelling Fig. 1). As reported for other imidazolium containing ILs,^{13d,f} in this case the anion–cation interaction comes about preferentially through the C_r site of the imidazolium ring; this feature, sustained because the C_r–H_a bond concentrates the majority of the cation charge, justifies the preferred interaction site with the anion. The location of the first peak (Fig. 11) is consistent with the optimised geometry obtained in this work by *ab initio* calculations. However, some significant differences appear when the results (Fig. 11) are compared with those reported for other [BMIM]⁺ containing ILs. The first peak for the C_r–S RDF at $r = 4$ Å coincides with the value obtained for [BMIM]PF₆[−],^{13f} but peak intensity is lower for [BMIM]OS (slightly greater than 5 for [BMIM]PF₆[−]).^{13f} The C_w–S RDF structures are also slightly different; for [BMIM]OS a more structured first peak appears, whereas for [BMIM]PF₆[−] a flatter peak is reported.^{13f} Thus, although for [BMIM]PF₆[−] the anion–cation interaction comes about preferentially through the C_r–H_a imidazolium site, this preference is less pronounced than for other imidazolium containing ILs.

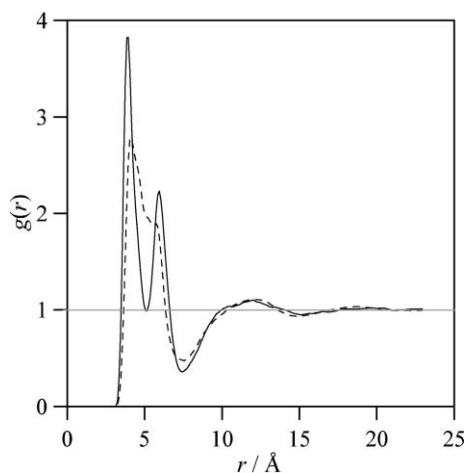


Fig. 11 Site-site radial distribution functions for [BMIM]OS at 318.15 K and 0.1 MPa. (—) C_r–S; (---) C_w–S.

Because of the ionic character of the species involved in the fluid, the RDFs extend to long distances, showing a long-range interactional ordering.

The presence of alkyl apolar chains both in the cation and in the anion poses the question of whether polar/non-polar domains appear in this fluid, as reported by Canongia and Padua for imidazolium-containing ILs with symmetrical, almost spherical anions like PF₆[−].^{13a} These authors have shown that increasing the chain length of the alkyl substituent in the imidazolium ring modifies the polar domains, even though these keep on for large substituents. Therefore, we also studied the effect of long alkyl chains in the anion, OS[−], in this nanostructural fluid ordering. Fig. 12 plots site–site RDFs between C_t–C_t tail carbons of imidazolium ring (to verify the cation–cation apolar chain interactions), between C_s–C_s anion carbons in the apolar chain (to study the interaction between apolar regions of anion), and C_t–C_s anion–cation apolar interactions. The RDFs reported in Fig. 11 show a well defined first peak at 4 Å for C_t–C_t interaction, a less intense first peak at 5 Å for C_s–C_s, and a first peak with complex shape (two small maxima at 4 and 5 Å) followed by a second well defined peak for C_t–C_s. The intensity and location of these peaks show that clustering of non-polar chains appears in [BMIM]OS; the RDF for C_t–C_s denote that non-polar clusters are made up of alkyl chains both in the anion and cation, although the intense and sharp first C_t–C_t peak compared with the less intense C_s–C_s shows that cation alkyl chains are closer within these non-polar domains. The long apolar OS[−] chain, together with the preferred interaction with the C_r site of the imidazolium ring, restricts the anion–anion non-polar chains clustering; that is, non-polar domains are structured through cation chains to which alkyl anion chains gather, as shown in Fig. 12 for C_t–C_s RDF. In any event, the presence of non-polar domains in this fluid, whose structure is dominated by electrostatic interactions, is clear, as for other [BMIM]⁺ containing ILs.^{13a}

A more detailed analysis of the fluid structure can be achieved through identification of polar/non-polar domains in the fluid microstructure.^{13a} The splitting between both domains for [BMIM]OS is based on the charge distribution analysis obtained from the above quantum mechanical

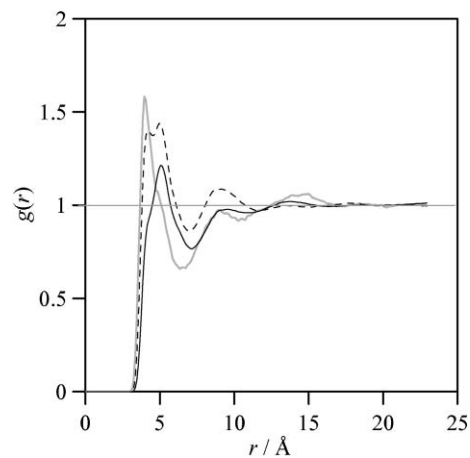


Fig. 12 Site-site radial distribution functions for [BMIM]OS at 318.15 K and 0.1 MPa. (—, grey) C_t–C_t, (—) C_s–C_s and (---) C_t–C_s.

calculations, and is shown in Fig. 13a. For [BMIM]⁺ the polar region is formed by the imidazolium ring together with the two methyl groups joined directly to the ring, whereas the non-polar region is formed by the three last carbons of the butyl chain. For OS⁻, the polar region comes from the sulfate group and the first carbon directly linked, whereas the non-polar region arises from the rest of the alkyl chain. Thus, inspection of the [BMIM]OS shows important non-polar regions that should have a noticeable effect on the fluid structure.

In Fig. 13b the final simulation box is plotted according to the coloring procedure for polar/non-polar domains. An analysis of Fig. 13b reveals that the fluid structure is dominated by non-polar domains that permeate the polar network. In spite of this, the polar regions seem to have a certain degree of continuity. Comparison of the literature results for [BMIM]PF₆⁻ with those reported for [BMIM]OS also reveal that for a small and almost spherical anion, such as PF₆⁻, the fluid structure is dominated by the polar domains.^{13a} However, for ILs with longer, non-spherical anions such as OS⁻, the non-polar domains disrupt the polar structure, because in this way the longer non-polar alkyl chains accommodate more efficiently. Thus, connectivity between non-polar fluid regions, structured through the cation alkyl chains but made up of anion and cation chains, is ubiquitous in [BMIM]OS together with a certain connection between polar domains, although strongly permeated by non-polar domains. In summary, the effect of alkyl chain length on perturbation of polar domains is greater for the anion than for the cation; this conclusion can also be drawn when comparing

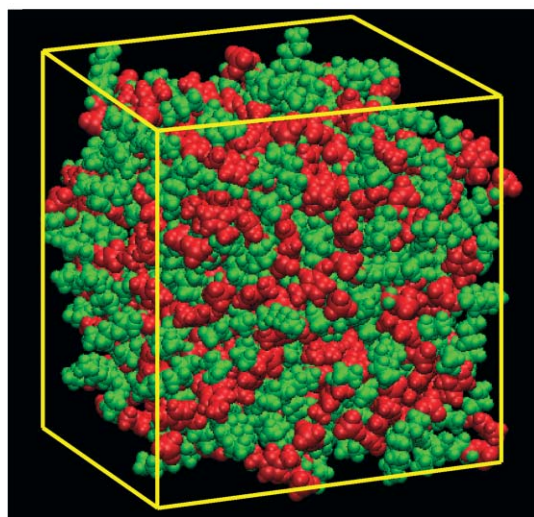
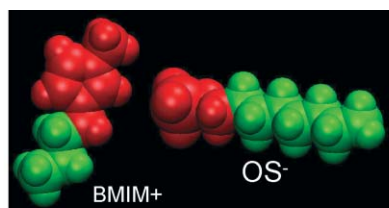


Fig. 13 (a) Coloring code to distinguish polar (red) and apolar (green) regions^{13a} in [BMIM]⁺ and OS⁻ ions; (b) snapshot of a simulation box containing 360 ions of [BMIM]OS after 200 ps of molecular dynamics simulation.

the results for 1-octyl-3-methyl imidazolium ILs with those for OS⁻ (with the same non-polar chain length).^{13a}

In the above analyses it is important to describe more in detail the polar domains structure. It has been reported that there is stronger spatial correlation between the tail groups of non-polar chains than with other groups in the same chains, but closer to the polar head of the corresponding ion.^{13a,43} In Fig. 14 the RDFs for different groups in the non-polar chain of the [BMIM]⁺ ion (around which the non-polar domains develop) are reported. It is clear that, as reported for other ILs,^{13a,43} the spatial correlation diminishes as one moves in the non-polar chain toward the polar head, with headgroups (C2) distributed relatively homogeneously. This structuring effect, termed liquid crystal-like structure,⁴³ is reinforced by longer anions such as OS⁻.

The self-diffusion coefficient, D , is calculated from the Einstein relation:

$$D = \frac{1}{6} \lim_{t \rightarrow \infty} \langle \Delta r(t)^2 \rangle \quad (13)$$

where the quantity in brackets is the mean square displacement, (msd). In Fig. 15 the msd for the cation and anion, calculated from the molecular dynamics simulation, are reported for the first 80 ps simulation. The diffusive behaviour of [BMIM]OS is very similar to those previously reported for other imidazolium ILs.^{13df,44} A linear behaviour of msd for $t > 40$ ps is observed in Fig. 15, providing the D coefficients from the slope of the linear fittings $D_{[BMIM]} = 5.3 \times 10^{-12}$ and $D_{OS} = 4.8 \times 10^{-12} \text{ m}^2 \text{ s}^{-1}$; hence, the self-diffusion coefficient of the fluid (calculated as $0.5(D_{[BMIM]} + D_{OS})$) is $D_{[BMIM]OS} = 5.1 \times 10^{-12} \text{ m}^2 \text{ s}^{-1}$ at 318.15 K and 0.1 MPa. This value is consistent with that reported for other [BMIM]⁺ containing ILs,^{13df} and is two orders of magnitude lower than those for common fluids such as water ($D_{\text{water},318.15\text{K}} = 3.601 \times 10^{-9} \text{ m}^2 \text{ s}^{-1}$).⁴⁵ This diffusion constant is reasonable in view of the large viscosity of [BMIM]OS. Viscosity, η , of [BMIM]OS at 318.15 K and 0.1 MPa is 197.0 mPa s (obtained from a polynomial fit of data reported by Wasserscheid *et al.*^{4a}) and for water $\eta = 0.596 \text{ mPa s}$.¹⁸ If the Stokes–Einstein relation applies to this system (eqn (14)) then the estimated value of the

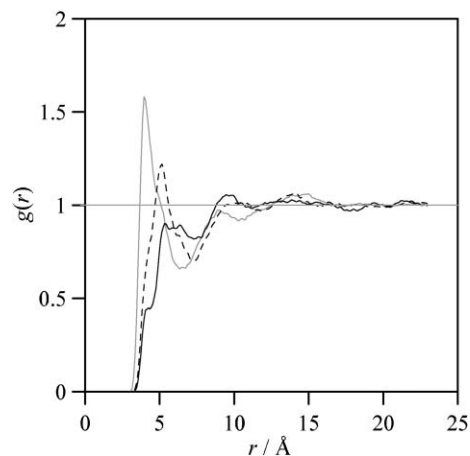


Fig. 14 Site-site radial distribution functions for [BMIM]OS at 318.15 K and 0.1 MPa. (—, grey) Ct–Ct; (---) C3–C3 and (—) C2–C2.

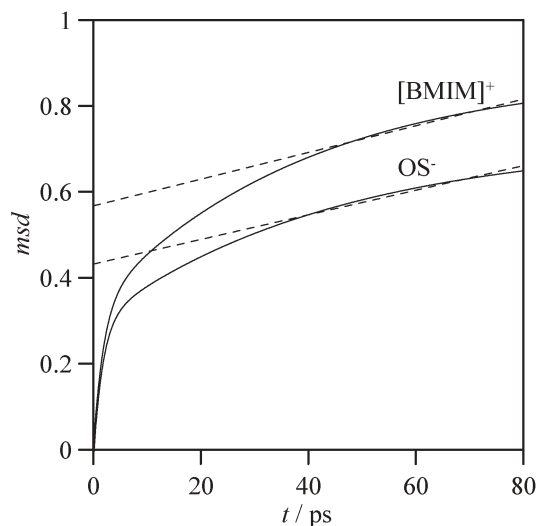


Fig. 15 (—) Center of mass mean square displacement, msd , of $[BMIM]^+$ and OS^- at 318.15 and 0.1 MPa. (---) Linear fits of the linear part of msd .

self-diffusion coefficient for $[BMIM]OS$ is $1.09 \times 10^{-11} \text{ m}^2 \text{ s}^{-1}$, which is very close to that computed through molecular dynamics simulations in spite of the simplifications beneath the Stokes–Einstein relation.

$$D_{[BMIM]OS} = D_{\text{water}} \frac{\eta_{\text{water}}}{\eta_{[BMIM]OS}} \quad (14)$$

Anyhow, the diffusion constant of $[BMIM]OS$ is lower compared to other $[BMIM]^+$ containing ILs; for instance, for $[BMIM]PF_6$, a value of $1.9 \times 10^{-11} \text{ m}^2 \text{ s}^{-1}$ for the cation at 313 K reported in the literature,^{13f} is almost four times greater than the value for the same cation in $[BMIM]OS$, in agreement with the larger viscosity of this IL.³² As for other ILs, for $[BMIM]OS$ the diffusion constant of the cation is greater than that of the anion.^{13d,f}

Conclusions

In this paper, a combined experimental and theoretical study on the structure and properties of the halogen-free $[BMIM]OS$ ionic liquid is reported. The measured PVT surface contributes both to a better understanding of ILs structure and to the setting of structure–property relationships, providing a fair set of thermophysical properties needed for industrial applications. The fluid behaviour shows a number of anomalies, such as the decrease of the α_P values with increasing temperature along isobars, or the increase in C_P as pressure is raised along isotherms, that can be related to the structural fluid complexity. The properties of the $[BMIM]OS$ IL make it a suitable candidate for a number of possible applications. The theoretical study shows the preferred interaction of the anion and cation through the C_r site of the imidazolium ring; also it presents a fluid structure dominated by the apolar domains formed by alkyl chains of cation and anion, which permeate the polar domains that are more reduced than in other imidazolium containing ILs with smaller, spherical anions. The structure and properties of the fluid are strongly conditioned

by the long anion alkyl chain that hampers the packaging, decreasing the density, and also slows down the ionic motion, as the low self-diffusion constants reveal.

Acknowledgements

The financial support by Junta de Castilla y León, Project BU10/03, and Ministerio de Educación y Ciencia, Project CTQ2005-06611/PPQ, (Spain) are gratefully acknowledged.

References

- 1 *Ionic Liquids: Industrial Applications for Green Chemistry*, ed. R. D. Rogers and K. R. Seddon, ACS Symp. Ser., vol. 818, ACS, Washington D.C., 2002.
- 2 (a) C. Pretti, C. Chiappe, D. Pieraccini, M. Gregori, F. Abramo, G. Monni and L. Intorre, *Green Chem.*, 2006, **8**, 238; (b) M. T. Garcia, N. Gathergood and P. J. Scammells, *Green Chem.*, 2005, **7**, 9; (c) N. Gathergood, M. T. Garcia and P. J. Scammells, *Green Chem.*, 2004, **6**, 166.
- 3 R. P. Swatloski, J. D. Holbrey and R. D. Rogers, *Green Chem.*, 2003, **5**, 361.
- 4 (a) P. Wasserscheid, R. van Hal and A. Bösmann, *Green Chem.*, 2002, **4**, 400; (b) J. D. Holbrey, W. M. Reichert, R. P. Swatloski, G. A. Broker, W. R. Pitner, K. R. Seddon and R. D. Rogers, *Green Chem.*, 2002, **4**, 407; (c) J. H. Davis and P. A. Fox, *Chem. Commun.*, 2003, 1209.
- 5 C. Hilgers and P. Wasserscheid, in *Ionic Liquids in Synthesis*, ed. P. Wasserscheid and T. Welton, Wiley–VCH, Weinheim, 2002.
- 6 (a) S. Wadud, R. Onodera, M. M. Or-Rashid and S. Oshiro, *Curr. Microbiol.*, 2001, **42**, 12; (b) N. Gathergood and P. J. Scammells, *Aust. J. Chem.*, 2002, **55**, 557.
- 7 (a) P. A. Suarez, S. Einof, J. E. L. Dullius, R. F. Souza and J. Dupont, *J. Chim. Phys. Phys.-Chim. Biol.*, 1998, **95**, 1626; (b) J. G. Huddleston, A. E. Visser, W. M. Reichert, H. D. Willauer, G. A. Broker and R. D. Rogers, *Green Chem.*, 2001, **3**, 156; (c) G. Law and P. R. Watson, *Langmuir*, 2001, **17**, 6138; (d) S. V. Dzuba and R. A. Barsch, *ChemPhysChem*, 2002, **3**, 161; (e) K. Kim, B. Shin, H. Lee and F. Ziegler, *Fluid Phase Equilib.*, 2004, **218**, 215.
- 8 (a) K. R. Cox, *Fluid Phase Equilib.*, 1993, **82**, 1; (b) R. Dohrn and O. Pföhl, *Fluid Phase Equilib.*, 2002, **15**, 194.
- 9 (a) R. Gomes de Azevedo, J. M. S. S. Esperanca, V. Najdanovic-Visak, Z. P. Visak, H. J. R. Guedes, M. Nunes da Ponte and L. P. N. Rebelo, *J. Chem. Eng. Data*, 2005, **50**, 997; (b) R. Gomes de Azevedo, J. M. S. S. Esperanca, J. Szydłowski, Z. P. Visak, P. F. Pires, H. J. R. Guedes and L. P. N. Rebelo, *J. Chem. Thermodyn.*, 2005, **37**, 888; (c) K. N. Marsh, J. A. Boxall and R. Lichtenthaler, *Fluid Phase Equilib.*, 2004, **219**, 93; (d) Z. Gu and J. F. Brennecke, *J. Chem. Eng. Data*, 2002, **47**, 339.
- 10 J. F. Brennecke and E. J. Magin, *AIChE J.*, 2001, **47**, 2384.
- 11 J. D. Holbrey and K. R. Seddon, *Clean Prod. Process.*, 1999, **1**, 223.
- 12 K. N. Marsh, A. Deev, A. C. T. Wu, E. Tran and A. Klamt, *Korean J. Chem. Eng.*, 2002, **19**, 357.
- 13 (a) J. N. A. Canongia and A. A. H. Pádua, *J. Phys. Chem. B*, 2006, **110**, 3330; (b) M. Bühl, A. Chaumont, R. Schurhammer and G. Wipff, *J. Phys. Chem. B*, 2005, **109**, 18591; (c) J. N. A. Canongia, J. Deschamps and A. A. H. Pádua, *J. Phys. Chem. B*, 2004, **108**, 2038; (d) Z. Liu, S. Huang and W. Wang, *J. Phys. Chem. B*, 2004, **108**, 12978; (e) M. Del Pópolo and G. A. Voth, *J. Phys. Chem. B*, 2004, **108**, 1744; (f) T. I. Morrow and E. J. Maginn, *J. Phys. Chem. B*, 2002, **106**, 12807.
- 14 R. Alcalde, S. Aparicio, B. García, M. J. Dávila and J. M. Leal, *New J. Chem.*, 2005, **29**, 817.
- 15 C. A. Cerdeiriña, J. A. Míguez, E. Carballo, C. A. Tovar, E. de la Puente and L. Romani, *Thermochim. Acta*, 2000, **347**, 37.
- 16 M. Zabransky, V. Ruzicka, V. Mayer and E. S. Domalski, *Heat Capacities of Liquids. Critical Review and Recommended Values*, *J. Phys. Chem. Ref. Data Monogr.*, 1996, **6**.
- 17 (a) B. García, S. Aparicio, R. Alcalde, M. J. Dávila and J. M. Leal, *Ind. Eng. Chem. Res.*, 2004, **43**, 3205; (b) S. Aparicio, B. García,

- R. Alcalde, M. J. Dávila and J. M. Leal, *J. Phys. Chem. B*, 2006, **110**, 6933.
- 18 *NIST Chemistry WebBook, NIST Standard Reference Database Number 69*, ed. P. J. Linstrom and W. G. Mallard, National Institute of Standards and Technology, Gaithersburg MD, June 2005, (<http://webbook.nist.gov>).
- 19 (a) O. Fandiño, A. S. Pensado, L. Lugo, E. R. López and J. Fernández, *Green Chem.*, 2005, **7**, 775; (b) R. Lundstrum, A. R. H. Goodwin, K. Hsu, M. Frels, D. R. Caudwell and J. P. M. Trusler, *J. Chem. Eng. Data*, 2005, **50**, 1377; (c) J. Bernhardt and H. Pauly, *J. Phys. Chem.*, 1980, **84**, 145; (d) S. J. Ashcroft, D. R. Booker and J. C. R. Turner, *J. Chem. Soc., Faraday Trans.*, 1990, **86**, 145.
- 20 M. J. Frisch, G. W. Trucks, H. B. Schlegel, G. E. Scuseria, M. A. Robb, J. R. Cheeseman, J. A. Montgomery, Jr., T. Vreven, K. N. Kudin, J. C. Burant, J. M. Millam, S. S. Iyengar, J. Tomasi, V. Barone, B. Mennucci, M. Cossi, G. Scalmani, N. Rega, G. A. Petersson, H. Nakatsuji, M. Hada, M. Ehara, K. Toyota, R. Fukuda, J. Hasegawa, M. Ishida, T. Nakajima, Y. Honda, O. Kitao, H. Nakai, M. Klene, X. Li, J. E. Knox, H. P. Hratchian, J. B. Cross, V. Bakken, C. Adamo, J. Jaramillo, R. Gomperts, R. E. Stratmann, O. Yazyev, A. J. Austin, R. Cammi, C. Pomelli, J. Ochterski, P. Y. Ayala, K. Morokuma, G. A. Voth, P. Salvador, J. J. Dannenberg, V. G. Zakrzewski, S. Dapprich, A. D. Daniels, M. C. Strain, O. Farkas, D. K. Malick, A. D. Rabuck, K. Raghavachari, J. B. Foresman, J. V. Ortiz, Q. Cui, A. G. Baboul, S. Clifford, J. Cioslowski, B. B. Stefanov, G. Liu, A. Liashenko, P. Piskorz, I. Komaromi, R. L. Martin, D. J. Fox, T. Keith, M. A. Al-Laham, C. Y. Peng, A. Nanayakkara, M. Challacombe, P. M. W. Gill, B. G. Johnson, W. Chen, M. W. Wong, C. Gonzalez and J. A. Pople, *GAUSSIAN 03 (Revision C.02)*, Gaussian, Inc., Wallingford, CT, 2004.
- 21 A. D. Becke, *Phys. Rev. A*, 1988, **38**, 3098.
- 22 C. Lee, W. Yang and R. G. Parr, *Phys. Rev. B: Condens. Matter Mater. Phys.*, 1988, **37**, 785.
- 23 A. D. Becke, *J. Chem. Phys.*, 1993, **98**, 5648.
- 24 V. Barone, *Chem. Phys. Lett.*, 1994, **226**, 392.
- 25 J. W. Ponder, *TINKER: Software tool for molecular design*, 4.2 edn, Washington University School of Medicine, 2004.
- 26 W. G. Hoover, *Phys. Rev. A*, 1985, **31**, 1695.
- 27 M. P. Allen and D. J. Tildesley, *Computer Simulation of Liquids*, Clarendon Press, Oxford, UK, 1989.
- 28 J. P. Rickaert, G. Ciccotti and H. J. Berendsen, *J. Comput. Phys.*, 1977, **23**, 327.
- 29 U. L. Essmann, M. L. Perera, T. Berkowitz, H. Darden, H. Lee and L. G. Pedersen, *J. Chem. Phys.*, 1995, **103**, 8577.
- 30 J. M. Martínez and L. Martínez, *J. Comput. Chem.*, 2003, **24**, 819.
- 31 K. J. Schweighofer, U. Essmann and M. Berkowitz, *J. Phys. Chem. B*, 1997, **101**, 3793.
- 32 J. Jacquemin, P. Husson, A. A. H. Padua and V. Mayer, *Green Chem.*, 2006, **8**, 172.
- 33 (a) L. Moens, D. M. Blake, D. L. Rudnicki and M. J. Hale, *J. Sol. Energy Trans. ASME*, 2003, **125**, 112; (b) B. Wu, R. G. Reddy and R. D. Rogers, *Proceedings of Solar Forum 2001*, Washington DC, 2001; (c) E. F. Camacho, M. Berenguel and F. R. Rubio, *Advanced control of solar plants*, Springer-Verlag, London, UK, 1997.
- 34 M. Deetlefs, K. R. Seddon and M. Shara, *New J. Chem.*, 2006, **30**, 317.
- 35 (a) A. M. Pereiro, F. Santamaría, E. Tojo, A. Rodríguez and J. Tojo, *J. Chem. Eng. Data*, 2006, **51**, 952; (b) K. S. Kim, B. K. Shin and H. Lee, *Korean J. Chem. Eng.*, 2004, **21**, 1010; (c) K. S. Kim, B. K. Shin, H. Lee and F. Ziegler, *Fluid Phase Equilib.*, 2004, **218**, 215.
- 36 E. C. Ihmehls and J. Gmehling, *Ind. Eng. Chem. Res.*, 2001, **40**, 4470.
- 37 I. Cibulka, *Fluid Phase Equilib.*, 1993, **89**, 1.
- 38 (a) T. I. Morrow and E. J. Maginn, *J. Phys. Chem. B*, 2002, **106**, 12807; (b) J. K. Shah, J. F. Brenneke and E. J. Maginn, *Green Chem.*, 2002, **4**, 112; (c) J. K. Shah and E. J. Maginn, *Fluid Phase Equilib.*, 2004, **222–223**, 195.
- 39 (a) L. P. N. Rebelo, V. Najdanovic-Visak, Z. P. Visak, M. Nunes da Ponte, J. Szydlowski, C. A. Cerdeiriña, J. Troncoso, L. Romani, J. M. S. S. Esperanca, H. J. R. Guedes and H. C. de Sousa, *Green Chem.*, 2004, **6**, 369–381; (b) M. Taravillo, V. G. Baonza, M. Cáceres and J. Nuñez, *J. Phys.: Condens. Matter*, 2003, **15**, 2979.
- 40 M. R. J. Dack, *Chem. Soc. Rev.*, 1975, **4**, 211.
- 41 (a) S. Y. Lee and S. B. Lee, *Chem. Commun.*, 2005, 3469; (b) K. Swiderski, A. McLean, C. M. Gordon and D. H. Vaughan, *Chem. Commun.*, 2004, 2178; (c) J. Laneta and M. Roth, *J. Phys. Chem. B*, 2004, **108**, 12444; (d) S. B. Lee, *J. Chem. Technol. Biotechnol.*, 2004, **80**, 133.
- 42 L. L. Williams, J. B. Rubin and H. W. Edwards, *Ind. Eng. Chem. Res.*, 2004, **43**, 4967.
- 43 Y. Wang and G. A. Voth, *J. Am. Chem. Soc.*, 2005, **127**, 12192.
- 44 C. J. Margulis, H. A. Stern and N. J. Berne, *J. Phys. Chem. B*, 2002, **106**, 12017.
- 45 M. Holz, S. R. Heil and A. Sacco, *Phys. Chem. Chem. Phys.*, 2000, **2**, 4740.

Imidazolium dialkylphosphates—a class of versatile, halogen-free and hydrolytically stable ionic liquids†

Esther Kuhlmann, Simone Himmler, Heidi Giebelhaus and Peter Wasserscheid*

Received 21st August 2006, Accepted 7th November 2006

First published as an Advance Article on the web 11th December 2006

DOI: 10.1039/b611974c

In this article a systematic and detailed study on the synthesis and the properties of dialkylphosphate ionic liquids is presented. This class of halogen-free ionic liquids is easily available in high quality and great variability by direct alkylation of nucleophiles, such as 1-methylimidazole, 1-ethylimidazole, 1-butylimidazole and 1-(2-methoxyethyl)-imidazole with different trialkylphosphates, such as trimethylphosphate, triethylphosphate or tributylphosphate. In general, these dialkylphosphate ionic liquids were found to display very attractive physico-chemical properties with great technical potential, especially in low temperature (<200 °C) applications with water present. For this specific application area, the materials described here clearly show superior properties compared with alkylsulfate ionic liquids due to their obviously much higher hydrolytic stability.

Introduction

Ionic liquids (ILs) have attracted a great deal of scientific attention during the last decade due to their often unique combination of physico-chemical properties. In particular, their exceptionally low vapour pressure at ambient temperatures makes them interesting substitutes for many applications for which the volatility of traditional organic solvents causes problems. Today, the areas of ionic liquid use range from electrochemistry^{1,2} and analytical^{3–5} to synthesis,^{6,7} transition metal catalysis⁸ and biocatalysis.⁹ Of particular interest, for short term industrial applications, is the use of ionic liquids as engineering or process fluids. Examples of this rapidly expanding area include their use in separation technologies (extractive distillation^{10,11} and extraction¹¹), as heat transfer agents,¹² as liquid pistons in gas compressors¹³ or as performance additives in paints.¹⁴ In all these applications the unique properties of the ionic liquids improve product performance or process efficiency (in particular with respect to energy consumption). However, for all these applications it is of critical importance that the ionic liquid does not decompose under the operating conditions. For most of the above-mentioned applications these conditions include a certain amount of water present in the operating system which makes the hydrolytic stability of the applied ionic liquid an issue of the greatest practical relevance. Apart from this, the viscosity of the ionic liquid is an important selection criterion, as the latter determines the rate of all heat and mass transport processes and heavily affects stirring, mixing and pumping operations.

Owing to their hydrolytic instability,¹⁵ the application of hexafluorophosphate and tetrafluoroborate ionic liquids is limited to strictly anhydrous conditions. Water-stable fluorinated ionic liquids, such as bis(trifluoromethylsulfonyl) imides,¹⁶ nonafluorobutane sulfonates¹⁷ or tris(pentafluoroethyl)trifluorophosphates,¹⁸ may be used regularly in many academic laboratories nowadays but their technical application is seriously limited by the high price of the respective anions.

In this context, the intense quest for low-viscosity, halogen-free ionic liquids that has been seen over the last three years is understandable. Published examples include alkyl- and aryl-sulfonates,¹⁹ alkyl- and oligoethersulfates²⁰ and organoborate-based anions.²¹ In particular, the hydrophilic ionic liquid [EMIM][EtSO₄] received great attention, becoming one of the first commercial “bulk” ionic liquids (available on a ton-scale) with a complete set of registration data available saying that it is a non-toxic chemical with no labelling required.²² Another class of intrinsically halogen- and halide-free ionic liquids that has attracted our special interest in recent times is based on dialkylphosphate ions. Ammonium dialkylphosphates were first described in 1952.²³ The alkylation products of pyridine and trialkylphosphates were described to be salts with very low melting points in 1989.²⁴ Recently Cytec filed patents on the synthesis of imidazolium-based dialkylphosphate ionic liquids.²⁵

In this paper we aim to present for the first time a detailed study on this new class of ionic liquids. A great variety of these ionic liquids have been synthesized and characterized, paying particular attention to those properties of practical relevance.

Results and discussion

Synthesis of phosphate based ILs

To develop an optimized synthetic protocol for the alkylation of 1-alkylimidazole compounds with trimethylphosphate, the kinetics of the synthesis of 1,3-dimethylimidazolium

Lehrstuhl für Chemische Reaktionstechnik der Friedrich-Alexander-Universität Erlangen-Nürnberg, Egerlandstrasse 3, Erlangen D-91058, Germany. E-mail: wasserscheid@crt.cbi.uni-erlangen.de; Fax: +499131-8527421; Tel: +499131-8527420

† Electronic supplementary information (ESI) available: 1-Vinylimidazole hydrogenation—additional kinetic information. See DOI: 10.1039/b611974c.



Scheme 1 Alkylation of 1-*N*-methylimidazole with trimethylphosphate.

dimethylphosphate ([MMIM][Me₂PO₄]) (see Scheme 1) were studied in detail.

The synthesis was carried out batch-wise in a round bottomed flask, in which isothermal conditions were maintained. The conversion was monitored by ¹H-NMR spectroscopy over time. To suppress further reaction after sampling, all samples were immediately cooled to room temperature (at this temperature no alkylation reaction is observed). To investigate the reaction order with respect to each of the two starting materials, 1-methylimidazole ([MIM]) and trimethylphosphate ([Me₃PO₄]) individually, two different experiments were carried out in which the initial concentration of one reactant was much larger than the concentration of the other reactant. Thus, the concentration of the reactant in large excess remained almost constant during the reaction, and the reaction order with respect to the other, stoichiometrically-limited compound could be investigated. The rate of depletion was found to be 1st order with respect to both starting materials, MIM and Me₃PO₄. Therefore the overall reaction order was found to be second order according to the following equation:

$$-\frac{d[\text{MIM}]}{dt} = k[\text{MIM}][\text{Me}_3\text{PO}_4]$$

A comparison of these findings with kinetic studies by Jess *et al.*, which describe the alkylation of 1-methylimidazole with butyl chloride, reveals that both alkylation reactions are similar with respect to reaction order.²⁶

If the initial concentrations of the reactants are chosen to be equal the former equation can be rewritten as

$$-\frac{d[\text{MIM}]}{dt} = k[\text{MIM}]^2$$

With [MIM] = [MIM]₀ at *t* = 0, the second order integrated rate equation reads

$$\frac{1}{[\text{MIM}]} - \frac{1}{[\text{MIM}]_0} = kt$$

To determine the activation energy of this quaternation reaction, experiments at 50 °C, 60 °C, 70 °C and 80 °C were carried out. Fig. 1 shows the rate constants *k* for the different temperatures.

The Arrhenius plot, based on the experiments at 50–80 °C, is shown in Fig. 2.

From the slope of the Arrhenius plot, an activation energy of 77 kJ mol⁻¹ can be deduced, and the collision factor was calculated to be 4.076 × 10⁷ l mol⁻¹ s⁻¹. This value is slightly lower than those given in literature for similar alkylation reactions, *i.e.* 87 kJ mol⁻¹ for the synthesis of [BMIM]Cl with a collision factor of 2.131 × 10¹⁰ l mol⁻¹ s⁻¹. The kinetic investigation showed that the synthesis of the dimethylimidazolium dimethylphosphate is slower than the synthesis of 1-butyl-3-methylimidazolium chloride.²⁶

As the alkylation strength of the trialkylphosphates decreases with increasing length of the alkyl chain, the reaction

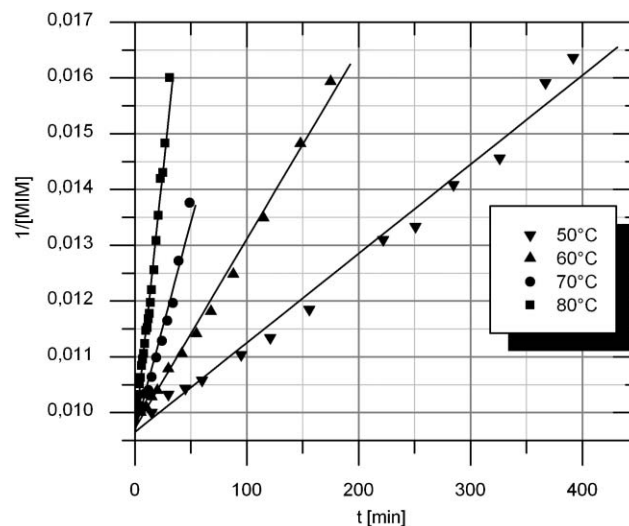


Fig. 1 Rate constant of the [MMIM][Me₂PO₄] synthesis based on experiments at different temperatures; (▼) reaction at 50 °C, (▲) reaction at 60 °C, (●) reaction at 70 °C, (■) reaction at 80 °C.

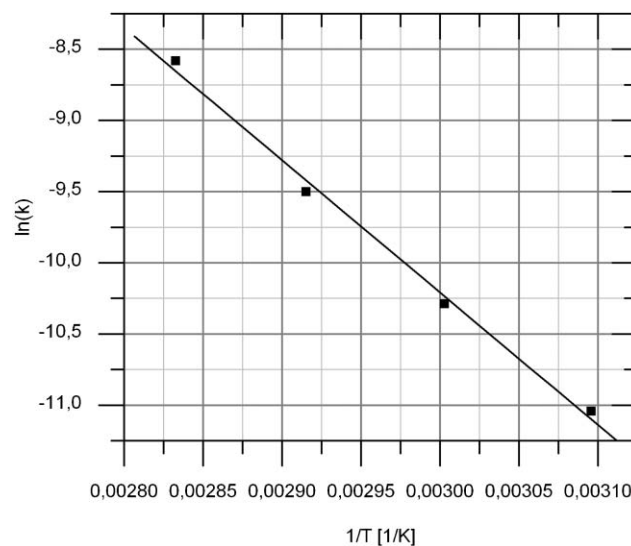


Fig. 2 Arrhenius plot of the rate constant *k* of the [MMIM][Me₂PO₄] synthesis.

rates become significantly slower, in the cases when triethylphosphate and tributylphosphate are used as the alkylation agent. Therefore the reaction conditions were modified step-wise to guarantee full conversion, even with these less-reactive alkylating agents. While full conversion could be achieved in the alkylation of 1-alkylimidazoles with trimethylphosphates within 24 h at 80 °C, 120 °C for three days was necessary to complete the reaction with triethylphosphate. For tributylphosphate as the alkylating agent, the conditions had to be set to 160 °C for three days to obtain full conversion of both reactants, in a stoichiometric reaction mixture. Further details concerning the synthesis, as well as the spectroscopic data for all the ionic liquids synthesized, can be found in the Experimental.

Table 1 1,3-dialkylimidazolium dialkylphosphate ionic liquids investigated in this study

Dimethylphosphates	Diethylphosphates	Dibutylphosphates
[MMIM][Me ₂ PO ₄]	[EMIM][Et ₂ PO ₄]	[BMIM][Bu ₂ PO ₄]
[EMIM][Me ₂ PO ₄]	[EEIM][Et ₂ PO ₄]	[BEIM][Bu ₂ PO ₄]
[BMIM][Me ₂ PO ₄]	[BEIM][Et ₂ PO ₄]	[BBIM][Bu ₂ PO ₄]
[HMIM][Me ₂ PO ₄]	[HEIM][Et ₂ PO ₄]	[BHIM][Bu ₂ PO ₄]
[OMIM][Me ₂ PO ₄]	[OEIM][Et ₂ PO ₄]	[BOIM][Bu ₂ PO ₄]
[(MeEG)MIM][Me ₂ PO ₄]		
[(MeEG ₂)MIM][Me ₂ PO ₄]		
[(MeEG ₃)MIM][Me ₂ PO ₄]		

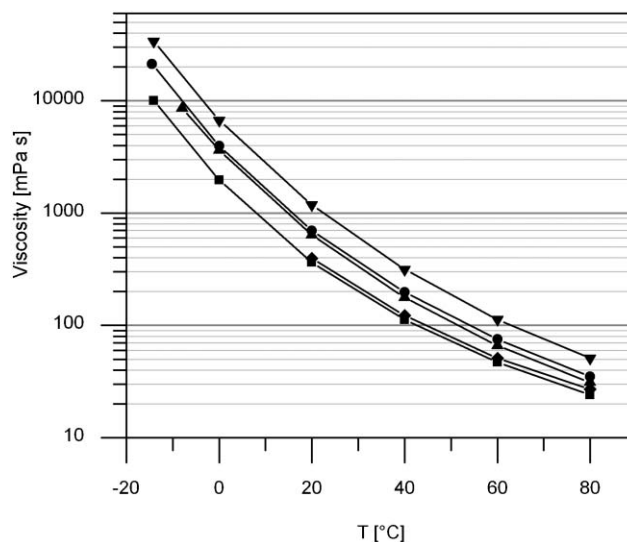
Synthesis of [EMIM][Me₂PO₄]*—*preparation of the precursor 1-ethylimidazole

In our quest for dialkylphosphate ionic liquids with low viscosity, we proposed that [EMIM][Me₂PO₄] would be an extremely interesting candidate. The [EMIM] cation is known for producing low-viscosity ionic liquids in combination with many anions, probably due to the fact that it provides the ideal combination of low symmetry and weak van der Waals interactions.²⁷ Since mixed trialkylphosphate alkylation agents are difficult to obtain synthetically, we opted for the alkylation of 1-ethylimidazole with trimethylphosphate to synthesize this liquid. However, 1-ethylimidazole is not currently commercially available. Therefore we decided to synthesize this compound ourselves by the hydrogenation of 1-*N*-vinylimidazole. The latter is an industrially-important chemical used as hardener for epoxy resins, in polymer and resin-bound foundry core production and in the oil industry.²⁸

The catalytic hydrogenation of 1-vinylimidazole was carried out without solvent. Pd on charcoal proved to be the most suitable hydrogenation catalyst in our study with a 100% conversion in a reaction time of less than 4 h (0.375 wt% Pd on charcoal, 30 bar hydrogen, 25 °C). Interestingly, the hydrogenation proceeds under these conditions in a highly selective manner, with no detectable product in the GC analysis after filtration of the catalyst except 1-ethylimidazole. More details concerning the vinylimidazole hydrogenation including results of our kinetic studies are found in the supporting information.

Physico-chemical properties

In this study, our aim was to explore the class of dialkylphosphate ionic liquids in much more detail—mainly with regard to their physico-chemical properties which are the key selection criteria for many applications. In particular, viscosity

**Fig. 3** Experimental viscosities of the dialkylimidazolium dimethylphosphates as a function of temperature: (■) [MMIM][Me₂PO₄], (◆) [EMIM][Me₂PO₄], (●) [BMIM][Me₂PO₄], (▲) [HMIM][Me₂PO₄], (▼) [OMIM][Me₂PO₄].

and density data should be addressed. An overview of the ionic liquids under investigation is given in Table 1.

Viscosity. All tested dialkylphosphates were found to be Newtonian liquids. All data given in Table 2 are average values, determined from 20 different shearing rates between 0.1 s⁻¹ and 100 s⁻¹ at 20 °C. Since it is known that the water content in ionic liquids can reduce the ionic liquid's viscosity significantly,²⁹ all ionic liquids were dried under reduced pressure to a defined water content (for details see Table 4 in the Experimental) before the viscosities were measured.

The viscosity measurements show (see Table 2) that ionic liquids of the general type [RMIM][Me₂PO₄] display increasing viscosity as the length of the alkyl chain, R, increases. This general trend is to be expected as it is consistent with the observations made for ionic liquids [RMIM]X, with other anions X.²⁷ We were surprised, however, to observe that [EMIM][Me₂PO₄] displayed a slightly higher viscosity than the highly symmetrical [MMIM][Me₂PO₄]. Fig. 3 presents an overview of the temperature-dependent viscosities of these 1-alkyl-3-methylimidazolium dimethylphosphates.

In contrast to the 1-alkyl-3-methylimidazolium dimethylphosphates, increasing chain-length of the *N*-imidazolium

Table 2 Experimental viscosities (η) of the dialkylimidazolium dialkylphosphates at 20 °C

Dialkylimidazolium dimethylphosphates		Dialkylimidazolium diethylphosphates		Dialkylimidazolium dibutylphosphates	
	η /mPa s		η /mPa s		η /mPa s
[MMIM][Me ₂ PO ₄]	363	[EMIM][Et ₂ PO ₄]	457	[BMIM][Bu ₂ PO ₄]	1896
[EMIM][Me ₂ PO ₄]	394	[EEIM][Et ₂ PO ₄]	518	[BEIM][Bu ₂ PO ₄]	2377
[BMIM][Me ₂ PO ₄]	696	[BEIM][Et ₂ PO ₄]	1115	[BBIM][Bu ₂ PO ₄]	2691
[HMIM][Me ₂ PO ₄]	638	[HEIM][Et ₂ PO ₄]	1068	[BHIM][Bu ₂ PO ₄]	3413
[OMIM][Me ₂ PO ₄]	1182	[OEIM][Et ₂ PO ₄]	1212	[BOIM][Bu ₂ PO ₄]	3797
[(MeEG)MIM][Me ₂ PO ₄]	769				
[(MeEG ₂)MIM][Me ₂ PO ₄]	398				
[(MeEG ₃)MIM][Me ₂ PO ₄]	324				

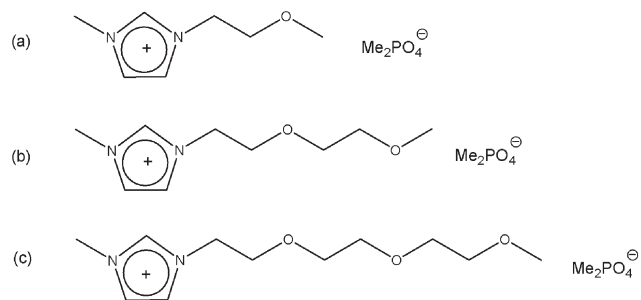


Fig. 4 Structures of the synthesized PEG-substituted ionic liquids: (a) [(MeEG)MIM][Me₂PO₄], (b) [(MeEG₂)MIM][Me₂PO₄], (c) [(MeEG₃)MIM][Me₂PO₄].

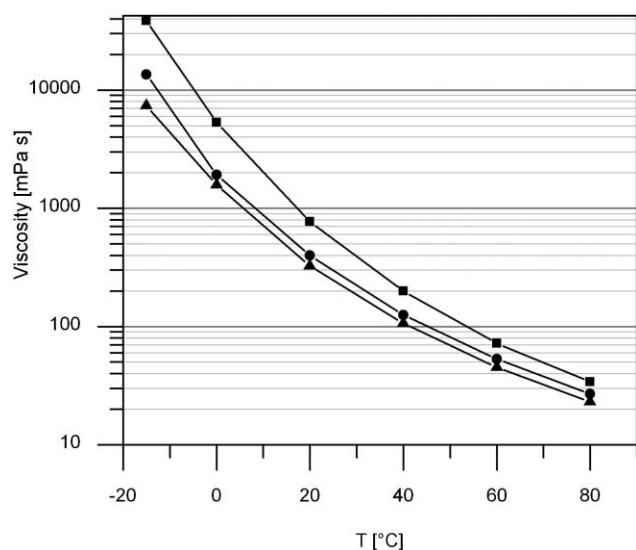


Fig. 5 Experimental viscosities of the PEG-functionalized dialkylimidazolium dimethylphosphates as a function of temperature: (■) [(MeEG)MIM][Me₂PO₄], (●) [(MeEG₂)MIM][Me₂PO₄], (▲) [(MeEG₃)MIM][Me₂PO₄].

substituent leads to decreasing viscosity of the ionic liquid for *N*-imidazolium substituents carrying ethylene glycol units! This surprising and very interesting effect has been demonstrated for the ionic liquid structures displayed in Fig. 4.

Fig. 5 illustrates this general finding with a comparison of the temperature-dependent viscosities of these ethylene glycol-functionalized imidazolium dimethylphosphates.

Furthermore, it is important to note that the ionic liquids with ethylene glycol-functionalized cations show generally very

low viscosities compared with the imidazolium cations with a similar length of side chain but no ether groups. For example [(MeEG₃)MIM][Me₂PO₄] shows only 324 mPa s at 20 °C compared with 1182 mPa s for [OMIM][Me₂PO₄], which has an even shorter side chain on the imidazolium nitrogen.

We assume that this effect is due to the increased flexibility of the ether side chain. “Shielding” effects of the positively charged imidazolium core, through interaction with the side chain’s oxygen atoms, can also not be excluded. In this context, it might also be of interest that the viscosity-decreasing effect of the ether-functionalized side chains is known both for phase transfer catalysts and surfactants,³⁰ as well as for oligoethersulfate ionic liquids.²⁰

Melting point. All synthesised ionic liquids were liquid at room temperature. However the exact melting points could not be determined due to the fact that these ionic liquids are supercooled melts at the temperature ranges investigated.

Density. The densities of the synthesised ionic liquids were measured at room temperature (Table 3). The quality of the ionic liquids under investigation was the same as for the viscosity measurements.

As known from previous work,^{31–34} the density of ionic liquids decreases with increasing chain-length at the imidazolium nitrogen.

Thermal and hydrolytic stability. As already pointed out in the introduction, our main intention in further developing dialkylphosphate ionic liquids was to access a class of hydrophilic ionic liquids, with high thermal and hydrolytic stability, that could be obtained by direct alkylation from cheap alkylation agents. It was therefore a key aspect of our study to investigate the long-term thermal stability (TGA measurement over 20 h at 120 °C) and hydrolytic stability of the dialkylphosphate ionic liquids, using the well-established, bulk ionic liquid [EMIM][EtSO₄] as a benchmark.

For the long-term stability measurements, [MMIM][Me₂PO₄] and [OEIM][Et₂PO₄] were selected to get some additional information about the alkyl chain-length on the thermal stability. While the short-chain ionic liquid [MMIM][Me₂PO₄] was found to be stable over the 20 h TGA experiment (<0.01% weight loss over 20 h), [OEIM][Et₂PO₄] showed a slight weight loss (0.018% per h; 0.36% over 20 h) over time. In contrast to the results for the dialkylphosphates, [EMIM][EtSO₄] was found to degrade

Table 3 Experimental densities of the dialkylimidazolium dialkylphosphates

Dialkylimidazolium dimethylphosphates		Dialkylimidazolium diethylphosphates		Dialkylimidazolium dibutylphosphates	
$\rho/\text{kg m}^{-3}$		$\rho/\text{kg m}^{-3}$		$\rho/\text{kg m}^{-3}$	
[MMIM][Me ₂ PO ₄]	1.26	[EMIM][Et ₂ PO ₄]	1.14	[BMIM][Bu ₂ PO ₄]	1.04
[EMIM][Me ₂ PO ₄]	1.21	[EEIM][Et ₂ PO ₄]	1.12	[BEIM][Bu ₂ PO ₄]	1.03
[BMIM][Me ₂ PO ₄]	1.18	[BEIM][Et ₂ PO ₄]	1.08	[BBIM][Bu ₂ PO ₄]	1.02
[HMIM][Me ₂ PO ₄]	1.11	[HEIM][Et ₂ PO ₄]	1.06	[BHIM][Bu ₂ PO ₄]	1.00
[OMIM][Me ₂ PO ₄]	1.08	[OEIM][Et ₂ PO ₄]	1.04	[BOIM][Bu ₂ PO ₄]	0.98
[(MeEG)MIM][Me ₂ PO ₄]	1.23				
[(MeEG ₂)MIM][Me ₂ PO ₄]	1.21				
[(MeEG ₃)MIM][Me ₂ PO ₄]	1.19				

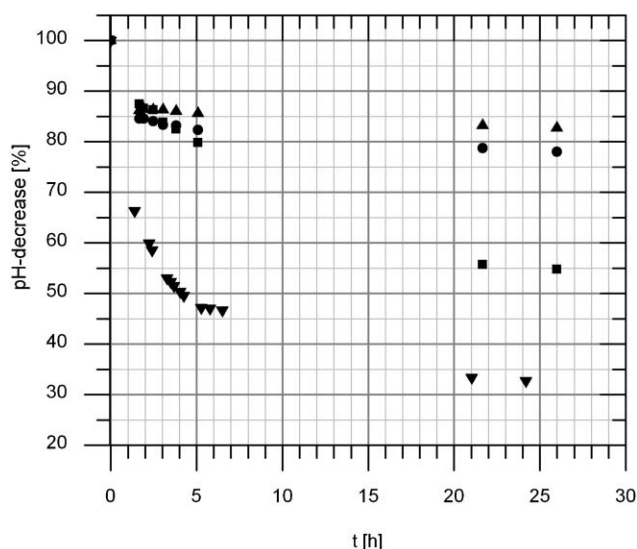


Fig. 6 pH-value–time–profile for (■) [MMIM][Me₂PO₄], (●) [OMIM][Me₂PO₄], (▲) [OEIM][Et₂PO₄], (▼) [EMIM][EtSO₄]. The pH value is given as a percentage of the starting value. Experimental conditions: molar ratio ionic liquid:water = 1:1000 at 95 °C.

much faster under identical conditions, with 9% of the ionic liquid lost after 20 h at 120 °C (0.45% weight loss per h).

The hydrolytic stabilities of the representative [MMIM][Me₂PO₄], [OMIM][Me₂PO₄] and [OEIM][Et₂PO₄] were studied in comparison with [EMIM][EtSO₄]. For this study, the alteration of pH values was recorded *vs.* time for mixtures of water and [EMIM][EtSO₄], [MMIM][Me₂PO₄], [OMIM][Me₂PO₄] and [OEIM][Et₂PO₄], respectively, with a molar ratio of ionic liquid:water = 1:1000 at 95 °C (Fig. 6).

These experiments impressively demonstrate the significantly higher hydrolytic stability of dialkylphosphate ionic liquids *vs.* the ethylsulfate melt. The quick loss in pH in the first two hours, as can be seen in Fig. 6, is due to traces of trialkylphosphate, which is extremely sensitive towards hydrolysis. Among the different dialkylphosphates, the results suggest a higher stability for the ionic liquids with hydrophobic cations, [OMIM][Me₂PO₄] and [OEIM][Et₂PO₄]. After the first two hours (pH loss due to traces of alkylating agent), the pH decreases only slightly (pH shift ~10% within 25 hours). This stability is higher than that of [MMIM][Me₂PO₄] (pH shift of 45% within 25 hours). The most drastic hydrolytic instability was observed for [EMIM][EtSO₄] with a pH shift of >68% over 25 hours.

Experimental

Chemicals

1-Vinylimidazole was received from BASF AG. The catalyst Pd/C was provided by Degussa AG. All other reagents used were purchased from Aldrich, Fluka, Riedel-de Haën, Rohm and Haas Co. and Solvent Innovation GmbH with commercial grades >99%.

General synthetic procedures

Synthesis of 1-ethylimidazole. The hydrogenation of 1-vinylimidazole to 1-ethylimidazole was carried out in a 600 ml

autoclave from Parr (autoclave 4843; pressure range 0–200 bars) with an external cooling bath using a gas intake stirrer. The stirring speed was kept at 1200 rpm for all experiments. 400 g of 1-vinylimidazole were mixed with 0.25 wt% or 0.375 wt% of catalyst (Pd/C 5% on activated charcoal). The autoclave was flushed three times with helium before hydrogen pressure was applied. The reaction was carried out at room temperature semi-batchwise with respect to hydrogen. Therefore the hydrogen pressure was always kept at 30 bars. The course of reaction was monitored *via* gas chromatography. After full conversion was reached the autoclave was flushed again three times with hydrogen and the slurry was filtered to remove the catalyst. Afterwards, 1-ethylimidazole was distilled at 85 °C and yielded a clear colourless liquid with a purity >99.5%.

Synthesis of dimethylphosphate ionic liquids. 1.0 equiv. of an amine was weighed into a dry Schlenk flask and 1.0 equiv. of trimethylphosphate was added dropwise to ensure isothermal reaction conditions. The reaction mixture was stirred for 24 h at 80 °C under an argon atmosphere.

Yield: [MMIM][Me₂PO₄] >99%, [EMIM][Me₂PO₄] >99%, [BMIM][Me₂PO₄] >99%, [HMIM][Me₂PO₄] >99%, [OMIM][Me₂PO₄] 99%, [(MeEG)MIM][Me₂PO₄] 99%, [(MeEG₂)MIM][Me₂PO₄] 99%, [(MeEG₃)MIM][Me₂PO₄] >99%.

Synthesis of diethylphosphate ionic liquids. 1.0 equiv. of an amine was weighed into a dry Schlenk flask and 1.0 equiv. of triethylphosphate was added dropwise to ensure isothermal reaction conditions. The reaction mixture was stirred for 3 days at 120 °C under an argon atmosphere.

Yield: [EMIM][Et₂PO₄] >99%, [EEM][Et₂PO₄] >99%, [BEIM][Et₂PO₄] >99%, [EHIM][Et₂PO₄] >99%, [EOIM][Et₂PO₄] 99%.

Synthesis of dibutylphosphate ionic liquids. 1.0 equiv. of an amine was weighed into a dry Schlenk flask and 1.0 equiv. of tributylphosphate was added dropwise to ensure isothermal reaction conditions. The reaction mixture was stirred for 3 d at 160 °C under an argon atmosphere.

Yield: [BMIM][Bu₂PO₄] >99%, [BEIM][Bu₂PO₄] >99%, [BBIM][Bu₂PO₄] 99%, [BHIM][Bu₂PO₄] 99%, [BOIM][Bu₂PO₄] 99%.

Synthesis of PEG-imidazoles. A solution of 2.5 equiv. sodium hydroxide, dissolved in the same amount of distilled water, a catalytic amount of hexadecyltrimethylammonium hydrogensulfate and 1.0 equiv. of a PEG-alcohol was prepared. 1.1 equiv. of benzenesulfonyl chloride were added dropwise at 70 °C (if necessary an ice bath was used to keep the temperature at 70 °C). The reaction mixture was refluxed for 3 h at 70 °C. The precipitate was removed by filtration and the aqueous solution was extracted four times with dichloromethane. The combined organic phases were washed once with distilled water, concentrated to a small volume and dried under reduced pressure to yield the PEG–benzenesulfonate. A solution of 3.0 equiv. sodium hydroxide, dissolved in the same amount of distilled water, a catalytic amount of hexadecyltrimethylammonium hydrogensulfate and 1.0 equiv. of

imidazole was prepared. 1.1 equiv. of PEG–benzenesulfonate was added dropwise at 70 °C (if necessary an ice bath was used to keep the temperature at 70 °C). Viscous mixtures were diluted with small amounts of toluene. The reaction mixture was stirred overnight at room temperature and then for 2 h at 70 °C. Water was added to the reaction mixture until the precipitate was dissolved. The aqueous solution was extracted four times with dichloromethane and the combined organic phases were concentrated to a small volume and distilled under reduced pressure to yield the final product.

Yield: (MeEG)IM 64%, (MeEG₂)IM 31%, (MeEG₃)IM 66%.

Kinetic experiments

For the kinetic investigations the reactions were carried out batch-wise at standard pressure in an isothermal round bottom flask using 1.0 equiv. of 1-methylimidazole and 1.0 equiv. of trimethylphosphate as reactants. Temperatures were varied from 50 °C to 80 °C in steps of 10 °C. The conversion to [MMIM][Me₂PO₄] was analysed by ¹H-NMR spectroscopy. All NMR spectra were recorded on a JEOL ECX 400 MHz spectrometer in CDCl₃.

Gas chromatography

GC-data was recorded on a Varian 8900 gas chromatograph with a Varian CP 8410 autoinjector and a Factor Four Capillary Column VF-1 ms 15 m × 0.25 mm id DF-0.25 (CO 8907). The temperature of injection was 270 °C and the temperature program was as follows: 1 min Iso 100 °C; 200 °C with 10 °C min⁻¹; 1 min Iso 200 °C. Hydrogen was used as the carrier gas with a volume flow of 1 ml min⁻¹. Acetone was used as the solvent.

NMR spectroscopy

NMR spectra were recorded on a JEOL ECX +400 spectrometer (¹H: 400 MHz, ¹³C: 100 MHz, ³¹P: 162 MHz). Deuterated solvents (CDCl₃ and d₆-DMSO) were used as internal standards. The chemical shifts are noted in parts per million (ppm), the coupling constants in Hz. The data is stated in the following way:

1,3-Dimethylimidazolium dimethylphosphate [MMIM][Me₂PO₄]. ¹H-NMR (400 MHz, d₆-DMSO, [ppm]) δ = 3.28 (6H, d, P(OCH₃)₂, *J* = 10.4 Hz), 3.87 (6H, s, H₃CNCHNCH₃), 7.85 (2H, m, NCHCHN), 9.66 (1H, s NCHN).

¹³C-NMR (100 MHz, d₆-DMSO, [ppm]) δ = 36.0 (H₃CNCHNCH₃), 51.8 (P(OCH₃)₂), 124.0 (NCHCHN), 138.3 (NCHN).

1-Ethyl-3-methylimidazolium dimethylphosphate [EMIM][Me₂PO₄]. ¹H-NMR (400 MHz, d₆-DMSO, [ppm]) δ = 1.22 (3H, t, NCH₂CH₃), 3.24 (6H, d, P(OCH₃)₂, *J* = 10.4 Hz), 3.72 (3H, s, NCH₃), 4.05 (2H, q, NCH₂CH₃, *J* = 7.3 Hz), 7.35 (2H, m, NCHCHN), 10.15 (1H, s, NCHN).

¹³C-NMR (100 MHz, d₆-DMSO, [ppm]) δ = 15.1 (NCH₂CH₃), 35.5 (NCH₃), 43.9 (NCH₂CH₃), 51.2 (P(OCH₃)₂), 121.9 (NCHCHN), 123.5 (NCHCHN), 136.7 (NCHN).

1-*n*-Butyl-3-methylimidazolium dimethylphosphate [BMIM][Me₂PO₄]. ¹H-NMR (400 MHz, d₆-DMSO, [ppm]) δ = 0.86 (3H, t, NCH₂CH₂CH₂CH₃, *J* = 7.4 Hz), 1.23 (2H, sex, NCH₂CH₂CH₂CH₃, *J* = 7.4 Hz), 1.75 (2H, p, NCH₂CH₂CH₂CH₃, *J* = 7.4 Hz), 3.28 (6H, d, P(OCH₃)₂, *J* = 10.4 Hz), 3.88 (3H, s, NCH₃), 4.19 (2H, t, NCH₂CH₂CH₂CH₃, *J* = 7.2 Hz), 7.85 (1H, s, NCHCHN), 7.94 (1H, s, NCHCHN), 9.77 (1H, s, NCHN).

¹³C-NMR (100 MHz, d₆-DMSO, [ppm]) δ = 13.2 (NCH₂CH₂CH₂CH₃), 18.7 (NCH₂CH₂CH₂CH₃), 31.4 (NCH₂CH₂CH₂CH₃), 35.5 (NCH₃), 48.3 (NCH₂CH₂CH₂CH₃), 51.2 (P(OCH₃)₂), 122.2 (NCHCHN), 123.5 (NCHCHN), 137.2 (NCHN).

1-*n*-Hexyl-3-methylimidazolium dimethylphosphate [HMIM][Me₂PO₄]. ¹H-NMR (400 MHz, d₆-DMSO, [ppm]) δ = 0.83 (3H, t, NCH₂CH₂CH₂CH₂CH₂CH₃, *J* = 6.7 Hz), 1.23 (6H, m, NCH₂CH₂CH₂CH₂CH₂CH₃), 1.77 (2H, p, NCH₂CH₂CH₂CH₂CH₂CH₃, *J* = 7.5 Hz), 3.28 (6H, d, P(OCH₃)₂, *J* = 10.3 Hz), 3.88 (3H, s, NCH₃), 4.19 (2H, t, NCH₂CH₂CH₂CH₂CH₂CH₃, *J* = 7.2 Hz), 7.84 (1H, s, NCHCHN), 7.92 (1H, s, NCHCHN), 9.74 (1H, s, NCHN).

¹³C-NMR (100 MHz, d₆-DMSO, [ppm]) δ = 13.7 (NCH₂CH₂CH₂CH₂CH₂CH₃), 21.8 (NCH₂CH₂CH₂CH₂CH₂CH₃), 25.1 (NCH₂CH₂CH₂CH₂CH₂CH₃), 29.4 (NCH₂CH₂CH₂CH₂CH₂CH₃), 30.5 (NCH₂CH₂CH₂CH₂CH₂CH₃), 35.5 (NCH₃), 48.6 (NCH₂CH₂CH₂CH₂CH₂CH₃), 51.2 (P(OCH₃)₂), 122.2 (NCHCHN), 123.5 (NCHCHN), 137.1 (NCHN).

1-Methyl-3-*n*-octylimidazolium dimethylphosphate [OMIM][Me₂PO₄]. ¹H-NMR (400 MHz, d₆-DMSO, [ppm]) δ = 0.82 (3H, t, NCH₂CH₂CH₂CH₂CH₂CH₂CH₂CH₃, *J* = 7.0 Hz), 1.21 (10H, m, NCH₂CH₂CH₂CH₂CH₂CH₂CH₂CH₃), 1.77 (2H, p, NCH₂CH₂CH₂CH₂CH₂CH₂CH₃, *J* = 7.4 Hz), 3.29 (6H, d, P(OCH₃)₂, *J* = 10.3 Hz), 3.88 (3H, s, NCH₃), 4.19 (2H, t, NCH₂CH₂CH₂CH₂CH₂CH₂CH₃, *J* = 7.2 Hz), 7.85 (1H, s, NCHCHN), 7.93 (1H, s, NCHCHN), 9.76 (1H, s, NCHN).

¹³C-NMR (100 MHz, d₆-DMSO, [ppm]) δ = 13.8 (NCH₂CH₂CH₂CH₂CH₂CH₂CH₃), 22.0 (NCH₂CH₂CH₂CH₂CH₂CH₂CH₃), 25.4 (NCH₂CH₂CH₂CH₂CH₂CH₂CH₃), 25.3 (NCH₂CH₂CH₂CH₂CH₂CH₂CH₃), 28.4 (NCH₂CH₂CH₂CH₂CH₂CH₂CH₃), 29.3 (NCH₂CH₂CH₂CH₂CH₂CH₂CH₃), 31.1 (NCH₂CH₂CH₂CH₂CH₂CH₂CH₃), 35.5 (NCH₃), 48.6 (NCH₂CH₂CH₂CH₂CH₂CH₂CH₃), 51.1 (P(OCH₃)₂), 122.2 (NCHCHN), 123.5 (NCHCHN), 136.9 (NCHN).

1-Ethyl-3-methylimidazolium diethylphosphate [EMIM][Et₂PO₄]. ¹H-NMR (400 MHz, d₆-DMSO, [ppm]) δ = 1.05 (6H, t, (OCH₂CH₃)₂, *J* = 7.1 Hz), 1.39 (3H, t, NCH₂CH₃, *J* = 7.3 Hz), 3.65 (4H, p, P(OCH₂CH₃)₂, *J* = 7.1 Hz), 3.90 (3H, s, NCH₃), 4.24 (2H, q, NCH₂CH₃, *J* = 7.3 Hz), 7.89 (1H, s, NCHCHN), 8.01 (1H, s, NCHCHN), 9.91 (1H, s, NCHN).

¹³C-NMR (100 MHz, d₆-DMSO, [ppm]) δ = 15.1 (NCH₂CH₃), 16.6 (P(OCH₂CH₃)₂), 35.5 (NCH₃), 43.9 (NCH₂CH₃), 58.9 (P(OCH₂CH₃)₂), 121.9 (NCHCHN), 123.5 (NCHCHN), 136.9 (NCHN).

1,3-Diethylimidazolium diethylphosphate [EEIM][Et₂PO₄]. ¹H-NMR (400 MHz, d₆-DMSO, [ppm]) δ = 1.06 (6H, t, P(OCH₂CH₃)₂, *J* = 7.2 Hz), 1.42 (6H, t, CH₃CH₂-NCHNCH₂CH₃, *J* = 7.2 Hz), 3.61 (4H, p, P(OCH₂CH₃)₂, *J* = 7.0 Hz), 4.21 (4H, q, CH₃CH₂NCHNCH₂CH₃, *J* = 7.3 Hz), 7.85 (2H, m, NCHCHN), 9.58 (1H, s, NCHN).

¹³C-NMR (100 MHz, d₆-DMSO, [ppm]) δ = 15.1 (NCH₂CH₃), 16.6 (P(OCH₂CH₃)₂), 43.9 (NCH₂CH₃), 59.0 (P(OCH₂CH₃)₂), 122.0 (NCHCHN), 136.3 (NCHN).

1-*n*-Butyl-3-ethylimidazolium diethylphosphate [BEIM][Et₂PO₄]. ¹H-NMR (400 MHz, d₆-DMSO, [ppm]) δ = 0.87 (3H, t, NCH₂CH₂CH₂CH₃, *J* = 7.4 Hz), 1.06 (6H, t, P(OCH₂CH₃)₂, *J* = 7.1 Hz), 1.23 (2H, sex, NCH₂CH₂-CH₂CH₃, *J* = 7.5 Hz), 1.41 (3H, t, NCH₂CH₃), 1.77 (2H, p, NCH₂CH₂CH₂CH₃, *J* = 7.4 Hz), 3.63 (4H, p, P(OCH₂CH₃)₂, *J* = 7.0 Hz), 4.23 (4H, m, CH₃CH₂NCHNCH₂CH₂CH₂CH₃), 7.95 (2H, m, NCHCHN), 9.95 (1H, s, NCHN).

¹³C-NMR (100 MHz, d₆-DMSO, [ppm]) δ = 13.2 (NCH₂CH₂CH₂CH₃), 15.0 (NCH₂CH₃), 16.6 (P(OCH₂-CH₃)₂), 18.7 (NCH₂CH₂CH₂CH₃), 31.3 (NCH₂CH₂-CH₂CH₃), 44.0 (NCH₂CH₃), 48.3 (NCH₂CH₂CH₂CH₃), 58.9 (P(OCH₂CH₃)₂), 122.1 (NCHCHN), 122.3 (NCHCHN) 136.5 (NCHN).

1-Ethyl-3-*n*-hexylimidazolium diethylphosphate [EHIM][Et₂PO₄]. ¹H-NMR (400 MHz, d₆-DMSO, [ppm]) δ = 0.81 (3H, m, NCH₂CH₂CH₂CH₂CH₂CH₃), 1.06 (6H, t, P(OCH₂-CH₃)₂, *J* = 7.1 Hz), 1.22 (6H, m, NCH₂CH₂CH₂CH₂-CH₂CH₃), 1.40 (3H, t, NCH₂CH₃, *J* = 7.3 Hz), 1.78 (2H, p, NCH₂CH₂CH₂CH₂CH₂CH₃, *J* = 6.9 Hz), 3.65 (4H, p, P(OCH₂CH₃)₂, *J* = 7.0 Hz), 4.24 (4H, m, CH₃CH₂NCHNC-H₂CH₂CH₂CH₂CH₂CH₃), 7.99 (2H, m, NCHCHN), 10.02 (1H, s, NCHN).

¹³C-NMR (100 MHz, d₆-DMSO, [ppm]) δ = 13.7 (NCH₂CH₂CH₂CH₂CH₂CH₃), 15.1 (NCH₂CH₃), 16.6 (P(OCH₂CH₃)₂), 21.8 (NCH₂CH₂CH₂CH₂CH₂CH₃), 25.1 (NCH₂CH₂CH₂CH₂CH₂CH₃), 29.3 (NCH₂CH₂CH₂CH₂-CH₂CH₃), 30.5 (NCH₂CH₂CH₂CH₂CH₂CH₃), 44.0 (NCH₂CH₃), 48.6 (NCH₂CH₂CH₂CH₂CH₂CH₃), 58.9 (P(OCH₂CH₃)₂), 122.0 (NCHCHN), 122.3 (NCHCHN) 136.4 (NCHN).

1-Ethyl-3-*n*-octylimidazolium diethylphosphate [EOIM][Et₂PO₄]. ¹H-NMR (400 MHz, d₆-DMSO, [ppm]) δ = 0.82 (3H, t, NCH₂CH₂CH₂CH₂CH₂CH₂CH₂CH₃, *J* = 6.8 Hz), 1.06 (6H, t, P(OCH₂CH₃)₂, *J* = 7.1 Hz), 1.22 (10H, m, NCH₂-CH₂CH₂CH₂CH₂CH₂CH₂CH₃), 1.41 (3H, t, NCH₂CH₃, *J* = 7.3 Hz), 1.78 (2H, p, NCH₂CH₂CH₂CH₂CH₂CH₂CH₃, *J* = 6.8 Hz), 3.65 (4H, p, P(OCH₂CH₃)₂, *J* = 7.0 Hz), 4.24 (4H, m, CH₃CH₂NCHNCH₂CH₂CH₂CH₂CH₂CH₂CH₂CH₃), 7.98 (2H, m, NCHCHN), 10.00 (1H, s, NCHN).

¹³C-NMR (100 MHz, d₆-DMSO, [ppm]) δ = 13.8 (NCH₂CH₂CH₂CH₂CH₂CH₂CH₃), 15.0 (NCH₂CH₃), 16.6 (P(OCH₂CH₃)₂), 21.9 (NCH₂CH₂CH₂CH₂CH₂-CH₂CH₃), 25.4 (NCH₂CH₂CH₂CH₂CH₂CH₂CH₃), 28.3 (NCH₂CH₂CH₂CH₂CH₂CH₂CH₃), 28.4 (NCH₂CH₂-CH₂CH₂CH₂CH₂CH₃), 29.3 (NCH₂CH₂CH₂CH₂CH₂-CH₂CH₃), 31.1 (NCH₂CH₂CH₂CH₂CH₂CH₂CH₃),

44.0 (NCH₂CH₃), 48.6 (NCH₂CH₂CH₂CH₂CH₂CH₂CH₂-CH₃), 59.0 (P(OCH₂CH₃)₂), 122.0 (NCHCHN), 122.3 (NCHCHN) 136.1 (NCHN).

1-*n*-Butyl-3-methylimidazolium dibutylphosphate [BMIM][Bu₂PO₄]. ¹H-NMR (400 MHz, d₆-DMSO, [ppm]) δ = 0.86 (9H, m, NCH₂CH₂CH₂CH₃, P(OCH₂CH₂CH₂CH₃)₂), 1.76 (2H, p, NCH₂CH₂CH₂CH₃, *J* = 7.3 Hz), 3.57 (4H, q, P(OCH₂CH₂CH₂CH₃)₂, *J* = 6.5 Hz), 3.88 (3H, s, NCH₃), 4.19 (2H, t, CH₃CH₂CH₂CH₂N, *J* = 7.2 Hz), 7.81 (1H, m, NCHCHN), 7.89 (1H, m, NCHCHN), 9.74 (1H, s, NCHN).

¹³C-NMR (100 MHz, d₆-DMSO, [ppm]) δ = 13.2 (NCH₂CH₂CH₂CH₃), 13.6 (P(OCH₂CH₂CH₂CH₃)₂), 18.6 (NCH₂CH₂CH₂CH₃), 18.7 (P(OCH₂CH₂CH₂CH₃)₂), 31.4 (NCH₂CH₂CH₂CH₃), 32.6 (P(OCH₂CH₂CH₂CH₃)₂), 35.5 (NCH₃), 48.2 (NCH₂CH₂CH₂CH₃), 63.1 (P(OCH₂CH₂-CH₂CH₃)₂), 122.2 (NCHCHN), 123.5 (NCHCHN), 137.3 (NCHN).

1-*n*-Butyl-3-ethylimidazolium dibutylphosphate [BEIM][Bu₂PO₄]. ¹H-NMR (400 MHz, CDCl₃, [ppm]) δ = 0.74 (6H, t, P(OCH₂CH₂CH₂CH₃)₂, *J* = 7.4 Hz), 0.79 (3H, t, NCH₂CH₂CH₂CH₃, *J* = 7.4 Hz), 1.22 (6H, m, NCH₂CH₂-CH₂CH₃, P(OCH₂CH₂CH₂CH₃)₂), 1.43 (7H, m, NCH₂CH₃, P(OCH₂CH₂CH₂CH₃)₂), 1.72 (2H, p, NCH₂CH₂CH₂CH₃, *J* = 7.6 Hz), 3.71 (4H, q, P(OCH₂CH₂CH₂CH₃)₂, *J* = 6.4 Hz), 4.2 (2H, t, NCH₂CH₂CH₂CH₃, *J* = 7.4 Hz), 4.25 (2H, q, CH₃CH₂N, *J* = 7.5 Hz), 7.29 (1H, m, NCHCHN), 7.45 (1H, m, NCHCHN), 10.71 (1H, s, NCHN).

¹³C-NMR (100 MHz, CDCl₃, [ppm]) δ = 13.2 (NCH₂CH₂CH₂CH₃), 13.6 (P(OCH₂CH₂CH₂CH₃)₂), 15.3 (NCH₂CH₃), 18.8 (NCH₂CH₂CH₂CH₃), 19.2 (P(OCH₂CH₂-CH₂CH₃)₂), 31.9 (NCH₂CH₂CH₂CH₃), 32.8 (P(OCH₂CH₂-CH₂CH₃)₂), 44.6 (NCH₂CH₃), 49.2 (NCH₂CH₂CH₂CH₃), 64.4 (P(OCH₂CH₂CH₂CH₃)₂), 121.4 (NCHCHN), 121.5 (NCHCHN), 138.8 (NCHN).

1,3-Di-*n*-butylimidazolium dibutylphosphate [BBIM][Bu₂PO₄]. ¹H-NMR (400 MHz, d₆-DMSO, [ppm]) δ = 0.86 (12H, m, CH₃CH₂CH₂CH₂NCHNCH₂CH₂CH₂CH₃, P(OCH₂CH₂-CH₂CH₃)₂), 1.26 (8H, m, CH₃CH₂CH₂CH₂NCHNCH₂-CH₂CH₂CH₃, P(OCH₂CH₂CH₂CH₃)₂), 1.44 (4H, p, P(OCH₂CH₂CH₂CH₃)₂, *J* = 7.0 Hz), 1.77 (4H, p, CH₃CH₂CH₂CH₂NCHNCH₂CH₂CH₂CH₃, *J* = 7.3 Hz), 3.63 (4H, q, P(OCH₂CH₂CH₂CH₃)₂, *J* = 6.5 Hz), 4.21 (4H, t, CH₃CH₂CH₂CH₂NCHNCH₂CH₂CH₂CH₃, *J* = 7.2 Hz), 7.92 (2H, m, NCHCHN), 9.85 (1H, s, NCHN).

¹³C-NMR (100 MHz, d₆-DMSO, [ppm]) δ = 13.1 (NCH₂CH₂CH₂CH₃), 13.6 (P(OCH₂CH₂CH₂CH₃)₂), 18.6 (NCH₂CH₂CH₂CH₃), 18.7 (P(OCH₂CH₂CH₂CH₃)₂), 31.4 (NCH₂CH₂CH₂CH₃), 32.7 (P(OCH₂CH₂CH₂CH₃)₂), 48.3 (NCH₂CH₂CH₂CH₃), 63.1 (P(OCH₂CH₂CH₂CH₃)₂), 122.4 (NCHCHN), 137.0 (NCHN).

1-*n*-Butyl-3-*n*-hexylimidazolium dibutylphosphate [BHIM][Bu₂PO₄]. ¹H-NMR (400 MHz, d₆-DMSO, [ppm]) δ = 0.85 (12H, m, CH₃CH₂CH₂CH₂NCHNCH₂CH₂CH₂CH₂CH₂CH₃, P(OCH₂CH₂CH₂CH₃)₂), 1.25 (12H, m, CH₃CH₂CH₂CH₂-NCHNCH₂CH₂CH₂CH₂CH₂CH₃, P(OCH₂CH₂CH₂CH₃)₂),

1.43 (4H, p, $\text{P}(\text{OCH}_2\text{CH}_2\text{CH}_2\text{CH}_3)_2$), $J = 6.93$ Hz), 1.78 (4H, m, $\text{CH}_3\text{CH}_2\text{-CH}_2\text{CH}_2\text{NCHNCH}_2\text{CH}_2\text{CH}_2\text{CH}_2\text{CH}_2\text{CH}_3$), 3.60 (4H, q, $\text{P}(\text{OCH}_2\text{CH}_2\text{CH}_2\text{CH}_3)_2$), $J = 6.4$ Hz), 4.23 (4H, t, $\text{CH}_3\text{CH}_2\text{CH}_2\text{CH}_2\text{NCHNCH}_2\text{CH}_2\text{CH}_2\text{CH}_2\text{CH}_2\text{CH}_3$), $J = 7.0$ Hz), 7.97 (2H, m, *NCHCHN*), 10.04 (1H, s, *NCHN*).

^{13}C -NMR (100 MHz, d_6 -DMSO, [ppm]) $\delta = 13.2$ ($\text{NCH}_2\text{-CH}_2\text{CH}_2\text{CH}_3$), 13.7 ($\text{NCH}_2\text{CH}_2\text{CH}_2\text{CH}_2\text{CH}_2\text{CH}_3$), 13.7 ($\text{P}(\text{OCH}_2\text{CH}_2\text{CH}_2\text{CH}_3)_2$), 18.6 ($\text{NCH}_2\text{CH}_2\text{CH}_2\text{CH}_3$), 18.7 ($\text{P}(\text{OCH}_2\text{CH}_2\text{CH}_2\text{CH}_3)_2$), 21.8 ($\text{NCH}_2\text{CH}_2\text{CH}_2\text{CH}_2\text{CH}_2\text{-CH}_3$), 25.1 ($\text{NCH}_2\text{CH}_2\text{CH}_2\text{CH}_2\text{CH}_2\text{CH}_3$), 29.2 ($\text{NCH}_2\text{CH}_2\text{-CH}_2\text{CH}_2\text{CH}_2\text{CH}_3$), 30.4 ($\text{NCH}_2\text{CH}_2\text{CH}_2\text{CH}_2\text{CH}_2\text{CH}_3$), 31.2 ($\text{NCH}_2\text{CH}_2\text{CH}_2\text{CH}_3$), 32.7 ($\text{P}(\text{OCH}_2\text{CH}_2\text{CH}_2\text{CH}_3)_2$), 48.4 ($\text{NCH}_2\text{CH}_2\text{CH}_2\text{CH}_3$), 48.7 ($\text{NCH}_2\text{CH}_2\text{CH}_2\text{CH}_2\text{CH}_2\text{CH}_3$), 63.0 ($\text{P}(\text{OCH}_2\text{CH}_2\text{CH}_2\text{CH}_3)_2$), 122.3 (*NCHCHN*), 136.4 (*NCHN*).

1-*n*-Butyl-3-*n*-octylimidazolium dibutylphosphate [BOIM] [Bu₂PO₄]. ^1H -NMR (400 MHz, d_6 -DMSO, [ppm]) $\delta = 0.84$ (12H, m, $\text{CH}_3\text{CH}_2\text{CH}_2\text{CH}_2\text{NCHNCH}_2\text{CH}_2\text{CH}_2\text{CH}_2\text{CH}_2\text{-CH}_2\text{CH}_2\text{CH}_3$, $\text{P}(\text{OCH}_2\text{CH}_2\text{CH}_2\text{CH}_3)_2$), 1.24 (16H, m, $\text{CH}_3\text{CH}_2\text{CH}_2\text{CH}_2\text{NCHNCH}_2\text{CH}_2\text{CH}_2\text{CH}_2\text{CH}_2\text{CH}_2\text{CH}_2\text{CH}_3$, $\text{P}(\text{OCH}_2\text{CH}_2\text{CH}_2\text{CH}_3)_2$), 1.43 (4H, p, $\text{P}(\text{OCH}_2\text{CH}_2\text{CH}_2\text{CH}_3)_2$), $J = 6.9$ Hz), 1.78 (4H, m, $\text{CH}_3\text{CH}_2\text{CH}_2\text{CH}_2\text{NCHNCH}_2\text{-CH}_2\text{CH}_2\text{CH}_2\text{CH}_2\text{CH}_2\text{CH}_2\text{CH}_3$), 3.60 (4H, q, $\text{P}(\text{OCH}_2\text{CH}_2\text{-CH}_2\text{CH}_3)_2$), $J = 6.4$ Hz), 4.22 (4H, t, $\text{CH}_3\text{CH}_2\text{CH}_2\text{CH}_2\text{-NCHNCH}_2\text{CH}_2\text{CH}_2\text{CH}_2\text{CH}_2\text{CH}_2\text{CH}_3$), $J = 7.0$ Hz), 7.96 (2H, m, *NCHCHN*), 10.02 (1H, s, *NCHN*).

^{13}C -NMR (100 MHz, d_6 -DMSO, [ppm]) $\delta = 13.2$ ($\text{NCH}_2\text{CH}_2\text{CH}_2\text{CH}_3$), 13.6 ($\text{NCH}_2\text{CH}_2\text{CH}_2\text{CH}_2\text{CH}_2\text{CH}_2\text{-CH}_2\text{CH}_3$), 13.8 ($\text{P}(\text{OCH}_2\text{CH}_2\text{CH}_2\text{CH}_3)_2$), 18.6 ($\text{NCH}_2\text{CH}_2\text{-CH}_2\text{CH}_3$), 18.7 ($\text{P}(\text{OCH}_2\text{CH}_2\text{CH}_2\text{CH}_3)_2$), 22.0 ($\text{NCH}_2\text{CH}_2\text{CH}_2\text{CH}_2\text{CH}_2\text{CH}_2\text{CH}_2\text{CH}_3$), 25.4 ($\text{NCH}_2\text{CH}_2\text{-CH}_2\text{CH}_2\text{CH}_2\text{CH}_2\text{CH}_3$), 28.2 ($\text{NCH}_2\text{CH}_2\text{CH}_2\text{CH}_2\text{-CH}_2\text{CH}_2\text{CH}_2\text{CH}_3$), 28.4 ($\text{NCH}_2\text{CH}_2\text{CH}_2\text{CH}_2\text{CH}_2\text{CH}_2\text{CH}_2\text{-CH}_3$), 29.3 ($\text{NCH}_2\text{CH}_2\text{CH}_2\text{CH}_2\text{CH}_2\text{CH}_2\text{CH}_3$), 31.0 ($\text{NCH}_2\text{CH}_2\text{CH}_2\text{CH}_2\text{CH}_2\text{CH}_2\text{CH}_3$), 31.3 ($\text{NCH}_2\text{CH}_2\text{-CH}_2\text{CH}_3$), 32.7 ($\text{P}(\text{OCH}_2\text{CH}_2\text{CH}_2\text{CH}_3)_2$), 48.4 ($\text{NCH}_2\text{CH}_2\text{-CH}_2\text{CH}_3$), 48.6 ($\text{NCH}_2\text{CH}_2\text{CH}_2\text{CH}_2\text{CH}_2\text{CH}_2\text{CH}_3$), 63.1 ($\text{P}(\text{OCH}_2\text{CH}_2\text{CH}_2\text{CH}_3)_2$), 122.3 (*NCHCHN*), 136.5 (*NCHN*).

1-(2-Methoxyethyl)-3-methylimidazolium dimethylphosphate [(MeEG)MIM][Me₂PO₄]. ^1H -NMR (400 MHz, d_6 -DMSO, [ppm]) $\delta = 3.24$ (1H, s, $\text{NCH}_2\text{CH}_2\text{OCH}_3$), 3.28 (6H, d, $\text{P}(\text{OCH}_3)_2$), $J = 10.3$ Hz), 3.69 (2H, m, $\text{NCH}_2\text{CH}_2\text{OCH}_3$), 3.89 (3H, s, H_3CN), 4.40 (2H, t, $\text{NCH}_2\text{CH}_2\text{OCH}_3$), $J = 5.0$ Hz), 7.81 (1H, s, *NCHCHN*), 7.89 (1H, m, *NCHCHN*), 9.66 (1H, s, *NCHN*).

^{13}C -NMR (100 MHz, d_6 -DMSO, [ppm]) $\delta = 35.5$ (NCH_3), 48.4 ($\text{NCH}_2\text{CH}_2\text{OCH}_3$), 51.2 ($\text{P}(\text{OCH}_3)_2$), 57.9 ($\text{NCH}_2\text{CH}_2\text{-OCH}_3$), 69.6 ($\text{NCH}_2\text{CH}_2\text{OCH}_3$), 122.6 (*NCHCHN*), 123.4 (*NCHCHN*), 137.4 (*NCHN*).

1-(2-(2-Methoxyethoxy)ethyl)-3-methylimidazolium dimethylphosphate [(MeEG₂)MIM][Me₂PO₄]. ^1H -NMR (400 MHz, d_6 -DMSO, [ppm]) $\delta = 3.21$ (1H, s, $\text{NCH}_2\text{CH}_2\text{-OCH}_2\text{CH}_2\text{OCH}_3$), 3.29 (6H, d, $\text{P}(\text{OCH}_3)_2$), $J = 10.4$ Hz), 3.40 (2H, m, $\text{NCH}_2\text{CH}_2\text{OCH}_2\text{CH}_2\text{OCH}_3$), 3.54 (2H, m, $\text{NCH}_2\text{CH}_2\text{OCH}_2\text{CH}_2\text{OCH}_3$), 3.76 (2H, t, $\text{NCH}_2\text{CH}_2\text{-OCH}_2\text{CH}_2\text{OCH}_3$), $J = 5.0$ Hz), 3.88 (3H, s, H_3CN), 4.37 (2H,

t, $\text{NCH}_2\text{CH}_2\text{OCH}_2\text{CH}_2\text{OCH}_3$), $J = 5.0$ Hz), 7.78 (2H, s, *NCHCHN*), 9.43 (1H, s, *NCHN*).

^{13}C -NMR (100 MHz, d_6 -DMSO, [ppm]) $\delta = 35.5$ (NCH_3), 48.5 ($\text{NCH}_2\text{CH}_2\text{OCH}_2\text{CH}_2\text{OCH}_3$), 51.2 ($\text{P}(\text{OCH}_3)_2$), 58.0 ($\text{NCH}_2\text{CH}_2\text{OCH}_2\text{CH}_2\text{OCH}_3$), 68.1 ($\text{NCH}_2\text{CH}_2\text{OCH}_2\text{CH}_2\text{-OCH}_3$), 69.2 ($\text{NCH}_2\text{CH}_2\text{OCH}_2\text{CH}_2\text{OCH}_3$), 71.0 ($\text{NCH}_2\text{CH}_2\text{-OCH}_2\text{CH}_2\text{OCH}_3$), 122.6 (*NCHCHN*), 123.3 (*NCHCHN*), 137.3 (*NCHN*).

1-(2-(2-(2-Methoxyethoxy)ethoxy)ethyl)-3-methylimidazolium dimethylphosphate [(MeEG₃)MIM][Me₂PO₄]. ^1H -NMR (400 MHz, d_6 -DMSO, [ppm]) $\delta = 3.23$ (3H, s, $\text{NCH}_2\text{CH}_2\text{-OCH}_2\text{CH}_2\text{OCH}_2\text{CH}_2\text{OCH}_3$), 3.27 (6H, d, $\text{P}(\text{OCH}_3)_2$), $J = 10.3$ Hz), 3.48 (8H, m, $\text{NCH}_2\text{CH}_2\text{OCH}_2\text{CH}_2\text{OCH}_2\text{CH}_2\text{-OCH}_3$), 3.77 (2H, t, $\text{NCH}_2\text{CH}_2\text{OCH}_2\text{CH}_2\text{OCH}_2\text{CH}_2\text{OCH}_3$), $J = 5.0$ Hz), 3.88 (3H, s, H_3CN), 4.38 (2H, t, $\text{NCH}_2\text{CH}_2\text{OCH}_2\text{-CH}_2\text{OCH}_2\text{CH}_2\text{OCH}_3$), $J = 5.0$ Hz), 7.79 (1H, m, *NCHCHN*), 7.82 (1H, m, *NCHCHN*), 9.48 (1H, s, *NCHN*).

^{13}C -NMR (100 MHz, d_6 -DMSO, [ppm]) $\delta = 35.5$ (NCH_3), 48.5 ($\text{NCH}_2\text{CH}_2\text{OCH}_2\text{CH}_2\text{OCH}_2\text{CH}_2\text{OCH}_3$), 51.1 ($\text{P}(\text{OCH}_3)_2$), 58.0 ($\text{NCH}_2\text{CH}_2\text{OCH}_2\text{CH}_2\text{OCH}_2\text{CH}_2\text{OCH}_3$), 68.1 ($\text{NCH}_2\text{CH}_2\text{OCH}_2\text{CH}_2\text{OCH}_2\text{CH}_2\text{OCH}_3$), 69.4 ($\text{NCH}_2\text{-CH}_2\text{OCH}_2\text{CH}_2\text{OCH}_2\text{CH}_2\text{OCH}_3$), 69.7 ($\text{NCH}_2\text{CH}_2\text{OCH}_2\text{-CH}_2\text{OCH}_2\text{CH}_2\text{OCH}_3$), 122.6 (*NCHCHN*), 123.3 (*NCHCHN*), 137.2 (*NCHN*).

Determination of water content

After synthesis, the ionic liquids were dried overnight under vacuum (<1 mbar) at 70 °C. The water content was determined by coulometric Karl-Fischer titration using a Metrohm 756 KF Coulometer with a Hydranal[®] Coulomat AG reagent.

Viscosity

The viscosities of the novel ionic liquids were measured under an argon atmosphere using a MCR 100 rheometer from Anton Paar, Graz. Temperature control was maintained by a peltier element. Viscosity measurements were always carried out with samples of defined water content that was determined directly prior to the measurement by coulometric Karl-Fischer titration.

Density

Density was measured at room temperature in a Blaubrand pycnometer with a defined volume of 5.330 ml according to DIN ISO 3507.

Thermal stability

Thermogravimetric measurements were conducted on a Netzsch TG 209 with the samples placed in an open Al₂O₃ pan and heated from room temperature up to 120 °C at a heating rate of 10 K min⁻¹ under a protective gas atmosphere. The loss of weight was detected over 20 h at 120 °C.

Hydrolytic stability

For the determination of the hydrolytic stability, samples of ionic liquids with molecularly defined water content

(1:1000 ratio of ionic liquid:water) were stirred at 95 °C while the pH values were recorded using a Schott CG 842 pH meter.

Conclusions

The results of our study demonstrate that low-melting dialkylphosphates indeed form an interesting and versatile class of halogen-free ionic liquids. The melts are readily accessible by a single reaction step from trialkylphosphates and 1-alkylimidazoles, as demonstrated for eighteen different representatives. However, reaction times to complete nucleophile conversion are significantly longer compared with *N*-alkylimidazole alkylation with diethyl sulfate or butyl chloride, due to the comparatively lower reactivity of the trialkylphosphates.

A detailed kinetic study of the reaction of 1-methylimidazole with trimethylphosphate revealed the synthesis to be of second order in total (first order with respect to each starting material), the activation energy was determined to be 77 kJ mol⁻¹. Furthermore, a way to prepare 1-*N*-ethylimidazole, the precursor needed for [EMIM][Me₂PO₄] synthesis, was devised. The compound was synthesised in excellent yield by hydrogenation of the industrially-available compound 1-vinylimidazole.

Regarding the physico-chemical properties of the new ionic liquids, the surprisingly low viscosity of dimethylphosphate ionic liquids with ethylene glycol-functionalized cations is remarkable. Moreover, our experiments provide evidence for good thermal and hydrolytic stability of dialkylphosphate ionic liquids, proving these materials to be significantly superior to the well-established bulk ionic liquid [EMIM][EtSO₄] at least regarding these specific aspects. Given the good availability, the known biodegradability and, in general, the low-toxicity of esters of phosphoric acid (except trimethylphosphate resp. tricresylphosphate),³⁵ we anticipate that dialkylphosphate ionic liquids will indeed develop as an interesting alternative to other halogen-free ionic liquids, in particular for technical applications, with a high degree of stability and sensitivity for a commercially-competitive price.

Nomenclature

[BBIM]	1,3-di- <i>n</i> -butylimidazolium
[BEIM]	1- <i>n</i> -butyl-3-ethylimidazolium
[BHIM]	1- <i>n</i> -butyl-3- <i>n</i> -hexylimidazolium
[BMIM]	1- <i>n</i> -butyl-3-methylimidazolium
[BOIM]	1- <i>n</i> -butyl-3- <i>n</i> -octylimidazolium
[Bu ₂ PO ₄]	dibutylphosphate
Pd/C	Palladium on activated charcoal
<i>E</i> _A	Arrhenius activation energy/kJ mol ⁻¹
[EMIM]	1-ethyl-3-methylimidazolium
[EEIM]	1,3-diethylimidazolium
[EHIM]	1-ethyl-3- <i>n</i> -hexylimidazolium
[EOIM]	1-ethyl-3- <i>n</i> -octylimidazolium
[Et ₂ PO ₄]	diethylphosphate
[HMIM]	1- <i>n</i> -hexyl-3-methylimidazolium
<i>k</i>	rate constant (for <i>n</i> th order reaction/ (mol L ⁻¹) ^{1-<i>n</i>} s ⁻¹)

<i>k</i> ₀	collision factor (for <i>n</i> th order reaction/ (mol L ⁻¹) ^{1-<i>n</i>} s ⁻¹)
<i>m</i>	reaction order
[(MeEG)MIM]	1-(2-methoxyethyl)-3-methylimidazolium
[(MeEG ₂)MIM]	1-(2-(2-methoxyethoxy)ethyl)-3-methylimidazolium
[(MeEG ₃)MIM]	1-(2-(2-(2-methoxyethoxy)ethoxy)ethyl)-3-methylimidazolium
[MMIM]	1,3-dimethylimidazolium
[Me ₂ PO ₄]	dimethylphosphate
NMR	nuclear magnetic resonance spectroscopy
[OMIM]	1-methyl-3- <i>n</i> -octylimidazolium
<i>p</i>	pressure/bar
<i>r</i>	reaction rate/mol L ⁻¹ s ⁻¹
<i>T</i>	temperature/°C

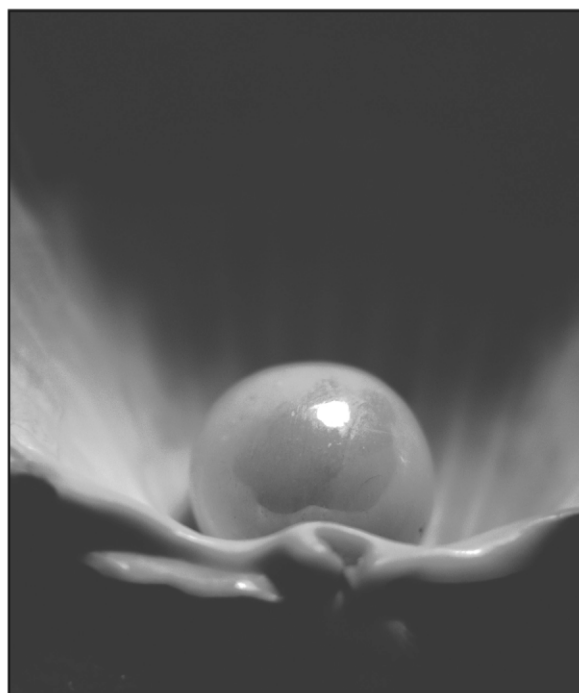
Acknowledgements

The authors would like to thank the BASF AG for providing 1-vinylimidazole and Degussa AG for providing samples of the catalyst Pd/C.

References

- 1 F. Endres and S. Z. El Abedin, *Phys. Chem. Chem. Phys.*, 2006, **8**, 2101–2116.
- 2 R. Kawano, H. Matsui, C. Matsuyama, A. Sato, M. A. B. H. Susan, N. Tanabe and M. Watanabe, *J. Photochem. Photobiol., A*, 2004, **164**, 87.
- 3 A. Bosmann and T. J. S. Schubert, GB 2005-10772 2414553, 2005.
- 4 T. Brinz and U. Simon, Robert Bosch GmbH, DE 2002-10245337 10245337, 2004.
- 5 K. Fukumoto, M. Yoshizawa and H. Ohno, *J. Am. Chem. Soc.*, 2005, **127**, 2398.
- 6 M. Maase, K. Massonne, K. Halbritter, R. Noe, M. Bartsch, W. Siegel, V. Stegmann, M. Flores, O. Huttenloch and M. Becker, BASF AG, WO 2003-EP545 2003062171, 2003.
- 7 M. Earle in *Ionic Liquids in Synthesis*, 2003, ed. P. Wasserscheid and T. Welton, Wiley-VCH, Weinheim, 2003, pp. 174–213.
- 8 T. Welton and P. J. Smith, *Adv. Organomet. Chem.*, 2004, **51**, 251.
- 9 R. A. Sheldon, R. M. Lau, M. J. Sorgedragger, F. van Rantwijk and K. R. Seddon, *Green Chem.*, 2002, **4**, 147.
- 10 Y. A. Beste, H. Schoenmakers, W. Arlt, M. Seiler and C. Jork, BASF AG, DE 2003-10336555 10336555, 2005.
- 11 J. Eßer, P. Wasserscheid and A. Jess, *Green Chem.*, 2004, **6**, 316.
- 12 M. E. Van Valkenburg, R. L. Vaughn, M. Williams and J. S. Wilkes, *Proc. Electrochem. Soc.*, 2002, **19**, 112.
- 13 M. Kömpf, in *Linde Technology*, 2006, pp. 24–29, http://www.linde.com/international/web/linde/likelindeeng.nsf/docbyalias/nav_technology.
- 14 B. Weyershausen and K. Lehmann, *Green Chem.*, 2005, **7**, 15.
- 15 R. P. Swatloski, J. D. Holbrey and R. D. Rogers, *Green Chem.*, 2003, **5**, 361.
- 16 F. Endres, *Z. Phys. Chem.*, 2004, **218**, 255.
- 17 P. Wasserscheid and C. Hilgers, Solvent Innovation GmbH, EP, 2000-118441 1182196, 2002.
- 18 M. Schmidt, U. Heider, W. Geissler, N. Ignatyev and V. Hilarius, Merck Patent GmbH, EP 2001-111953 1162204, 2001.
- 19 M. Maase, K. Massonne and L. Szarvas, BASF AG, WO, 2005-EP752 2005070896, 2005.
- 20 S. Himmler, S. Hörmann and P. Wasserscheid, *Green Chem.*, DOI: 10.1039/b617498a, submitted.
- 21 Z. -B. Zhou, H. Matsumoto and K. Tatsumi, *Chem. Lett.*, 2004, **33**, 680.
- 22 Available, e.g., from Solvent Innovation GmbH, Cologne (www.solvent-innovation.de) or BASF AG (www.basionics.de).
- 23 J. H. Werntz, E. I. du Pont de Nemours & Co., Wilmington, DE, USA, 1951.
- 24 A. M. Modro and T. A. Modro, *J. Phys. Org. Chem.*, 1989, **2**, 377.

- 25 Y. Zhou, A. J. Robertson, J. H. Hillhouse, D. Baumann, Cytec Canada Inc., WO, 2004016631, 2004.
- 26 A. Grosse Boewing and A. Jess, *Green Chem.*, 2005, **7**, 230.
- 27 R. D. Rogers and R. Swatlowksi, in *Ionic Liquids in Synthesis, 2003*, ed. P. Wasserscheid and T. Welton, Wiley-VCH, Weinheim, 2003, pp. 56–68.
- 28 E.g. BASF AG (www2.basf.de/de/intermed).
- 29 K. R. Seddon, A. Stark and M. -J. Torres, *ACS Symp. Ser.*, 2002, **819**, 34.
- 30 K. Kosswig, Surfactants, in *Ullmann's Encyclopedia of Industrial Chemistry*, Wiley-VCH, 2002.
- 31 J. G. Huddleston, A. E. Visser, W. M. Reichert, H. D. Willauer, G. A. Broker and R. D. Rogers, *Green Chem.*, 2001, **3**, 156.
- 32 K. N. Marsh, J. A. Boxall and R. Lichtenthaler, *Fluid Phase Equilib.*, 2004, **219**, 93.
- 33 S. V. Dzyuba and R. A. Bartsch, *ChemPhysChem*, 2002, **3**, 161.
- 34 J. Jacquemin, P. Husson, A. A. H. Padua and V. Majer, *Green Chem.*, 2006, **8**, 172.
- 35 *Römpf-Chemie-Lexikon*, Thieme Verlag, Stuttgart, 1995.



Looking for that **special** chemical biology research paper?

TRY this free news service:

Chemical Biology

- highlights of newsworthy and significant advances in chemical biology from across RSC journals
- free online access
- updated daily
- free access to the original research paper from every online article
- also available as a free print supplement in selected RSC journals.*

*A separately issued print subscription is also available.

Registered Charity Number: 207890

RSC Publishing

www.rsc.org/chembiology

22030681

New developments in emulsion–PVC polymerisation to produce polymers with the potential of reduced or zero VOC requirements when used in plastisol applications

Christopher Howick*

Received 25th July 2006, Accepted 24th November 2006

First published as an Advance Article on the web 14th December 2006

DOI: 10.1039/b610722b

Poly(vinylchloride) (chloroethene) resins have been used for the preparation of plastisols for a number of years. PVC plastisols are dispersions of such resins in liquid plasticisers, the plasticiser having the dual function of imparting softness and flexibility to the final article and for providing a liquid medium for the preparation of the plastisol that enables it to be coated, dipped or sprayed. For many years plastisol viscosity modification has involved the use of various volatile organic compounds (VOCs), which have an impact on their use in the workplace, and can also cause emitted VOCs from the end product. Control of the latter is of particular interest in new developments to combat indoor air quality (IAQ) problems. This paper shows that newly developed PVC resins are capable of producing the correct plastisol viscosity without the need for VOC addition to the plastisol. Moreover, new PVC additive technologies are available which enable end articles to be made from PVC plastisols that show greatly reduced or zero impact on IAQ when tested with newly developed equipment such as the Field and Laboratory Emission Cell (FLEC).

1 Introduction

Poly(vinylchloride) (chloroethene) represents one of the world's major commodity polymers, with a diverse range of applications including pipes, window profiles, packaging, flooring, cable insulation and sheathing and many more. The majority of the volume of PVC produced in the world is made using suspension polymerisation technologies: the polymerisation of droplets of vinyl chloride monomer in water, generally using monomer soluble initiators. However, a small but significant range of PVC resins are made using emulsion polymerisation. This is a term which covers a number of similar technologies which are intended to produce PVC resins of a relatively small particle size, typically 0.1 to 2.0 microns *ex-reactor*. The reason for this small particle size requirement is that these resins, unlike their suspension-derived counterparts, are required to form stable dispersions in a liquid plasticiser. The name given to these liquid polymer dispersions is *PVC plastisols*.

PVC plastisols have been produced for many years, and they continue to be used today to produce a number of commercially important end products such as safety flooring, corrosion resistant coatings for automobiles and synthetic leather products for use in car dashboards and fascias. Plastisols are also used in the manufacture of vinyl coated wallcoverings and external coated fabrics such as tarpaulins, advertising banners and stadium roofs. These plastisols have many processing advantages over resins made using suspension polymerisation in that they can be coated rather than extruded or calendered, and since such products have not been subject to shear they do

not possess a thermal history. Moreover, the laying down of very thin coatings is much easier *via* the plastisol route.

A simple PVC plastisol consists of an emulsion-type PVC resin and liquid plasticiser, typically an organic ester such as di-isononylphthalate. The function of the plasticiser in the plastisol is two-fold: (i) it provides the liquid medium to allow the plastisol to be formed and (ii) when the plastisol is fused and turned into the final article it provides the flexibility and softness required in that final article. These two requirements can be opposing: if a plastisol possesses too high a viscosity to allow it to be coated, addition of more plasticiser may solve that problem but it is likely that it will make the final product too soft and flexible. This is the reason why, over time, resin manufacturers have tailored their products to certain applications so as to give the optimum plastisol properties for an end product manufacturer targeting a given softness. However, in order to develop new products in certain areas, fabricators some time ago developed plastisols for the production of articles of relatively hard appearance that required relatively low levels of plasticiser addition. Since the low level of plasticiser was insufficient to provide enough liquid for plastisol formation, the viscosity of the plastisol was reduced with hydrocarbon solvents. These would flash off in processing and, since they had no plasticising action, enabled the processor to make lightly plasticised articles.

This situation continued for many years, although in recent times such use of volatile diluents has become a concern. Statutory instruments such as the 1990 Environmental Protection Act in the United Kingdom has required users of volatile plastisol diluents to either reduce use or install solvent recovery systems. Many have done so and the use continues with the necessary recovery and abatement systems.

Ineos Chlorvinyls, The Heath, Runcorn, Cheshire, UK WA7 4QZ.
E-mail: chris.howick@ineosvinyls

Although solvent evaporation during the processing operation does take place, complete removal of solvent at this stage is not 100% efficient and some solvent remains in the product, from which it evaporates during the first part of its lifetime. The emission of hydrocarbon solvents from these systems can be monitored using classical headspace gas chromatography² although modern assessment methods for indoor air quality (IAQ) can detect such evaporation from some products at exceedingly low levels (see below). Reduction programmes for this and all sources of volatile organic compound (VOC) in interior building products are one of the essential requirements of the EU's Construction Products Directive.³

Since the demand for plastisol resins remains healthy there was a need to establish whether the requirement of plastisol viscosity reduction could be met through changes in the polymerisation technologies that are used to manufacture plastisol grade PVC resins, since particle size and particle size distribution of the resin and other solid plastisol ingredients, as well as the level and type of the liquid plasticiser phase, will determine the viscosity of the plastisol. This paper reports and reviews some recent developments within the plastisol industry.

2 Emulsion PVC polymerisation technologies

Several historical developments set the scene for the development of plastisol-grade PVC resins in the second half of the 20th century. These were adequately reviewed by Bunten,¹ and the key technologies reviewed are still in commercial operation today. They are all used to produce resins of relatively small primary particle size which enable the formation of a plastisol when mixed with the desired level of liquid plasticiser.

The main technologies available are (i) microsuspension polymerisation (ii) seeded emulsion polymerisation and (iii) continuous emulsion polymerisation. Microsuspension polymerisation resembles suspension polymerisation technology except that the monomer–water mix is subject to high shear forces that enable a proportion of it to be homogenised into small monomer droplets. These droplets are then stabilised with a surfactant to prevent coalescence. The particle size distribution of the resulting resin made using this technology tends to be broad. This favours a good wetting out of the polymer in the plasticiser which means that plastisol formation tends to occur at relatively low levels of plasticiser. These plastisols, however, tend to suffer from high shear dilatancy. This is an increase in plastisol viscosity with shear which makes coating at higher speeds difficult, and resolution of this issue with hydrocarbons solvents is another source of VOC use in this industry. A solution to this is to use a resin produced *via* a seeded emulsion or continuous emulsion technology. Seeded emulsion polymerisation produces discrete particle size families by using water-soluble initiators, the monomer being dispersed into droplets through the use of surfactants and the polymerisation taking place *via* the monomer–surfactant–water micelles. Continuous polymerisation is an extension of this, and allows the polymerisation to be carried out continuously through the continuous removal of polymer and water with the concomitant replenishment of reactants to produce a broad particle size distribution of a multi-modal

resin. Both of these technologies tend to form pseudoplastic flow resins, that is resins whose plastisols show a shear thinning behaviour. This allows the processing of the plastisol to be made easily at high speeds but these resins tend to require more plasticiser for initial plastisol formation, thus rendering them unsuitable for the production of “hard” articles. Typical electron micrographs from standard microsuspension and seeded emulsion polymerisations are shown in Fig. 1.

Therefore plastisol formulators were presented with a dilemma for the production of hard articles at a commercially acceptable production rate: resins which formed plastisols at the correct plasticiser level could not be coated at high speeds without the use of volatile diluents and resins whose plastisols could be coated at high speeds could not be prepared at low plasticiser contents without the use of volatile diluents.

3 Indoor air quality

Many articles made from PVC plastisols are used in the indoor environment and, as a result, legislation requires that their potential for the emission of VOCs in use be assessed. One method that has been developed for this evaluation is the Field and Laboratory Emission Cell (FLEC) (see Fig. 2), which can be used to produce emission data using methods compliant with European Standard EN13419.⁴ The cell blows air of given humidity across the surface of the sample and collects gases emitted onto an absorbent. These can then be desorbed and analysed using Thermal Desorption–Gas Chromatography–Mass Spectrometry techniques (TD-GC-MS). The cell has wide reaching fields of application, since, in addition to the above attributes, it is portable and can therefore be taken to sites that are thought to be presenting a specific IAQ problem.

4 PVC plastisols

In addition to PVC resin and plasticiser, plastisols can contain a variety of ingredients, each present for a specific purpose. A summary is given in Table 1. In terms of the ingredients which can affect IAQ, studies centre on the plastisol diluents or rheology modifiers, as described above, and the thermal stabiliser package. These are used for two main purposes: to impart improved thermal stability to the resin and, in the case of foamed articles, to catalyse the decomposition of chemical

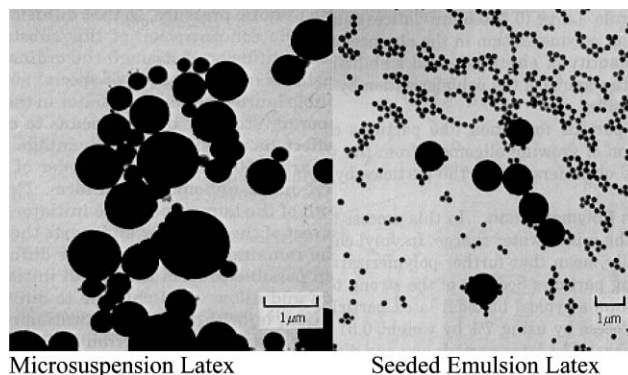


Fig. 1 Electron micrographs of standard microsuspension latex (left) and seeded emulsion latex (right).



Fig. 2 Field and Laboratory Emission Cell[®].

Table 1 Typical plastisol ingredients

INGREDIENT	TYPICAL LEVEL (%)	POTENTIAL EFFECT ON CHEMICAL EMISSION
PVC Resin	50–60	None
Fillers	10–30	None
Pigments	1–10	None
Plasticiser	20–40	Low (as SVOC)
Stabiliser	1–2	High (depends on type)
Chemical blowing agent	0–2	Low (gases lost in processing)
Viscosity modifiers	0.5–1	High (depends on type)
Solvents	0–2	High

blowing agents. The active ingredients are typically mixed metal soaps, but the stabiliser package frequently contains solvents, boosters, phosphite chelators and other ingredients to aid plastisol dispersion or aid the main ingredients in the bringing about of the desired effects.

5 VOC reduction

In an attempt to bring about significant reductions in VOC emission, the following aspects of plastisol formulating need to be addressed:

Can the need for volatile plastisol diluents be avoided?

Can the desired thermal stability and foam activation be achieved without species which have an impact on IAQ?

In order to study the first part, a full review of typical plastisol formulations by market was made. This enabled detailed knowledge of the typical levels of PVC, plasticiser and other key plastisol ingredients. The desire was to enable a flowable plastisol to be formed using the required formulation without the need for dilution. Moreover this plastisol was also required to coat at high speeds, *i.e.* not possess a dilatant rheology, again without recourse to volatile diluents. Since the factors controlling the plastisol viscosity and rheology are primarily related to the particle size and particle size distribution, the means of deriving new particle size distributions for the resin were studied. The influence of the polymerisation technology was studied using experimental design software,⁵ which showed the influence of the key

technologies on particle size distribution and therefore on the plastisol viscosity and rheology. Through an understanding of these parameters a number of experimental resins were developed using a pilot plant facility and these were then studied in detail, and finally a modified microsuspension resin was produced on a production facility.

6 Results from experimental resins

Fig. 3 shows the effect on typical plastisol viscosity—at low and high shear—of the resin modifications made as a result of the study.

Three plastisol formulations were studied: (i) 66.6% PVC, 33.3% plasticiser (ii) 71.4% PVC, 28.6% plasticiser and (iii) 50% PVC, 25% plasticiser and 25% calcium carbonate. In all cases the plasticiser used was di-2-ethylhexylphthalate (DEHP). For plastisol (i) the modified microsuspension resins showed a slightly lower plastisol viscosity. This difference was significantly larger for formulation (ii), which represented the known extreme of plastisol formation for the standard microsuspension resin. For this level of plasticiser the modified microsuspension resin formed a plastisol with ease and gave a plastisol viscosity some 30% of that of the standard resin. This equates to a potential 70% reduction in the use of a hydrocarbon diluent and in many cases would be sufficient to eliminate their use from the process. For the third plastisol, a 60% drop in plastisol viscosity was observed indicating that this resin had the potential of producing cost effective (*i.e.* filled) articles without the need to use volatile diluents to bring about the viscosity reduction needed.

7 Further experimental resins and the use of new thermal stabilisers

New resins have also been developed for application areas using the same methods. One particular area of interest is the use of thicker clear PVC layers on the top of PVC floorings for use in contract applications such as schools and hospitals. PVC is frequently the material of choice in these areas on account of its high mechanical properties, its ease of cleaning and compliance to a number of European Standards.⁶ One particularly useful aspect is that through PVC plastisol technology, foamed layers can be produced, and these give the required compression resistance and compression recovery.

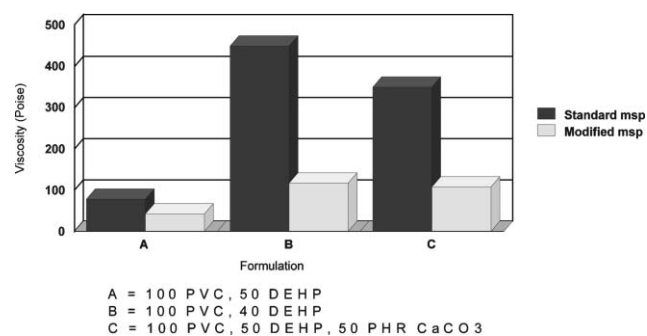


Fig. 3 Effect of standard and modified microsuspension resins on the low shear (Brookfield) viscosity of simple PVC plastisols.

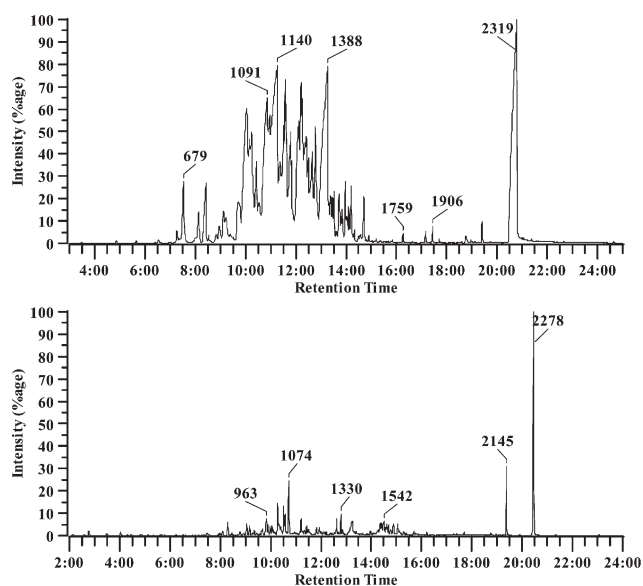


Fig. 4 Emission profiles of (i) standard flooring top coat and (ii) flooring top coat based on modified microsuspension resin with new stabiliser (both figures to same scale).

The top coats of these products consist of a thick, clear plastisol coating. This is generally based on a simple plastisol consisting of *ca.* 70% PVC and 30% plasticiser with a small addition of thermal stabiliser. The key properties of this layer are clarity and high thermal stability, in addition to the normal physical requirements as laid down in the relevant European standards.⁵ More recently attention has been turned to the level of VOCs emitted from these products. The use of diluents can be avoided through use of the appropriate resin, and this work has also studied a range of new thermal stabilisers that have been developed so as to give low potential for chemical emission.

Plastisols were prepared using “Evipol” MP8058 PVC resin (Ineos Chlorvinyls), di-isonylphthalate (Exxon Mobil) and the newly developed Akrostab stabiliser (Akcros Chemicals). Despite the lack of plastisol diluent, plastisol viscosity, both at low and high shear, was at acceptable levels. The film produced had clarity and thermal stability which were acceptable when compared with a control sample. Films of this polymer and that of a control were then tested for

emission of VOCs in accordance with EN13419. Volatiles emitted were absorbed onto Tenax[®] and then desorbed using TD-GC-MS.

The emission profiles are shown in Fig. 4, where the clear benefits of the new system—significantly reduced VOC emission—are seen. These products are now on the market and are enabling industry to bring about significant reductions in VOC use, and thus reduce the environmental impact of these products. Further work has shown that the emission profiles of these products are significantly lower than not only traditional PVC based systems but also those of other materials used in this area.

8 Conclusions

This paper has described the recent development of new PVC resins for the plastisol area that enable plastisol formulations with significantly reduced volatile organic compound (VOC) levels to be used, by enabling plastisol formation to be made through PVC polymer and plasticiser alone at the low plasticiser levels that traditionally have required VOC use to aid plastisol formation. These resins can be used in standard plastisol applications as well as foaming and clear coat applications. These can be combined with newly developed thermal stabiliser systems to allow for further significant VOC reductions in products for indoor applications. These products are all now commercially available.

Further work is planned on taking these resins into more diverse plastisol applications.

References

- 1 M. J. Bunten, M. W. Newman, P. V. Smallwood and R. C. Stephenson, *Encyclopaedia of Polymer Science and Engineering*, vol. 17 and Supplement, pp 241–392, 1989.
- 2 C. J. Howick and S. A. McCarthy, *J. Vinyl Addit. Technol.*, 1996, **2**(2), 134–142.
- 3 EU Directive 89/106/EEC, *Official Journal of the European Communities L40*, pp 12–26, 11th February 1989.
- 4 European Standard EN13419 (1999), European Committee for Standardisation, Rue de Stassart 36, B-1050 Brussels.
- 5 Conference Proceedings, Vinyltec 2002, Society of Plastics Engineers, Itasca, IL, USA, Sept. 30–Oct. 2 2002.
- 6 European Standards EN424 (1993), EN425 (1994), EN433 (1994), European Committee for Standardisation, Rue de Stassart 36, B-1050 Brussels.

Use of a green and cheap ionic liquid to purify gasoline octane boosters†

Alberto Arce,* Héctor Rodríguez and Ana Soto

Received 2nd August 2006, Accepted 24th November 2006

First published as an Advance Article on the web 15th December 2006

DOI: 10.1039/b611139d

This work demonstrates the ability of the ionic liquid 1-ethyl-3-methylimidazolium ethylsulfate ([emim][EtSO₄]) to act as an extraction solvent for liquid–liquid extraction and as an azeotrope breaker for extractive distillation, to separate the azeotropic mixture ethyl *tert*-butyl ether (ETBE) + ethanol, thus purifying the tertiary ether, which is the most used additive to improve the octane index of gasolines. To assess the suitability of [emim][EtSO₄] to perform the mentioned separation, the liquid–liquid equilibrium (LLE) at 298.1 K and the isobaric vapour–liquid equilibrium (VLE) at 101.3 kPa have been determined for the ternary system ETBE + ethanol + [emim][EtSO₄]. The separation sequence for the extractive distillation has been obtained from the residue curve map and checked by simulation. The equilibrium data have been adequately correlated by means of the NRTL equation, thus facilitating their computerized treatment.

Introduction

The world energy demand is nowadays experiencing a dramatic increase. In spite of numerous governmental and institutional policies looking for a more controlled and rational consumption of energy, forecasts prognosticate a continuation of the raising trend in the near future, closely related to the global population growth.¹ Linked to this problem, the growth of concepts such as sustainable development in the second half of the 20th century has been a major impetus, over the last decades, for the exploration and exploitation of renewable sources for the generation of energy. Nevertheless, fossil fuels continue to supply much of the energy used worldwide,² so the development of energy from renewable sources must be accompanied in parallel by an optimized use of traditional sources of energy.

A relevant end-use sector in energy consumption is transportation. As in the general case, many efforts are currently being made to promote the penetration of sustainable alternatives in this field as fuels. For example, important research is carried out in trying to develop fuel cells powered with hydrogen.³ But, to date, the main results and developments have undoubtedly been reached for biofuels and, particularly, bioethanol.⁴ The use of this sort of ethanol, obtained by fermentation from agricultural products, is being encouraged by legislators in many places in Europe and the Americas, to feed engines either alone or as an additive to gasoline. However, the intensified production of bioethanol is not exempted of controversy, since issues such as the use of pesticides and fertilizers, the large demand of soil or the biodiversity preservation related to its production lead to important concerns in a considerable part of the scientific and industrial communities. The most intelligent use of bioethanol

as fuel for the future, as at present, will probably be conditioned by local circumstances. Thus, in countries like Brazil and the USA, with a large availability of fertile land for harvesting sugar cane and corn, bioethanol is an interesting alternative as direct fuel for vehicles or direct additive to gasolines; whereas in regions where the space is more limited or valuable for other uses, mainly in Europe, a preferable option may be the use of bioethanol for the production of a tertiary ether, then using the latter as the oxygenating additive in gasoline blending. Actually, ethyl *tert*-butyl ether (ETBE) produced from bioethanol (which means a 47% biofuel contribution⁵) is currently a major biofuel contributor in Europe.

ETBE has come to replace methyl *tert*-butyl ether (MTBE) as the most widely used anti-knock additive for gasolines, basically due to two reasons: the possibility of involving ethanol from renewable sources in the synthesis, instead of the more valuable and fossil-originated methanol; and a lower solubility in water, thus reducing the risk of aquifers contamination from leaks in underground storage tanks, as reported for MTBE in the past.⁶ ETBE is produced by an etherification reaction between isobutene and ethanol, the latter possibly having an agricultural origin. In the mentioned reaction, an excess of the alcohol is used. Consequently, the outlet stream of the reactor is mainly constituted by a mixture of ETBE and the unreacted ethanol. A downstream separation stage is then required to obtain the purified ether and to recycle the ethanol to the reactor. ETBE and ethanol have close boiling points and form an azeotropic mixture; therefore it is hard to separate them by conventional distillation. Interesting alternatives may be solvent (or liquid–liquid) extraction at ambient temperature or extractive distillation. Both techniques require, nonetheless, the introduction of an auxiliary substance (called a solvent in liquid–liquid extraction, and an entrainer in extractive distillation) to carry out the separation; thus, their successful implementation will be critically dependent on the discovery of a suitable compound to act either as extracting solvent or as entrainer.

Dpt of Chemical Engineering, University of Santiago de Compostela, E-15782, Santiago de Compostela, Spain. E-mail: eqaaarce@usc.es; Fax: +34 981 528050; Tel: +34 981 563100

† Electronic supplementary information (ESI) available: Tables S.1–3 and equipment for the measurement of the physical properties. See DOI: 10.1039/b611139d

The selection of an effective solvent or entrainer for use in the mentioned processes is controlled by several factors.⁷ It must preferably be chemically stable, non-corrosive and cheap, showing low toxicity and being easily recoverable from the outlet streams of the unit. In addition, it must exhibit the thermodynamic ability to carry out the aimed separation. For liquid–liquid extraction the solvent must have a favourable selectivity and also a high solvent capacity, whereas for extractive distillation the entrainer must exalt the relative volatility in the mixture.

The family of low melting point salts known as ionic liquids (ILs) has attracted an increasing interest from academia and industry over the last decade.⁸ Their use as environmentally benign solvents, replacing the polluting and hazardous volatile organic compounds (VOCs), has been one of the major potential applications pointed out.⁹ This is mainly due to their extremely low vapour pressure, particularly at normal operation conditions in processes,¹⁰ thus avoiding loss of the IL by evaporation to the atmosphere. Their non-volatile nature would also play a crucial role in facilitating the downstream recovery and recycling to the unit, as flash distillation could be used instead of the more expensive and aggressive rectification. Moreover, the adequate selection of cation and anion may lead to a stable non-corrosive IL with low toxicity and an affordable cost, in addition to acceptable values of properties such as viscosity or melting point in an extracting solvent or an entrainer. A further requirement, taking into account the list of characteristics in the previous paragraph, is the suitability from a thermodynamic point of view. In the literature, a few works focusing on the analysis of ILs as solvents in extraction processes can be found, with liquid–liquid equilibrium (LLE) data being the basis for their evaluation.¹¹ Even more scarcely available are papers reporting vapour–liquid equilibrium (VLE) data involving ILs and their potential use as entrainers for extractive distillation processes.¹²

Alkylsulfate-based ILs with a cation derived from imidazolium¹³ are, to date, some of the most promising ILs to be applied in industrial processes. In general, they can be easily synthesized in an atom-efficient and halide-free way, at a reasonable cost. They show chemical and thermal stability, low melting points and relatively low viscosities. Particularly, 1-ethyl-3-methylimidazolium ethylsulfate ([emim][EtSO₄]) combines those features in a suitable way to be used as solvent in liquid–liquid extraction or as an azeotrope breaker in extractive distillation. In addition to this and to the general properties of ILs, recent studies have shown that [emim][EtSO₄] presents an acceptable level of toxicity,¹⁴ lying in the range of many other chemical substances currently used in the role aimed herein.

From the above, [emim][EtSO₄] seems to be a good candidate to test as an extracting solvent or entrainer in purifying ETBE from its mixtures with ethanol. To evaluate such a possibility, an equilibrium thermodynamic study of the ternary system ETBE + ethanol + [emim][EtSO₄] has been carried out in this work. Its LLE at 298.1 K and its isobaric VLE at 101.3 kPa have been determined. To the best of our knowledge, this is the first time that both LLE and VLE are jointly reported for a ternary system involving an IL, which may be kindly welcomed by researchers working within

prediction modelling for systems with ILs. The experimental data have been successfully correlated, thus facilitating their implementation and use in computerized applications.

Results and discussion

Experimental data

Liquid–liquid equilibrium. The compositions of both phases in equilibrium were determined at 298.1 K for mixtures with different global compositions in the heterogeneous region of the system ETBE + ethanol + [emim][EtSO₄]. The results are reported in Table 1, alongside the corresponding values of solute distribution ratio (β) and selectivity (S), which are defined by the following expressions:

$$\beta = \frac{x_2^{\text{II}}}{x_2^{\text{I}}} \quad (1)$$

$$S = \frac{x_1^{\text{I}} x_2^{\text{II}}}{x_1^{\text{II}} x_2^{\text{I}}} \quad (2)$$

where x is the molar composition, subscripts 1 and 2 refer to ETBE (inert) and ethanol (solute), and superscripts I and II indicate the organic-rich phase (top or less dense phase) and the solvent rich-phase (bottom or denser phase), respectively. The solute distribution ratio gives an idea of the solvent capacity of the IL, being related to the amount of solvent required for the process. Selectivity provides a measurement of the separation power of the IL, conditioning the number of equilibrium stages needed in the unit. Values as high as possible for both parameters are desired.

A triangular diagram is a common method for the visualization of the LLE for a ternary system at constant pressure and temperature. In Fig. 1, such a diagram is drawn for the system ETBE + ethanol + [emim][EtSO₄], with the vertices of the triangle representing each of the pure compounds: left for ETBE (the inert in this case, since it is the compound not dissolved preferentially by the IL); top for ethanol (the solute, because it mainly goes into the IL-rich phase); and right for [emim][EtSO₄] (the solvent). The LLE is described in the diagram by plotting the experimental tie-lines,

Table 1 Composition of the experimental tie-line ends, solute distribution ratio (β) and selectivity (S) for the system ETBE + ethanol + [emim][EtSO₄] at 298.1 K. The mole fractions of ETBE, ethanol and ionic liquid are represented by x_1 , x_2 and x_3 , respectively

Organic phase			Ionic liquid phase			β	S
x_1	x_2	x_3	x_1	x_2	x_3		
1.000	0.000	0.000	0.031	0.000	0.969	—	—
0.991	0.009	0.000	0.028	0.064	0.908	7.11	251.7
0.976	0.024	0.000	0.046	0.141	0.813	5.88	124.7
0.960	0.040	0.000	0.052	0.224	0.724	5.60	103.4
0.916	0.084	0.000	0.059	0.358	0.583	4.26	66.2
0.875	0.125	0.000	0.060	0.458	0.482	3.66	53.4
0.794	0.206	0.000	0.078	0.540	0.382	2.62	26.7
0.709	0.289	0.002	0.103	0.602	0.295	2.08	14.3
0.651	0.347	0.002	0.133	0.632	0.235	1.82	8.9
0.546	0.441	0.013	0.180	0.646	0.174	1.46	4.4
0.481	0.493	0.026	0.223	0.636	0.141	1.29	2.8

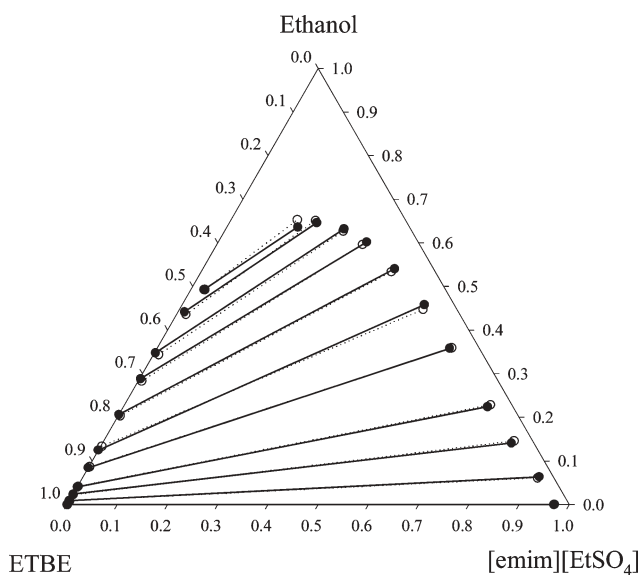


Fig. 1 Experimental (●, solid line) and correlated (○, dotted line) tie-lines for the LLE of the ternary system ETBE + ethanol + [emim][EtSO₄] at 298.1 K and atmospheric pressure. The correlated data were calculated by means of the NRTL equation, with a value of $\alpha = 0.2$ and an *a priori* established value of β_{∞} .

whose extremes correspond to pairs of equilibrium compositions. The positive slope shown by the tie-lines is readily interpretable as a desirable feature, since it implies values greater than the unity for the solute distribution ratio, or, equivalently, that the solute goes preferentially to the solvent-rich phase. Additionally, Fig. 1 provides a clear idea of the shape and size of the immiscibility region of the system.

From these results, it turns out that [emim][EtSO₄] can successfully act as a solvent for the separation of ETBE and ethanol in a liquid–liquid extractor. Together with this, it should not be forgotten that the non-volatile nature of the IL would facilitate considerably its downstream recovery, thus confining it in the process with negligible loss of solvent.

Vapour–liquid equilibrium. Before investigating the VLE for the ternary system, the completely miscible constituent binaries were analyzed. The VLE for the binary system ETBE + ethanol was already reported in the literature.¹⁵ However, the VLE for the pair ethanol + [emim][EtSO₄] had not been previously reported. The equilibrium temperatures for this binary system at 101.3 kPa are summarized in the temperature–composition diagram shown in Fig. 2. The numerical raw data are provided in Table S.1 in the ESI.† Since the IL is essentially non-volatile, the vapour in equilibrium with the boiling liquid phase is exclusively constituted by ethanol. No equilibrium temperatures could be determined in the range of very low ethanol concentrations, due to problems of decomposition of [emim][EtSO₄]. Himmler *et al.*¹⁶ determined the decomposition temperature to be 630 K, higher temperatures leading to the back alkylation of the anion.

Concerning the ternary system ETBE + ethanol + [emim][EtSO₄], its isobaric VLE was determined in the homogeneous region. The experimental compositions calculated for the liquid and vapour phases in equilibrium, as well

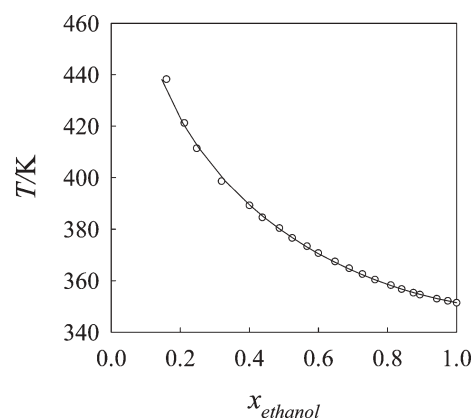


Fig. 2 Experimental VLE data at 101.3 kPa (○) and corresponding NRTL ($\alpha = 0.2$) correlation (solid line) for the binary system ethanol + [emim][EtSO₄].

as the equilibrium temperatures, are listed in Table 2. Fig. 3 shows the compositions triangular diagram, where each arrow has its origin in the point corresponding to the composition of the liquid phase and its final end in the point corresponding to the composition of the vapour phase in equilibrium. As can be inferred from the diagram, the system does not exhibit a ternary azeotrope. The calculated liquid isotherms are depicted in Fig. 4, indicating the different compositions of ternary liquid mixtures which would boil at the same temperature.

Correlation

Liquid–liquid equilibrium. The experimental LLE data were correlated by means of a classical model such as the NonRandom Two-Liquid (NRTL) equation,¹⁷ despite the fact that this model was not originally intended for systems with electrolytes. The nonrandomness parameter of the model, α , was previously set to three different values: 0.1, 0.2 and 0.3. The NRTL binary interaction parameters were obtained using a software program described by Sørensen and Ait.¹⁸ The goodness of the correlation was evaluated by calculating the residual function F and the mean error of the solute distribution ratio, $\Delta\beta$, defined as:

$$F = 100 \times \left[\sum_k \min \sum_i \sum_j \frac{(x_{ijk} - \hat{x}_{ijk})^2}{6M} \right]^{0.5} \quad (3)$$

$$\Delta\beta = 100 \times \left[\sum_k \frac{((\beta_k - \hat{\beta}_k) / \beta_k)^2}{M} \right]^{0.5} \quad (4)$$

where subscripts and sum indices i, j and k refer to compounds, phases and tie-lines, respectively; M is the total number of experimental tie-lines; and the circumflex symbol on top indicates a calculated value.

The program was run twice for each value of α : first, without previous assignment of a value for the solute distribution ratio at infinite dilution, β_{∞} ; and then, establishing an *a priori* optimum value for β_{∞} , found by trial and error with $\Delta\beta$ as the optimality criterion. The resulting binary interaction

Table 2 Boiling temperatures (T) and liquid and vapour mole fractions (x_i , y_i) for ETBE (1) + ethanol (2) + [emim][EtSO₄] (3) at 101.3 kPa

T/K	x_1	x_2	y_1	y_2
349.06	0.0369	0.7198	0.4067	0.5933
350.49	0.0288	0.7382	0.3444	0.6556
351.32	0.0197	0.7772	0.2731	0.7269
346.93	0.0480	0.7522	0.4143	0.5857
343.47	0.0707	0.7321	0.5246	0.4754
343.83	0.0876	0.7723	0.4706	0.5294
342.27	0.1213	0.7410	0.5298	0.4702
341.08	0.1582	0.7080	0.5777	0.4223
340.49	0.1930	0.6758	0.6052	0.3948
340.29	0.2395	0.6536	0.6116	0.3884
340.20	0.2828	0.6306	0.6052	0.3948
340.96	0.2326	0.6914	0.5546	0.4454
341.97	0.1783	0.7463	0.5026	0.4974
343.01	0.1416	0.7884	0.4537	0.5463
344.27	0.1081	0.8242	0.3986	0.6014
345.49	0.0848	0.8546	0.3387	0.6613
346.75	0.0702	0.8761	0.2791	0.7209
351.04	0.0100	0.9816	0.0316	0.9684
349.86	0.0251	0.9550	0.1046	0.8954
348.58	0.0423	0.9374	0.1666	0.8334
347.11	0.0687	0.9108	0.2374	0.7626
346.24	0.0801	0.8754	0.2924	0.7076
344.58	0.1104	0.8450	0.3633	0.6367
342.86	0.1510	0.7859	0.4587	0.5413
341.92	0.1884	0.7503	0.4996	0.5004
340.61	0.2979	0.6503	0.5673	0.4327
340.27	0.3482	0.6041	0.5929	0.4071
340.29	0.4083	0.5690	0.5859	0.4141
340.04	0.4886	0.4929	0.6128	0.3872
340.87	0.3420	0.6403	0.5381	0.4619
341.81	0.2560	0.7278	0.4821	0.5179
343.17	0.1792	0.8064	0.4139	0.5861
344.50	0.1332	0.8540	0.3511	0.6489
354.13	0.0093	0.8570	0.0577	0.9423
353.02	0.0131	0.8526	0.1037	0.8963
353.69	0.0077	0.8759	0.0490	0.9510
353.82	0.0063	0.8878	0.0243	0.9757
351.73	0.0146	0.8838	0.1194	0.8806
348.68	0.0430	0.8536	0.2498	0.7502
347.08	0.0560	0.8412	0.3154	0.6846
349.59	0.0304	0.8258	0.2671	0.7329
351.47	0.0188	0.8466	0.1762	0.8238
353.30	0.0105	0.8127	0.1638	0.8362
364.54	0.0011	0.6777	0.0154	0.9846
360.97	0.0036	0.6859	0.1341	0.8659
355.05	0.0200	0.6879	0.3103	0.6897
346.55	0.0527	0.6751	0.5220	0.4780
340.15	0.1095	0.6589	0.6683	0.3317
342.77	0.0813	0.7262	0.5602	0.4398
346.50	0.0517	0.7131	0.4738	0.5262
343.45	0.0637	0.7130	0.5605	0.4395
340.15	0.1230	0.6554	0.6634	0.3366
369.49	0.0102	0.5609	0.1414	0.8586
365.26	0.0300	0.5798	0.1989	0.8011
366.42	0.0020	0.6061	0.1290	0.8710
357.08	0.0589	0.6079	0.2704	0.7296
352.42	0.0280	0.6613	0.4041	0.5959
348.33	0.0715	0.6154	0.5097	0.4903
398.81	0.0275	0.2601	0.0855	0.9145
386.01	0.0227	0.3591	0.1206	0.8794
382.30	0.0144	0.3825	0.1121	0.8879
377.79	0.0320	0.4038	0.1626	0.8374
372.55	0.0119	0.4927	0.1489	0.8511

parameters and residuals for the correlation with $\alpha = 0.2$ are listed in Table 3. For best comparison, Fig. 1 shows the correlated tie-lines plotted along with the experimental ones, for the particular case of the NRTL correlation with $\alpha = 0.2$

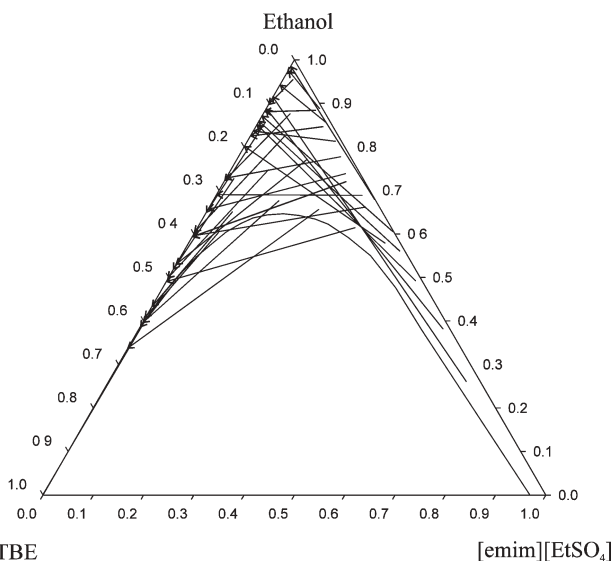


Fig. 3 Experimental VLE data at 101.3 kPa for the ternary system ETBE + ethanol + [emim][EtSO₄].

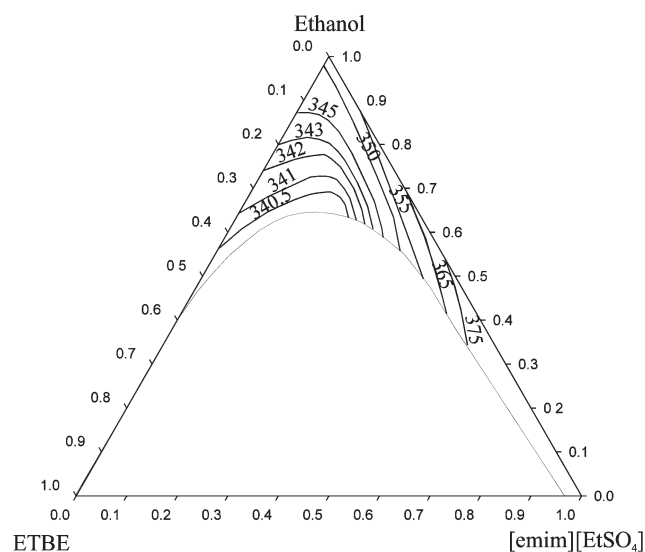


Fig. 4 Calculated isothermal liquid phase compositions for VLE at 101.3 kPa for the ternary system ETBE + ethanol + [emim][EtSO₄]. Temperature values of the isotherms are expressed in Kelvin.

Table 3 Binary interaction parameters (BIPs) and residuals from the correlation of the LLE data of the ternary system ETBE (1) + ethanol (2) + [emim][EtSO₄] (3) by the NRTL equation ($\alpha = 0.2$)

β_∞	Components $i-j$	BIPs		Residuals	
		$\Delta g_{ij}/J \text{ mol}^{-1}$	$\Delta g_{ji}/J \text{ mol}^{-1}$	F	$\Delta\beta$
8.33	1-2	-1015.0	2928.7	0.4879	12.1
	1-3	15308	4710.8		
	2-3	1951.9	-6002.3		
	1-2	-511.93	2595.9	0.5208	9.5
	1-3	14497	4644.9		
	2-3	2940.7	-5929.0		

and setting the optimum value of β_{∞} . When the optimal value of β_{∞} is laid down in advance, it is observed that the residual function F increases slightly, whereas $\Delta\beta$ decreases extensively.

Vapour–liquid equilibrium. The correlation of the experimental (P , T , x , y) results was carried out with a computer program that runs a non-linear regression method based on the maximum likelihood principle. Due to the lack of thermodynamic parameters for the IL, the vapour phase was considered ideal. For the binary system ethanol + [emim][EtSO₄] this approximation is adequate, since the IL is basically non-volatile and ethanol is therefore the only component in the vapour phase. For the ternary system, this assumption might mean high deviations between model and experimental data. Saturation pressures were calculated from Antoine's equation:

$$\log(P_i^{\text{sat}}/\text{kPa}) = A - \frac{B}{(T/\text{K}) + C} \quad (5)$$

using values for the coefficients A , B , and C taken from literature in the case of ETBE and ethanol,¹⁹ and arbitrarily setting them to fictional values in order to lead to a negligible vapour pressure for [emim][EtSO₄] (see Table S.2 in the ESI).†

Assuming the same considerations stated for LLE data correlation, the NRTL equation was used to model the liquid-phase activity coefficients, setting the nonrandomness parameter, α , to different values and selecting the value giving the best correlation. The values of the binary interaction parameters are summarized in Table 4 for the binary and ternary systems, respectively, along with the corresponding root mean standard deviations in temperature, pressure and compositions of the liquid and vapour phases.

With the parameters obtained in the correlation of the ternary system, the residue curve map was plotted (Fig. 5). A residue curve represents the liquid residue composition with time as the result of a simple, one-stage batch distillation. Residue curve maps are used to make preliminary estimates of regions of feasible product compositions for distillation of non-ideal ternary mixtures. Fig. 5 shows that [emim][EtSO₄] induces a liquid phase heterogeneity over a portion of the composition triangle, but does not split the components to be

Table 4 Binary interaction parameters (BIPs) and root mean square deviations (rmsd) from the correlation of the VLE data of the ternary system ETBE (1) + ethanol (2) + [emim][EtSO₄] (3) or the binary system ethanol (2) + [emim][EtSO₄] (3) by the NRTL equation ($\alpha = 0.2$)

		Binary system	Ternary system
BIPs	$\Delta g_{12}/\text{J mol}^{-1}$	—	707.45
	$\Delta g_{21}/\text{J mol}^{-1}$	—	3235.6
	$\Delta g_{13}/\text{J mol}^{-1}$	—	21399
	$\Delta g_{31}/\text{J mol}^{-1}$	—	11632
	$\Delta g_{23}/\text{J mol}^{-1}$	1667.3	1869.3
	$\Delta g_{32}/\text{J mol}^{-1}$	1909.8	3816.0
rmsd(T/K)		0.08	0.27
rmsd(P/kPa)		0.001	0.005
rmsd(x_1)		—	0.0112
rmsd(x_2)		0.0046	0.0073
rmsd(y_1)		—	0.0038
rmsd(y_2)		0.0001	0.0038

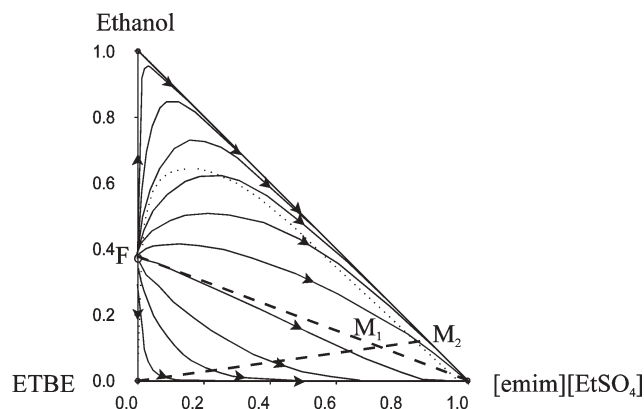


Fig. 5 Residue curve map for the extractive distillation of a mixture ETBE + ethanol using [emim][EtSO₄] as entrainer.

separated into different distillation regions. Therefore, the suitability of [emim][EtSO₄] as an entrainer in extractive distillation is confirmed, and the corresponding column sequence can be established. The purpose of the IL is to separate into its pure components the azeotropic binary mixture of ETBE and ethanol (F) feeding the process. The hypothetical ternary mixture formed with the addition of the IL (M_1) is separable in a distillation column, obtaining pure ETBE and a mixture of ethanol and [emim][EtSO₄] (M_2). Due to the negligible vapour pressure of the IL, this mixture will be easily separated in a flash column, then recycling the IL to the extractive distillation column.

Simulation

The separation column sequence mentioned in the paragraph above was simulated using the software HYSYS[®] (v3.2) by Aspen Technology, Inc. (Cambridge, MA, USA). The corresponding flowsheet is shown in Fig. 6. The first column is a distillation column, working at atmospheric pressure, with 10 equilibrium stages. Equal mass flows of solvent and feed are introduced at the second and fifth stages, respectively. The top product is ETBE totally pure. The bottom product (a mixture of ethanol and [emim][EtSO₄]) is firstly heated at 423.1 K, well below the decomposition temperature of the ionic liquid and therefore avoiding such a problem in the proposed purification system. After this, it is fed to a flash vessel working at reduced

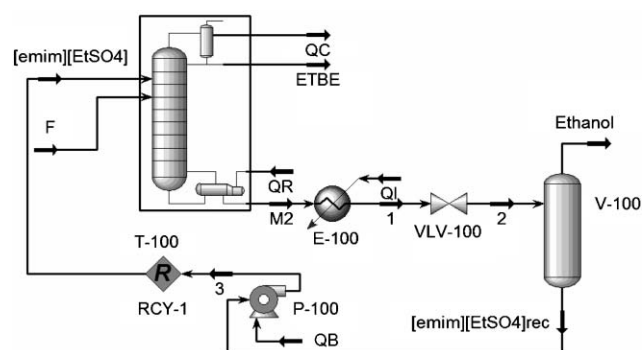


Fig. 6 Column sequence for the extractive distillation of mixtures ETBE + ethanol with [emim][EtSO₄] as entrainer.

pressure (20 kPa). From that vessel are obtained pure ethanol and [emim][EtSO₄] (99.1 mass%), the latter being recycled to the first column. The process is not optimized and the output compositions are only approximated because some of the data used to solve the process (*e.g.* equilibrium at 20 kPa, heat capacities) were not supported by experimentation; instead, they were just estimated by the simulator itself, based on a poor description of the ionic liquid when it was defined and introduced in the database. Nonetheless, the ability of the ionic liquid [emim][EtSO₄] as azeotrope breaker in extractive distillation for the separation of the mixture ETBE + ethanol is corroborated by the simulation test carried out.

Conclusions

The LLE and VLE for the ternary system ETBE + ethanol + [emim][EtSO₄] were determined. The results, together with the intrinsic characteristics of [emim][EtSO₄], show that this IL can be successfully used as a solvent in liquid–liquid extraction or as an entrainer in extractive distillation for the separation of mixtures of ETBE + ethanol. This would lead to both a more purified ETBE, ready to use in gasoline blending to achieve fuels with higher octane index, and, in addition, to an optimization in the use of the ethanol involved in the synthesis of the tertiary ether.

IL technology, thanks to the non-volatile nature of the IL under the operational temperature and pressure conditions, facilitates downstream separations to recover the IL, and will avoid its loss to the atmosphere by evaporation. Since cost and toxicity of [emim][EtSO₄] are relatively low, these should not be unavoidable barriers for its implementation in the processes at an industrial level. Additional features of [emim][EtSO₄], such as atom efficiency in its synthesis, enhance from an overall perspective the greener character of the new proposed processes.

The LLE and VLE data were adequately correlated by the NRTL equation. Although this model is theoretically developed for systems not involving electrolytes, a high number of model parameters leads to an accurate “mathematical” correlation. Research on equilibrium modelling of systems with ionic liquids, as well as on thermophysical properties of these neoteric solvents, seems to be an imminent objective for chemical engineers. The availability of both LLE and VLE data for the same system, as done in this work, may be particularly useful in the development and improvement of theoretical models for ILs.

The good correlation of the experimental data permits them to be handled them in a computerized fashion. This makes possible, for instance, their implementation in specialized software to perform process simulation. Together with the introduction in such software of a complete set of properties to characterize the [emim][EtSO₄], the simulation of the processes suggested herein can be run, and help in the design of units and operation conditions. Simulation could eventually be a useful tool in choosing between solvent extraction and extractive distillation to achieve the purification of ETBE. Local circumstances concerning availability of feedstocks, energy cost, *etc.* should be considered in taking the final decision. In

the current work, an example was presented of how simulation software might be useful for practical purposes.

Experimental

Materials

The synthesis of [emim][EtSO₄] was carried out by reaction of equimolar quantities of 1-methylimidazole (Aldrich, >99%, GC) and diethylsulfate (Aldrich, >98%, GC) in toluene.^{13,20} A solution of 1-methylimidazole in toluene was prepared first and then diethyl sulfate was added dropwise under inert atmosphere. The reaction was done in an ice bath to prevent the temperature rising above 313 K. As [emim][EtSO₄] is non-soluble in toluene, it was separated from reagents and solvent and then washed three times with fresh toluene. Removal of residual volatile compounds in the IL was carried out first in a rotary evaporator, and later under high vacuum for 48 h while heating at 353 K with stirring. Synthesis of [emim][EtSO₄] by this method ensures complete absence of halide ions, whose presence could affect the performance of the IL in the experiments.²¹

ETBE with a purity of 99.4%, checked by gas chromatography, was obtained from the Department of Chemical Engineering of the University of Barcelona, Spain. Ethanol with a nominal purity of 99.9% was purchased from Merck.

Several physical properties were measured for all pure compounds in this work. Results are summarized in Table S.3 in the ESI,† along with the description of the apparatuses used to carry out the measurements. Comparisons with literature values are also shown and good agreement of the data can be observed, which highlights the quality of the materials and their potential to generate reliable results in the experiments.

Since the water content of an IL can dramatically vary its properties and behaviour,²¹ it is important to ensure that it is thoroughly dried. In this case, the water content of [emim][EtSO₄] was found to be as low as 0.01%, measured by Karl-Fischer titration with a Metrohm 737 KF Coulometer. The water contents of ETBE and ethanol were also measured, being 0.03% and 0.04% respectively.

Determination of LLE

For the experimental determination of the LLE tie-lines of the system studied, ternary mixtures (or just binary, for the immiscible pair ETBE–IL) with compositions lying in the immiscible region were introduced inside jacketed glass cells. The mixtures were kept at constant temperature using water from a Selecta Ultraterm 6000383 thermostat, whose temperature was checked by means of a Heraeus Quat 100 thermometer with a precision of ± 0.01 K. All the mixtures were vigorously stirred for at least 1 hour, and then allowed to settle for a minimum of 4 hours to guarantee that the equilibrium state was completely reached. The indicated protocol was established according to results from preliminary tests. A sample of each layer in equilibrium was taken using glass syringes with coupled stainless steel needles. Then the samples were dissolved in deuterated solvent inside NMR-tubes which were properly sealed.

The composition of these samples was determined by proton nuclear magnetic resonance spectroscopy (^1H NMR). The spectrometer used to perform the analysis was a shielded magnet Bruker DRX-500. These measurements were estimated to be precise to ± 0.005 in molar fraction, according to results from test samples previously prepared by weight. All weighing involved in the experimental work was carried out in a Mettler Toledo AT 261 balance, with a precision of ± 0.0001 g.

Determination of VLE

The VLE data were obtained using a Labodest 602 equilibrium still (Fischer Labor und Verfahrenstechnik, Germany). This still is equipped with a Fischer digital manometer that measures pressure to within ± 0.01 kPa and an ASL F250 Mk II Precision Thermometer, operating with a wired PT100 PRT, that maintains the temperature of the system with an overall accuracy of ± 0.02 K. The Labodest 602 recirculates both the liquid and vapour phases, and is suitable for the determination of either isobaric or isothermal VLE data. Isobaric operation was developed in this work, at a constant pressure of 101.3 kPa. Contact with water in the open atmosphere was avoided by flushing the system with gaseous argon.

The compositions of the phases in equilibrium were determined by an indirect method based on physical properties, namely densities and refractive indices. These physical properties for homogeneous ternary mixtures ETBE + ethanol + [emim][EtSO₄] at 298.1 K and atmospheric pressure had been determined in a previous work.²² The determination of the equilibrium compositions in such way was estimated to be precise to 0.002 in molar fraction.

Acknowledgements

The authors are grateful to the Ministerio de Educación y Ciencia (Spain) for financial support through project PPQ2003-01326. HR also wants to thank them for the award of the FPI grant with reference BES-2004-5311 under the same project.

References

- 1 K. Weissermel and H.-J. Arpe, *Industrial Organic Chemistry*, VCH, Weinheim, 3rd edn, 1997.

- 2 *International Energy Outlook 2006*, Energy Information Administration, Office of Integrated Analysis and Forecasting, U.S. Department of Energy, Washington DC, 2006 (<http://www.eia.doe.gov/oiaf/ieo/index.html>).
- 3 See, for instance: http://www.hydrogen.energy.gov/fuel_cells.html.
- 4 See, for instance: <http://ethanol.org>.
- 5 See, for instance: Directive 2003/30/EC of the European Parliament and of the Council of 8 May 2003 on the promotion of the use of biofuels or other renewable fuels for transport, *Official Journal of the European Union*, 17 May 2003.
- 6 P. J. Squillace, D. A. Pope and C. V. Price, *Occurrence of the gasoline additive MTBE in shallow ground water in urban and agricultural areas*, U.S. Geological Survey, National Water Quality Assessment Program, Rapid City, SD, USA, 1995 (<http://sd.water.usgs.gov/nawqa/pubs/factsheet/fs114.95/fact.html>).
- 7 D. M. T. Newsham, in *Science and Practice of Liquid-Liquid Extraction*, ed. J. D. Thornton, Clarendon Press, Oxford, 1992, vol. 1; Z. Lei, B. Chen and Z. Ding, *Special Distillation Processes*, Elsevier, Amsterdam, 1st edn, 2005.
- 8 *Ionic Liquids IIIA: Fundamentals, Progress, Challenges, and Opportunities*, ed. R. D. Rogers and K. R. Seddon, ACS Symposium Series, Washington, 2005, vol. 901.
- 9 J. G. Huddleston, H. D. Willauer, R. P. Swatloski, A. E. Visser and R. D. Rogers, *Chem. Commun.*, 1998, **16**, 1765.
- 10 M. J. Earle, J. M. S. S. Esperança, M. A. Gilea, J. N. Canongia Lopes, L. P. N. Rebelo, J. W. Magee, K. R. Seddon and J. A. Widegren, *Nature*, 2006, **439**, 831–834.
- 11 A. Heintz, *J. Chem. Thermodyn.*, 2005, **37**, 525–535.
- 12 Y. A. Beste, M. Eggersmann and H. Schoenmakers, *Chem.-Ing.-Tech.*, 2005, **77**, 1800; Y. A. Beste, M. Eggersmann and H. Schoenmakers, *Chem.-Ing.-Tech.*, 2004, **76**, 1407; Y. A. Beste, C. Jork and H. Schoenmakers, *Chem.-Ing.-Tech.*, 2003, **75**, 1148.
- 13 J. D. Holbrey, W. M. Reichert, R. P. Swatloski, G. A. Broker, W. R. Pitner, K. R. Seddon and R. D. Rogers, *Green Chem.*, 2002, **4**, 407.
- 14 J. D. Holbrey, N. V. Plechkova and K. R. Seddon, *Green Chem.*, 2006, **8**, 411–414.
- 15 A. Arce, J. Martínez-Ageitos, E. Rodil and A. Soto, *ELDATA: Int. Electron. J. Phys.-Chem. Data*, 1998, **4**, 135.
- 16 S. Himmler, S. Hörmann, R. van Hal, P. S. Schulz and P. Wasserscheid, *Green Chem.*, 2006, **8**, 887–894.
- 17 H. Renon and J. M. Prausnitz, *AIChE J.*, 1968, **14**, 135.
- 18 J. M. Sørensen and W. Arlt, *Liquid-Liquid Equilibrium Data Collection. Binary Systems*, DECHEMA Chemistry Data Series, DECHEMA, Frankfurt, 1979, vol. 5 (1).
- 19 A. Arce, J. Martínez-Ageitos, E. Rodil and A. Soto, *Fluid Phase Equilib.*, 1999, **165**, 121–139; A. Heine, K. Fischer and J. Gmehling, *J. Chem. Eng. Data*, 1999, **44**, 373–378.
- 20 J. Z. Yang, X. M. Lu, J. S. Gui and W. G. Xu, *Green Chem.*, 2004, **6**, 541.
- 21 K. R. Seddon, A. Stark and M.-J. Torres, *Pure Appl. Chem.*, 2000, **72**, 2275–2287.
- 22 A. Arce, E. Rodil and A. Soto, *J. Chem. Eng. Data*, 2006, **51**, 1453–1457.

Solute–solvent interactions within aqueous poly(ethylene glycol): solvatochromic probes for empirical determination and preferential solvation

Pallavi Singh and Siddharth Pandey*

Received 2nd March 2006, Accepted 28th November 2006

First published as an Advance Article on the web 18th December 2006

DOI: 10.1039/b603210a

Due to their vast industrial importance, poly(ethylene glycols) [PEGs] have become substances of major investigations. The hypothesis that aqueous PEG rather than pure PEG may provide substantially improved physicochemical properties for many industrial applications is addressed. Solvatochromic electronic absorbance probes are utilized to gather important information about these systems. Response from a water-soluble betaine dye suggests a decrease in dipolarity/polarizability and/or hydrogen-bond donating (HBD) acidity as the PEG is added to water. This is further confirmed by the response of *N,N*-diethyl-4-nitroaniline, which shows a decrease in dipolarity/polarizability and, in concert with the response from the betaine dye, a decrease in HBD acidity as the amount of PEG is increased. Response from 4-nitroaniline combined with dipolarity/polarizability is used to show that hydrogen-bond accepting (HBA) basicity increases with the addition of PEG to water. The extent of change in these important physicochemical properties depends on the PEG molecular mass. A simple mole-fraction weighted solvation model suggests significant preferential solvation of the betaine dye by PEG molecules in aqueous PEG solutions.

Introduction

The role of the solvent in chemical reactions is one of immediate and daily concern to practising chemists.¹ The majority of the solvents used in industry are volatile organic compounds (VOCs) which have a high vapour pressure and low water solubility. Lately, there have been efforts from both academic and industrial research communities to seek neoteric and plausible greener alternatives to these VOCs.^{2–8} Among many such alternatives being explored currently (*e.g.*, supercritical fluids, room-temperature ionic liquids, *etc.*), polymers and aqueous polymer-based solvents are gaining widespread acceptance.⁸ As a result, investigations and applications of polymer-based solutions have increased many fold. Especially, exploration and assessment of the structural and dynamical properties of molten polymers and polymer solutions has become a topic of great interest. In particular, poly(ethylene glycols) (PEGs) are of great industrial, pharmaceutical, and biomedical importance due to their physicochemical properties and high solubility in many solvents, especially water.^{9–11}

PEGs are condensation polymers of ethylene oxide with water having the general formula $H(OCH_2CH_2)_nOH$. The most widespread uses of low-volatile non-toxic PEGs are in detergents and as emulsifiers and plasticizers.^{9,10} The wide range of chain lengths provides physical and chemical properties for application in many areas, such as polyester resin preparation to enhance water dispersibility, water-based coatings, anti-dusting in agricultural formulations, brightening

effect and adhesion enhancement in electroplating processes, coupling agent, humectant, solvent, and lubricant in cosmetics and personal care bases, dimensional stabilizer in wood working operations, dye carrier in paints and inks, heat transfer fluid formulation and de-foamer formulations, low volatile, water soluble and non-corrosive lubricant without staining residue in food and package process, mucoadhesive drug carrier, DNA condensation in aqueous methanol solutions, among others.^{12,13}

Many of the aforementioned and other biomedical applications of PEG are solely possible due to the high aqueous solubility of most low molecular mass PEGs. This could be attributed to the hydrogen-bonding within PEG solutions.¹⁴ As a result, a greater understanding of solute–solvent and solvent–solvent interactions within aqueous PEG solutions becomes imperative. For example, one of the important applications of PEGs is in protein precipitation. The intra-diffusion studies performed in order to understand the precipitation mechanism of proteins suggested formation of a network which may be due to the presence of water bridges between two ether oxygens of the PEG chain. The network is regarded as an assembly of chains connected together through hydrogen bonds between H of water and O of PEG and the stoichiometry is suggested to be 0.5 water molecules for each ether oxygen.¹⁵ The structure is similar to that of cross-linked polymerized gels.

Towards obtaining a better understanding of the solute–solvent interactions within aqueous PEG solutions comprised of varying molecular mass PEGs, we have utilized selected solvatochromic molecular electronic absorbance probes.¹⁶ Depending on the solute–solvent interaction(s) involved,

Department of Chemistry, Indian Institute of Technology Delhi, Hauz Khas, New Delhi-110016, India. E-mail: sipandey@chemistry.iitd.ac.in; Fax: +91-11-26581102; Tel: +91-11-26596503

solubilizing medium may exert a profound effect on the position, shape and intensity of a molecular absorption band. Many of such interactions, *e.g.*, dipolarity/polarizability, hydrogen bond donating ability, hydrogen bond accepting ability, *etc.*, are readily manifested through molecular absorbance spectra of various solvatochromic probes.¹⁷ Further, specific solute–solvent interaction(s) may result in preferential solvation of the solute by one of the components in the solution.¹⁸ We present the behaviour of a variety of molecular absorbance probes when dissolved in aqueous PEG solutions of different molecular masses. On the basis of these probe responses, using empirical relationships established in the literature, dipolarity/polarizability (π^*), hydrogen-bond donating ability (α) and hydrogen bond accepting ability (β) of aqueous PEG solutions are reported. Finally, the extent of preferential solvation, if any, is also explored.

It is important to mention some earlier attempts to investigate aqueous PEG systems. Zaslavsky *et al.* used a structurally different betaine dye to probe aqueous PEG systems (a buffered aqueous phase was used): however, aqueous PEG systems with lower molecular mass PEGs were not investigated in the entire concentration range.¹⁹ Another report by Park and co-workers also has the same problem.²⁰ Further, many empirical parameters are not reported for the aqueous PEGs, rather only neat PEGs constituted the main systems of interest. Huddleston and Rogers have also measured similar empirical parameters: however, their investigations mostly dealt with PEG–salt aqueous biphasic systems.^{11,21} Interested readers are referred to pertinent references provided in ref. 11 for further information on Huddleston and Rogers work in the related area.

Experimental

Materials. 2,6-Diphenyl-4-(2,4,6-triphenylpyridinium-1-yl)phenolate [betaine dye 1] and 2,6-dichloro-4-(2,4,6-triphenylpyridinium-1-yl)phenolate [betaine dye 2] were purchased from Aldrich Chemical Co. in the highest purity possible and Fluka ($\geq 99\%$ by HPLC), respectively. It is important to mention that betaine dyes are usually crystallized with ~ 2 moles of crystal water, and as a result are not close to 100% pure. For spectrophotometric purposes, however, they can be considered close to 100% pure. 4-Nitroaniline ($\geq 90\%$) and *N,N*-diethyl-4-nitroaniline were purchased from Spectrochem Co. Ltd. and Frinton Laboratories, respectively. PEGs of average molecular mass 200, 400, 600 4000, and 6000 were purchased from Central Drug House (CDH) and HPLC grade water was obtained from Merck. Ethanol (99.9%) was obtained from sd fine-chem. Ltd.

Method. All probe stock solutions were prepared in ethanol and stored in amber glass vials at 4 ± 1 °C. The required amounts of probes were weighed using Mettler–Toledo AB104-S balance with a precision of ± 0.1 mg. Aqueous PEG solutions with different molecular mass PEGs were prepared by mass using an Ohaus AR2130 balance with a precision of ± 1 mg. If required, solutions were gently heated to 40 °C in a water bath with continuous stirring to obtain a

homogeneous solution at room temperature. An appropriate amounts of the probe solution from the stock was transferred a 10 mL volumetric flask. The ethanol was evaporated using a gentle stream of high purity nitrogen gas. PEG, water or aqueous-PEG solution was added to the volumetric flask to achieve the desired probe concentration.

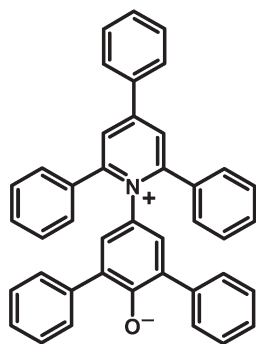
A PerkinElmer LambdaBio 20 double beam spectrophotometer with variable band width was used for acquisition of the UV-vis molecular absorbance data. All the data were acquired using 1 cm² path length quartz cuvettes. The spectral response from appropriate blanks was subtracted before data analysis. It was observed that Beer's law was followed for all four probes within the concentration ranges used in our studies (*i.e.*, the electronic absorbance values of all probes were within the linear range of the respective absorbance *versus* concentration plots). All the measurements were taken in triplicate and averaged. All data are acquired under ambient conditions. Data analysis was performed using Microsoft Excel and SigmaPlot 8.0 software.

Results and discussion

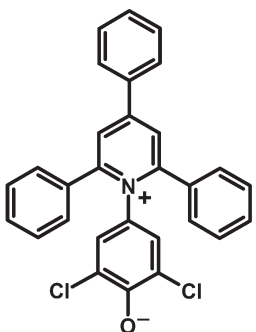
Behaviour of 2,6-dichloro-4-(2,4,6-triphenylpyridinium-1-yl)phenolate and $E_T(33)$

2,6-Diphenyl-4-(2,4,6-triphenylpyridinium-1-yl)phenolate (betaine dye 1) exhibits an unusually high solvatochromic band shift.^{22–24} The lowest energy intramolecular charge-transfer absorption band of the betaine dye 1 is hypsochromically shifted by *ca.* 357 nm on going from relatively non-polar diphenyl ether ($\lambda_{\max} \sim 810$ nm) to water ($\lambda_{\max} \sim 453$ nm). The negative solvatochromism of the betaine dye 1 originates from the differential solvation of its highly polar equilibrium ground state and the less polar first Franck–Condon excited states with increasing solvent polarity. There is a considerable charge transfer from the phenolate to the pyridinium part of the zwitterionic molecule (see structure in Scheme 1). Because of its zwitterionic nature, the solvatochromic probe behaviour of betaine dye 1 is strongly affected by the hydrogen-bond donating (HBD) acidity of the solvent; hydrogen-bond donating solvents stabilize the ground state more than the excited state. Betaine dye 1 is one of the most widely used probes of its kind: the empirical scale of solvent “polarity”, $E_T(30)$, is defined as the molar transition energy of the dye in kcal.mol^{−1} at room temperature and normal pressure according to the expression $E_T(30) = 28\,591.5/\lambda_{\max}$ in nm. However, in the present work a derivative of the betaine dye 1, 2,6-dichloro-4-(2,4,6-triphenylpyridinium-1-yl)phenolate (Scheme 1, henceforth named betaine dye 2) is used due to certain advantages over betaine dye 1.²⁵ Firstly, betaine dye 1 has a high pK_a value of 8.65 ± 0.05 , which restricts measurements to being performed preferably in alkaline solutions. Secondly, the low solubility ($< 10^{-6}$ M) of betaine dye 1 in water renders it somewhat unsuitable for investigating aqueous-based solutions.²⁶ Betaine dye 2 has a pK_a value of 4.78 ± 0.05 and it remains unprotonated at physiological pH.

Absorbance spectra of betaine dye 2 were collected in PEG 200, PEG 400, PEG 600, PEG 4000, PEG 6000 and PEG 20000, and aqueous solutions of these PEGs in 10 wt%



2,6-Diphenyl-4-(2,4,6-triphenylpyridinium-1-yl)phenolate
(Betaine dye 1)



2,6-Dichloro-4-(2,4,6-triphenylpyridinium-1-yl)phenolate
(Betaine dye 2)

Scheme 1 Structures of betaine dyes 1 and 2.

increments of water at ambient conditions. Fig. 1 shows absorbance spectra of betaine dye 2 ($\sim 100 \mu\text{M}$) in aqueous PEG 600. Similar betaine dye 2 spectral behaviour is observed in all the other aqueous PEG solutions as well. The well-established empirical solvent “polarity” parameter, $E_T(33)$ (the molar transition energy of the probe in kcal mol^{-1} , $E_T(33) = 28591.5/\lambda_{\text{max}}$ in nm) was calculated and is reported in Table 1. As expected, a bathochromic shift in λ_{max} [a decrease in $E_T(33)$] is clearly evident as the wt% of the PEG is increased, indicating a decrease in the dipolarity and/or HBD acidity of

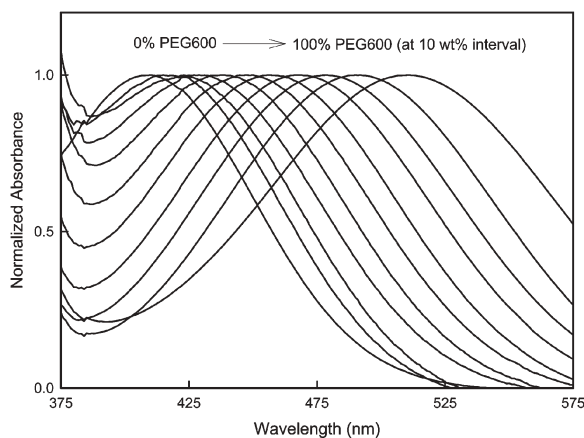


Fig. 1 Normalized absorbance spectra of betaine dye 2 [$\sim 100 \mu\text{M}$] in aqueous PEG 600.

Table 1 $E_T(33)$ values (kcal mol^{-1}) within aqueous PEG solutions. Maximum standard deviation associated with the $E_T(33)$ of $\pm 0.20 \text{ kcal mol}^{-1}$ is observed within neat water

PEG (wt%)	PEG 200	PEG 400	PEG 600	PEG 4000	PEG 6000
0%	69.96	69.96	69.96	69.96	69.96
10%	69.91	68.73	68.73	67.59	68.48
20%	69.57	67.43	67.59	66.41	67.59
30%	68.56	66.34	66.49	65.35	66.72
40%	66.80	65.13	65.13	64.54	65.43
50%	64.91	63.12	63.68	63.19	63.54
60%	63.68	62.70	62.70	61.55	61.49
70%	62.56	61.36	61.22	60.32	60.38
80%	61.71	59.32	59.75	Opaque	Opaque
90%	60.79	58.83	58.23	Opaque	Opaque
100%	59.65	57.36	55.95	Solid	Solid

the solubilizing microenvironment (*i.e.*, the cybotactic region) around this probe. These results are in accord with those reported by Zaslavsky *et al.*¹⁹ for buffered water as they established earlier that the static dielectric constant of water in aqueous solutions of PEG 6000 decreases directly with the PEG concentration.²⁷ Further, as the PEG molecular mass is increased in going from PEG 200 to PEG 600, $E_T(33)$ in neat PEG decreases, again indicating decreased dipolarity and/or HBD acidity of the solubilizing microenvironment for the probe with PEG molecular mass (a decrease in $E_T(33)$ of 10.3 ± 0.2 , 12.6 ± 0.2 , and $14.0 \pm 0.2 \text{ kcal mol}^{-1}$ from neat water to PEG200, PEG400, and PEG600, respectively, is observed). Surprisingly, a fair-to-good linear correlation is observed between $E_T(33)$ and wt% PEG for each PEG, as indicated by the results of the linear regression analysis (Table 2). A close inspection reveals the slopes to be higher for higher PEGs, *i.e.*, PEG 600, PEG 4000, PEG 6000, indicating higher sensitivity of the probe response as the wt% of PEG is increased for higher molecular mass PEGs. Similar outcomes were reported by Zaslavsky *et al.*¹⁹, albeit with a significant difference. Their results show a linear behaviour only up to a limiting PEG concentration, after which the slope increases (the limiting concentration for all PEGs is $< 40 \text{ wt}\%$). Their results with another probe, thymol blue, however, showed linear behaviour up to around 30 wt% PEG for PEG 6000. As was mentioned earlier, whole concentration range was not investigated by these authors even for lower molecular mass PEGs. Tentatively, we can attribute these differences to the fact that the structures of the two probes are different along with the fact that buffered water was used in their studies.

Significantly poor r^2 values were recovered from the linear regression analysis of $E_T(33)$ versus PEG mole fraction (Table 2, the mole fractions of PEG are calculated using the mean molecular mass of the corresponding PEG). As was suggested in the literature,^{28,29} the concentration scale may be recalculated in terms of monomer molar fraction, x' , defined as

$$x' = \frac{n_{\text{OE}}}{n_{\text{OE}} + n_{\text{w}}} \quad (1)$$

n_{OE} being the mean number of oxyethylene units of PEG chains in solution and n_{w} the number of water molecules. The linear regression analysis of $E_T(33)$ versus x' shows

Table 2 Results of linear regression analysis for $E_T(33)$ versus wt% PEG, $E_T(33)$ versus mole fraction PEG, and $E_T(33)$ versus x' for aqueous PEG systems

	$E_T(33)$ vs. wt% PEG		$E_T(33)$ vs. mole fraction PEG		$E_T(33)$ vs. x'	
	r^2	Slope	r^2		r^2	Slope
PEG 200	0.9769	-0.1152 ± 0.0018	0.6059		0.9097	-11.4566 ± 0.3627
PEG 400	0.9952	-0.1272 ± 0.0010	0.4740		0.9263	-12.5997 ± 0.3572
PEG 600	0.9930	-0.1350 ± 0.0011	0.4927		0.9674	-13.6941 ± 0.2526
PEG 4000	0.9870	-0.1290 ± 0.0022	0.8754		0.9597	-18.3958 ± 0.5440
PEG 6000	0.9825	-0.1377 ± 0.0011	0.9218		0.9826	-20.1026 ± 0.3865

some improvement in r^2 values: however, a linear behaviour, for all analytical purposes, cannot be suggested. Surprisingly, the slope increases as the PEG molecular mass is increased.

Further, solute–solvent interaction for betaine dye 2 and aqueous PEG is also manifested through the broadening in the electronic absorption band in going from neat water to neat PEG—increases in FWHMs of 22.6 ± 0.8 , 34.6 ± 0.8 and 36.6 ± 0.8 nm are observed for PEG 200, PEG 400, and PEG 600, respectively. This is conceivable as the less dipolar (with respect to the ground state) excited state of this probe would perhaps encounter enhanced interactions with its milieu as the dipolarity of the cybotactic region is decreased. Further, a greater decrease in $E_T(33)$ with increasing PEG molecular mass is also understandable as there are more ethylene oxide moieties on each polymer unit, giving rise to lower dipolarity and/or HBD acidity. A more interesting observation, however, is the extent of the difference in the spectral behaviour between PEG200/PEG400 and PEG400/PEG600. The changes in both $E_T(33)$ and FWHM are more drastic for the former. These results may be explained on the combined effect of the presence of shorter oxyethylene chains as well as a larger number of terminal polar OH functionalities in PEG 200 as compared with PEG 400 and PEG 600 (the number of terminal OH groups decreases in the ratio 6:3:2 for PEG 200, PEG 400, and PEG 600, respectively). While the longer oxyethylene chains may provide a cybotactic region with decreased dipolarity, the presence of more OH termini will impart enhanced hydrogen bond donating acidity along with increased dipolarity. A cumulative effect will result in lower $E_T(33)$ and higher FWHM as the PEG molecular mass is increased.

Preferential solvation as indicated by betaine dye 2 [$E_T(33)$]

The study of physicochemical properties that depend on solute–solvent interactions is much more complex in mixed solvent systems than in pure solvents.^{30–33} On one hand, the solute can be preferentially solvated by any of the solvents present in the mixture: on the other, solvent–solvent interactions can strongly affect solute–solvent interactions. Studying solute–solvent interactions by means of solvatochromic probes is both simple and convenient.^{18,34} Preferential solvation arises whenever the bulk mole fraction solvent composition is different from the solvation microsphere solvent composition. The response of spectroscopic probes is dependent upon the composition of the solvation microsphere and therefore provides a convenient means to measure the extent of preferential solvation. Most spectroscopic probe

techniques assume an idealized situation where solvent–solvent interactions can be neglected and the measured spectral response, R , in a binary solvent mixture is given by^{18,34–38}

$$R = Y_A R_A^0 + (1 - Y_A) R_B^0 \quad (2)$$

a weighted local mole fraction of the probe's spectral response in the two pure solvents, R_A^0 and R_B^0 . Here Y_A and $(1 - Y_A)$ refer to the solvation sphere composition, which, in the case of preferential solvation, may be quite different from the overall bulk liquid-phase composition.

Considering spectral response as $E_T(33)$, we have calculated the Y_{PEG} for PEG 200, PEG 400, and PEG 600 (calculations were not possible for higher molecular mass PEGs due to the lack of $E_T(33)$ in neat PEG). Figs. 2 and 3 present Y_{PEG} versus mole fraction PEG and Y_{PEG} versus x' , respectively, for PEG 200, PEG 400, and PEG 600. It is clear that $Y_{\text{PEG}} >$ mole fraction PEG at most PEG concentrations for all three PEG systems. It can be deduced that the probe betaine dye 2 is significantly preferentially solvated by the PEG molecules. It is conceivable that the non-polar functionalities of the probe are inducing this effect (see probe structure in Scheme 1). Further, the extent of preferential solvation increases rapidly and reaches a maximum before gradually decreasing again (see Fig. 2). The highest extent of preferential solvation is observed in the 0.15–0.22 mole fraction PEG region for all three PEGs investigated. The extent of preferential solvation, on the average, is decreased if the similar analysis is carried out with x' instead of mole fraction PEG. The trend is very similar nonetheless (Fig. 3). It is important to remind the reader that the calculations are based on $E_T(33)$ in neat PEGs, whereas x' is defined in terms of oxyethylene units.

Empirical Kamlet–Taft parameters

Additional insight into these aqueous PEG systems can be provided using Kamlet–Taft solvatochromic indicators of solvent dipolarity/polarizability (π^*), HBD acidity (α), and hydrogen bond accepting (HBA) basicity (β).^{39–42}

The π^* parameters were estimated from the absorption maximum (ν_{DENA} , in kK) of *N,N*-diethyl-4-nitroaniline (DENA), a non-hydrogen bond donor solute, using:

$$\pi^* = 8.649 - 0.314 \nu_{\text{DENA}} \quad (3)$$

β values were determined from the enhanced solvatochromic shift of 4-nitroaniline (NA) relative to its homomorph

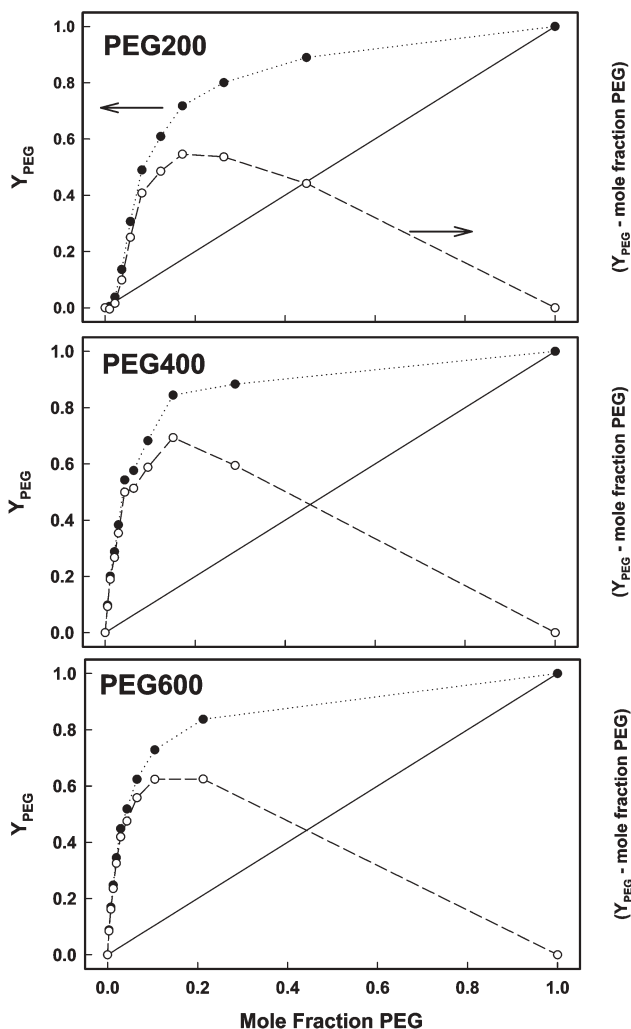


Fig. 2 Solvation sphere composition of PEG (Y_{PEG}) calculated from eqn. (2) (closed circles) and [$Y_{\text{PEG}} - \text{mole fraction PEG}$] (open circles) versus mole fraction PEG. Continuous line indicates ideal behaviour.

N,N-diethyl-4-nitroaniline, $-\Delta\nu(\text{DENA-NA})/kK$, resulting in eqn. (4).

$$\beta = -0.357\nu_{\text{NA}} - 1.176\pi^* + 11.12 \quad (4)$$

α parameters were in turn calculated from $E_{\text{T}}(30)$ and π^* values.

$$\alpha = 0.061E_{\text{T}}(30) - 0.885\pi^* - 1.837 \quad (5)$$

$E_{\text{T}}(30)$ were calculated from $E_{\text{T}}(33)$. For this, both $E_{\text{T}}(30)$ and $E_{\text{T}}(33)$ were obtained in 20 different solvents and the following relationship was obtained from the linear regression analysis:

$$E_{\text{T}}(30) = 0.9953 (\pm 0.0287) E_{\text{T}}(33) - 8.1132 (\pm 1.6546)$$

$$R = 0.9926, \text{ standard error of estimate} = 0.8320, n = 20 \quad (6)$$

As expected, a gradual hypsochromic shift in DENA λ_{max} ($[\text{DENA}] \sim 25 \mu\text{M}$) accompanied by a reduction in FWHM is observed as the amount of PEG is increased (data not shown). Calculated π^* are presented in Figs. 4 and 5. For PEG 200,

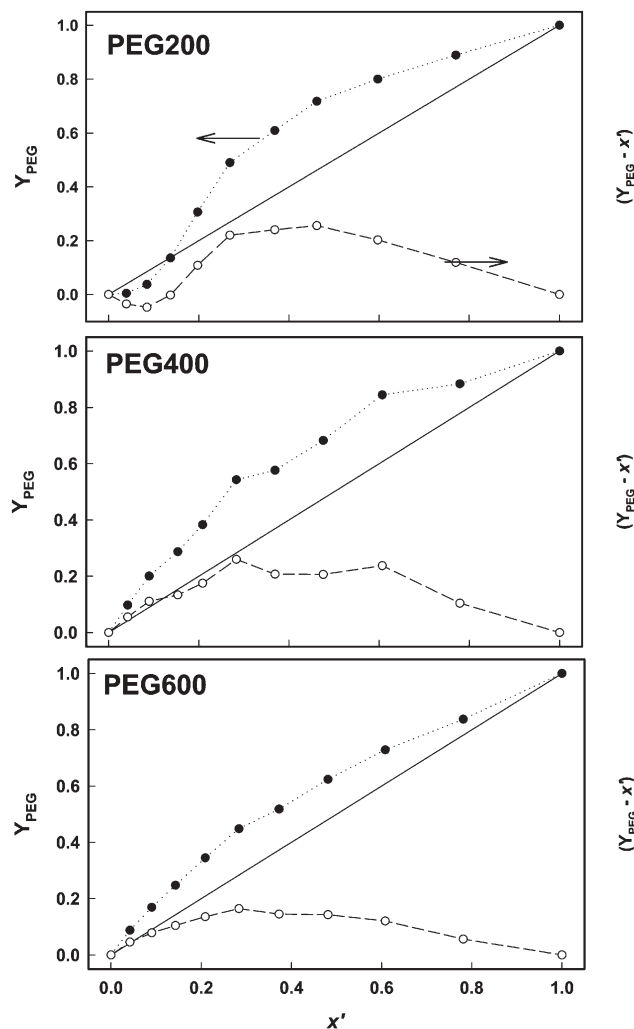


Fig. 3 Solvation sphere composition of PEG (Y_{PEG}) calculated from eqn. (2) (closed circles) and [$Y_{\text{PEG}} - \text{monomer molar fraction PEG (x')}$] (open circles) versus x' . Continuous line indicates ideal behaviour.

PEG 400, and PEG 600, a systematic decrease in π^* is observed with increasing amount of PEG (Fig. 4). For PEG 4000 and PEG 6000, however, the trend in π^* is not as systematic; upon addition of PEG to water an overall trend of decrease in π^* may be suggested (Fig. 5). For neat PEG 200, PEG 400 and PEG 600, as the molecular mass of the PEG is increased, π^* is decreased ($\pi^* = 0.915 \pm 0.009, 0.867 \pm 0.010$ and 0.838 ± 0.008 for PEG 200, PEG 400, and PEG 600, respectively). This could be attributed to the increase in less dipolar longer oxyethylene chains on higher molecular mass PEGs. It is important to mention that these results are in contradiction with what is reported by Park *et al.*²⁰ For PEG 8000 in the concentration range 0–30 wt%, their π^* probes did not show any solvatochromic shifts. This is surprising as all the betaine dye results also confirm a decrease in dipolarity/polarizability and/or HBD acidity as the amount of PEG is increased in the solution. Further, they also report their π^* to be essentially the same regardless of PEG molecular mass. Again, our results, along with those by Zaslavsky *et al.*,¹⁹ using various betaine dyes, suggest otherwise. No change in π^*

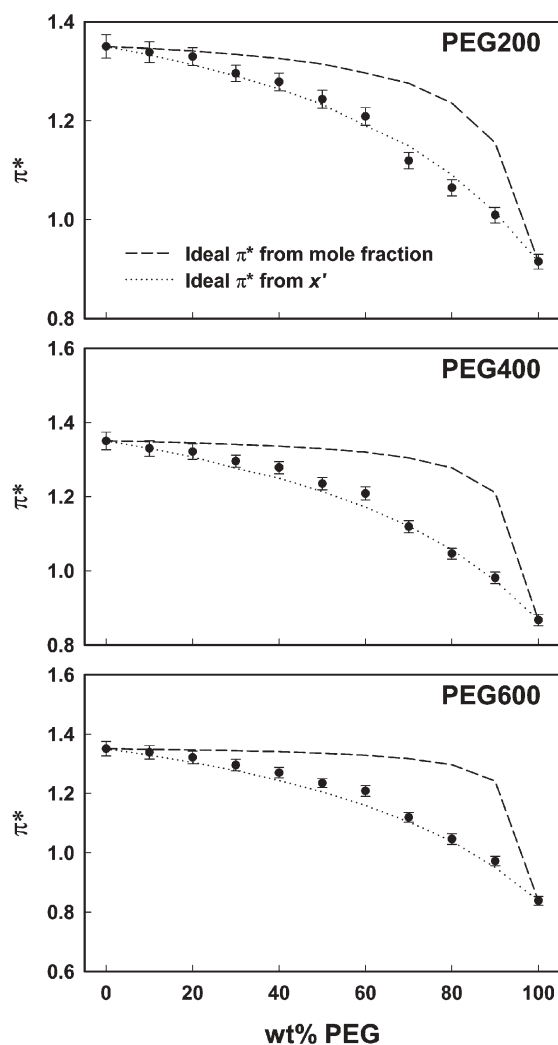


Fig. 4 Dipolarity/polarizability (π^*) (closed circles) versus wt% PEG in aqueous PEG. Dashed and dotted curves represent ideal π^* calculated using mole fractions and monomer molar fractions, x' , respectively.

with addition of water and changing PEG molecular mass, as reported by Park *et al.*, is difficult to comprehend.

Next, further information is obtained through the estimation of ideal π^* values. Ideal π^* are estimated as weighted mole fraction averaged values and as weighted x' averaged values (dashed and dotted curves in Fig. 4, respectively). It is clear that while the estimated values using mole fraction PEG are not in good agreement with the measured π^* , the ones using x' provided fairly reasonable agreement. This further emphasizes the role played by the oxyethylene units in the dipolarity/polarizability of aqueous PEG systems.

The measured HBA basicity (β) is presented in Figs. 5 and 6 ([NA] $\sim 25 \mu\text{M}$). It is clear from the data that β increases as wt% PEG is increased. This could be easily attributed to the fact that each PEG molecule offers more hydrogen bond accepting centres (two HOCH_2CH_2 and, depending on PEG molecular mass, many $\text{CH}_2\text{CH}_2\text{OCH}_2\text{CH}_2$) than water. As a consequence, the measured β are closer to the ideal β calculated using weighted x' averaged values than the ideal β calculated from weighted mole fraction averaged values

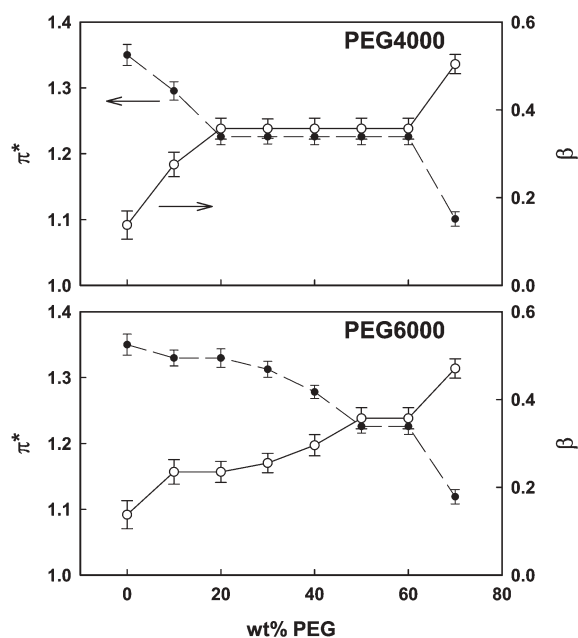


Fig. 5 Dipolarity/polarizability (π^*) (closed circles, dashed lines) and hydrogen-bond accepting basicity (β) (open circles, continuous lines) versus wt% PEG for PEG 4000 and PEG 6000 in aqueous PEG.

(Fig. 6). The observation that measured β are always higher than the calculated ideal β from weighted x' averaged values could be tentatively attributed to the difference in the hydrogen bond accepting ability of the terminal OH and the oxyethylene moieties. Again, for PEG 4000 and PEG 6000, β also increases with increase in PEG amount in the solution (Fig. 5, ideal β could not be calculated due to the lack of β in neat PEG 4000 and PEG 6000, respectively). It is important to mention here that, to our surprise, analyses by Park and co-workers²⁰ again show no changes in the β value upon addition of PEG to water. We are unable to offer an explanation for this at present. The π^* and β values reported by them in neat PEG are very similar to our values nonetheless.

Finally, the HBD acidities (α) were calculated for each of the aqueous PEG systems using eqns (5) and (6) and are plotted in Figs. 7 and 8. For neat PEGs our α values are in good agreement with those reported by Park and co-workers;²⁰ similar to our results, they also report a decrease in α as more and more PEG is added to the water. However, they have calculated α only up to 40 wt% PEG in water. A careful examination of α reported in Figs. 7 and 8 reveals some interesting information. First, as the PEG molecular mass increases, α in neat PEG decreases. This could be attributed to the fact that although every PEG molecule possesses two HBD sites at the termini (the ability of oxyethylene hydrogens for HBD can be considered negligible), there would be a lower number of HBD sites for longer PEG chains around a probe molecule in its cybotactic region. Second, as the amount of PEG is increased, α decreases. This is easy to comprehend as water is one of the best HBD solvents. It appears that the decrease in α is not as drastic at higher PEG weight fractions as in aqueous solutions with lower amounts of PEG. Further, ideal α are calculated using PEG mole fractions and x' (long dashed and dotted curves in Fig. 7, respectively). It is clear

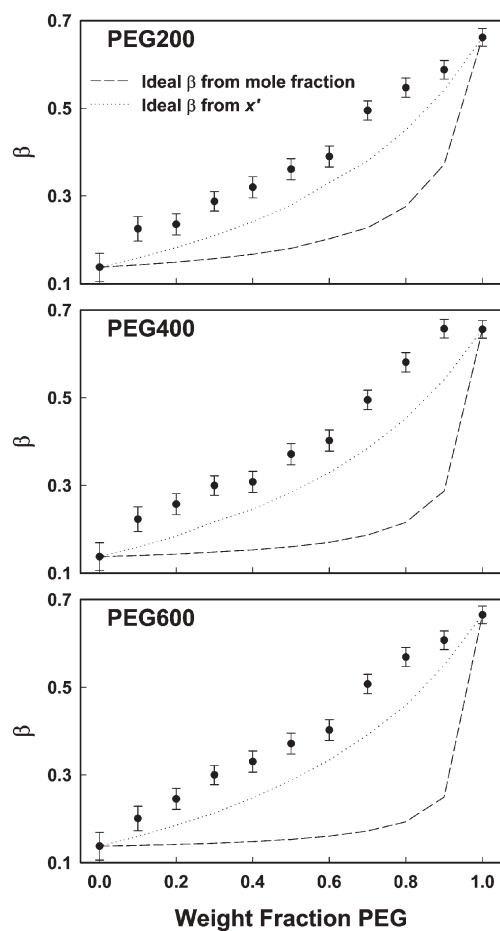


Fig. 6 Hydrogen-bond accepting basicity (β) (closed circles) versus weight fraction PEG in aqueous PEG. Dashed and dotted curves represent ideal β calculated using mole fractions and monomer molar fractions, x' , respectively.

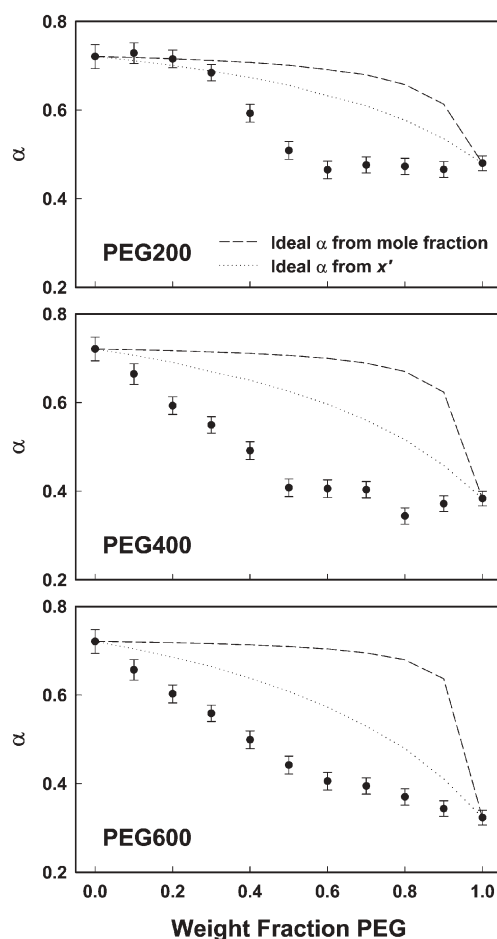


Fig. 7 Hydrogen-bond donating acidity (α) (closed circles) versus weight fraction of PEG in aqueous PEG. Dashed and dotted curves represent ideal α calculated using mole fractions and monomer molar fractions, x' , respectively.

from the plot that the experimental α values do not conform to any of the two calculated ideal α . Of the two ideal α , the one calculated using x' is closer to the experimentally observed α nonetheless.

Conclusions

Solvatochromic molecular electronic absorbance probes have furnished important information regarding the solute solvation and properties of aqueous PEG systems with varying PEG molecular mass. It is demonstrated that the commonly used E_T scale linearly decreases with PEG weight fraction. This decrease in E_T value is a combined effect of the decrease in the dipolarity/polarizability and the HBD acidity of the aqueous PEG. HBA basicity, on the other hand, increases with increasing PEG. A simplistic solvation model suggests the betaine dye used in the investigation to be preferentially solvated by PEG in the aqueous PEG solution. The outcomes of these investigations may be used to better model chemical and biological processes within aqueous PEG systems. This may further help to enhance the potential overall use and applications of these environmentally-benign systems.

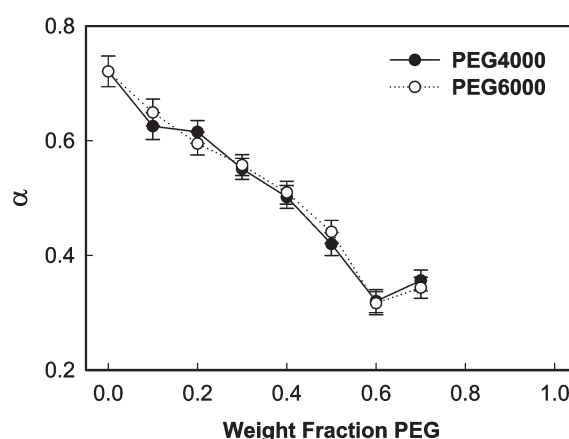


Fig. 8 Hydrogen-bond donating acidity (α) versus weight fraction of PEG in aqueous PEG for PEG 4000 (closed circles, continuous lines) and PEG 6000 (open circles, dotted lines).

Acknowledgements

S.P. would like to thank the Department of Science and Technology, Government of India, and Council of Scientific

and Industrial Research, Government of India, for the partial support of this work.

References

- 1 C. Reichardt, *Solvents and Solvent Effects in Organic Chemistry*, Wiley-VCH, Weinheim, 3rd edn., 2003.
- 2 T. J. Collins, *J. Chem. Educ.*, 1995, **72**, 965.
- 3 C. J. Cusamano, *CHEMTECH*, 1992, **22**, 482.
- 4 J. F. Brennecke and M. A. Stadtherr, *Comput. Chem. Eng.*, 2002, **26**, 307.
- 5 J. H. Clark, *Green Chem.*, 1999, **1**, 1.
- 6 *Green Chemistry: Challenging Perspectives*, eds. P. Tundo and P. T. Anastas, Oxford Science, Oxford, 1999.
- 7 D. Noble, *Anal. Chem.*, 1993, **65**, 693A.
- 8 *Clean Solvents, Alternate Media for Chemical Reactions and Processing*, ed. M. A. Abraham and L. Moens, ACS Symposium Series 819, American Chemical Society, Washington, DC, 2002.
- 9 *Poly(Ethylene Glycol) Chemistry: Biotechnical and Biomedical Applications*, ed. J. M. Harris, Plenum, New York, 1992.
- 10 *Poly(Ethylene Glycol) Chemistry and Biological Applications*, ed. J. M. Harris and S. Zalipsky, ACS Symposium Series 680, American Chemical Society, Washington, DC, 1997.
- 11 J. Chen, S. K. Spear, J. G. Huddleston and R. D. Rogers, *Green Chem.*, 2005, **7**, 64.
- 12 B. S. Lele and S. A. Hoffman, *J. Controlled Release*, 2000, **69**, 237.
- 13 G. Kleideiter and E. Nordmeier, *Polymer*, 1999, **40**, 4013.
- 14 G. D. Smith, D. Y. Yoon, R. L. Jaffe, R. H. Colby, R. Krishnamoorti and L. J. Fetters, *Macromolecules*, 1996, **29**, 3462.
- 15 A. Vergara, G. Paduano, G. D'Errico and R. Sartorio, *Phys. Chem. Chem. Phys.*, 1999, **1**, 4875.
- 16 W. E. Acree, Jr., in *Encyclopedia of Analytical Chemistry: Theory and Instrumentation*, ed. R. A. Meyers, John Wiley & Sons, Ltd., Chichester, 2000, p. A5412 and references cited therein.
- 17 P. Suppan and N. Ghoneim, *Solvatochromism*, Royal Society of Chemistry, Cambridge, 1997.
- 18 *Solvent Mixtures: Properties and Selective Solvation*, Y. Marcus, Marcel Dekker, New York, 2002.
- 19 B. Y. Zaslavsky, L. M. Miheeva, E. A. Masimov, S. F. Djafarov and C. Reichardt, *Phys. Chem. Chem. Phys.*, 1999, **86**, 519.
- 20 I. W. Kim, M. D. Jang, Y. K. Ryu, E. H. Cho, Y. K. Lee and J. H. Park, *Anal. Sci.*, 2002, **18**, 1357.
- 21 J. G. Huddleston, H. D. Willauer and R. D. Rogers, *Phys. Chem. Chem. Phys.*, 2002, **4**, 4065.
- 22 C. Reichardt, *Chem. Rev.*, 1994, **94**, 2319.
- 23 C. Reichardt, *Pure Appl. Chem.*, 2004, **76**, 1903.
- 24 C. Reichardt, S. Asharin-Fard, A. Blum, M. Eschner, A. M. Mehranpour, P. Milart, T. Niem, G. Schafer and M. Wilk, *Pure Appl. Chem.*, 1993, **65**, 2593.
- 25 M. A. Kessler and O. S. Wolfbeis, *Phys. Chem. Liq.*, 1989, **50**, 51.
- 26 S. N. Baker, G. A. Baker and F. V. Bright, *Green Chem.*, 2002, **4**, 165.
- 27 B. Y. Zaslavsky, L. M. Miheeva, M. N. Rodnikova, G. V. Spivak, V. S. Harkin and A. U. Mahmudov, *J. Chem. Soc., Faraday Trans. 1*, 1989, 2857.
- 28 M. Pochylski, F. Aliotta, Z. Blaszcak and J. Gapinski, *J. Phys. Chem. B*, 2006, **110**, 485; Z. Blaszcak, M. Pochylski, I. I. Kostka, P. Ziobrowski, M. Drozdowski and M. Farhoud, *J. Mol. Liq.*, 2005, **121**, 75.
- 29 K. Miki, P. Westh and Y. Koga, *J. Phys. Chem. B*, 2005, **109**, 19536.
- 30 M. Roses, C. Rafols, J. Ortega and E. Bosch, *J. Chem. Soc., Perkin Trans. 2*, 1995, 1607.
- 31 M. Roses, C. Rafols, J. Ortega and E. Bosch, *J. Chem. Soc., Perkin Trans. 2*, 1996, 1497.
- 32 M. Roses, E. Bosch, F. Rived, U. Buhvestov and C. Rafols, *J. Chem. Soc., Perkin Trans. 2*, 1997, 1341.
- 33 M. Roses and E. Bosch, *J. Chem. Soc., Faraday Trans.*, 1992, **88**, 3541.
- 34 Y. Marcus, *Chem. Soc. Rev.*, 1993, 409.
- 35 K. A. Fletcher and S. Pandey, *Appl. Spectrosc.*, 2002, **56**, 266.
- 36 K. A. Fletcher and S. Pandey, *Appl. Spectrosc.*, 2002, **56**, 1498.
- 37 K. A. Fletcher, G. A. Baker, S. N. Baker and S. Pandey, *New J. Chem.*, 2003, **27**, 1706.
- 38 K. A. Fletcher and S. Pandey, *J. Phys. Chem. B*, 2003, **107**, 13532.
- 39 M. J. Kamlet, J. L. Abboud and R. W. Taft, *J. Am. Chem. Soc.*, 1977, **99**, 6027.
- 40 R. W. Taft and M. J. Kamlet, *J. Am. Chem. Soc.*, 1976, **98**, 2886.
- 41 M. J. Kamlet and R. W. Taft, *J. Am. Chem. Soc.*, 1976, **98**, 377.
- 42 M. J. Kamlet, J. L. Abboud, M. H. Abraham and R. W. Taft, *J. Org. Chem.*, 1983, **48**, 2877.

Liquid phase behaviour of 1-butyl-3-methylimidazolium 2-(2-methoxyethoxy)-ethylsulfate with organic solvents and water†

Urszula Domańska* and Andrzej Marciniak

Received 29th June 2006, Accepted 5th December 2006

First published as an Advance Article on the web 22nd December 2006

DOI: 10.1039/b609205e

Liquid–liquid equilibria of binary systems containing a room-temperature ionic liquid (1-butyl-3-methylimidazolium 2-(2-methoxyethoxy)-ethylsulfate [BMIM][MDEGSO₄], with: a hydrocarbon (*n*-hexane, cyclohexane, or benzene); a ketone (pentan-3-one, nonan-5-one or cyclopentanone); an alcohol (methanol, ethanol, butan-1-ol or octan-1-ol); 1,1-dimethylpropyl methyl ether or water were measured at normal pressure by a dynamic method from 287 K to the boiling point of the solvent or to 373 K. This paper includes thermophysical basic characterization of pure ionic liquid, obtained *via* differential scanning calorimetry (DSC), temperature of decomposition, temperature of glass phase transition, and heat capacity at half the *C_p* extrapolated temperature. The solubility of [BMIM][MDEGSO₄] in ketones decreases with an increase of the molecular weight of the ketone and is much higher in cycloketones than in a linear ketone. The solubility of the investigated IL is higher in aromatic hydrocarbons than in cyclic or linear hydrocarbons with the same number of carbon atoms. As a result of its strong interactions with alcohols, [BMIM][MDEGSO₄] shows complete miscibility with methanol, ethanol, butan-1-ol and octan-1-ol above 293 K. The experimental results of LLE have been correlated using the binary parameters of the non-random two liquid (NRTL) equation. The average root-mean-square deviation for the equilibrium mole fraction for all the calculated values was found to be 0.0031.

Introduction

Ionic liquids (ILs) are promising media to replace toxic and volatile organic solvents in industrial processes. They have negligible vapour pressures and are in the liquid state over a wide temperature range.¹ Another very important feature of ionic liquids is that their physicochemical properties depend upon both the cation and the anion structure, which provides the opportunity to design a solvent having certain properties (for example melting temperature, density, viscosity, liquidus range, *etc.*) for specific applications. Replacement of an organic solvent by an ionic liquid increases selectivity, yield and speed of reaction in many cases.^{2–4}

To design any process involving ionic liquids on an industrial scale it is necessary to know a range of basic thermophysical properties such as: temperature and enthalpy of melting; temperature and enthalpy of phase transition; heat capacity; viscosity; density and some thermodynamic properties including vapour–liquid equilibrium (VLE), liquid–liquid equilibrium (LLE), solid–liquid equilibrium (SLE) and activity coefficients at infinite dilution. Thermophysical properties and equilibrium data are also important to better understand the nature of ionic liquids and to develop thermodynamic models such as UNIFAC(Do).⁵ In recent work,⁶ the liquid–liquid phase equilibria for another ionic liquid/organic solvent system

have been reported and a review of the literature in the field presented with possible aggregates also discussed for the different systems.

This work is a continuation of our previous studies on liquid–liquid equilibrium in binary systems containing various ionic liquids and organic solvents.^{7–14} The liquid–liquid equilibrium of many binary systems containing 1-hexyloxy-methyl-3-methylimidazolium tetrafluoroborate, [C₆H₁₃OCH₂-MIM][BF₄] and 1-hexyloxymethyl-3-methylimidazolium bis(trifluoromethylsulfonyl)-imide, [C₆H₁₃OCH₂MIM][Tf₂N] with aliphatic hydrocarbons, aromatic hydrocarbons, cyclohexane, alcohols, ketones, or water have been determined.^{7,8} The impact of various factors on the phase behaviour of alkoxy-imidazolium-based ionic liquids with hydrocarbons has been reported.⁸ All the systems examined showed upper critical solution temperature (UCST) behaviour, with low solubility of the IL in *n*-alkanes and cycloalkanes and high solubility in aromatic hydrocarbons. An increase in the alkyl chain length of a *n*-alkane, or an increase in the alkyl chain length of substituent group on a benzene ring resulted in an increase in the UCST. The choice of anion was shown to have a large impact on the UCST of these systems, by changing the anion from [Tf₂N][−] to [BF₄][−] the solubility dramatically decreased and the UCST increased.⁷ The solubility of the dialkoxy-imidazolium salts: 1,3-dihexyloxymethyl-imidazolium tetrafluoroborate, [(C₆H₁₃OCH₂)₂IM][BF₄] and 1,3-dihexyloxymethyl-imidazolium bis(trifluoromethylsulfonyl)-imide, [(C₆H₁₃OCH₂)₂IM][Tf₂N] in hydrocarbons, alcohols and in water have previously been measured.⁷ Most of the examined systems showed immiscibility in the liquid phase at the upper critical solution temperature, or complete miscibility

Physical Chemistry Division, Faculty of Chemistry, Warsaw University of Technology, Noakowskiego 3, 00-664, Warsaw, Poland.

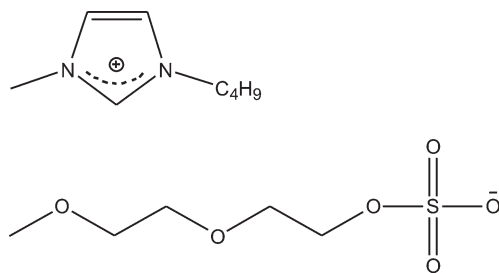
E-mail: ula@ch.pw.edu.pl; Fax: +48-22-6282741; Tel: +48-22-6213115

† Electronic supplementary information (ESI) available: TG/TGA data (Fig. S1) and equilibrium data (Table S1). See DOI: 10.1039/b609205e

of the IL with polar solvents at room temperature. An increase in the alkyl chain length of the alcohol resulted in an increase in the UCST as observed in previous work for imidazolium, ammonium or pyridinium ionic liquids.^{1,7,9,11,13} The increasing interaction between the IL and the solvent was undoubtedly the result of the specific interaction between the oxygen on the alkoxyethyl group of the cation with the solvent. The resulting increase in solubility was achieved by replacing a methyl group with a second alkoxy- group on the imidazolium ring.⁷

In this study, we investigated the liquid–liquid equilibrium of 1-butyl-3-methylimidazolium 2-(2-methoxyethoxy)-ethyl-sulfate with hydrocarbons, ketones, 1,1-dimethylpropyl methyl ether (*tert*-amyl methyl ether, TAME), water and alcohols. In our previous work the activity coefficients at infinite dilution for various solutes in this ionic liquid have been measured.¹⁵ For comparison with our previous work,^{7,8} the alkoxy groups are attached to the anion of the ionic liquid.

The structure of the ionic liquid under study is presented below:



Results and discussion

The investigated IL shows a high temperature of decomposition and the value of 632 K corresponds to 57% mass loss. The decomposition of the compound progresses in one step. The shape of the decomposition curve and the decomposition temperature are similar to the ionic liquid [BMIM][CH₃SO₄], which we have previously investigated (see Fig. S1 of the ESI†).¹² From differential scanning calorimetry data, the temperature of glass phase transition and the heat capacity at half the C_p extrapolated temperature were measured and was determined to be 199.32 K and 192.9 J mol⁻¹ K⁻¹, respectively.

In this work the liquid-phase behaviour for a number of binary ionic liquid–organic solvent systems were determined. Table S1 of the ESI includes direct experimental results of the equilibrium temperature, T versus x_1 , the mole fraction of the IL for the investigated systems.† For some systems the binodal curve, T_b (recorded with increasing temperature) and the cloud point curve, T_c (observed during cooling) are presented. Fig. 1–4 show the liquid–liquid phase diagrams (binodal curves) of the investigated systems. The left-hand limits of the equilibrium curves are very close to zero mole fraction of IL, *i.e.* $x_1 \approx 10^{-4}$.

Complete miscibility at temperatures higher than 293 K was observed for the binary systems containing [BMIM][MDEGSO₄] with methanol, ethanol, butan-1-ol and octan-1-ol. In previous work complete miscibility was found for solutions of: [MMIM][CH₃SO₄] with an alcohol (methanol,

ethanol, or butan-1-ol) and with water, solutions of [BMIM][CH₃SO₄] with: an alcohol (methanol, ethanol, butan-1-ol, hexan-1-ol, octan-1-ol or decan-1-ol) and with water and also for solutions of [BMIM][OcSO₄] with an alcohol (methanol, butan-1-ol, hexan-1-ol, octan-1-ol or decan-1-ol) at a temperature of 310 K.^{13,14} The immiscibility in the liquid phase with UCST was observed in binary systems containing 1-hexyloxymethyl-3-methylimidazolium tetrafluoroborate, [C₆H₁₃OCH₂MIM][BF₄], or 1-hexyloxymethyl-3-methylimidazolium bis(trifluoromethylsulfonyl)-imide, [C₆H₁₃OCH₂MIM][Tf₂N] and alcohols.⁸ In binary systems with the dialkoxy-imidazolium salts: 1,3-dihexyloxymethyl-imidazolium tetrafluoroborate, [(C₆H₁₃OCH₂)₂IM][BF₄] and 1,3-dihexyloxymethyl-imidazolium bis(trifluoromethylsulfonyl)-imide, [(C₆H₁₃OCH₂)₂IM][Tf₂N] with alcohols, complete miscibility in the liquid phase was observed over the liquidus curve (solid–liquid equilibrium).⁷ It is evident that it is mainly the sulfate group of the anion that is responsible for the strong interaction when the polar solvent is either alcohol or water.

The maximum of the curves (upper critical solution temperature), was not observed for the systems under study in this work, as the boiling temperature of the solvent was lower (dashed lines in Fig. 1 and Fig. 3). The shape of the equilibrium curve was similar for every measured system. Unfortunately, it was impossible to detect visually the mutual solubility of the IL with the solvent in the solvent rich phase for the investigated system. From our previous measurements^{7–9} and COSMO-RS predictions^{12,13} it is known that the concentrations at equilibrium temperatures are very low with $x_1 \approx 10^{-4}$. Fig. 1 shows the liquid phase behaviour for the investigated IL with benzene, cyclohexane and hexane. From Fig. 1, it is clear that the solubility of the IL in benzene is greater than its solubility in either cyclohexane or hexane. This result is in very good agreement with the values of experimental activity coefficients at infinite dilution, γ_{13}^∞ and

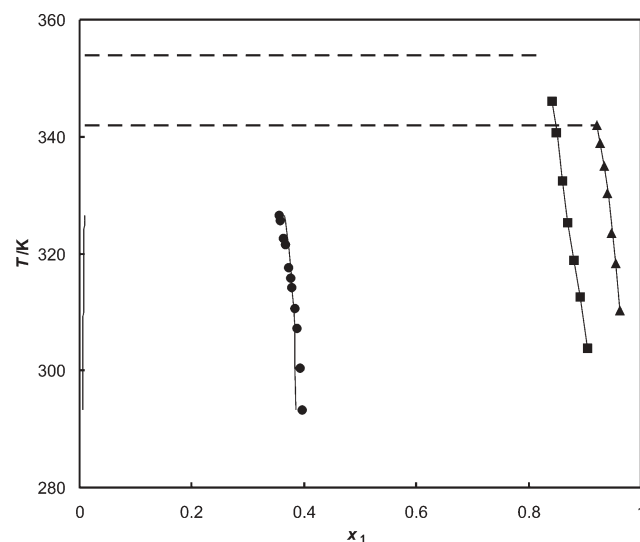


Fig. 1 Liquid–liquid equilibrium diagrams for $\{x_1$ [BMIM][MDEGSO₄] + $(1 - x_1)$ hydrocarbon}: \blacktriangle , *n*-hexane; \blacksquare , cyclohexane; \bullet , benzene; dotted line designated boiling temperature of a solvent; thin solid line calculated by the NRTL equation (see text).

with calculated selectivity at infinite dilution, $S_{298.15K}^{\infty}$ for hexane–benzene which is equal to 39.7.¹⁵ For the aromatic compounds, the values of γ_{13}^{∞} are small (2.04 at 298.15 K), the value of γ_{13}^{∞} being greater for toluene than for benzene. The value of γ_{13}^{∞} for methanol is even smaller than for the aromatic hydrocarbons (0.34 at 298.15 K). It appears that the more polar the solute, the greater is the interaction with the ionic liquid and the smaller the value of γ_{13}^{∞} becomes.¹⁵ Benzene (with its six π -delocalized electrons) presumably interacts through π – π interactions with the cation, or anion species. Methanol with its single lone pair of electrons can form strong intermolecular interactions with the cation moiety of the ionic liquid and the oxygen atoms of the IL's anion (hydrogen bonding). The results show that methanol interacts significantly stronger with the ionic liquid (complete miscibility with alcohols in this work) than does benzene. The expected strong π – π interaction between benzene and the imidazolium ring causes a small immiscibility gap in the liquid–liquid equilibrium. The difference in solubility for cyclohexane and hexane in [BMIM][MDEGSO₄] is small, with the solubility of cyclohexane greater than that of hexane. It can be simply explained by a packing effect, the cyclohexane molecule having a smaller molecular volume than that of the hexane molecule.

In this work the solubility of other *n*-alkanes, cycloalkanes and aromatic hydrocarbons in [BMIM][MDEGSO₄] were not measured because the influence of the length of the alkyl group in these compounds has been studied and discussed previously.^{7,8,10–14} Additionally, from the activity coefficient at infinite dilution, γ_{13}^{∞} , measurements,^{15,16} it is clear that the solubility of *n*-alkanes, cycloalkanes and aromatic hydrocarbons in [BMIM][MDEGSO₄] decreases with increasing alkyl chain in the hydrocarbon. A similar trend was observed for [BMIM][MDEGSO₄] + a linear ketone (Fig. 2) with the solubility of pentan-3-one being greater than that of nonan-5-one in the IL. Fig. 2 shows the large effect that the structure of the ketone has on solubility. The solubility of cyclopentanone

in IL is greater than the solubility of pentan-3-one in the same ionic liquid. In the latter case not only has the molecular volume an influence, but also the very similar structure of cyclopentanone to the imidazolium ring produces an affect on solubility. The cyclopentanone molecule composed of a five-segment hydrocarbon ring and a polar keto-group can strongly interact with the cationic imidazolium ring of the IL. Strong dipole–dipole interactions between the solvent and solute and the cyclic moiety cause enhanced mutual solubility.

The immiscibility gap for the system [BMIM][MDEGSO₄] + TAME is very large as may be seen with reference to Fig. 3. TAME is used as an octane booster in gasoline blending and in the production of TAME methanol is used in excess and must be separated after synthesis. Our measurements show that the investigated IL can successfully be used to separate methanol from TAME. The feasibility of using other ILs in the separation of ethanol from TAE and ETBE has been studied by Arce *et al.*^{17–20}

The mutual solubility of [BMIM][MDEGSO₄] with water is shown in Fig. 4 and it may be seen that the miscibility gap is very small. The strong interaction of water with the anion and cation cause complete miscibility in the region $x_1 = 0.1$ to $x_1 = 1$.

Experimental

Materials

The origins of the chemicals (in parentheses Chemical Abstract registry numbers, the manufactures reported, and mass percent purities) were as follows: [BMIM][MDEGSO₄] (595565-54-1, Solvent Innovation GmbH, >98%); *n*-hexane (110-54-3, Fluka, 99%); cyclohexane (110-82-7, Fluka, 99%); benzene (71-43-2, Aldrich, 99.9%); methanol (67-56-1, Aldrich, 99.8%); ethanol (64-17-5, Aldrich, 99.5%); butan-1-ol (71-36-3, Aldrich, 99.8%); octan-1-ol (111-87-5, Fluka, 99.7%);

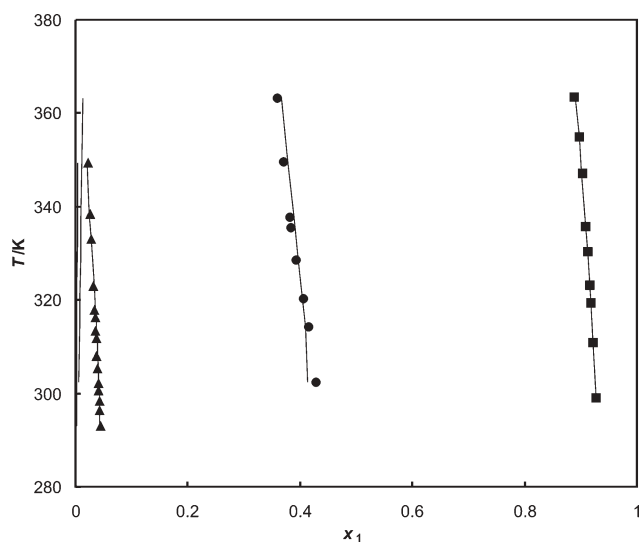


Fig. 2 Liquid–liquid equilibrium diagrams for $\{x_1$ [BMIM][MDEGSO₄] + $(1 - x_1)$ ketone}: \blacktriangle , cyclopentanone; \bullet , pentan-3-one; \blacksquare , nonan-5-one; thin solid line calculated by the NRTL equation (see text).

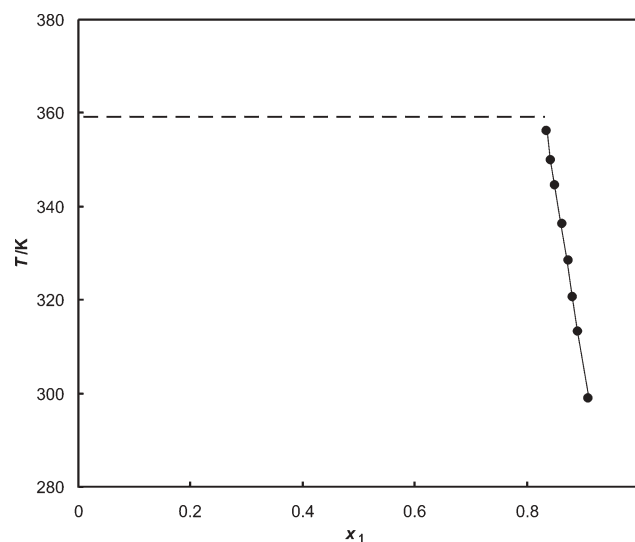


Fig. 3 Liquid–liquid equilibrium diagram for $\{x_1$ [BMIM][MDEGSO₄] + $(1 - x_1)$ *tert*-amyl methyl ether}: \bullet , experimental points; dotted line designated boiling temperature of the solvent; solid line calculated by the NRTL equation (see text).

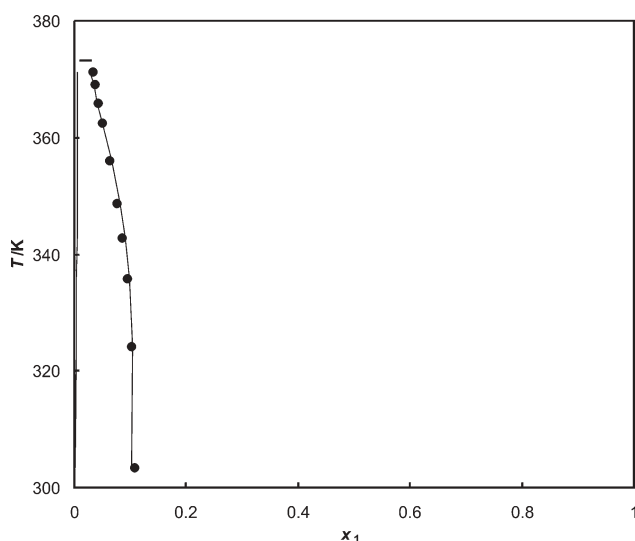


Fig. 4 Liquid-liquid equilibrium diagram for $\{x_1$ [BMIM][MDEGSO₄] + $(1 - x_1)$ water}: ●, experimental points; dotted line designated boiling temperature of the solvent; thin solid line calculated by the NRTL equation (see text).

pentan-3-one (96-22-0, Fluka, 99.5%); cyclopentanone (120-92-3, Fluka, 99.5%); nonan-5-one (502-56-7, Aldrich, 98%); *tert*-amyl methyl ether (994-05-8, Aldrich, 97%). ILs were dried 24 h at 300 K in a vacuum before use. All solvents were fractionally distilled over different drying reagents to mass fraction purity better than 99.8% and were stored over freshly activated molecular sieves of type 4A (Union Carbide). All compounds were checked by GLC analysis and no significant impurities were found. Analysis, using the Karl Fischer technique, showed that the water content in solvents was less than 0.02 mass percent. Sample of ionic liquids used in the experiment have been checked regularly concerning water content using Karl Fischer titration. In all cases, the content of water was less than 160 ppm.

Decomposition of compounds

Simultaneous thermogravimetry/differential thermal analysis (TG/DTA) experiments were performed using a MOM Derivatograph-PC (Hungary). Generally, runs were performed using matched labyrinth platonic crucibles with Al₂O₃ in the reference pan. The crucible design hampered the migration of volatile decomposition products, reducing the rate of gas evolution and, in turn, increasing contact time of the reactants. The TG/DTA curves were obtained at a heating rate of 5 K min⁻¹ with a dynamic nitrogen atmosphere (flow rate of 20 dm³ h⁻¹). Temperatures of decomposition and percentages of mass loss are presented in Fig. S1 of the ESI.†

Differential scanning microcalorimetry (DSC)

The glass transition temperature and heat capacity at half C_p extrapolated temperature were measured by a Perkin-Elmer Pyris 1 differential scanning calorimetry (DSC), apparatus. Measurements were carried out at a scan rate of 10 K min⁻¹, with a power sensitivity of 16 mJ s⁻¹ and a recorder sensitivity of 5 mV. Each time the instrument was used, it was calibrated

with the 99.9999 mol% purity indium sample. The calorimetric accuracy was $\pm 1\%$, and the calorimetric precision was $\pm 0.5\%$.

Liquid-liquid phase equilibria apparatus and measurements

Liquid-liquid equilibrium temperatures were determined using a dynamic method as described in detail previously.¹⁰ Appropriate mixtures of IL and solvent were placed, under nitrogen in a drybox, into a Pyrex glass cell and heated or cooled very slowly (less than 2 K h⁻¹ near the equilibrium temperature), with continuous stirring inside the cell. The mixture was then placed in a glass thermostat filled with water. A sample of known composition was heated until it became one phase (binodal curve) then cooled until two phases appeared (cloud point curve), these measurements were repeated three to five times. The temperature was measured with an electronic thermometer P 550 (DOSTMANN electronic GmbH) with the probe totally immersed in the thermostating liquid. The thermometer was calibrated on the basis of ITS-90. The accuracy of the temperature measurements was judged to be ± 0.01 K. Mixtures were prepared by mass, and errors did not exceed $x_1 = 0.0002$ and $T_1 = 0.1$ K in mole fraction and temperature, respectively. The LLE measurements were limited at the upper temperature by the boiling temperature of the solvent or thermostating liquid. The results of the solubility measurements are presented in Table S1 of the ESI.†

Modelling

In addition to the experimental curves (binodal curves), all IL/organic solvent systems with liquid-liquid phase behavior were correlated using the binary parameters nonrandom two-liquid equation²¹ for a mixtures of two components. From our previous measurements⁷⁻⁹ and COSMO-RS predictions^{12,13} the mole fraction at equilibrium temperatures of the dilute ionic liquid solutions were assumed to be $x_1 = 10^{-4}$.

The solute activity coefficients, γ_1 , of the saturated solutions were correlated by the NRTL model describing the excess Gibbs energy²¹

$$\frac{G^E}{RT} = x_1 x_2 \left[\frac{\tau_{21} G_{21}}{x_1 + x_2 G_{21}} + \frac{\tau_{12} G_{12}}{G_{12} x_1 + x_2} \right] \quad (1)$$

$$\tau_{12} = (g_{12} - g_{22})/RT \quad (2)$$

$$\tau_{21} = (g_{21} - g_{11})/RT \quad (3)$$

$$G_{12} = \exp(-\alpha_{12} \tau_{12}) \quad (4)$$

$$G_{21} = \exp(-\alpha_{12} \tau_{21}) \quad (5)$$

$$\ln(\gamma_1) = x_2^2 \left[\tau_{21} \left(\frac{G_{21}}{x_1 + x_2 G_{21}} \right)^2 + \frac{\tau_{12} G_{12}}{(x_2 + x_1 G_{12})^2} \right] \quad (6)$$

Model adjustable parameters ($g_{12}-g_{22}$) and ($g_{21}-g_{11}$) were found by minimization of the objective function OF:

$$\text{OF} = \sum_{i=1}^n [(\Delta x_1)_i^2 + (\Delta x_1^*)_i^2] \quad (7)$$

Table 1 Correlation of the liquid–liquid equilibria data by means of the NRTL equation: parameters g_{12} – g_{22}/g_{21} – g_{11} and the deviation σ_x

System	NRTL parameters ^a		Deviations
	g_{12} – $g_{22}/J \text{ mol}^{-1}$	g_{21} – $g_{11}/J \text{ mol}^{-1}$	σ_x
[BMIM][MDEGSO ₄] + benzene	–1782.33	12808.48	0.0073
[BMIM][MDEGSO ₄] + <i>n</i> -hexane	10093.03	37118.81	0.0002
[BMIM][MDEGSO ₄] + cyclohexane	8375.89	29572.47	0.0003
[BMIM][MDEGSO ₄] + cyclopentanone	–9422.54	22604.53	0.0021
[BMIM][MDEGSO ₄] + pentan-3-one	–1500.77	12517.28	0.0093
[BMIM][MDEGSO ₄] + nonan-5-one	8434.78	29181.63	0.0005
[BMIM][MDEGSO ₄] + TAME	8477.88	29995.57	0.0005
[BMIM][MDEGSO ₄] + water	–6803.13	19150.53	0.0049

^a Calculated with the third non-randomness parameter $\alpha = 0.3$.

where n is the number of experimental points and Δx is defined as

$$\Delta x = x_{\text{calc.}} - x_{\text{exp.}} \quad (8)$$

The root-mean-square deviation of mole fraction was defined as follows:

$$\sigma_x = \left(\frac{\sum_{i=1}^n (\Delta x_1)_i^2 + \sum_{i=1}^n (\Delta x_1^*)_i^2}{2n-2} \right)^{1/2} \quad (9)$$

Table 1 shows the adjustable parameters and root-mean-square deviations for the constant nonrandomness factor, $\alpha = 0.3$. The modelled binodal curves reproduced the experimentally observed data to a satisfactory degree (Fig. 1–4).

Conclusion

In this work the liquid–liquid phase behaviour of the imidazolium ionic liquid with different organic solvents is presented. Due to the differences in solubility, the IL used in this work has attracted significant attention as a potential solvent for industrial applications. The significant differences in the mutual solubility of [BMIM][MDEGSO₄] with alkanes and aromatic hydrocarbons indicate that the IL may be considered as a possible alternative solvent for aliphatic/aromatic extraction. Complete miscibility of the investigated IL with methanol and the huge miscibility gap in the system with TAME indicates that [BMIM][MDEGSO₄] may successfully be utilised in the separation of methanol from TAME.

Acknowledgements

Funding for this research was provided by the Polish Ministry of Education and Sciences for the Joint Project of

Polish-South African Scientific and Technological International Cooperation (grant 504/G/1020/0602/0613).

References

- J. M. Crosthwaite, M. J. Muldoon, S. N. V. K. Aki, E. J. Maginn and J. F. Brennecke, *J. Phys. Chem. B*, 2006, **110**, 9354–9361.
- T. Welton, *Coord. Chem. Rev.*, 2004, **248**, 2459–2477.
- R. Sheldon, *Chem. Commun.*, 2001, **23**, 2399–2407.
- J. Dupont, R. F. de Souza and P. A. Z. Suarez, *Chem. Rev.*, 2002, **102**, 3667–3692.
- R. Kato and J. Gmehling, *J. Chem. Thermodyn.*, 2005, **37**, 603–619.
- J. Łachwa, J. Szydłowski, A. Makowska, K. R. Seddon, J. M. S. S. Esperanca, H. J. R. Guedes and L. P. N. Rebelo, *Green Chem.*, 2006, **8**, 262–267.
- U. Domańska and A. Marciniak, *Fluid Phase Equilib.*, 2006, DOI: 10.1016/j.fluid.2006.07.005.
- U. Domańska and A. Marciniak, *J. Chem. Thermodyn.*, 2005, **37**, 577–585.
- U. Domańska and A. Marciniak, *J. Phys. Chem. B*, 2004, **108**, 2376–2382.
- U. Domańska and A. Marciniak, *J. Chem. Eng. Data*, 2003, **48**, 451–456.
- U. Domańska, A. Marciniak and R. Bogel-Łukasik, *ACS Sym. Ser.*, 2005, **901**, 256–269.
- U. Domańska, A. Pobudkowska and F. Eckert, *Green Chem.*, 2006, **8**, 268–276.
- U. Domańska, A. Pobudkowska and F. Eckert, *J. Chem. Thermodyn.*, 2006, **38**, 685–695.
- U. Domańska, A. Pobudkowska and A. Wiśniewska, *J. Solution Chem.*, 2006, **35**, 311–334.
- T. M. Letcher, U. Domańska, M. Marciniak and A. Marciniak, *J. Chem. Thermodyn.*, 2005, **37**, 587–593.
- M. Krummen, P. Wasserscheid and J. Gmehling, *J. Chem. Eng. Data*, 2002, **47**, 1411–1417.
- A. Arce, O. Rodríguez and A. Soto, *J. Chem. Eng. Data*, 2004, **49**, 514–517.
- A. Arce, O. Rodríguez and A. Soto, *Ind. Eng. Chem. Res.*, 2004, **43**, 8323–8327.
- A. Arce, O. Rodríguez and A. Soto, *Chem. Eng. J.*, 2006, **115**, 219–223.
- A. Arce, O. Rodríguez and A. Soto, *Fluid Phase Equilib.*, 2006, **242**, 164–168.
- H. Renon and J. M. Prausnitz, *AIChE J.*, 1968, **14**, 135–144.

Solvent-free selective oxidation of benzyl alcohol by molecular oxygen over uranium oxide supported nano-gold catalyst for the production of chlorine-free benzaldehyde

Vasant R. Choudhary,* Rani Jha and Prabhas Jana

Received 12th June 2006, Accepted 12th December 2006

First published as an Advance Article on the web 3rd January 2007

DOI: 10.1039/b608304h

A detailed investigation on the production of chlorine-free benzaldehyde in the solvent-free oxidation of benzyl alcohol by O₂ over nano-gold supported on U₃O₈ has been carried out. Influence of different catalyst parameters (different methods of gold deposition on U₃O₈, gold loading and particle size, and catalyst calcination temperature) and reaction conditions (reaction period and temperature) on the process performance has been studied. The catalyst containing gold at higher concentration and with smaller gold particles showed the better process performance (higher benzyl alcohol conversion and benzaldehyde yield or selectivity). The benzyl alcohol conversion is largely increased but the selectivity for benzaldehyde is slightly decreased (while that of benzyl benzoate is increased) with increasing the reaction period or temperature. In the presence of solvent (*viz.* toluene, *p*-xylene, DMF or DMSO), the process performance was found to be inferior to that observed in the absence of any solvent. Substituted benzyl alcohols also can be oxidized by O₂ to corresponding aldehydes with high yield and/or selectivity, using the catalyst in the absence of any solvent.

1. Introduction

Unlike the gas phase oxidation of toluene, chlorine-free benzaldehyde can be produced by the liquid phase oxidation of benzyl alcohol without loss of carbon in the form of CO₂, a green house gas. A large amount of toxic waste is produced in the conventional preparation of benzaldehyde by reacting benzyl alcohol with stoichiometric or excess amounts of potassium or ammonium permanganate in aqueous acidic medium.¹ In order to avoid the use of organic solvent, a use of supercritical carbon dioxide as an effective reaction medium to perform the oxidation of primary and secondary aliphatic alcohols to corresponding carbonyl compounds with chromium trioxide supported silica has been reported.² In this case, the chromic oxide acts as an oxidizing agent. A use of environmentally clean oxidizing agent, such as H₂O₂ or more preferably O₂, but in the presence of organic solvent, has been reported earlier for the benzyl alcohol-to-benzaldehyde oxidation using different solid catalysts.^{3–9} Solvent-free oxidation of benzyl alcohol to benzaldehyde by TBHP, using the easily separable/reusable MnO₄[–] exchanged hydrotalcite or transition metal containing layered double hydroxide as a catalyst, has also been reported earlier.^{10,11} The use of TBHP as the oxidizing agent, however, leads to the formation of tert-butanol as a by-product in the oxidation. To make the liquid phase benzyl alcohol-to-benzaldehyde oxidation process environmentally clean/green, it should be carried out in the absence of any solvent, using a clean oxidizing agent (*e.g.* O₂ or H₂O₂), preferably using molecular oxygen for favorable process economics.

Recently, in our preliminary communication,¹² we have reported a totally green process for the solvent-free selective benzyl alcohol-to-benzaldehyde oxidation by molecular oxygen (at close to atmospheric pressure), using an easily separable/reusable nano-gold catalyst supported on different metal oxides (particularly the Au/MgO, Au/Al₂O₃, Au/ZrO₂ and Au/U₃O₈ catalysts), prepared by a homogeneous deposition precipitation (HDP) method for depositing nano-gold on the supports. Among the supported nano-gold catalysts, the Au/U₃O₈ showed the best performance in the process.¹² Later, Hutching and coworkers also reported the solvent-free oxidation of benzyl alcohol to benzaldehyde by O₂ using Au–Pd/TiO₂ catalyst.¹³

In this paper, we report our detailed investigation on the solvent-free selective oxidation of benzyl alcohol to benzaldehyde by O₂ over Au/U₃O₈ catalyst, which showed the best process performance (among the different supported nano-gold catalysts) in our preliminary work reported earlier.¹¹ Influence of the method of gold deposition, gold loading and calcination temperature of the catalyst on the benzyl alcohol conversion and benzaldehyde selectivity in the process has been investigated. The influence of the reaction conditions (*viz.* reaction time and temperature) on the process performance has also been studied. Use of the catalyst in the solvent-free oxidation of substituted benzyl alcohols by O₂ to corresponding aldehydes has also been investigated.

2. Experimental

2.1 Preparation and characterization of Au/U₃O₈ catalysts

The Au/U₃O₈ catalysts were prepared by different methods for depositing gold on U₃O₈ support by impregnation, deposition

Chemical Engineering & Process Development Division, National Chemical Laboratory, Pune, 411 008, India.
E-mail: vr.choudhary@ncl.res.in; Fax: +91 20 25902612

precipitation, homogeneous deposition precipitation and co-precipitation methods, as follows [in all the four methods, the gold available for its deposition/incorporation in the catalyst was the same (8.0 wt% of the support)]:

(i) Deposition of gold on U₃O₈ by impregnation (IMP). The Au/U₃O₈ (IMP) catalyst was prepared by contacting the U₃O₈ (2.0 g) with concentrated aqueous solution of HAuCl₄·3H₂O (Thomas Baker Chem. Ltd., Mumbai, India), evaporating the extra liquid on water bath, drying at 100 °C for 12 h and finally calcining the solid in air at 400 °C for 2 h. The uranium oxide (U₃O₈) was obtained by hydrolyzing uranyl nitrate [UO₂(NO₃)₂·6H₂O] (BDH, Mumbai) by aqueous ammonia (30%), washing the resulting precipitate, drying and then calcining at 500 °C for 4 h in air. The catalyst was denoted as Au/U₃O₈ (IMP).

(ii) Deposition of gold on U₃O₈ by deposition precipitation (DP). The Au/U₃O₈ (DP) catalyst was prepared by contacting the U₃O₈ under stirring with aqueous NaOH solution containing HAuCl₄·3H₂O at a pH of 7.0 and 70 °C for 1 h, aging the mixture at 30 °C for 1 h, filtering and thoroughly washing the solid with deionised water, drying and calcining the dried solid in air at 400 °C for 2 h. The catalyst was denoted as Au/U₃O₈ (DP). The deposition precipitation method was developed earlier by Haruta and coworkers¹⁴ for depositing nano-gold on metal oxide support.

(iii) Deposition of gold on U₃O₈ by homogeneous deposition precipitation (HDP). The Au/U₃O₈ (HDP) catalyst was prepared by the HDP method described elsewhere.^{15–17} The U₃O₈ (2.0 g) was contacted under stirring with aqueous solution of urea (5.19 g) containing HAuCl₄·3H₂O (0.32 g). The temperature of the reaction mixture was gradually increased up to 95 °C and maintained for 6 h. Thereafter, the mixture was aged at 30 °C for 12 h and then the solid was filtered, thoroughly washed with deionised water, dried at 90 °C for 12 h and finally calcined in air at 400 °C for 2 h. The catalyst was denoted as Au/U₃O₈ (HDP).

(iv) Preparation of Au/U₃O₈ by co-precipitation (CP). The appropriate quantities of uranyl nitrate, [UO₂(NO₃)₂·6H₂O], and aqueous gold chloride solution were taken in a three-necked round bottom flask and diluted with 200 ml distilled water. This solution was then heated to 60 °C. The pH and temperature of the solution was monitored continuously. An aqueous solution of Na₂CO₃ (0.5 N) was added drop-wise to the heated solution until the pH of the solution reached 8.0. The stirring was continued further for 1 h at 60 °C. The reaction mixture was aged overnight at room temperature, filtered, washed thoroughly with distilled water (500 ml × 8 times), dried at 90 °C for 12 h and finally calcined in air at 400 °C for 2 h. The catalyst was denoted as Au/U₃O₈ (CP).

The U₃O₈ used in the above first three methods was prepared by hydrolyzing uranyl nitrate at a pH > 8.0, filtering, washing and drying the precipitate and then calcining in air at 400 °C for 2 h.

The catalysts were characterized for their Au content by ICP-OES (using a Perkin-Elmer analyzer) and also for their

Au particle size by the XRD peak (at $2\theta = 38.2^\circ$) broadening [using a Philips X-ray diffractometer (1730 series) and Cu K α radiation]. The surface area of the Au/U₃O₈ catalysts was measured by the single point N₂ adsorption method (using a surface area analyzer, Quanta Chrome, USA).

2.2 Catalytic oxidation reaction

The liquid phase oxidation of benzyl alcohol over the supported Au catalysts, was carried out in a magnetically stirred reactor (capacity: 10 cm³), provided with a mercury thermometer (for measuring the reaction temperature) and reflux condenser, at the following general reaction conditions: reaction mixture = 29 mmol benzyl alcohol (or substituted benzyl alcohol) + 0.1 g catalyst, temperature = 130 °C, pressure = 1.5 atm, and reaction time = 5 h. Unless otherwise mentioned, the reaction was carried out at the above general conditions. For studying the solvent effects, 5.0 ml of solvent (toluene, *p*-xylene, DMF or DMSO) were added to the reaction mixture. After the reaction, the reaction mixture was filtered, the solid catalyst was washed with hot toluene, and the reaction products and unconverted reactants from the filtrate were analyzed by gas chromatograph with flame ionisation detector, using a SE-30 column and N₂ as a carrier gas. Under the prevailing reaction conditions, no oxidation of solvent (toluene or xylene) was observed.

The conversion, product selectivity and product yield were calculated as follows: conversion (%) = [(moles of reactant converted) × 100] ÷ [(moles of reactant in feed)], product selectivity (%) = [(moles of product formed) × 100] ÷ [(moles of reactant converted)] and product yield (%) = (percentage of reactant converted to a particular product) or [conversion (%) × product selectivity (%) ÷ 100].

3. Results and discussion

Influence of the method of gold deposition, gold loading and calcination/pretreatment temperature of the catalyst (prepared by the HDP method), and also that of the reaction conditions (*viz.* absence or presence of different solvents, temperature and reaction period) have been studied on the conversion of benzyl alcohol and selectivities for benzaldehyde and benzyl benzoate in the benzyl alcohol oxidation over Au/U₃O₈ catalyst. The results are presented in Fig. 1–5 and Table 1. Influence of the catalyst preparation/pretreatment temperature on the surface properties (*viz.* surface area and gold particle size) and also on the turn-over-frequency (TOF), expressed as the rate of the reaction per unit mass of the catalyst or the deposited Au per unit time, is shown in Table 2. Results of the solvent-free oxidation of different substituted benzyl alcohols to their corresponding aldehydes are presented in Table 3.

3.1 Influence of the method of gold deposition

The results in Fig. 1 show a strong influence of the method of gold deposition on the catalyst performance in the solvent-free benzyl alcohol oxidation. The catalyst performance (benzaldehyde yield) observed for the different methods of gold deposition/catalyst preparation is in the following order: HDP > DP > CP > IMP.

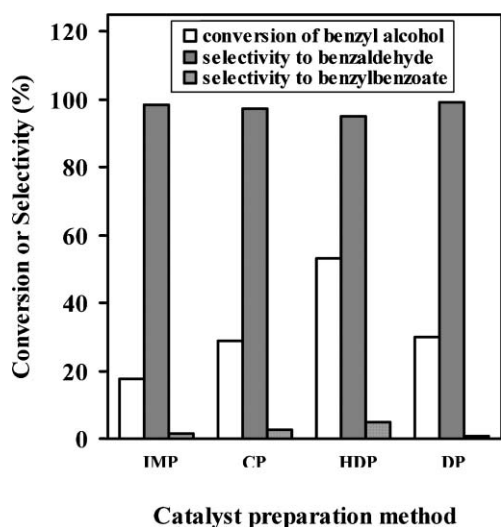


Fig. 1 Performance of the Au/U₃O₈ catalysts (calcined at 400 °C), prepared by the different gold deposition methods, in the solvent-free oxidation of benzyl alcohol (at 130 °C).

For the catalysts prepared by the different methods, the benzaldehyde selectivity was found to be more or less the same but they differ in their benzyl alcohol conversion activity, either because of the difference in their Au particle size or due to different gold loadings (Table 2).

The Au/U₃O₈ (HDP) showed the best performance. The lowest performance of the Au/U₃O₈ (IMP), having similar gold loading (8.0 wt%), is mostly attributed to its larger Au particle size, and consequently to its lower gold surface area. Whereas, the lower gold loading is responsible for the lower activity of the Au/U₃O₈ (CP) and Au/U₃O₈ (DP) catalysts containing smaller gold particles. When, the same amount of gold (8 wt% of U₃O₈) was available for its incorporation in the

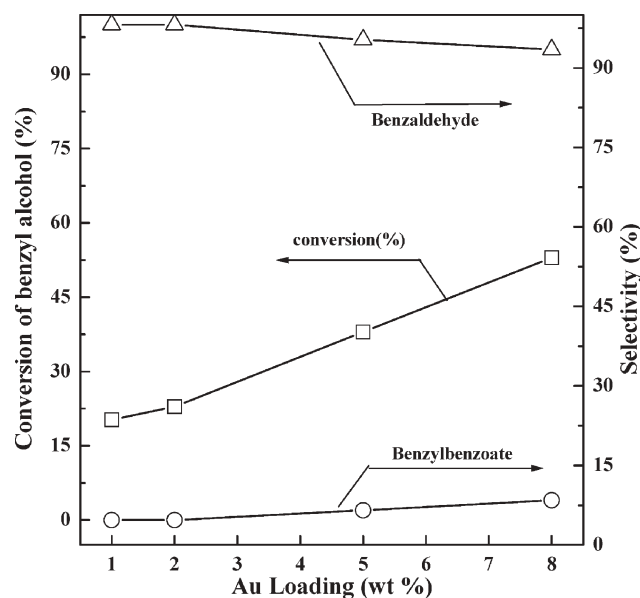


Fig. 2 Effect of the Au loading in the Au/U₃O₈ (HDP) catalyst (calcined at 400 °C) on the conversion and selectivity in the solvent-free oxidation of benzyl alcohol (at 130 °C).

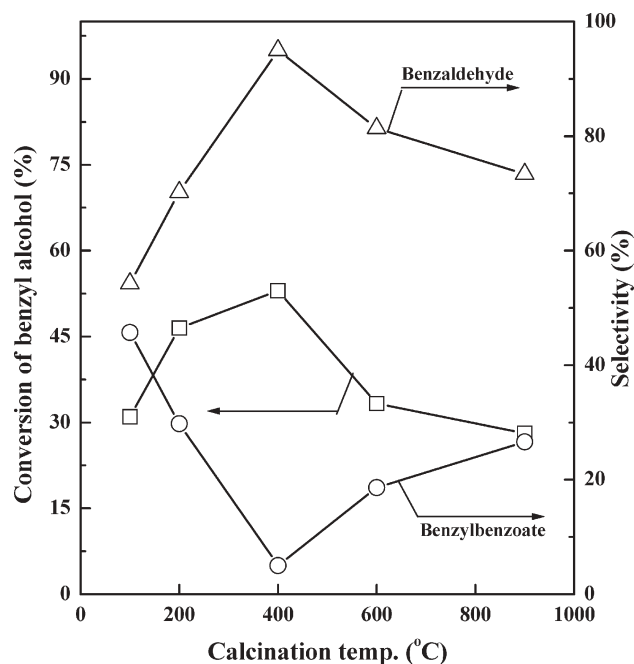


Fig. 3 Influence of the calcination temperature of the Au(8 wt%)/U₃O₈ (HDP) catalyst on the solvent-free oxidation of benzyl alcohol (at 130 °C).

catalysts, the gold deposited by the DP and CP methods was appreciably lower than that of the HDP; in the later (HDP) method, the gold deposition is complete (*i.e.* 100% of the available gold).

In our earlier communication,¹² the Au/U₃O₈ (HDP) catalyst showed excellent reusability in the reaction (after the 1st, 3rd and 5th reuse of the catalyst, the benzaldehyde yields

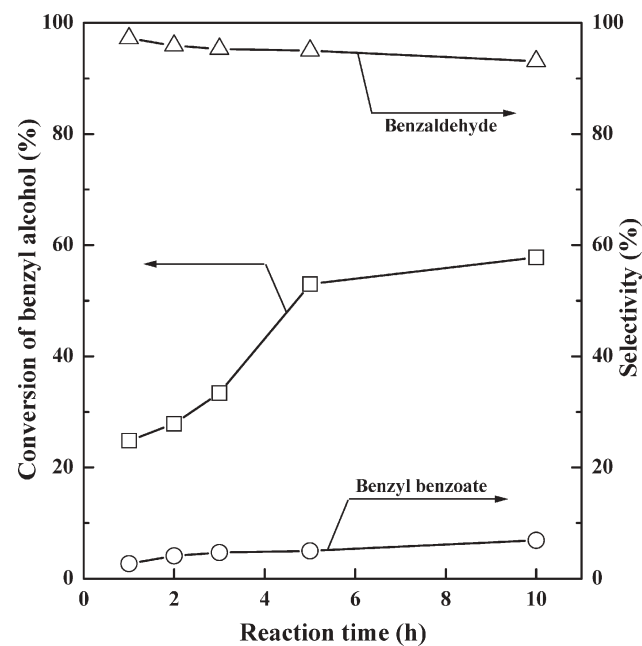


Fig. 4 Effect of the reaction time on the conversion and selectivity in the solvent-free oxidation of benzyl alcohol (at 130 °C) over the Au(8 wt%)/U₃O₈ (HDP) catalyst (calcined at 400 °C).

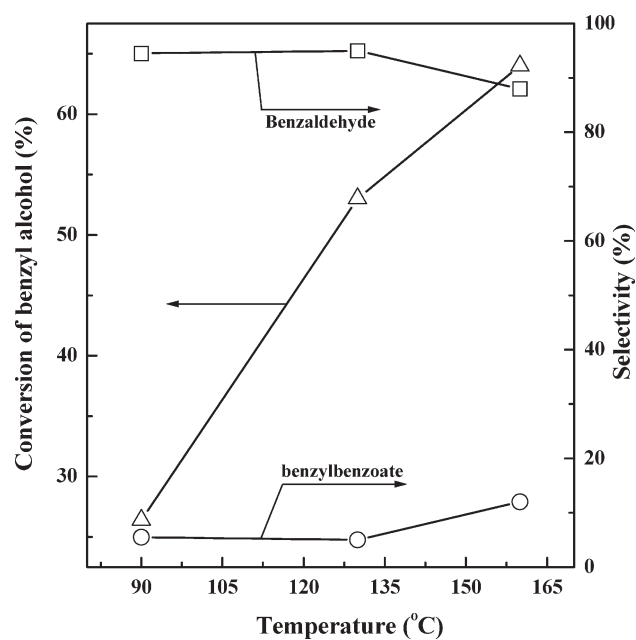


Fig. 5 Influence of the reaction temperature (reaction time = 5 h) on the conversion and selectivity in the solvent-free oxidation over the Au(8 wt%)/U₃O₈ (HDP) catalyst (calcined at 400 °C).

were 50, 50.3 and 49.8%, respectively) and the reaction was found to be essentially catalyzed by the heterogeneous supported gold catalyst (when the catalyst from the reaction mixture was removed after the initial reaction period of 30 min, there was no further appreciable increase in the conversion or yield).

All the further work was, therefore, carried out using the catalyst prepared by depositing gold on U₃O₈ by the HDP method.

3.2 Influence of gold loading

The results in Fig. 2 show that, with increasing the Au loading in Au/U₃O₈ (HDP) catalyst, its benzyl alcohol oxidation activity is increased markedly, almost linearly, while its selectivity for benzaldehyde is decreased due to the simultaneous formation of benzyl benzoate; the decrease in the benzaldehyde selectivity is, however, smaller.

It may be noted that the deposition of gold on the U₃O₈ support by the HDP method was quantitative; even no traces of gold was detected in the filtrate. This is most probably expected because of the strong adsorption of positively charged gold complexes under the basic conditions. Formation of [Au(urea)₄]Cl₃·2H₂O and/or [Au₂(NH₂)₂Cl₂(NCO)(OH)]·H₂O complexes¹⁸ has been observed earlier in the presence of urea at room temperature and 90 °C, respectively. Under the basic conditions of the HDP, the surface of U₃O₈ support becomes negatively charged [this is expected because of the fact that the pH corresponding to the isoelectric point of U₃O₈ (≈4.0) is much lower than the actual pH of the system]. The adsorption of positively charged Au complexes on the U₃O₈ support is, therefore, facilitated, leading to a complete deposition of gold from the solution.

The results (Fig. 2) also reveal that the selectivity of benzaldehyde is decreased with increasing the benzyl alcohol conversion. This is because of the fact that benzaldehyde is an intermediate product. The overall benzyl alcohol oxidation process involves the reaction pathway presented in Fig. 6. Since, no net formation of benzoic acid was observed over the Au/U₃O₈ catalysts and other metal oxide supported Au catalysts,¹¹ the benzoic acid reacts instantly with benzyl alcohol, which is available in much higher concentration, forming benzyl benzoate.

Table 1 Results for the oxidation of benzyl alcohol by molecular oxygen over the Au(8 wt%)/U₃O₈ (HDP) catalyst in the absence and presence of different solvents

Solvent used	Temp./°C	Conversion (%)	Selectivity (%)		Benzaldehyde yield (%)	TOF ^a /mol g ⁻¹ _(Au) h ⁻¹
			Benzaldehyde	Benzylbenzoate		
Nil	130	53.0	95.0	5.0	50.4	0.37
Nil	110	40.5	96.5	3.5	39.1	0.29
Toluene	110	27.0	86.6	13.4	23.4	0.17
<i>p</i> -Xylene	110	45.0	82.5	17.5	37.1	0.27
DMF	135	49.6	72.0	28.1	35.7	0.26
DMSO	130	15.7	99.5	0.5	15.6	0.11

^a Rate of the formation of benzaldehyde per unit mass of the deposited gold per unit time.

Table 2 Surface area and Au particle size of the Au/U₃O₈ catalysts prepared by different methods (Au available for deposition on U₃O₈ = 8.0 wt%) and turn-over frequency (TOF) of the catalysts in the benzylalcohol-to-benzaldehyde oxidation

Method of catalyst preparation	Concentration of Au in the catalyst (wt%)	Calcination temp./°C	Surface area/m ² g ⁻¹	Particle size of Au/nm	TOF ^a	
					/mol g ⁻¹ _(cat) h ⁻¹	/mol g ⁻¹ _(Au) h ⁻¹
Impregnation	8.0	400	6.2	34.6	0.010	0.13
Co-precipitation	4.7	400	5.2	12.2	0.016	0.35
DP	5.1	400	8.0	19.1	0.017	0.34
HDP	8.0	400	6.5	14.2	0.029	0.37
HDP	8.0	600	5.0	—	0.016	0.20
HDP	8.0	900	3.8	33.2	0.012	0.15

^a Rate of the formation of benzaldehyde per unit mass of the catalyst or deposited gold per unit time.

Table 3 Results for the solvent-free oxidation of different benzyl alcohols by molecular oxygen over the Au(8 wt%)/U₃O₈ (HDP) catalyst (calcined at 400 °C)

Substrate	Conversion (%)	Selectivity (%)			TOF ^a /mol g ⁻¹ _(Au) h ⁻¹
		Aldehyde	Ester	Aldehyde yield (%)	
3-NO ₂ PhCH ₂ OH	40.8	98.5	1.5	40.2	0.30
3-PhOPhCH ₂ OH	42.5	98.0	2.0	41.7	0.31
4-MeOPhCH ₂ OH	67.0	92.5	7.5	62.0	0.46
PhCH ₂ CH ₂ OH	42.1	43.0	57.0	18.0	0.13

^a Rate of the formation of benzaldehyde per unit mass of the deposited gold per unit time.

3.3 Influence of catalyst calcination temperature

The results in Fig. 3 show a strong influence of the temperature, at which the Au(8 wt%)/U₃O₈ (HDP) catalyst (after the gold deposition) was calcined, on the performance of the catalyst in the oxidation. With increasing calcination temperature, both the catalytic activity (benzyl alcohol conversion) and benzaldehyde selectivity pass through a maximum, while the selectivity for the benzyl benzoate formation is passed through a minimum, at the catalyst calcination temperature of 400 °C. This shows that the catalyst shows best performance when it is calcined at 400 °C. The lower performance of the catalyst at higher calcination temperatures (600 and 900 °C) is because of the increased gold particle size (Table 2) and consequently due to the decreased gold surface area. However, the lower catalyst performance at the lower calcination temperatures (100 and 200 °C) may be due to the presence of moisture in the catalyst.

3.4 Influence of reaction time

When the reaction period is increased from 1 to 10 h, the benzyl alcohol conversion and the selectivity for benzyl benzoate are increased but the selectivity for benzaldehyde is decreased (Fig. 4). The decrease in the benzaldehyde selectivity is attributed to the increase in the rate of benzyl benzoate formation due to the increase in the conversion of benzyl alcohol with increasing the reaction period. The benzaldehyde selectivity decrease is, however, quite small.

It is interesting to note that, at the lower reaction periods, the conversion is increased almost exponentially with the time,

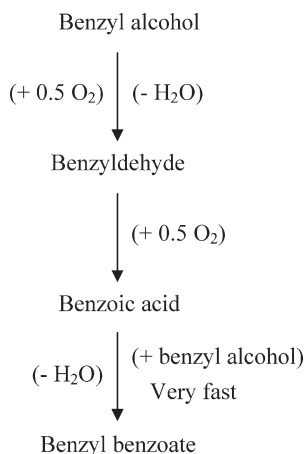


Fig. 6 Reaction scheme for the benzyl alcohol-to-benzaldehyde oxidation over Au/U₃O₈ catalyst.

indicating autocatalytic conversion of benzyl alcohol. This is expected because of the fact that the benzoic acid formed in the oxidation reacts instantly with the reactant (benzyl alcohol), thereby increasing the benzyl alcohol conversion with the formation of benzyl benzoate.

3.5 Influence of reaction temperature

As expected, the influence of reaction temperature on the benzyl alcohol conversion is very strong (Fig. 5). However, the selectivity for benzaldehyde or benzyl benzoate is influenced appreciably only when the temperature is increased from 130 °C to 160 °C. Even at the higher temperature (160 °C), no net formation of benzoic acid was observed.

As observed in the earlier studies (Fig. 2 and Fig. 4), the benzaldehyde selectivity was decreased with increasing the benzyl alcohol conversion, further confirming benzaldehyde as an intermediate product as shown in the reaction scheme (Fig. 6).

3.6 Influence of the presence of solvent

The results in Table 1 clearly reveal that, the benzyl alcohol-to-benzaldehyde oxidation process shows the best performance in the absence of any solvent. Both the conversion and benzaldehyde selectivity in the oxidation in the presence of toluene, *p*-xylene, DMF (dimethylformamide) or DMSO (dimethylsulfoxide), as a solvent, are lower than that observed in the absence of any solvent.

The observed lower benzyl alcohol conversion activity of the catalyst in the presence of different solvents is mostly attributed to the competitive adsorption between the solvent and benzyl alcohol on the catalyst and thereby occupying part of the active sites of the catalyst by the adsorbed solvent molecules.

3.7 Oxidation of substituted benzyl alcohols

Results of the solvent-free oxidation of different substituted benzyl alcohols to corresponding aromatic aldehydes over the Au/U₃O₈ (HDP) are presented in Table 3.

The results reveal that, apart from benzyl alcohol, substituted benzyl alcohols can also be oxidized by molecular oxygen to their corresponding aldehydes with good to high selectivity and conversion in the absence of any solvent, using the environmentally-friendly, easily separable and reusable Au/U₃O₈ (HDP) catalyst. The catalytic activity in the oxidation, however, depends upon the substituent group in the benzyl alcohols. For 4-methoxy benzyl alcohol, the catalyst

shows both high activity and high benzaldehyde selectivity. Whereas, for PhCH₂CH₂OH, the catalyst shows good activity but comparable selectivity for both aldehyde and benzyl benzoate. For 3-nitro- or 3-hydroxy-benzyl alcohol, the catalyst shows high aldehyde selectivity at a good conversion (Table 3).

4. Conclusions

Chlorine-free benzaldehyde can be produced by an environmentally-friendly solvent-free liquid phase oxidation of benzyl alcohol with molecular oxygen, even at low pressure (1.5 atm), using nano-gold supported U₃O₈, particularly prepared by the homogeneous deposition precipitation method. The Au/U₃O₈ (HDP) is a highly promising, easily separable and reusable catalyst for the solvent-free selective oxidation process. There is an optimum catalyst calcination temperature (400 °C) for achieving the highest benzyl alcohol conversion and benzaldehyde selectivity. The better process performance (*i.e.* higher benzaldehyde yield and selectivity) is achieved when the catalyst contains gold at higher concentration and also with smaller particle size.

With increasing reaction period or temperature, the benzyl alcohol conversion is increased markedly, but there is a small decrease in the selectivity for benzaldehyde and a small increase in the formation of benzyl benzoate. In the presence of commonly used solvent (toluene, *p*-xylene, dimethyl formamide or dimethyl sulfoxide), the process performance (both the benzaldehyde yield and selectivity) is found to be inferior to that observed in the absence of any solvent.

The Au/U₃O₈ (HDP) is also a highly promising catalyst for the solvent-free oxidation of substituted benzyl alcohols by O₂ to corresponding aldehydes and/or esters with their good selectivity and yields.

Acknowledgements

R. J. and P. J. are grateful to the CSIR and UGC (New Delhi) for the award of a Senior Research Fellowship, respectively.

All the authors are grateful to CMC group of NCL for the XRD of the catalysts.

References

- (a) L. Kotai, B. Kazinczy, A. Keszler, H. Sandor, I. Gacs and K. Banerji, *Z. Naturforsch., B: Chem. Sci.*, 2001, **56**, 823; (b) A. Corma, V. Lambies, F. V. Melo and J. Palou, *An. Quim., Ser. A*, 1980, **76**, 304.
- M. E. Gonzalez-Nunez, R. Mello, A. Olmos, R. Acerete and G. Asensio, *J. Org. Chem.*, 2006, **71**, 1039.
- B. M. Choudary, M. Lakshmi Kantum, Ateeq Rahman, Ch. Venkat Reddy and K. Koteswara Rao, *Angew. Chem., Int. Ed.*, 2001, **40**, 763.
- L. F. Liotta, A. M. Venezia, G. Deganello, A. Longo, A. Martorana, Z. Schay and L. Guzzi, *Catal. Today*, 2001, **66**, 271.
- N. S. Bijlani and S. B. Chandalia, *Indian Chem. Eng.*, 1981, **23**, 44.
- I. Matsushita, K. Ebitani and K. Kaneda, *Chem. Commun.*, 1999, 265.
- T. Kawabata, Y. Shinozuka, Y. Ohishi, T. Shishido, K. Takaki and K. Takehira, *J. Mol. Catal. A: Chem.*, 2005, **236**, 206.
- T. Nishimura, N. Kakiuchi, M. Inoue and S. Uemura, *Chem. Commun.*, 2000, 1245; T. Nishimura, N. Kakiuchi, M. Inoue and S. Uemura, *Bull. Chem. Soc. Jpn.*, 2001, **74**, 165.
- H. Ji, T. Wang, M. Zhang, Y. She and L. Wang, *Appl. Catal., A*, 2005, **282**, 25.
- V. R. Choudhary, D. K. Dumbre, V. S. Narkhede and S. K. Jana, *Catal. Lett.*, 2003, **86**, 229.
- V. R. Choudhary, D. K. Dumbre, B. S. Uphade and V. S. Narkhede, *J. Mol. Catal. A: Chem.*, 2004, **215**, 129.
- V. R. Choudhary, A. Dhar, P. Jana, R. Jha and B. S. Uphade, *Green Chem.*, 2005, **7**, 768.
- D. I. Enache, J. K. Edwards, P. Landon, B. Solsana-Espriu, A. F. Carley, A. A. Herzing, M. Watanabe, C. J. Kiely, D. W. Knight and G. J. Hutchings, *Science*, 2006, **311**(5759), 362.
- S. Tsubota, M. Haruta, T. Kobayashi, A. Ueda and Y. Nakahara, *Stud. Surf. Sci. Catal.*, 1991, **72**, 695.
- R. Zanela, S. Giorgio, C. R. Henry and C. Louis, *J. Phys. Chem. B*, 2002, **106**, 7634.
- N. S. Patil, B. S. Uphade, P. Jana, S. K. Bhargava and V. R. Choudhary, *J. Catal.*, 2004, **223**, 236.
- N. S. Patil, B. S. Uphade, P. Jana, R. S. Sonawane, S. K. Bhargava and V. R. Choudhary, *Catal. Lett.*, 2004, **94**, 89.
- S. A. Sadeek and M. S. Refat, *J. Coord. Chem.*, 2005, **58**, 1727.

Aqueous medium Ullmann reaction over a novel Pd/Ph–Al–MCM-41 as a new route of clean organic synthesis

Hexing Li,^{*a} Jia Chen,^a Ying Wan,^a Wei Chai,^a Fang Zhang^a and Yunfeng Lu^b

Received 29th August 2006, Accepted 9th November 2006

First published as an Advance Article on the web 1st December 2006

DOI: 10.1039/b612370h

By using the Ph- and Al-functionalized MCM-41 (Ph–Al–MCM-41) as a support, a new and powerful Pd/Ph–Al–MCM-41 catalyst was designed and used in iodobenzene (Ar–I) Ullmann coupling reaction with the attempt to develop new routes of clean organic synthesis by using water instead of organic solvents as the reaction medium. The as-prepared Pd/Ph–Al–MCM-41 exhibited higher activity, better selectivity to biphenyl (Ar–Ar) and stronger durability than other supported Pd catalysts and the maximum Ar–Ar yield reached 79.8% at the optimum Ph/Al/Si molar ratio (15/1/60). Meanwhile, the Pd/Ph–Al–MCM-41 catalyst could be recycled 5 times, indicating the good stability, especially good hydrothermal stability. According to various characterizations, such as FTIR, XRD, TEM, ICP, NMR, N₂ sorption isotherms, the correlation of the catalytic performance to the structural characteristics of the Pd/Ph–Al–MCM-41 was discussed. Besides the high dispersion of Pd active sites on the surface and the easy diffusion in the pore channels of the Ph–Al–MCM-41 owing to the mesoporous structure, the higher activity of the Pd/Ph–Al–MCM-41 could be attributed to the increase of both the surface hydrophobicity resulting from Ph-modification and the surface Lewis acidity owing to the Al-modification, which were favorable for the adsorption of the Ar–I molecules, and thus enhanced the activity. The surface hydrophobicity could also account for the promotion on the selectivity to Ar–Ar by the Ph-modification, since less water could enter the pore channels, which was favorable for Ar–I dehalogenation to form the Ar–H byproduct. The promoting effect of the Al-modification on the selectivity was limited since the Lewis acidic site could adsorb Ar–I molecules in two modes, which were favorable for both the coupling reaction to form Ar–Ar and dehalogenation to form Ar–H. The hydrothermal stability test demonstrated that both the Ph-groups and Al-dopants could stabilize the mesoporous structure in aqueous solution, which could account for the strong durability of the Pd/Ph–Al–MCM-41 catalyst.

1. Introduction

Organic solvents are widely used in the fine chemical and pharmaceutical industries as media for reactions or as solutions for product isolation. The use of large quantities of organic solvents obviously causes environmental problems because volatile organic compounds are a principal cause of industrial pollution. To reduce the use of organic solvents, a great number of attempts have been made to develop new routes for conducting organic reactions in the aqueous solution, since water could be considered as the cleanest and safest substance on Earth. At the present stage, most of the aqueous medium organic reactions involve the use of homogeneous catalysts due to the solubility limitation.^{1,2} Although homogeneous catalysts in general have a high reactivity, their applications are still quite limited. They may not be recovered easily, which obviously increases cost and also leads to heavy-metal pollution in water. In addition, the water-soluble homogeneous catalysts often exhibit poor intermiscibility with

the organic substrates, and thus phase-transferring catalysts are frequently employed. Heterogeneous catalysts could be easily separated from the products and used repetitively,^{3,4} but their lower activity or/and selectivity seems a problem. One of the promising ways is to deposit active sites on the supports with mesoporous structure, since the high surface area may ensure the high dispersion of active sites while the large pores may facilitate the diffusion of reactant molecules from bulk solution onto the catalyst surface. The traditional mesoporous silica materials, such as MCM-41, SBA-15,^{5,6} usually exhibit poor adsorption for organic substrates in aqueous medium due to the hydrophilic surface. The preparation of the inorganic support modified with organic groups could improve the surface hydrophobicity, which may promote the entrance, diffusion and adsorption of organic reagents on the active sites within the pore channels, resulting in higher catalytic activity and selectivity.^{7–9} Meanwhile, the improvement of stability of the mesoporous structure, especially the hydrothermal stability during aqueous organic reactions, should also be considered.^{10,11} In this paper, we report the synthesis of a novel mesoporous Ph–Al–MCM-41 used as the support for depositing metallic Pd particles, with an attempt to improve both the hydrophobicity and hydrothermal stability by surface

^aDepartment of Chemistry, Shanghai Normal University, Shanghai, China. E-mail: HeXing-Li@shnu.edu.cn

^bDepartment of Chemical and Biomolecular Engineering, Tulane University, New Orleans, USA. E-mail: ylu@tulane.edu

modification with Ph-groups and Al-dopants in the framework. The catalytic performance of the as-prepared Pd/Ph–Al–MCM-41 was examined in an aqueous-medium iodobenzene (Ar–I) Ullmann reaction, an important type of organic reaction widely used in the fine chemical, agrochemical and pharmaceutical industries.^{12,13} The correlation of catalytic properties to the structural characteristics is discussed briefly.

2. Experimental

2.1 Catalyst preparation

The Ph–Al–MCM-41 was prepared according to following procedure: an aqueous solution containing TEOS, phenyltrimethoxysilane (PTMS), NaAlO₂, *n*-tetradecyltrimethylammonium bromide (CTMABr), NaOH and tetramethylammonium hydroxide (TMAOH), with a molar ratio of TEOS : PTMS : NaAlO₂ : CTMABr : NaOH : TMAOH : H₂O = 1 : 0.25 : *x* : 0.23 : 0.30 : 0.17 : 125, was kept stirring for 20 h at 25 °C and then heated at 120 °C for 72 h. After being filtered, water-washed, and dried in vacuum at 80 °C for 24 h, the surfactant template and other organic residues were removed by extracting in 1.0 M HCl–EtOH solution at 80 °C 4 times, followed by drying under vacuum at 80 °C for another 10 h. The Al-content was adjusted by changing the NaAlO₂ amount in the initial mixture and was denoted as Ph–Al–MCM-41–*x*, where *x* = Si/Al molar ratio.

The Pd/Ph–Al–MCM-41 catalyst was prepared by impregnating the as-prepared Ph–Al–MCM-41 with a PdCl₂ aqueous solution containing 1.67 wt% Pd at 25 °C for 24 h, followed by drying in air at 100 °C and activating in 10% H₂/N₂ at 200 °C for 3 h. For comparison, the Pd/MCM-41 and Pd/Ph–MCM-41 catalysts were also prepared in a similar way by using MCM-41 and Ph–MCM-41 supports, respectively.

2.2 Characterization

Small-angle X-ray diffraction (XRD) measurements were performed on a Rigaku D/maxrB diffractometer with CuKα X-ray. N₂ sorption isotherms were measured with a Quantachrome NOVA 4000e analyzer, based on which, the surface area (*S*_{BET}) was calculated by using the multiple-point Brunauer–Emmett–Teller (BET) method in the relative pressure range of *P*/*P*₀ = 0.05–0.25, and the pore size distribution curves, together with the average pore size (*d*_p) and the pore volume (*V*_p), were obtained according to the Barrett–Joyner–Halenda (BJH) model. Transmission electron microscopy (TEM) images were obtained on a JEOL JEM2011 electron microscope. X-ray photoelectron spectroscopy (XPS) measurements were performed on a Perkin–Elmer PHI 5000CESCA system with a base pressure of 10^{−9} Torr. All the binding energies were calibrated by using the contaminant carbon (C_{1s} = 284.6 eV) as a reference. FT-IR spectra were recorded with a Nicolet Magna 550 IR spectrometer. Temperature-programmed reduction (TPR) and hydrogen chemisorptions analysis were conducted on a Quantachrome CHEMBET-3000 system. ¹³C MAS NMR, ²⁹Si MAS NMR and ²⁷Al MAS NMR spectra were recorded on a Bruker DRX-400 NMR spectrometer.

2.3 Activity test

The Ar–I coupling reaction (Ullmann reaction) was used as a probe to examine performance of the as-prepared Pd-based catalysts. Under present conditions, only two products were identified during Ar–I Ullmann coupling reaction over different Pd-based supported catalysts. One is the target product biphenyl (Ar–Ar) resulting from the coupling reaction of Ar–I. The other is the side-product benzene resulting from dehalogenation of Ar–I to Ar–H. Thus, the reaction mechanism could be simply described in Scheme 1 (ref. 14), where HCOONa was used to reduce Pd(II) for the catalyst regeneration and KOH was used to neutralize the HI resulted from the reduction of PdI₂.

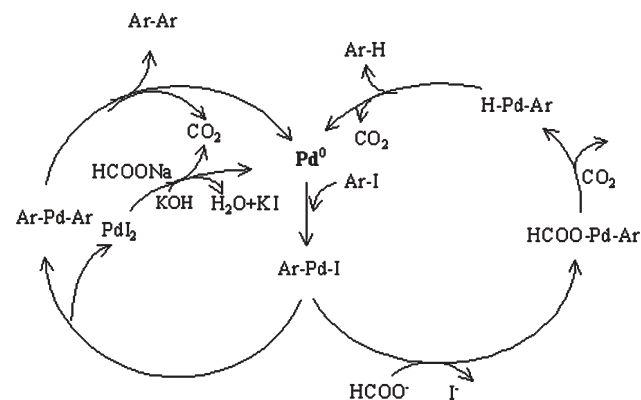
In a typical run of activity tests, 4.46 mmol Ar–I, 10 ml H₂O, 0.50 g catalyst with Pd-loading of 6 wt%, 1.1 g HCOONa and 1.4 g KOH were mixed in a 50 ml round-bottomed flask. The mixture was well stirred so that the diffusion effect could be neglected. After reaction at 100 °C for 10 h, the mixture was filtrated and then extracted with toluene. The products were analyzed by GC analysis (Agilent 1790) equipped with a JW DB-5, 95% dimethyl 1-(5%)-diphenylpolysiloxane column and a FID detector. The column temperature was programmed from 100 °C to 250 °C at a ramp speed of 15 °C min^{−1}. N₂ was used as carrier gas. All tests were repeated at least three times, and it was found that the experimental errors were within ±5%.

In order to determine the catalyst durability, the Pd/Ph–Al–MCM-41 catalyst was allowed to settle and filtered after each run of reactions, followed by washing thoroughly with diethyl ether, water and diethyl ether, respectively. After being dried in vacuum for 8 h, the catalyst was re-used a with fresh charge of solvent and reactants for subsequent recycle runs under the same reaction conditions. The content of Pd species leached off from the Pd/Ph–Al–MCM-41 heterogeneous catalyst in each run was determined by ICP analysis.

The hydrothermal stability was examined by refluxing the aqueous solution containing one of the as-prepared supports at 100 °C for desired time, followed by structural characterizations.

3. Result and discussion

The FTIR spectra (Fig. 1) revealed that, besides the absorbance peaks indicative of the MCM-41 sample at 3500,



Scheme 1

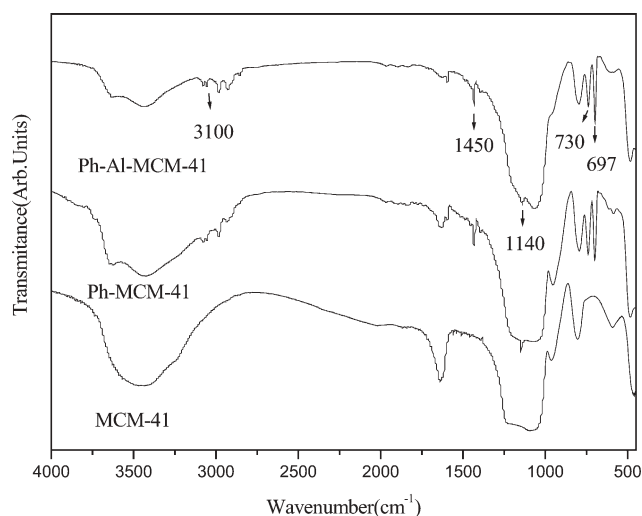


Fig. 1 FTIR spectra of the MCM-41, the Ph-MCM-41 and the Ph-Al-MCM-41-60 samples.

1474, 600, 456 and $1000\text{--}1300\text{ cm}^{-1}$, corresponding to $\nu(\text{O-H})$, $\delta(\text{O-H})$, $\omega(\text{O-H})$, $\nu_{\text{as}}(\text{Si-O})$ and $\delta(\text{Si-O})$ vibrations, both the Ph-Al-MCM-41 and the Ph-MCM-41 samples displayed additional peaks indicative of the $\nu(\text{C-H})$, $\delta(\text{C-H})$ and $\nu(\text{C-C})$ vibrations from the benzene ring at $3100\text{--}3000$, $690\text{--}740$ and $1450\text{--}1460\text{ cm}^{-1}$, respectively. These results demonstrated the successful incorporation of the Ph-group in the wall of MCM-41.¹⁵ The peak characteristic of the $\nu(\text{Si-C})$ vibration at $1160\text{--}1170\text{ cm}^{-1}$ could not be clearly distinguished since it was overlapped by the peak corresponding to the $\nu_{\text{as}}(\text{Si-O})$ in the network of MCM-41. It was found that the peak intensity at 3500 cm^{-1} decreased abruptly in the order of MCM-41, Ph-MCM-41 and Ph-Al-MCM-41, possibly due to the substitution of surface OH groups by Ph-groups and Al-dopants.

The incorporation of the Ph-groups and Al-dopants into the MCM-41 network could be further confirmed by solid NMR spectra. As shown in Fig. 2a, the ^{29}Si MAS NMR spectrum revealed that the Ph-Al-MCM-41 displayed three resonance up-field peaks corresponding to Q^4 ($\delta = -111\text{ ppm}$), Q^3 ($\delta = -102\text{ ppm}$), and Q^2 ($\delta = -95\text{ ppm}$), and two down-field peaks corresponding to T^3 ($\delta = -80\text{ ppm}$) and T^2 ($\delta = -72\text{ ppm}$), respectively,^{16,17} where $\text{Q}^n = \text{Si}(\text{OSi})_n(\text{OH})_{4-n}$ ($n = 2\text{--}4$) and $\text{T}^m = \text{RSi}(\text{OSi})_m(\text{OH})_{3-m}$ ($m = 1\text{--}3$).¹⁸ The presence of T^m peaks confirmed the formation of Si-C bonding, *i.e.*, the successful incorporation of the organic silane moieties as a part of the silica wall structure. The $\text{T}^m/(\text{T}^m + \text{Q}^n)$ ratio in the Ph-Al-MCM-41 sample was determined as 0.21, almost the same as the PTMS/(PTMS + TEOS) molar ratio in the initial mixture (0.20), suggesting that nearly all the PTMS incorporated with the TEOS, *i.e.*, the loss of PTMS during the co-condensation could be neglected. Meanwhile, the ^{13}C CPMAS NMR spectrum, shown in Fig. 2b, clearly displayed two peaks around 134 and 127 ppm, indicative of the C atoms in the benzene ring bonding with the MCM-41.¹⁹ The ^{27}Al MAS NMR spectra (Fig. 2c) further confirmed that the Al-dopants in the Ph-Al-MCM-41 samples were present in two modes depending on the Al-content. At low Al-content (Ph-Al-MCM-41-60), only one NMR peak around 45 ppm, indicative

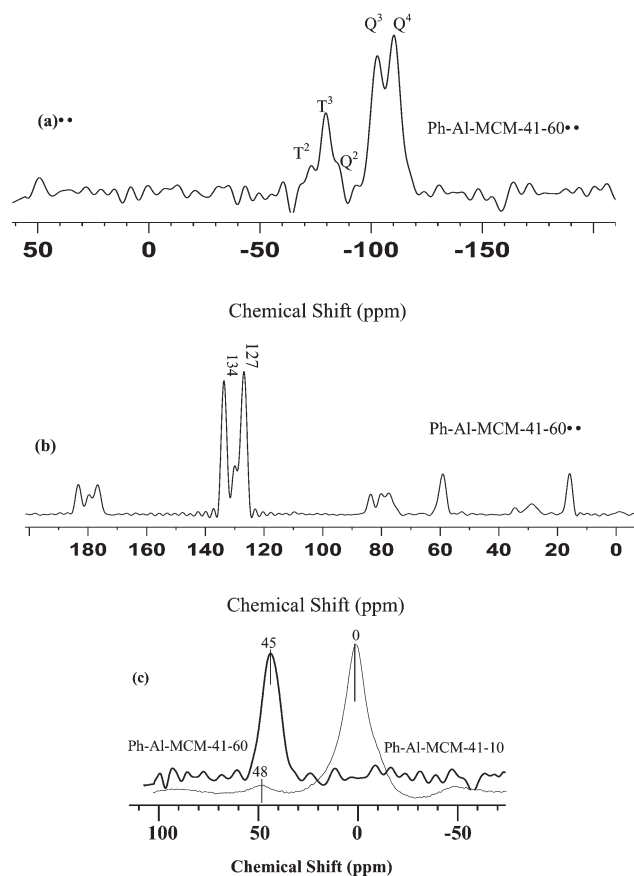


Fig. 2 (a) ^{13}C CP MAS, (b) ^{29}Si CP MAS and (c) ^{27}Al CP MAS NMR spectra of the Ph-Al-MCM-41-60 and the Ph-Al-MCM-41-10 samples.

of the tetrahedral Al, was observed, suggesting that almost all the Al-dopants were incorporated in the framework of the MCM-41. However, at high Al-content (Ph-Al-MCM-41-10), most of Al-dopants were present in the form of octahedral coordination, corresponding to an NMR signal around 0 ppm, while only a small fraction of Al-dopants were present in the form of tetrahedral coordination, corresponding to an NMR signal around 48 ppm. This indicates that, at high Al-content, most Al-dopants were anchored on the outer surface rather than incorporated in the framework of the MCM-41.²⁰

The XRD patterns (Fig. 3) revealed that the Ph-Al-MCM-41 exhibited a well resolved (100) diffractive peak around $2\theta = 2.4^\circ$ indicative of the hexagonal mesoporous structure.²¹ The decrease of the peak intensity and the disappearance of peaks characteristic of (110) and (200) diffractions around $2\theta = 3\text{--}6^\circ$ suggested that the ordered mesoporous structure was partially damaged after incorporation of Ph-groups and Al-dopants, since their interactions with the micelles may disturb the cooperative assembly of silica and CTMABr into a highly ordered mesostructure.²² The peak indicative of (100) diffraction shifted to the higher 2θ , indicating a decrease in basal spacing (d_{100}) owing to the increase of wall thickness of the pore channels.²³ The Pd/Ph-Al-MCM-41 exhibited an even weaker and broader peak indicative of (100) diffraction, which demonstrated that the deposition of metallic Pd particles on the Ph-Al-MCM-41 could further decrease the ordering degree

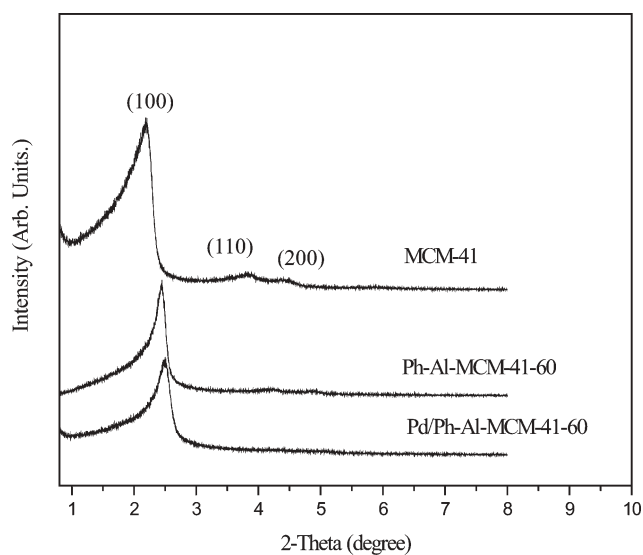


Fig. 3 Small-angle XRD patterns of the pure MCM-41, Al-MCM-41-60 and the 6 wt% Pd/Ph-Al-MCM-41-60 samples.

of the mesoporous structure. Since the Pd/Ph-Al-MCM-41 was obtained by the impregnation method, it was impossible for the Pd particles to enter the framework of the Ph-Al-MCM-41. Thus, the damage of the ordered mesoporous structure could be mainly attributed to the blockage of the pore channels by these Pd particles. This was confirmed by the TEM morphologies. As shown in Fig. 4, the Pd/Ph-Al-MCM-41-60 still preserved the ordered hexagonal mesoporous structure. The Pd particles deposited on the Ph-Al-MCM-41-60 support in two ways. Most Pd particles anchored on the outer surface of the support with a diameter ranging from 3 to 7 nm. However, a small fraction of the Pd particles were distributed in the pore channels, which could account for the positive shift of the peak position observed in Fig. 3 owing to the increase of the pore wall thickness.

Fig. 5 demonstrated that, similar to the pure MCM-41, both the Ph-Al-MCM-41 and the Pd/Ph-Al-MCM-41 displayed typical IV-type N_2 adsorption-desorption isotherms characteristic of the capillary condensation of N_2 in the mesopores.²⁴ Based on the N_2 adsorption-desorption isotherms, some structural parameters were calculated based on the BJH model. As shown in Table 1, both the Al-modification and the Ph-modification caused the decrease in the S_{BET} , V_P and d_P , possibly due to the coverage of the pore wall of the MCM-41 by the Ph-groups and Al-dopants, which caused an increase in the wall thickness.²⁵ Depositing Pd particles on the Ph-MCM-41 support further decreased the S_{BET} , V_P and d_P , which could be easily understood by considering the coverage of the Pd particles on the outer surface, which may result in the blockage of the pore channels, and the occupation of Pd particles in the pore channels, which may increase the pore wall thickness (see Table 1).

As shown in Fig. 6, the XPS spectra revealed that all the Pd species in the Pd/Ph-Al-MCM-41 sample was present in the metallic state, corresponding to the binding energies of 335.2 eV in $Pd_{3d5/2}$ level and 340.3 eV in $Pd_{3d3/2}$ level,²⁶ respectively, which implied that the Pd(II) species deposited on

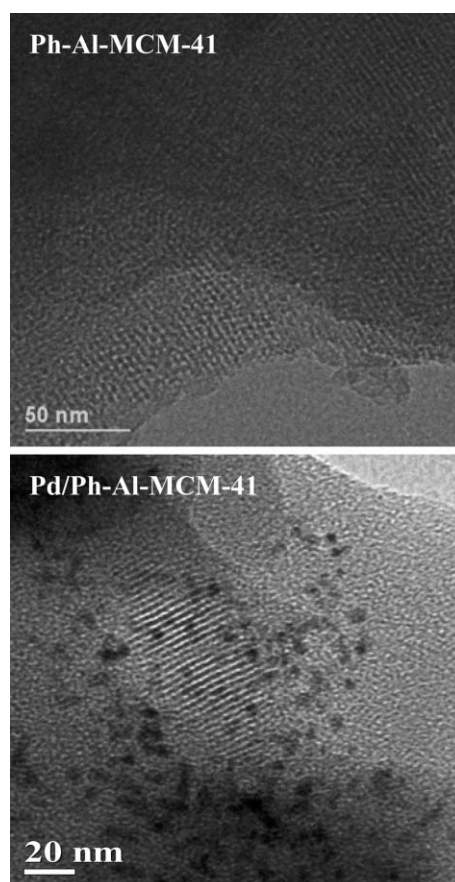


Fig. 4 TEM morphologies of the Ph-Al-MCM-41-60 and the 6 wt% Pd/Ph-Al-MCM-41-60 samples.

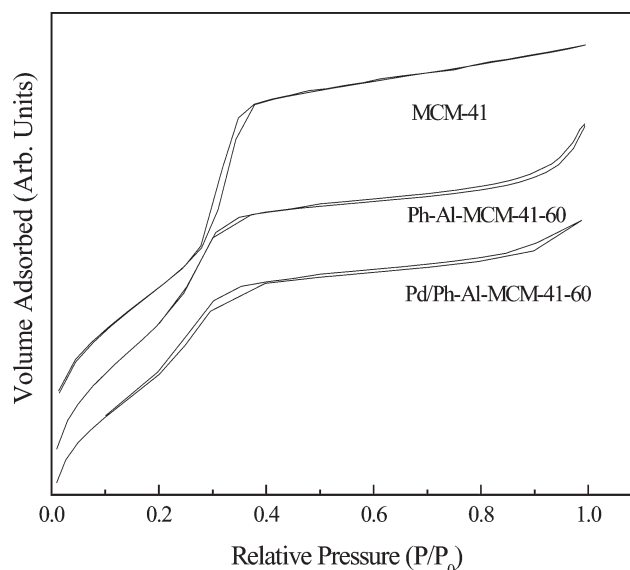


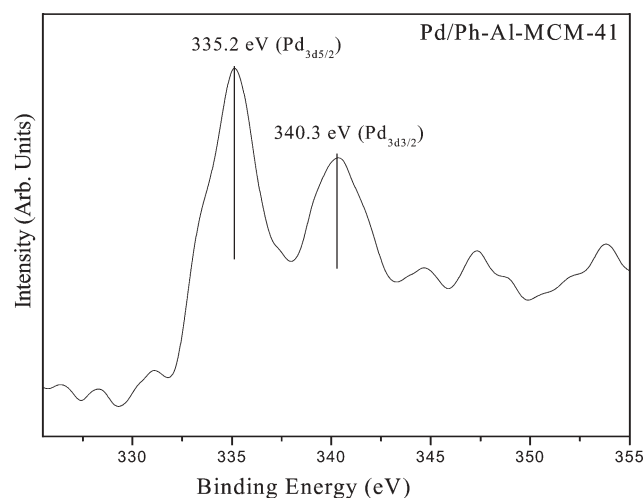
Fig. 5 N_2 adsorption-desorption isotherms of the MCM-41, the Ph-Al-MCM-41-60 and the 6 wt% Pd/Ph-Al-MCM-41-60 samples.

the Ph-Al-MCM-41 could be completely reduced by 10% H_2/N_2 under present conditions. Meanwhile, the TPR curve of the catalyst precursor (Fig. 7) displayed one strong negative peak around 86 °C characteristic of the decomposition of

Table 1 Structural parameters of the as-prepared samples

Sample	$d_{100}/$ nm	$S_{\text{BET}}/$ $\text{m}^2 \text{g}^{-1}$	$d_{\text{p}}/$ nm	$V_{\text{p}}/$ $\text{m}^3 \text{g}^{-1}$	Wall thickness ^a / nm
MCM-41	4.02	1442.4	2.6	1.3	2.0
Al-MCM-41-60	4.01	1361.2	2.6	1.2	2.1
Ph-MCM-41	3.66	989.8	1.9	0.51	2.3
Ph-Al-MCM-41-90	3.98	1028.7	1.8	0.93	2.5
Ph-Al-MCM-41-60	3.48	1017.8	1.5	0.87	2.6
Ph-Al-MCM-41-30	3.59	1010.6	1.4	0.85	2.7
Ph-Al-MCM-41-10	3.77	1008.0	1.3	0.81	3.1
Pd/Ph-Al-MCM-41-60	4.24	904.5	1.0	0.48	3.8

^a Pore wall thickness = a_0 - pore size, where a_0 (lattice parameter) = $2d_{100}/3^{1/2}$

**Fig. 6** XPS spectrum of the 6 wt% Pd/Ph-Al-MCM-41-60 sample.

PdH_2 ,²⁷ and one broad peak around 334 °C due to the hydrogen spillover rather than to the reduction of Pd(II) species.¹⁴ These results demonstrated that most Pd(II) species on the Ph-Al-MCM-41 support could be reduced in the 10% H_2/N_2 to PdH_2 even at ambient temperature.

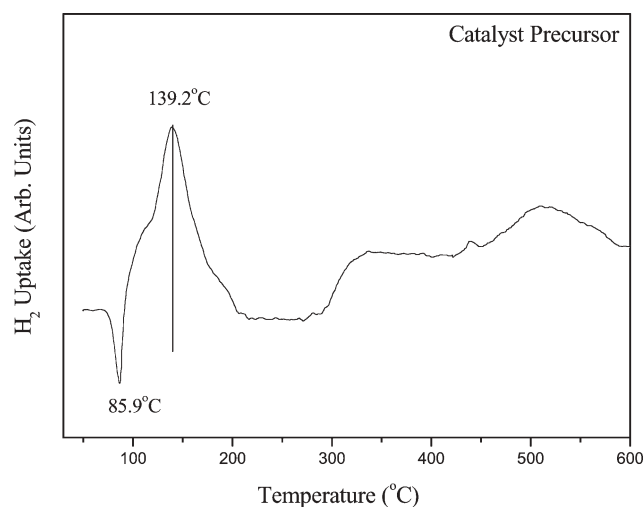
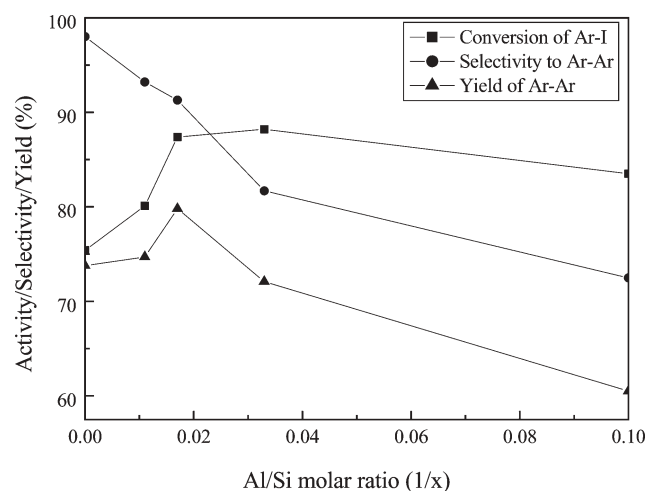
**Fig. 7** TPR profile of the precursor of the 6 wt% Pd/Ph-Al-MCM-41-60 catalyst.

Fig. 8 shows the dependence of the activity and selectivity on the Al-content during the aqueous medium Ar-I Ullmann reaction over Pd/Ph-Al-MCM-41 catalysts with the Pd loading of 6 wt%. One could see that the activity first increased and then decreased with the Al-content. Very high Al-content was harmful for the activity, possibly due to the damage of the ordered mesoporous structure. The selectivity to Ar-Ar decreased consistently with the increasing Al-content, owing to the increase of Lewis acidity, which might be favorable for the dehalogenation to produce Ar-H byproduct (as discussed below). The maximum Ar-Ar yield (79.8%) was obtained over the Pd/Ph-Al-MCM-41-60. Comparing the catalytic performance and durability of the Pd/Ph-Al-MCM-41-60 with other Pd-based catalysts (Table 2), the roles of various supports could be discussed as follows.

1. The Pd/MCM-41 exhibited much higher activity and better selectivity to biphenyl (Ar-Ar) than the Pd/SiO₂. Obviously, the higher activity of the Pd/MCM-41 could be attributed to both the larger surface area of MCM-41, which

**Fig. 8** Dependence of the Ar-I conversion, the selectivity to Ar-Ar and the yield of the Ar-Ar on the Al-content in the 6 wt% Pd/Ph-Al-MCM-41.**Table 2** Activity and recycle test of different catalysts in the Ar-I Ullmann reaction

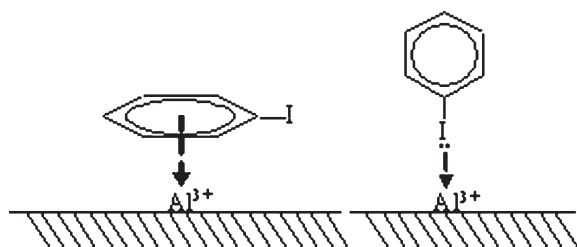
Catalysts	$S_{\text{Pd}}/$ $\text{m}^2 \text{g}^{-1}$	Cycle	Conversion (%)	Selectivity (%)	Yield (%)
Pd/SiO ₂	35.6	1	27.0	26.0	7.0
Pd/MCM-41	85.2	1	63.4	45.3	28.7
		2	45.2	30.1	13.6
Pd/Al-MCM-41-60	78.9	1	81.5	51.0	41.6
Pd/Ph-MCM-41	97.8	1	75.4	98.0	73.8
		2	78.0	88.8	70.0
		3	74.1	85.7	63.5
		4	68.3	73.8	50.4
Pd/Ph-Al-MCM-41-60	90.1	1	87.4	91.3	79.8
		2	88.3	87.1	76.9
		3	86.1	86.7	74.6
		4	84.1	83.4	70.2
		5	75.1	73.5	55.2

^a Reaction conditions: 2.0 g 6.0 wt% Pd/support, 3.24 g Ar-I, 40.0 ml H₂O, 4.40 g HCOONa and 5.60 g KOH, reaction temperature = 100 °C, reaction time for each run = 10 h.

ensured the wide dispersion of Pd active sites (see the S_{Pd} values in Table 2), and the larger pore size, which facilitated the diffusion and adsorption of the Ar–I molecules. The better selectivity of the Pd/MCM-41 could be attributed to the uniform mesopores, taking into account that the micropores in the SiO_2 were unfavorable for the formation of large Ar–Ar molecules.

2. The Pd/Al-MCM-41–60 exhibited much higher activity than the Pd/MCM-41. As the S_{Pd} of the Pd/Al-MCM-41–60 was even lower than that of the Pd/MCM-41, the promoting effect of the Al-dopants on the activity could be mainly attributed to the increase of the surface acidity. As is well known, the Al^{3+} incorporated in the MCM-41 may serve as Lewis type acidic sites which may adsorb Ar–I molecules easily, and thus could enhance the activity. The Ar–I molecule may be adsorbed on the Al^{3+} acidic sites by either the donation of the π -electrons in the benzene ring or the donation of lone electron-pair from the iodine atom, as shown in Scheme 2. The former was favorable for the coupling reaction to produce Ar–Ar while the latter was favorable for the dehalogenation to produce the Ar–H byproduct.¹⁴ The promoting effect of the Al-modification on the selectivity to Ar–Ar was quite limited due to the coincidence of both adsorption modes.

3. The Pd/Ph-MCM-41 exhibited much higher activity and selectivity to Ar–Ar than the Pd/MCM-41. The presence of the Ph-groups on both the outer surface and the pore surface may inhibit the agglomeration of Pd particles, which could improve the dispersion of Pd active sites (see S_{Pd} values), and thus enhance the activity. In addition, the incorporation of the Ph-groups in the MCM-41 may enhance the surface hydrophobicity, which is favorable for both the diffusion of the Ar–I molecules in the porous channels and the adsorption of Ar–I on the catalyst surface, especially in the aqueous medium. This could also account for the increase of the reaction activity. The promoting effect of the Ph-groups on the selectivity could be understood based on the reaction mechanism of the Ar–I Ullmann reaction.¹⁴ As shown in Scheme 1, the byproduct Ar–H was formed mainly through a transition state of $HCOO-Pd-Ar$ obtained by nucleophilic substitution of $I-Pd-Ar$ by $HCOO^-$.²⁸ As mentioned above, the Ph-modification could reduce the concentration of surface OH groups and enhance the surface hydrophobicity. Therefore, fewer water molecules could enter the pore channels, which may retard the dissociation of $HCOONa$ to $HCOO^-$, reducing the side reaction and, as a result, increasing the selectivity to biphenyl, since the formation of $HCOO-Pd-Ar$ species could be effectively inhibited.



Scheme 2

4. The Pd/Ph-Al-MCM-41–60 exhibited higher activity but lower selectivity to Ar–Ar, and in general, a higher Ar–Ar yield than the Pd/Ph-MCM-41. The promoting effect of the Al-modification could be attributed to the increase of Lewis acidic sites from Al^{3+} species, as discussed above. The rapid decrease of the selectivity to Ar–Ar could be attributed to the strong adsorption of the Al^{3+} for the iodine atom in the Ar–I molecule (Scheme 2), which was favorable for the dehalogenation to produce the Ar–H byproduct.¹⁴

5. The durability test revealed that the Pd/MCM-41 lost its activity and selectivity rapidly and could not be used repetitively, while the Pd/Ph-MCM-41 and the Pd/Ph-Al-MCM-41–60 could be used repetitively for 4 and 5 times, respectively. Since only less than 5 ppm Pd species in the solution was detected by ICP analysis, the leaching of Pd active sites during the reaction could be neglected. From Fig. 9, one could see that the Pd/Ph-Al-MCM-41 catalyst completely lost its mesoporous structure after being used for 5 times, which might be a principal reason responsible for the deactivation. Therefore, hydrothermal stability tests were performed by refluxing the MCM-41, Ph-MCM-41 and Ph-Al-MCM-41 samples in boiling water (100 °C), respectively. The N_2 adsorption–desorption isotherms, shown in Fig. 10, demonstrated that the MCM-41 lost its mesoporous structure completely after being treated for 8 h. However, the Ph-MCM-41 still displayed a resolved mesoporous structure after being treated for 12 h and the mesoporous structure disappeared completely after being treated for 18 h. The mesoporous structure could still be observed even after the Ph-Al-MCM-41 was treated for 18 h and was completely destroyed after being treated for 24 h. These results demonstrated the hydrothermal stability changed in the order Ph-Al-MCM-41–60 > Ph-MCM-41 > MCM-41, showing the promoting effects of both the Ph-modification and the Al-modification on the hydrothermal stability of the mesoporous structure. On the basis of ^{29}Si MAS NMR study, Kim and Ryoo claimed that the degradation of the mesoporous structure of Si-MCM-41 in water was mainly attributed to the hydrolysis of Si–O–Si

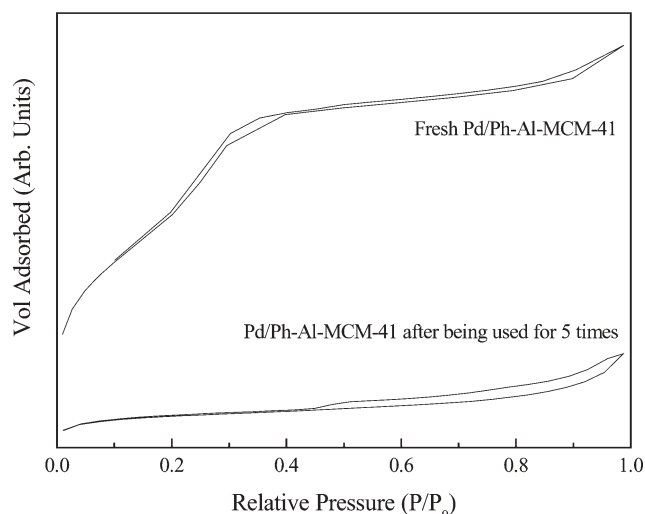


Fig. 9 N_2 sorption isotherms of the fresh 6 wt% Pd/Ph-Al-MCM-41 and the Pd/Ph-Al-MCM-41 after being used repetitively for 5 times.

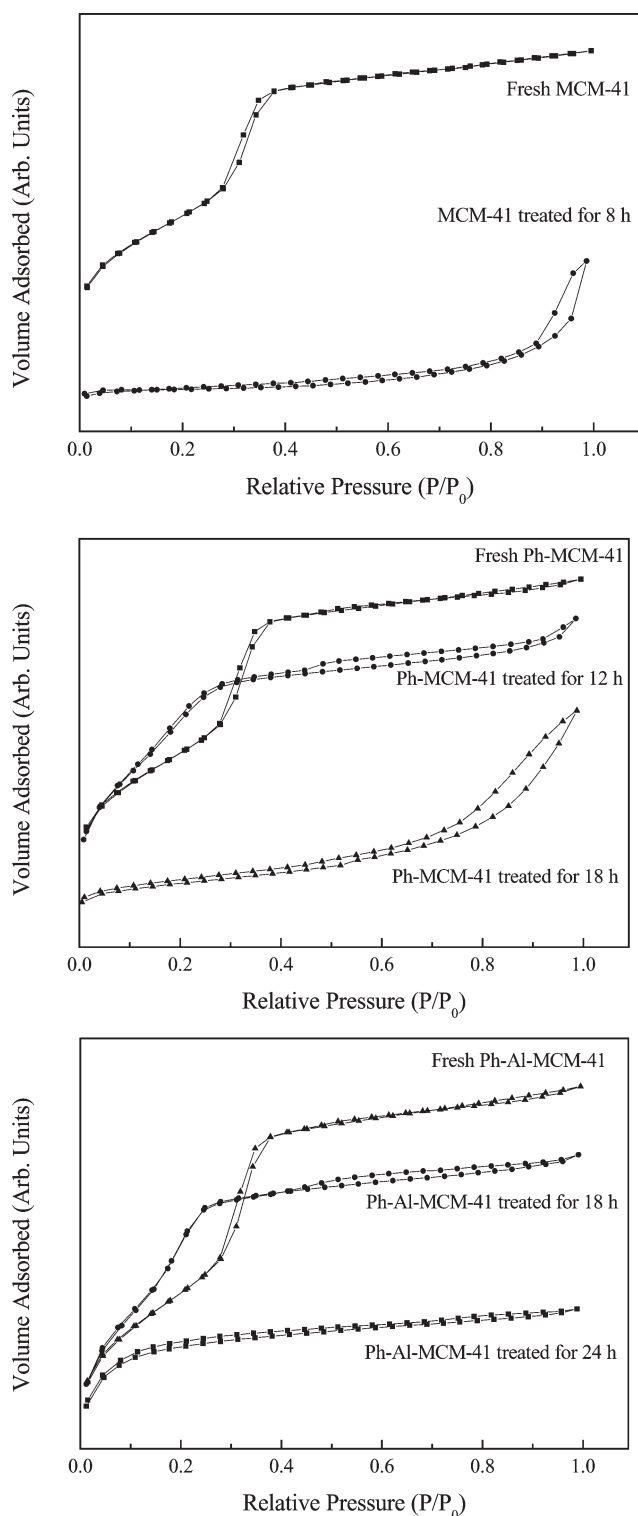


Fig. 10 N_2 sorption isotherms of MCM-41, Ph-MCM-41 and Ph-Al-MCM-41-60 before and after being refluxed in boiling water for different times.

linkages.²⁹ Modification of the MCM-41 with Ph-groups could enhance the surface hydrophobicity, which could inhibit the entrance of water molecules into the pore channels, and thus might protect the mesoporous structure from H_2O attack.^{28,30} The promoting effect of the Al-modification could be

understood by considering the following factors. Firstly, the incorporation of the Al-dopants in the framework of the MCM-41 might cause a structural distortion and enhance the straining force which could stabilize the mesoporous structure against the hydrothermal treatment.³¹ Secondly, the formation of the Si–O–Al bonding may reduce the concentration of silanol groups (see Fig. 1) which could inhibit the contact and adsorption of water molecules and, in turn, decrease the hydrolysis of Si–O–Si linkages.²⁹ Furthermore, a protective layer of aluminosilicate is possibly formed during the initial hydrolysis, which may protect the mesostructure from further hydrolysis.³² The improvement of the hydrothermal stability may protect the mesoporous structure of the catalyst from collapse, which ensured the high dispersion of Pd particles on the support and the free diffusion of organic molecules in the pore channels. Thus, the Pd/Ph–Al-MCM-41 retained its excellent activity and selectivity for a long time.

Conclusions

The present work developed a new supported Pd catalyst by using the mesoporous Ph–Al-MCM-41 as the support, which exhibited high activity and selectivity, as well as strong durability during an aqueous-medium iodobenzene (Ar–I) Ullmann reaction. The optimum Ph/Al/Si molar ratio was determined as 15/1/60, *i.e.*, Ph/Si = 1/4 and Al/Si = 1/60. Besides the high surface area and the large pore size, which ensured the well dispersion of the Pd particles and the easy diffusion and adsorption of Ar–I molecules, the Ph- and Al-modification played key roles in the improvement of the catalytic performance. The promoting effect of the Ph-modification on the activity and selectivity could be attributed to the enhancement of surface hydrophobicity. The Al-modification could greatly enhance the activity owing to the increase of surface Lewis acidity, which was favorable for the adsorption of Ar–I molecules. However, its promoting effect on the selectivity to Ar–Ar was limited, since the Lewis acidic sites could adsorb Ar–I molecules in two modes which were favorable for both the coupling reaction to produce Ar–Ar and the dehalogenation to form Ar–H byproduct. Both the Ph-modification and the Al-modification could enhance the hydrothermal stability of the mesoporous structure, showing strong durability during the Ar–I Ullmann reaction in aqueous medium.

References

- 1 M. R. J. Dack, *Chem. Soc. Rev.*, 1975, **4**, 211.
- 2 Y. Zhang, D. Wang and Z. T. Huang, *J. Prog. Chem.*, 1999, **11**, 394.
- 3 S. Zhang, D. Zhang and L. S. Liebeskind, *J. Org. Chem.*, 1997, **62**, 2312.
- 4 J. Hassan, *Chem. Rev.*, 2002, **102**, 1360.
- 5 A. Corma, *Chem. Rev.*, 1997, **97**, 2373.
- 6 C. T. Kresge, M. E. Leonowicz, W. J. Roth, J. C. Vartuli and J. S. Beck, *Nature*, 1992, **39**, 710.
- 7 A. P. Wight and M. E. Davis, *Chem. Rev.*, 2002, **102**, 3589.
- 8 A. Stein, B. J. Melde and R. C. Schroden, *Adv. Mater.*, 2000, **12**, 1403.
- 9 Q. Yang, Y. Li, L. Zhang, J. Yang, J. Liu and C. Li, *J. Phys. Chem. B*, 2004, **108**, 7934.
- 10 Y. Liu, W. Zhang and T. J. Pinnavaia, *Angew. Chem., Int. Ed.*, 2001, **40**, 1255.

- 11 Y. Xia and R. Mokaya, *Microporous Mesoporous Mater.*, 2004, **68**, 1.
- 12 G. Bringmann, R. Alter and R. Weirich, *Angew. Chem., Int. Ed. Engl.*, 1990, **102**, 1006.
- 13 S. Svenkatraman and C. J. Li, *Org. Lett.*, 1999, **1**, 1133.
- 14 J. Panpranot, J. G. Goodwin and A. Sayari, *Catal. Today*, 2002, **77**, 269.
- 15 H. Y. Huang, R. T. Yang, D. Chinn and C. L. Munson, *Ind. Eng. Chem. Res.*, 2003, **42**, 2427.
- 16 H. Hata, S. Saeki, T. Kimura, Y. Sugahara and K. Kuroda, *Chem. Mater.*, 1999, **11**, 1110.
- 17 P. T. Tenev, M. Chibwe and T. Pinnavaia, *Nature*, 1994, **368**, 321.
- 18 R. H. Simon, E. F. Christabel, L. Benedicte and M. Stephen, *Chem. Commun.*, 1999, 201.
- 19 J. Y. Choi, C. H. Kim and D. K. Kim, *J. Am. Ceram. Soc.*, 1998, **81**, 1184.
- 20 R. Ryong, H. K. Chang and F. H. Russ, *Chem. Mater.*, 1997, **9**, 1607.
- 21 Y. D. Xia, W. X. Wang and R. Mokaya, *J. Am. Chem. Soc.*, 2005, **127**, 790.
- 22 R. Mokaya, *J. Phys. Chem. B*, 2000, **104**, 8279.
- 23 S. J. Gergg and K. S. Sing, *Adsorption, Surface Area and Porosity*, Academic, New York, 2nd edn, 1982, p. 10.
- 24 J. Beck, J. Vartuli and W. Roth, *J. Am. Chem. Soc.*, 1992, **114**, 10834.
- 25 Y. D. Xia and R. Mokaya, *J. Phys. Chem. B*, 2003, **107**, 6954.
- 26 A. C. Thomas, *Photoelectron and Auger Spectroscopy*, Plenum, New York, 1st edn, 1975, p. 352.
- 27 J. Panpranot, K. Pattamakomsan and P. Praserttham, *J. Phys. Chem. B*, 2004, **105**, 6014.
- 28 W. H. Zhang, X. B. Lu and J. H. Xiu, *Adv. Funct. Mater.*, 2004, **14**, 544.
- 29 J. M. Kim and R. Ryoo, *Bull. Korean Chem. Soc.*, 1996, **17**, 66.
- 30 X. S. Zhao, G. Q. Lu, A. K. Whittaker, G. J. Millar and H. Y. Zhu, *J. Phys. Chem. B*, 1997, **101**, 6525.
- 31 C. Y. Chen, S. Q. Xiao and M. E. Davis, *Microporous Mater.*, 1995, **4**, 1.
- 32 W. Lutz, W. Gessner, R. Bertran, I. Pitsch and R. Fricke, *Microporous Mater.*, 1997, **12**, 131.



STOP!

searching...

Save valuable time searching for that elusive piece of vital chemical information.

Let us do it for you at the Library and Information Centre of the RSC.

We are your chemical information support, providing:

- Chemical enquiry helpdesk
- Remote access chemical information resources
- Speedy response
- Expert chemical information specialist staff

Tap into the foremost source of chemical knowledge in Europe and send your enquiries to

library@rsc.org

RSCPublishing

www.rsc.org/library

12120515

Supramolecular Chemistry Anniversary Issue

“The issue augurs well to be a precious help for students as well as specialist researchers wishing to get a quick update on a specific topic”
Javier de Mendoza

“This promises to be a landmark issue that will surely stand the test of time as a seminal contribution to the all-important area of supramolecular chemistry.”
Jon Sessler



- **easy-to-read and fully updated tutorial reviews**
- **authored by pioneering researchers in the field**
- **drawing together the most relevant topics in supramolecular chemistry today**

In its February 2007 special issue *Chem Soc Rev* celebrates two landmark anniversaries in the field of Supramolecular Chemistry:

1967: Charles Pedersen's first paper on the synthesis and metal binding properties of crown ethers is published in the *Journal of the American Chemical Society*.

1987: the Nobel prize in chemistry is awarded to Charles Pedersen, Jean-Marie Lehn and Donald Cram in recognition of their pioneering work in Supramolecular Chemistry.



years of publishing

Organic & Biomolecular Chemistry ...

- now one of the leading journals in the field
- Impact Factor 2.55
- high exposure - top papers highlighted in the wider scientific press
- indexed in MEDLINE and other major databases
- short publication times, as low as 24 days from acceptance for papers, and 14 days for communications

OBC has achieved tremendous success since the first issue was published in January 2003. Can any other 'young' journal boast such highly cited papers, published quickly to such exacting standards?

... celebrating 5 years of publishing

Environmental Science Books

Issues in Environmental Science & Technology

Series Editors:

R E Hester and R M Harrison

Format: **Hardback**

Price: **£45.00**

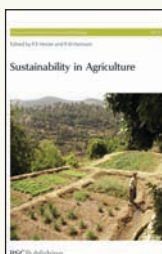
RSC Member Price: **£29.25**

Written by leading experts, this series presents a multidisciplinary approach to pollution and the environment. Focussing on the science and broader issues including economic, legal and political considerations.

Sustainability in Agriculture Vol. No. 21

Discusses the key factors impacting on global agricultural practices including fair trade, the use of pesticides, GM products and government policy.

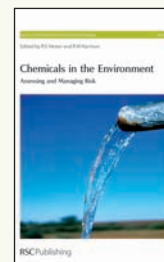
2005 | xiv+130 pages | ISBN-10: 0 85404 201 6
ISBN-13: 978 0 85404 201 2



Chemicals in the Environment Assessing and Managing Risk Vol. No. 22

Beginning with a review of the current legislation, the books goes on to discuss scientific and technical issues relating to chemicals in the environment and future developments.

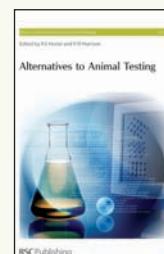
2006 | xvi+158 pages | ISBN-10: 0 85404 206 7
ISBN-13: 978 0 85404 206 7



Alternatives to Animal Testing Vol. No. 23

Provides an up-to-date discussion on the development of alternatives to animal testing including; international validation, safety evaluation, alternative tests and the regulatory framework.

2006 | xii+118 pages | ISBN-10: 0 85404 211 3
ISBN-13: 978 0 85404 211 1

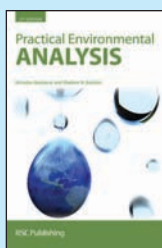


Practical Environmental Analysis 2nd Edition

By *M Radojevic and V N Bashkin*

A new edition textbook providing an up-to-date guide to practical environmental analysis. Ideal for students and technicians as well as lecturers wishing to teach the subject.

Hardback | 2006 | xxiv+458 pages | £39.95 | RSC member price
£25.75 | ISBN-10: 0 85404 679 8 | ISBN-13: 978 0 85404 679 9



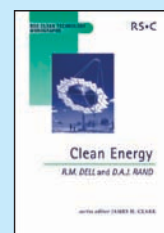
Clean Energy (RSC Clean Technology Monographs)

By *R M Dell and D A J Rand*

Series Editor *J H Clark*

Covering a broad spectrum of energy problems, this highly accessible book discusses in detail strategies for the world's future energy supply.

Hardback | 2004 | xxxvi+322 pages | £89.95 | RSC Member Price
£58.25 | ISBN-10: 0 85404 546 5 | ISBN-13: 978 0 85404 546 4

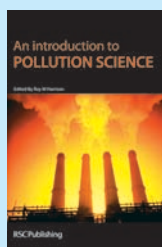


An Introduction to Pollution Science

By *R M Harrison*

A student textbook looking at pollution and its impact on human health and the environment. Covering a wide range of topics including pollution in the atmosphere, water and soil, and strategies for pollution management.

Hardback | 2006 | ca xii+322 pages | £24.95 | RSC Member Price
£16.50 | ISBN-10: 0 85404 829 4 | ISBN-13: 978 0 85404 829 8

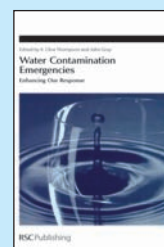


Water Contamination Emergencies Enhancing Our Response

By *J Gray and K C Thompson*

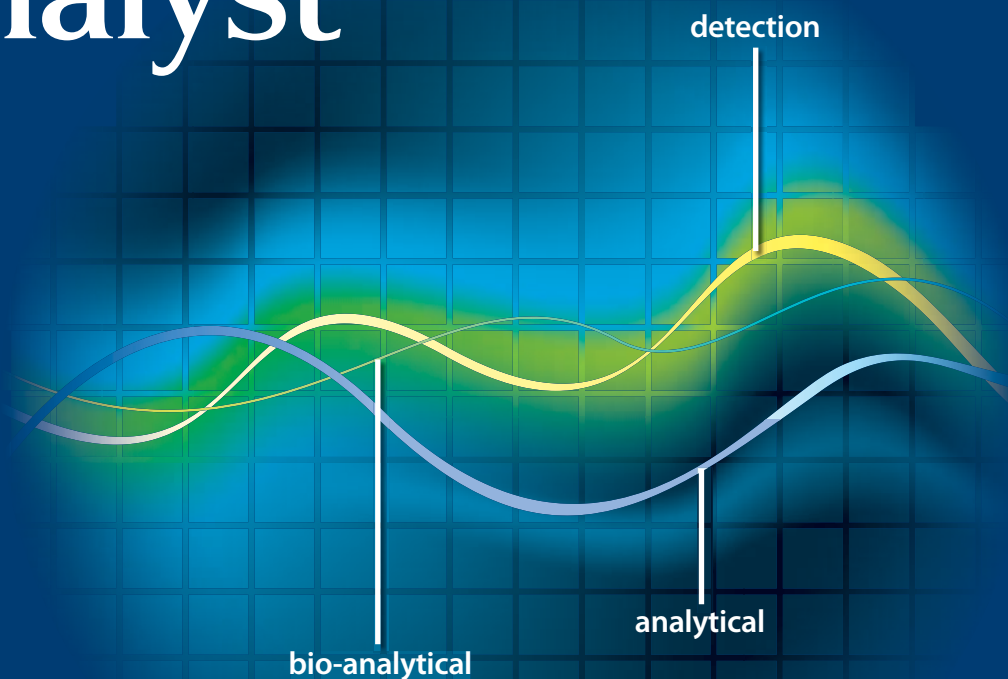
A look at the impact and response of contaminated water supplies including the threat of chemical, biological, radiological and nuclear (CBRN) events.

Hardback | 2006 | x+372 pages | £99.95 | RSC Member Price
£64.75 | ISBN-10: 0 85404 658 5 | ISBN-13: 978 0 85404 658 4



The Analyst

Not just an
analytical
chemistry
journal



Reporting on the latest innovations in detection science

With over a century of experience The Analyst is used to responding to the changing needs of the analytical community.

Focussing on innovative, interdisciplinary science The Analyst reports on significant advances made in the theory, practice and application of (bio) analytical and detection science.

With a new impact factor of 2.858 The Analyst just keeps getting better. It has an international audience and is the second highest general journal publishing primary research in all areas of analytical science.

Registered Charity No. 207890

RSC Publishing

www.rsc.org/analyst